CORROSION INHIBITION STUDIES OF GA9 MAGNESIUM ALLOY IN CHLORIDE AND SULPHATE MEDIA

Thesis

Submitted in partial fulfillment of the requirements for the degree of

DOCTOR OF PHILOSOPHY

by

SUDARSHANA SHETTY

DEPARTMENT OF CHEMISTRY

NATIONAL INSTITUTE OF TECHNOLOGY KARNATAKA

SURATHKAL, MANGALORE -575 025

DECEMBER, 2019

DEDICATED TO MY FAMILY

D E C L A R A T I O N

I hereby *declare* that the Research Thesis entitled "**CORROSION INHIBITION STUDIES OF GA9 MAGNESIUM ALLOY IN CHLORIDE AND SULPHATE MEDIA**" which is being submitted to the **National Institute of Technology Karnataka Surathkal,** in partial fulfillment of the requirements for the award of the Degree of **Doctor of Philosophy** in **Chemistry** is a *bonafide report of the research work carried out by me*. The material contained in this Research Thesis has not been submitted to any University or Institution for the award of any degree.

<div align="right">

Sudarshana Shetty

Register Number: 112016CY11P01

Department of Chemistry

</div>

Place: NITK - SURATHKAL

Date:

C E R T I F I C A T E

This is to *certify* that the Research Thesis entitled **"CORROSION INHIBITION STUDIES OF GA9 MAGNESIUM ALLOY IN CHLORIDE AND SULPHATE MEDIA"** submitted by **SUDARSHANA SHETTY** (Register Number**: 112016CY11P01)** as the record of the research work carried out by him, is *accepted as the Research Thesis submission* in partial fulfillment of the requirements for the award of degree of **Doctor of Philosophy.**

Dr. A. Nityananda Shetty   **Dr. Jagannatha Nayak**

Research Guides

Chairman – DRPC

ACKNOWLEDGEMENT

ABSTRACT

The corrosion behaviour of GA9 magnesium alloy in two different media, namely, sodium chloride and sodium sulphate in different concentrations and temperatures have been studied by potentiodynamic polarization and electrochemical impedance spectroscopy techniques. The effect of pH of the medium on the corrosion behaviour of GA9 magnesium alloy have also been studied in both the media. The results revealed a trend of higher corrosion rate associated with higher medium concentration, lower pH and higher temperature. The corrosion rate in the sodium chloride medium was higher than that in the sodium sulphate medium.

Four different alkyl sulfonates namely sodium dodecylbenzenesulfonate (SDBS), sodium 4-n-octylbenzenesulfonate (SOBS), sodium 2,4-dimethylbenzenesulfonate (SDMBS) and sodium benzenesulfonate (SBS) were tested as corrosion inhibitors for GA9. The results pertaining to the corrosion inhibition studies of four inhibitors in two different media at different temperatures in the presence of varying concentrations of inhibitors are reported in the thesis. The inhibition efficiencies of all the four inhibitors decrease with the increase in temperature and increase in the concentration of the media. Activation parameters for the corrosion of the alloy and thermodynamic parameters for the adsorption of the inhibitors have been calculated and have been documented in the thesis.

The sulfonates predominately physisorbed and adsorption was in accordance with Langmuir adsorption isotherm. The studied sulfonates were found to function as mixed type inhibitors. The sulfonates were more efficient at lower temperatures in both the media. Inhibition efficiency is in the order SDBS > SOBS >SDMBS > SBS. Proposed mechanism attributed the cathodic inhibition to the blockage of the reaction spots by chemisorbed sulphonates. The anodic inhibition resulted from the compaction of the porous film by precipitated magnesium sulfonates.

Keywords: GA9 alloy, Corrosion, Inhibitor, Adsorption.

CONTENTS   **Page No**

CHAPTER 1   INTRODUCTION

LIST OF FIGURES

x

NOMENCLATURE

Abbreviations	Nomenclature
ASTM	American Society for Testing and Materials
CPE	Constant phase element
DC	Direct Current
EDTA	Ethylenediamine tetraacetic acid
EDX	Electron dispersive x-ray analysis
EIS	Electrochemical impedance spectroscopy
EW	Equivalent weight of the corroding material
Fig	Figure
HF	High frequency
IUPAC	International Union of Pure and Applied Chemistry
LF	Low frequency
MF	Medium frequency
OCP	Open circuit potential
SBS	Sodium benzenesulfonate
SCC	Stress Corrosion Cracking
SCE	Saturated calomel electrode
SEM	Scanning electron microscopy
SDBS	Sodium dodecylbenzenesulfonate
SDMBS	Sodium 2,4-dimethylbenzenesulfonate
SOBS	Sodium 4-n-octylbenzenesulfonate
VPI	Vapour phase inhibitor

LIST OF SYMBOLS

Symbol	Definition
T	Absolute temperature
E_a	Activation energy
η_{act}	Activation overpotential
E_0	Amplitude of the signal
ω	Angular frequency
N	Avagadro's number
W_i	Atomic weight of the ith element in the alloy
b_c	Cathodic Tafel slope
E	Cell potential
R_{ct}	Charge transfer resistance
C_{inh}	Concentration of the inhibitor
Y_0	Constant phase element constant
B	Constant
K	Constant
i_{corr}	Corrosion current density
$i_{corr(inh)}$	Corrosion current density in the presence of inhibitor
E_{corr}	Corrosion potential
υ_{corr}	Corrosion rate
ρ	Density of the corroding material
C_{dl}	Double layer capacitance
R_e	Electrolyte resistance
$\Delta H^{\#}$	Enthalpy of activation
$\Delta S^{\#}$	Entropy of activation
i_o	Exchange current density
F	Faraday constant
ΔG	Free energy change
ω_{max}	Frequency at which imaginary part of the impedance has a maximum
R	Gas constant
Z''	Imaginary part impedance
Z_{mod}	Impedance modulus
η	Inhibition efficiency
R^2	Linear regression coefficient
f_i	Mass fraction of the ith element in the alloy
n	Number of electrons in a reaction
θ_{max}	Phase maximum
φ	Phase shift
h	Plank's constant
R_p	Polarization resistance

Z'	Real part of impedance
E^0	Standard cell potential
ΔH^0_{ads}	Standard enthalpy of adsorption
ΔS^0_{ads}	Standard entropy of adsorption
ΔG^0_{ads}	Standard free energy of adsorption
θ	Surface coverage
d	Thickness of the film
t	Time
n_i	Valence of the ith element of the alloy
f_i	Weight fraction of alloying element

CHAPTER 1

INTRODUCTION

1.1 INTRODUCTION TO CORROSION

The origin of term "corrosion" can be traced to Latin. The Latin term "rodere" means 'gnawing' and "corrodere" means 'gnawing to pieces'. The word corrosion is old as the earth, but it has been known by different names. Corrosion is commonly known as rusting, an undesirable phenomena which destroys the luster and beauty of objects and shortens their life (Einar Bardal). Even though it is a natural phenomenon in which the gases present in the atmosphere react chemically with metals to convert them into their salts, it results in loss of material and money. Metals have a strong crystalline structure and when they are converted into their salts they lose the metallic strength, resulting in the damage to machineries in which they are used. Thus corrosion causes damage to metals and thereby to the society. The estimate of loss due to corrosion is approximately 2.5 billion dollars/ annum all over the world. Hence it is necessary to understand the mechanism of corrosion. Corrosion is defined as "the destruction or deterioration of a metal by chemical or electrochemical reactions with its environment". The definition in general sense is often extended to beyond metals; to other nonmetallic materials of interest, such as ceramics, plastics, concrete, wood, rubber, etc. Corrosion of metals can be considered as 'extractive metallurgy in reverse'. As per IUPAC, "Corrosion is an irreversible interfacial reaction of a material (metal, ceramic and polymer) with its environment which results in its consumption or dissolution into the material of a component of the environment. Often, but not necessarily, corrosion results in effects detrimental to the usage of the material considered. Exclusively, physical or mechanical processes such as melting and evaporation, abrasion or mechanical fracture are not included in the term corrosion". Generally it is applicable mainly to metals and where a metal undergoes corrosion, its properties are changed due to the unintentional but destructive reaction with the environment. Most of the metals, except noble metals, occur in nature as thermodynamically stable compounds such as oxides, sulfides, carbonates, chlorides, etc. The extraction of pure metal from ore is an endothermic process. As a result pure metals exist at higher energy state compared to respective metal compounds in ores and possess a natural tendency to revert back to thermodynamically stable combined state. Hence process of corrosion is spontaneous and exposed metals corrode by combining with various constituents of the surrounding environment. Due to corrosion the useful

properties of a metal like malleability, ductility, electrical conductivity and also the surface appearance are lost.

1.2 CONSEQUENCES OF CORROSION

The consequences of corrosion are many and varied and the effects of these on the safe, reliable and efficient operation of equipment or structures are often more serious than the simple loss of a mass of metal. Some of the major harmful effects of corrosion can be summarized as follows:

- Reduction of metal thickness leading to loss of mechanical strength and structural failure or breakdown.

- Hazards or injuries to people arising from structural failure or breakdown (e.g. bridges, cars, aircraft).

- Loss of time in availability of profile - making industrial equipment.

- Reduced value of goods due to deterioration of appearance.

- Contamination of fluids in vessels and pipes (e.g. beer goes cloudy when small quantities of heavy metals are released by corrosion).

- Perforation of vessels and pipes allowing escape of their contents and possible harm to the surroundings. For example, a leaky domestic radiator can cause expensive damage to carpets and decorations, while corrosive sea water may enter the boilers of a power station if the condenser tubes perforate.

- Loss of technically important surface properties of a metallic component. These could include frictional and bearing properties, ease of fluid flow over a pipe surface, electrical conductivity of contacts, surface reflectivity or heat transfer across a surface.

- Mechanical damage to valves, pumps, etc. or blockage of pipes by solid corrosion products.

- Added complexity and expense on equipment, which needs to be designed to withstand a certain amount of corrosion, and to allow corroded components to be conveniently replaced.

1.3 IMPORTANCE OF CORROSION STUDIES

Corrosion is a complex phenomenon influenced by so many environmental factors such as atmospheric constituents, underground/soil wastes, acidic/alkaline

solutions and combinations of these. Many of the corrosion problems generated in the industries involve the surroundings associated with acids and in certain cases alkalies and solvents. The rapid growth in different sectors and the increasing pollution of the environment produces a more corrosive atmosphere. Thus the contamination of the industrial and other environmental factors is unavoidable. This leads to the destruction of materials. There are three primary reasons for concern about and study of corrosion: safety, economy, and conservation. Premature failure of bridges or structures due to corrosion can result in human injury or even loss of life. Failure of operating equipment can have the same disastrous results. (Schweitzer 2010).

To cope with the potential problems of corrosion, it is necessary to understand:

- Mechanisms of corrosion,
- Forms of metallic corrosion,
- Corrosive attack on nonmetallic materials,
- Corrosion-resistance properties of various materials,
- Proper fabrication and installation techniques,
- Methods to prevent or control corrosion,
- Corrosion testing techniques,
- Corrosion monitoring techniques.

Some of the economic and social consequences of corrosion are:

- Poor appearance,
- Contamination of a product,
- Loss of efficiency,
- Loss of valuable product,
- Effects on safety and reliability in handling hazardous materials,
- Depletion of natural resources including metals and fuels used to manufacture them.

1.4 ELECTROCHEMICAL THEORY OF CORROSION

According to this theory, corrosion of metals takes place due to the formation of anodic and cathodic regions on the same metal surface or when two different metals are in contact with each other in the presence of a conducting medium. Anodic reactions in

metallic corrosion are relatively simple. At the anodic region metal undergoes oxidation forming metal ions and liberates electrons. During alloy corrosion, this will result in the formation of metallic ions of many alloying elements. Metals that are capable of exhibiting multiple valence states may go through several stages of oxidation during the corrosion process. At the cathodic region, reduction reaction takes place. Since the metal cannot be reduced further, metal atoms at the cathodic region are unaffected by the cathodic reaction. Some of the constituents of the corrosion medium undergo reduction at the cathode. A corroding metal does not spontaneously accumulate any charge. It therefore follows that these two partial reactions of oxidation and reduction must proceed simultaneously and at the same rate to maintain electro neutrality. The electrons liberated by anodic reaction constitute corrosion current and are consumed in the cathodic process. The metal ions liberated at the anode and some anions formed at the cathode diffuse towards each other through the conducting medium and form a corrosion product somewhere between the anode and cathode (Fontana 2005). An illustrative cell established at a corroding metal surface is shown in Fig. 1.1.
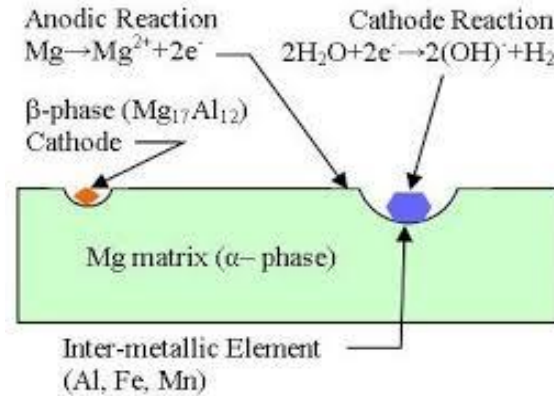
Fig. 1.1: An illustrative electrochemical cell formed at a corroding metal surface.

Corrosion reactions:

At the anodic region: Due to oxidation, the metal gets converted into its ions by liberating electrons.

$$M \rightarrow M^{n+} + ne^- \qquad (1.1)$$

At the cathodic region: Depending on the nature of the atmosphere the following reactions take place at the cathode.

1. Hydrogen evolution: These reactions are dependent upon pH of the medium and occur in the absence of oxygen. In acidic media protons are reduced and in neutral or alkaline media reduction of water takes place.

$$2H^+ + 2e^- \rightarrow H_2 \uparrow \tag{1.2}$$

$$2H_2O + 2e^- \rightarrow 2OH^- + H_2 \uparrow \tag{1.3}$$

2. Reduction of oxygen: At acidic pH oxygen is reduced to water, whereas at alkaline or neutral pH hydroxyl ion formation is favoured.

$$4H^+ + O_2 + 4e^- \rightarrow 2H_2O \tag{1.4}$$

$$2H_2O + O_2 + 4e^- \rightarrow 4OH^- \tag{1.5}$$

3. Metal ion reduction: Impurity metal ions get reduced at cathode.

$$M^{n+} + e^- \longrightarrow M^{(n-1)+} \tag{1.6}$$

4. Metal deposition: Secondary metal ions get reduced and deposited at cathode.

$$M^{n+} + n\ e^- \longrightarrow M \tag{1.7}$$

1.5 CLASSIFICATION OF CORROSION

Corrosion can be classified in different ways. Classification is usually based on one of the three factors.

- **Nature of the corrodent:**

  i] Wet corrosion: Occurs in the presence of liquid or moisture.

  ii] Dry corrosion: Occurs in the absence of a liquid phase or above the dew point of the environment.

- **Mechanism of corrosion:**

  i] Electrochemical corrosion: Corrosion in presence of destructive electrolytes and involve participation of electrons.

  ii] Chemical corrosion: Direct chemical oxidation of metal by surrounding atmosphere.

- **Appearance of the corroded metal:**

  Corrosion is either uniform and the metal corrodes at the same rate over the entire surface, or it is localized, in which case only small areas are affected (Davis 2000).

1.5.1 Forms of corrosion

Most conveniently corrosion can be classified in the forms in which it manifests itself. On the basis of their appearance of the corroded metal or mechanism of attack it can be divided into following eight forms.

1.5.1.1 Uniform corrosion

Uniform attack is the most common form of corrosion. It is characterized by corrosive attack proceeding evenly over the entire surface area, or a large fraction of the total area. General thinning takes place until failure. The most familiar example is the plate of zinc immersed in dilute sulfuric acid.

1.5.1.2 Galvanic corrosion

This type of electrochemical corrosion is also called bimetallic corrosion. Galvanic corrosion occurs when two dissimilar metals or alloys are electrically connected and immersed in an electrolyte. Dissimilar metals and alloys have different electrode potentials and when two or more of them come into contact in an electrolyte, one metal acts as anode and the other as cathode. The potential difference between the dissimilar metals is the driving force for the accelerated attack on the anode member of the galvanic couple. Example is copper rivets in steel utensils; steel corrodes whereas copper does not.

The three important requirements for the occurrence of galvanic corrosion are:

- Materials possessing different surface potential
- A common electrolyte
- A common electrical path

1.5.1.3 Crevice corrosion

Crevice corrosion is a localized and insidious type of corrosion occurring within or adjacent to narrow gaps or openings formed by metal-to-metal or metal-to-nonmetal contact. A concentration cell is formed between the electrolyte within the crevice, which is oxygen starved, and the electrolyte outside the crevice, where oxygen is more plentiful. The material within the crevice acts as the anode, and the exterior material becomes the cathode. Example is corrosion of steel in an industrial environment resulting from wetted area within crevice.

1.5.1.4 Pitting corrosion

Pitting is a highly localized form of corrosion that produces sharply defined holes. These holes may be small or large in diameter, but in most cases, they are relatively small. Pits may be isolated from each other on the surface or so close together that they resemble a roughened surface. Pitting occurs when one area of a metal becomes anodic with respect to the rest of the surface or when highly localized changes in the corrodent in contact with the metal, as in crevices, cause accelerated localized attack. Example: stainless steel exposed to chloride containing water.

1.5.1.5 Intergranular corrosion

Intergranular corrosion is defined as the selective dissolution of grain boundaries, or closely adjacent regions, without appreciable attack of the grains themselves. The grain boundary region is an area of crystallographic mismatch between the orderly structures within the adjacent grains. Due to this, it is slightly chemically more active than the grain area. Under certain conditions, the grain boundaries remain very reactive and under corrosive conditions, the attack along the grain boundaries results in intergranular corrosion. The grain boundary material, which is a limited area, acts as an anode, and the larger area of grains acts as cathodes. This results rapid and accelerated attack penetrating deeply into the metal. Example is depletion of chromium in the grain boundary regions results in intergranular corrosion of stainless steel.

1.5.1.6 Selective leaching

Selective leaching is the removal of one particular element from a solid alloy by corrosion processes. It is the preferential dissolution of one element from an alloy. The result of this corrosion is that of leaving a porous and usually brittle shadow of the original component. Two types of mechanism have been proposed, continuous selective removal of the more active metal of the alloy or general dissolution of the alloy followed by redeposition of the more noble constituents. The most common example of this phenomenon is dezincification of brass.

1.5.1.7 Erosion corrosion

Erosion-corrosion is the acceleration or increase in the rate of deterioration of a metal resulting from relative movement between the corrosive fluid and the metal

surface. Depending on the rate of this movement, abrasion takes place. Metal is removed from the surface as dissolved ions, or it forms solid corrosion products which are mechanically swept from the metal surface. It is characterized by the development of a surface profile of grooves, gullies, waves, rounded holes etc. Example: propellers, impellers exposed to moving fluids.

1.5.1.8 Stress corrosion cracking (SCC)

Stress corrosion cracking refers to failure under simultaneous presence of a corrosive medium and tensile stress. During stress corrosion, the metal or alloy is virtually unattacked over most of its surface, while fine cracks progress through it normal to the direction of tensile stress. Stress cracking of different alloys does occur depending on the type of corrosive environment. Stainless steels crack in chloride atmosphere. Major variables influencing SCC include solution composition, metal/alloy composition and structure, stress and temperature. Example: season cracking of brass in the presence of ammonia.

1.6 FACTORS INFLUENCING CORROSION RATE

There are various factors which influence the rate of corrosion of a metal or alloy under natural circumstances. For convenience these factors are categorized as nature of metal and nature of corrosive environment (Gadag and Shetty 2010).

1.6.1 Nature of the metal

The tendency of the metal to undergo corrosion is mainly dependent on the nature of the metal. In general the metals with lower electrode potential are more reactive and more susceptible for corrosion and metals with high electrode potential are less reactive and less susceptible for corrosion. For example the potential difference between iron and copper is 0.78 V which is more than that between iron and tin (0.3 V). Therefore, iron corrodes faster when in contact with copper than that with tin.

1.6.1.1 Purity of the metal

A very pure metal is more corrosion resistant than its commercial counterpart. But metal of highest purity is expensive and mechanically week, restricting their use. During commercial manufacture of metals certain undesirable factors get developed such as inclusion of impurities, precipitated phases, localized stress, and scratches, etc.

These factors contribute to increased susceptibility to corrosion. While impurities in a metal form a local galvanic cell (metal as anode and impurity as cathode) and result in the corrosion of metal. Rate of corrosion increases due to more exposure of impurities. For alloys the system is a homogeneous solid solution, hence no local action and no corrosion.

1.6.1.2 Electrode potential of metal

The standard electrode potential of metals is the benchmark to compare their tendency to undergo corrosion. The tendency of a metal to undergo corrosion decreases with increase in the standard electrode potential. Thus metals like magnesium and zinc with low electrode potential are more susceptible to corrosion than noble metals like platinum and gold with very high electrode potential. However an exception to this trend is seen with metals exhibiting passivity like aluminium due to surface passivation.

1.6.1.3 Hydrogen overvoltage on metal surface

The metal with lower hydrogen over voltage on its surface is more susceptible for corrosion, when cathodic reaction is hydrogen evolution type. Since lower hydrogen over voltage, liberation of hydrogen gas is easy. Therefore cathodic reaction is very fast, which in turn makes anodic reaction very fast. Thus increases the rate of corrosion. Higher the over voltage lesser is the corrosion.

1.6.1.4 Nature of corrosion product

The nature of corrosion product formed on surface largely decides the rate of further corrosion. The corrosion product formed like metal oxide may act as protective film. If the oxide layer, which forms on the surface, is stoichiometric, highly insoluble and non-porous in nature with low ionic and electronic conductivity then that type of products layer effectively prevents further corrosion, which acts as a protective film by acting as barrier between metal surface and corrosion medium. On the other hand if corrosion product is unstable, porous, and soluble, it further enhances corrosion.

1.6.1.5 Relative areas of anodic and cathodic region

The rate of the corrosion is greatly influenced by the relative sizes of cathodic and anodic areas. If the metal has smaller anodic area and larger the cathodic area exposed to corrosive atmosphere, more intense and faster is the corrosion occurring at the anodic

area. When anode is smaller and cathode region is larger all the liberated electrons at anode are rapidly consumed. This process makes the anodic reaction to takes place at its maximum rate, thus increasing the corrosion rate.

1.6.1.6 Physical state of the metal

Small granular metal will corrode faster than the larger one. Also the type of structure formed by a metal will have effect on the corrosion rate. A bent metal (stress) is rapidly corroded due to stress.

1.6.2 Environmental factors

Nature of corrosive medium has an equal influence on rate of metal corrosion as that of nature of metal. The corrosion behaviour depends on the surrounding environment. Some influential aspects of environment are given below.

1.6.2.1 Temperature

Corrosion rate increases with increase in temperature. This is due to the increase in conductance of the medium with increase in temperature and hence an increase in the diffusion rate. As a consequence, corrosion progresses faster at higher temperatures. In some cases, rise in temperature decreases passivity, which again leads to an increase in the corrosion rate.

1.6.2.2 pH of medium

The pH of solution is the factor that decides the type of cathodic reaction. In general rate of corrosion is higher in acidic pH than in neutral and alkaline pH. Exception exists with some metals like aluminum and zinc which show pronounced rate of corrosion in highly alkaline medium.

1.6.2.3 Humidity

In general it is observed that corrosion rate increases with increase in humidity of environment. The presence of moisture provides conducting medium for formation of galvanic cell, thus facilitating corrosion of metal.

1.6.2.4 Presence of impurities

Presence of some impurities in the atmosphere increases the rate of metal corrosion. For example, impurity like SO_2 combines with the moisture in the

environment forming sulphuric acid. Enhanced acidity often results in increased corrosion rate in most of the metals.

1.6.2.5 Electrical conductivity of the medium

Corrosion rate increases with the increase in conductivity of the medium. Higher the conductivity, faster will be migration of ions between the cathodic and anodic regions of corrosion cell, which enhances rate of corrosion. It is due to higher electrical conductivity that sea water is more corrosive than fresh water.

1.6.2.6 Presence of oxygen and oxidizers

The presence of oxidizing agents increases the corrosion rate of the metal. Even noble metals undergo corrosion in the presence oxidizing agents. Presence of oxygen or oxidizers provides more means of disposal of electrons arising from the anodic region, leading to increased rate of reduction, coupled with the increased rate of metal corrosion.

1.6.2.7 Velocity of medium

For corrosion processes that are controlled by activation polarization, agitation and velocity have no effect on the corrosion rate. If the corrosion process is under cathodic diffusion control, then agitation increases the corrosion rate. If the process is under diffusion control and the metal is readily passivated then corrosion rate increases. When passivated metals are exposed to extremely high corrosive velocity, mechanical damage or removal of these protective films occurs resulting in accelerated attack.

1.6.2.8 Concentration of medium

Increase in the concentration of medium will increase the amount of corrosive ions in the medium, which increases the corrosion rate to a greater extent. However exception is observed in acid medium where with the gradual increase in acid concentration corrosion rate reaches to a maximum and then decreases.

1.6.2.9 Polarization of anodic and cathodic regions

Polarization of cathode or anode decreases the rate of corrosion. If anodic polarization takes place, then the tendency of the metal to undergo oxidation decreases, hence the dissolution of metals as metal ions decreases. This is usually due to the increase in concentration of ions of the dissolved metals in the vicinity of electrode or

also due to the anodic passivity. Cathode polarization decreases the rate of the cathodic reaction hence hindering the combination of cathode reactant and electron. For the corrosion to continue both anodic and cathodic reaction should takes place simultaneously and if any one of the reactions is slower than the rate of corrosion is slower.

1.7 THERMODYNAMICS OF CORROSION

When corrosion is examined from the point of view of energetics, the study offers a great deal in understanding the overall process. Thermodynamics is the field that deals with energy and its change during chemical reactions. The principles of thermodynamics applicable to corrosion phenomena are described below (Schweitzer 2010).

1.7.1 Concept of free energy

In thermodynamic studies reactions are viewed in terms of changes in free energy. Corrosion reactions are spontaneous and are governed by the laws of thermodynamics. A process will be spontaneous only if there is a negative free energy change (ΔG). For electrochemical reactions, the free energy change is calculated from:

$$\Delta G = - nFE \qquad \qquad (1.8)$$

where, ΔG is the free energy change, n is the number of electrons involved in the reaction, F is the Faraday constant and E is the cell potential.

Therefore, for a given corrosion reaction to take place, the cell potential should be positive. Cell potential is taken as the difference between the potential of two half-cell reactions, the one at the cathode minus the one at the anode. Assuming hydrogen evolution as reaction at cathode, following relations are obtained.

$$E_{Cell} = E (H^+ / H_2) - E (M^{n+}/ M) \qquad \qquad (1.9)$$

It follows that metals with negative standard electrode potential, electrochemical cell potential will be positive and thus process of corrosion occurs (ΔG = -ve). Corrosion will not occur unless the reaction of metal oxidation (anodic metal dissolution) is spontaneous.

1.7.2 Application of thermodynamics to corrosion

The major application of thermodynamics to corrosion lies in the development of potential-pH plots or Pourbaix diagrams. Pourbaix diagrams are graphical

representations of the stability of a metal and its corrosion products as a function of the potential and pH of the aqueous solution. The potential is shown on the vertical axis and the pH on the horizontal axis. Such diagrams are constructed from calculations based on the Nernst equation and the solubility data for various metal compounds. In the diagram, the horizontal line represents pure electron transfer reaction equilibrium dependent solely on potential, but independent of pH. The vertical line represents equilibrium where there is no electron transfer involved and the reactions are solely dependent on pH. The sloping line represents equilibrium involving participation of electrons, H^+ and OH^- ions.

The Pourbaix diagram for pure magnesium-water system at 25 °C is shown in Fig. 1.2 (Pourbaix 1974). The diagram predicts that magnesium corrosion will occur spontaneously under positive potential conditions of -2.37 V ($E°$ of magnesium) and pH below 10.5. Magnesium remains insensitive to corrosion when its potential is maintained at more negative value than its E^0. The precipitation of magnesium hydroxide ($Mg(OH)_2$) from the corrosion product is favoured under highly alkaline conditions with pH above 10.5. $Mg(OH)_2$ is deposited to form a surface film that is expected to passivate the underlying metal.
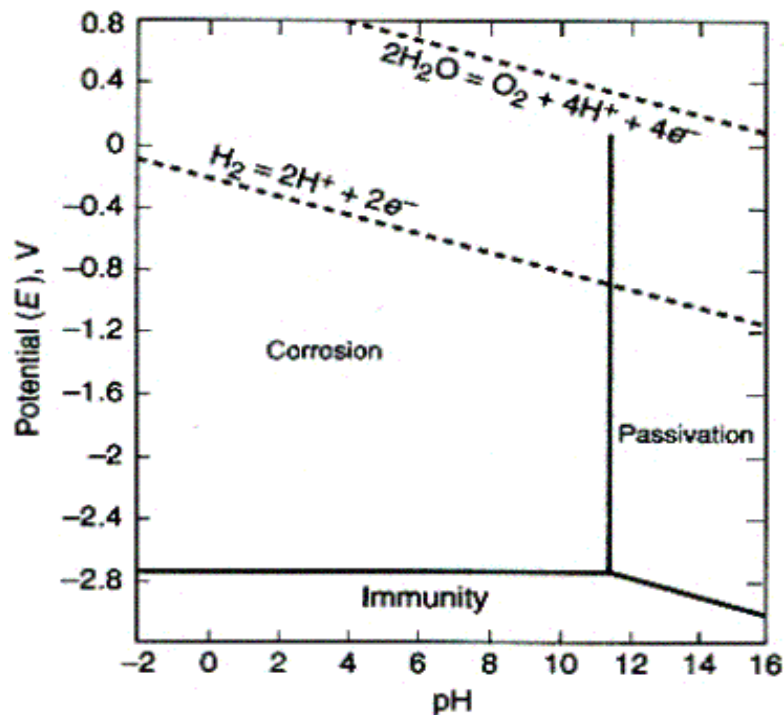
Fig. 1.2: Pourbaix diagram of magnesium and water system at 25 °C, showing the theoretical domains of corrosion, immunity and passivation (Pourbaix 1974).

The potential–pH diagram shows three clear-cut zones:

- **Immunity zone:** Under these conditions of potential and pH, metal remains in metallic form and corrosion are thermodynamically impossible.
- **Corrosion zone:** Under these conditions of potential and pH, metal corrodes spontaneously, forming various stable corrosion products.
- **Passive zone:** Under these conditions of potential and pH, protective passivating layer of corrosion product develops on surface of metal and retard further corrosion.

Pourbaix diagrams can be used for:

- Predicting the spontaneous direction of corrosion reactions.
- Estimating the stability and composition of corrosion products.
- Predicting environmental changes that will prevent or reduce corrosion.

Some limitations of Pourbaix diagrams are listed below.
- Data is purely thermodynamic and convey no information on rate of corrosion.
- Fails to predict the efficiency of passive film to protect the metal from corrosive attack.
- Most developed Pourbaix diagrams for corrosion behaviour of metals are in aqueous medium. However the medium under natural circumstances can be completely different.

1.8 CORROSION KINETICS

Naturally corroding systems never exist in a state of perfect equilibrium and therefore applicability of concepts of thermodynamics is limited. Moreover from an engineering standpoint, major interest lies in rate of corrosion. Hence concepts of electrode kinetics have great application in determining the rate of corrosion. Few such concepts are listed below.

1.8.1 Polarization

Electrode polarization can be defined as the extent of deviation of electrode potential from equilibrium value, resulting from a net current flowing from or to the electrode surface. Polarization is measured in volts. An electrochemical reaction is said to be polarized when the reaction is retarded by chemical, physical or environmental

factors. Hence polarization is also referred to as reaction inertia. Electrode polarization reduces the overall potential difference between two half cells, hence decreases the electrochemical corrosion. The degree of polarization is called as overvoltage or overpotential given by the following equation:

$$\text{Overvoltage} = E - E_0 \tag{1.10}$$

Where E is the electrode potential for some condition of current flow and E_0 is the electrode potential for zero current flow at equilibrium (also termed as the open circuit potential (OCP), corrosion potential, rest potential) (McCafferty 2010).

Depolarizers added to corrosion medium increase corrosion rate. Chelating ligands act as anodic depolarizers and oxidizers like ferric ions or O_2 act as cathodic depolarizers. (McCafferty 2010).

1.8.1.1 Activation polarization

Activation polarization usually is the controlling factor during corrosion in a media which contains a high concentration of active species (e.g. concentrated acids). Activation polarization refers to an electrochemical process that is controlled by the slowest step of reaction sequence taking place at the metal-electrolyte interface. In other words activation polarization is caused by a slow reaction of the electrode because the reaction at the electrode requires activation energy. Both anodic and cathodic reactions can be under activation polarization. A reaction for which an activation polarization predominates is referred as 'activation controlled'.

1.8.1.2 Concentration polarization

Concentration polarization refers to an electrochemical process controlled by the diffusion in the electrolyte bulk rather than at interface. Concentration polarization is predominant at cathode and negligible at anode, because supply of oxidizer at cathodic surface form electrolyte bulk is diffusion controlled but at anode there is unlimited supply of metal atoms for oxidation. Concentration polarization usually is the controlling factor during corrosion in a media which contains a scarce amount of reducible species or oxidizers (e.g. diluted acids and aerated salt solution). Any electrochemical process where agitation leads to increased rate of reaction is controlled by concentration polarization.

1.8.1.3 Ohmic polarization

Electrolyte solutions have a rather low conductivity compared to metals, especially in dilute solutions. In corrosion systems, if the metal surface is covered with paint or other insulating films or the electrolyte resistance surrounding the electrode has high resistance, a voltage drop over a portion of the electrolyte or the film covering the metal surface or both, which is known as resistance polarization. If resistance polarization dominates a reaction, it is referred as resistance or the ohmic drop controlled. This ohmic polarization is caused by the IR drops resulting from solution resistance, arising due to the inability to place reference electrode in contact with metal under investigation or due to the resistance across surface films, such as oxides.

1.8.2 Exchange current density

Exchange current density is the rate of exchange reactions or redox reactions expressed in terms of current density, for electrochemical equilibria involving participation of electrons. At equilibrium,

$$r_{\text{oxidation}} = r_{\text{reduction}} = i_o / nF \tag{1.11}$$

where 'r' is rate of reaction and i_o is exchange current density [A / cm^2] (Fontana 2005). Some factors influencing the exchange current density are mentioned below.

- Ratio of concentration of oxidized to reduced species at the electrodes.
- Temperature of medium. Higher the temperature higher will be i_o.
- Electrode surface roughness. Greater the roughness of the electrode surface, more will be the surface area, hence higher will be i_o. Example: platinized platinum has higher i_o for hydrogen evolution than bright platinum.

1.8.3 Mixed potential theory

Mixed potential theory was put forwarded by Wagner and Truad in 1938. This theory is based on two hypotheses.

- Any electrochemical reaction is divided into two or more partial oxidation and reduction reactions.
- There can be no net accumulation of electric charge during an electrochemical reaction.

The second hypothesis is merely restatement of the law of conservation of charge. That is a metal immersed in an electrolyte cannot spontaneously accumulate electric charge, as a result during corrosion, rate of oxidation must be equal to rate of reduction.

Mixed electrodes, according to above theory, refer to electrode or metal sample in contact with two or more oxidation- reduction systems. According to mixed potential theory a corroding system is viewed as combination of non-corroding metal in a reversible equilibrium with solution of its ions of unit activity and hydrogen electrode (as if non-corroding metal was saturated with H_2 gas at unit activity at unit pressure). Mixed potential theory in combination with concepts of exchange current density forms the basis for modern electrode-kinetic theory (Fontana 2005).

1.9 ELECTROCHEMICAL CORROSION TESTING

During corrosion, at least two electrochemical reactions, an oxidation and a reduction reaction, occur at a metal-electrolyte interface. Because corrosion is due to an electrochemical mechanism, it is clear that electrochemical techniques can be used to study corrosion reactions and mechanisms. Unlike weight loss or gravimetric methods, electrochemical methods are fast in determining and analyzing the electrochemical properties. Electrochemical corrosion testing is a simple and fast way to determine the corrosion resistance of an alloy in a particular environment. Mixed potential theory forms the basis for two electrochemical methods used to determine corrosion rate. These are tafel extrapolation and linear polarization techniques. According to mixed potential theory any electrochemical reactions can be divided into two or more partial oxidation and reduction reactions. Electrochemical techniques can be used to measure the kinetics of electrochemical process, in specific environment and also to measure the oxidizing power of the environment.

Thus corrosion rate can electrochemically be determined by a number of methods that result in a corrosion current density which is converted to corrosion rate using Faraday's laws,

$$\text{Corrosion rate (mm y}^{-1}) = \frac{0.00327 \, (E.W) \, i_{corr}}{D} \quad (1.12)$$

where i_{corr} = corrosion current density $\mu A/cm^2$

$E. W$ = equivalent weight of the corroding species (atomic wt. / oxidation number)

D = density of the corroding species, g/cm^3

The corrosion measurement techniques are classified in to two types.

    a)   DC Electrochemical monitoring techniques

    b)   AC Electrochemical monitoring techniques.

1.9.1 DC Electrochemical monitoring techniques

      Electrochemical technique has been used to study both speed data development and to better understand the corrosion mechanisms. DC polarization test is a potentiodynamic corrosion testing technique. This method involves changing potential of the working electrode and measuring the current produced as a function of time or potential. When an electrode is polarized, it can cause current to flow through electrochemical reactions that occur at the electrode surface. The amount of current produced is controlled by the kinetics of the reactions and the diffusion of reactants both towards and away from the electrode. DC polarization technique utilizes a typical three electrode system. The metal sample is turned as the working electrode. Inert metal like platinum constitutes the auxiliary electrode. The potential of working electrode is measured with respect to the reference electrode (Thompson and Payer 1998).

1.9.1.1 Tafel extrapolation method

      The Tafel extrapolation method can be used to determine the corrosion rate of a metal when metallic dissolution is under activation control. This technique uses data obtained from cathodic and anodic polarization measurements. The metal sample is termed the working electrode, and the cathodic current is supplied to it by means of an auxillary electrode as platinum. Cathodic data are preferred, since these are easier to measure experimentally. The Tafel plots are generated by applying a potential of 250 mV in both the positive and negative directions from the potential of the open circuit against the reference electrode. The current density is measured and usually plotted on a logarithmic scale. As shown in Fig. 1.3 a typical Tafel plot consists of an anodic and a cathodic branch, the corrosion potential (E_{corr}) and the corrosion current density (i_{corr}) are obtained from the Tafel plots. The corrosion potential (E_{corr}) or the open-circuit potential is the potential a metal will assume when placed in contact with a conductive medium. The value of the corrosion potential is determined by the half-reactions of the

corrosion process. E_{corr} is a characteristic of the corroding system. The Tafel plot provides a direct measure of corrosion current, which can be used to calculate the corrosion rate. The corrosion plot consists of an anodic and a cathodic branch, the intersection of these branches can be projected on the X and Y axes to give us the i_{corr} and the E_{corr} values. Tangents are drawn to the anodic and cathodic regions of the Tafel curve, the intersection of these provide the values of E_{corr} and i_{corr} when projected on the corresponding axes.

An electrochemical reaction under kinetic control [controlled by the kinetics of the electron transfer reaction at the metal surface] obeys the following Tafel equation,

$$i = i_0 \, e^{(2.3(E-E_0)/b)}$$

(1.13)

where, i is the current resulting from the reaction, i_0 is exchange current density, E is the electrode potential, E_o is the equilibrium potential, b is the Tafel slope (constant for a given reaction expressed in units of volts/decade).

The Tafel equation describes the behaviour of one isolated reaction. In a corrosion system, there exists two opposing reactions – anodic and cathodic. The Tafel equations for both the anodic and cathodic reactions in a corrosion system can be combined to generate the Butler-Volmer Equation, as represented below.

$$i = i_a + i_c = i_{corr} \, [e^{(2.3(E-Eo)/b_a)} - e^{(-2.3(E-Eoc)/b_c)}]$$

(1.14)

where, i is the measured cell current in amps, i_{corr} is the corrosion current in amps, E is the cell potential, E_o is the corrosion potential in volts, b_a is the anodic Tafel Constant in volts/decade, b_c is the cathodic Tafel Constant in volts/decade.

The slopes of the linear portions of these plots are called the Tafel constants, which are used to calculate the polarization resistance using the Stern-Geary equation (EI- Sayed, 1997).

$$R_p = \frac{B}{i_{corr}}$$

(1.15)

$$B = \frac{b_a b_c}{2.303(b_a + b_c)}$$

(1.16)
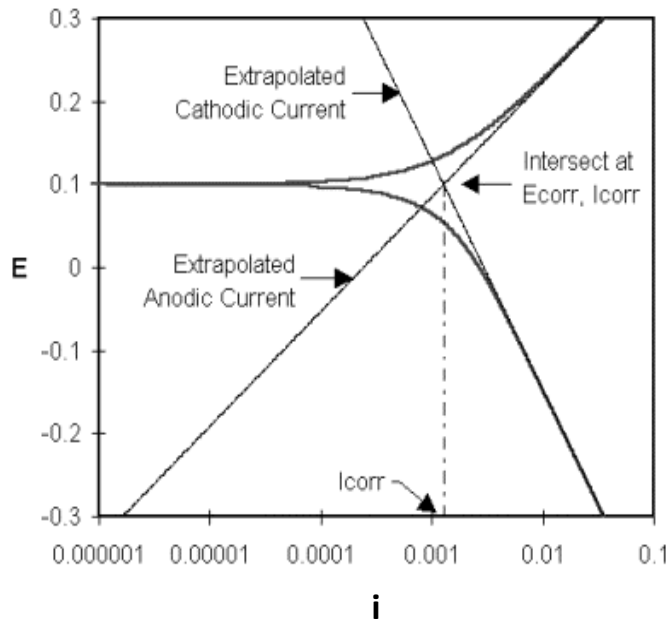
Fig. 1.3: A representative Tafel flot showing extrapolation.

Advantages of Tafel plots

- It is possible to continuously measure very low corrosion rates.
- It can be used for continuous monitoring of corrosion rate of a system.
- This technique is more rapid than the conventional weight loss methods.
- The Tafel constants b_a and b_c can be used with linear polarization data.

Disadvantages of Tafel plots

- The test electrode can be polarized only a limited number of times because some degree of electrode surface roughening occurs with each polarization.
- The method can be applied only to systems containing one reduction process since Tafel region is distorted if more than one reduction process occurs.
- The system gets disturbed due to polarization of material under test by several hundred mV from corrosion potential.

1.9.1.2 Linear polarization method

Linear polarization technique is another method that uses polarization behaviour to determine the corrosion rate of metals. The disadvantages of the Tafel extrapolation can be overcome to a large extent using linear polarization analysis. It is observed that within ± 10 mV nobler or more active than the corrosion potential, the applied current

20

density is linear function of the electrode potential. In this method the metal is polarized within ± 20 mV from the rest potential and the polarization plot is obtained by plotting overvoltage versus applied anodic and cathodic current densities on a linear scale. The usefulness of this measurement is that the slope of potential versus current plot, i.e., $\Delta E/\Delta i_{app}$ as shown in the fig. 1.4. The relationship of the slope of the linear polarization curve to the corrosion current, the anodic and the cathodic Tafel slopes are

$$\frac{\Delta E}{\Delta i_{app}} = \frac{b_a b_c}{2.303(b_a + b_c)i_{corr}} \tag{1.17}$$

where, $\Delta E/\Delta i_{app}$ is the slope of the linear portion of the curve, b_a and b_c are the anodic and cathodic Tafel slopes respectively, i_{corr} is the corrosion current density.
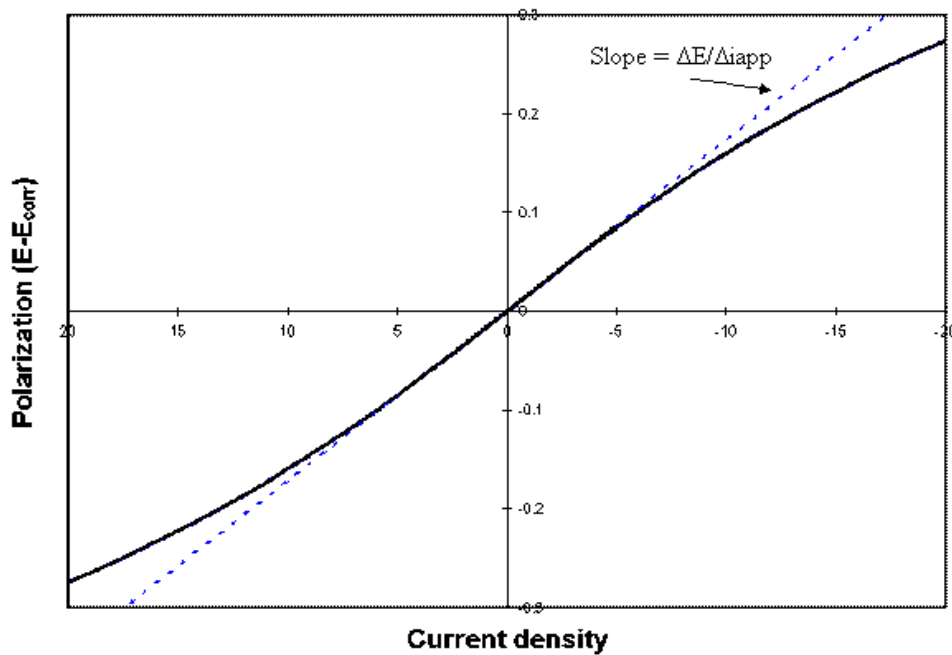
Fig. 1.4: Linear Polarization Curve.

The slope of the linear polarization curves is determined experimentally, and the values of the anodic and cathodic slopes are determined either experimentally or estimated. After these values are obtained, the corrosion rate can be calculated from the calculated value of the corrosion current density i_{corr}. For example for a system where anodic and cathodic slopes are equal to 0.12V per decade, the relationship between the slope of linear polarization curve and corrosion current is

$$\frac{\Delta E}{\Delta i_{app}} = \frac{0.026}{i_{corr}} \tag{1.18}$$

Test results obtained from linear polarization method should always be compared with weight-loss or other corrosion rate measurements to ensure the accuracy of the technique and its suitability to particular medium.

Advantages of linear polarization method
- It can be used for measuring very low corrosion rates in nuclear, pharmaceutical and food   processing industries.
- They permit rapid corrosion rate measurement and can be used to monitor corrosion rate in various process streams.
- It can be used to measure the corrosion rate of structures that cannot be visually inspected or subjected to weight loss tests, like underground pipes tanks and large chemical plant components.

Disadvantages of linear polarization method
- It is impossible to measure localized corrosion.
- Oxide formation, which may or may not lead to passivation, can alter the surface of the sample being tested. The original surface and the altered surface may have different values for the slopes of linear polarization curves.

1.9.2 Electrochemical impedance spectroscopy (EIS)

EIS method has been applied to corroding systems for characterization and analysis of complex interfaces. Electrical resistance is the ability of a circuit element to resist the flow of electrical current. Ohm's law defines resistance in terms of the ratio between voltage, E, and current, I.

$$R = E / I \tag{1.19}$$

While this is a well-known relationship, its use is limited to only one circuit element, the ideal resistor. An ideal resistor has several simplifying properties:
- It follows Ohm's law at all current and voltage levels.
- The value of its resistance is independent of frequency.
- AC current and voltage signals through a resistor are in phase with each other.

However, the real world contains circuit elements that exhibit much more complex behaviour. Like resistance, impedance is a measure of the ability of a circuit to resist the flow of electrical current, but unlike resistance, it is not limited by the simplified properties listed above. In electrochemical impedance measurements, a sinusoidal perturbation is imposed on the system centered on a DC condition of interest. In practice a small amplitude AC voltage perturbation about the corrosion potential is applied to electrode-electrolyte interface. The response of the system to such voltage perturbation is AC current signal which is further analyzed. Electrochemical impedance is normally measured using a small excitation signal. This is done so that the cell's response (output) is pseudo-linear. In a linear (or pseudo-linear) system, the current response to a sinusoidal potential will be a sinusoid at the same frequency but shifted in phase.
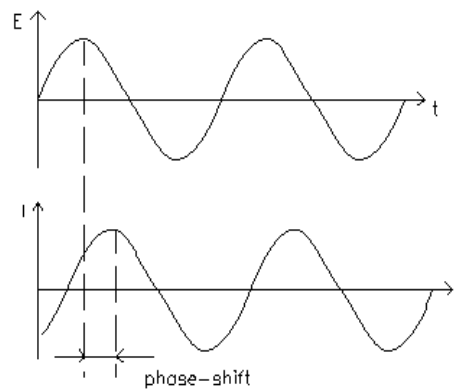
Fig. 1.5: Sinusoidal current response in a linear system.

The excitation signal, expressed as a function of time, has the form

$$E_t = E_0 \sin(\omega t)$$

(1.20)

where, E_t is the potential at time t, E_0 is the amplitude of the signal, ω is the radial frequency.

The relationship between radial frequency ω (expressed in radians/second) and frequency f (expressed in hertz) is:

$$\omega = 2\pi f$$

(1.21)

In a linear system, the response signal, I_t, is shifted in phase (φ) and has a different amplitude,

$$I_t = I_0 \sin(\omega t + \varphi)$$

<div align="right">(1.22)</div>

An expression analogous to Ohm's Law provides expression for the impedance of the system as:

$$Z = \frac{E_t}{I_t} = \frac{E_0 \sin(\omega t)}{I_0 \sin(\omega t + \phi)} = Z_0 \frac{\sin(\omega t)}{\sin(\omega t + \phi)}$$

<div align="right">(1.23)</div>

The impedance is therefore expressed in terms of a magnitude, Z_0 and a phase shift, φ. The impedance, $Z(\omega)$ may also be expressed in terms of real $Z^l(\omega)$ and imaginary $Z^{ll}(\omega)$ components in Cartesian coordinates.

$$Z(\omega) = Z^l(\omega) + Z^{ll}(\omega)$$

<div align="right">(1.24)</div>

For simplified Randles circuit the plot of Z^1 versus Z^{11} at various frequencies gives a semicircle which cuts the real axis at higher and lower frequencies [lower frequency data appear on right side of plot and higher frequency data on the left side] which is shown in the Nyquist plot (Fig.1.6). On the Nyquist Plot the impedance can be represented as a vector (arrow) of length |Z|. The angle between this vector and the X-axis, commonly called the "phase angle", φ. At very high frequency, the imaginary component Z^{11} disappears, leaving only the solution resistance, R_s. At very low frequency, Z^{11} again disappears, leaving a sum of R_s and the Faradaic reaction resistance or polarization resistance R_p, thus diameter of semicircle corresponds to R_p. The Faradaic reaction resistance or polarization resistance R_p is inversely proportional to the corrosion rate. Rs measured at high frequency can be subtracted from the sum of $R_p + R_s$ at low frequency to give a compensated value of R_p.

Nyquist plots have one major short coming. That is the plot provides no information about the exact frequency at which any data point is recorded. To overcome this limitation another popular presentation of Bode plot has been developed. In Bode magnitude plot, log|Z| along y-axis is plotted against log f along x-axis [frequency in hertz]. In Bode phase angle plot, φ [phase angle] along y-axis is plotted against log f along x-axis.
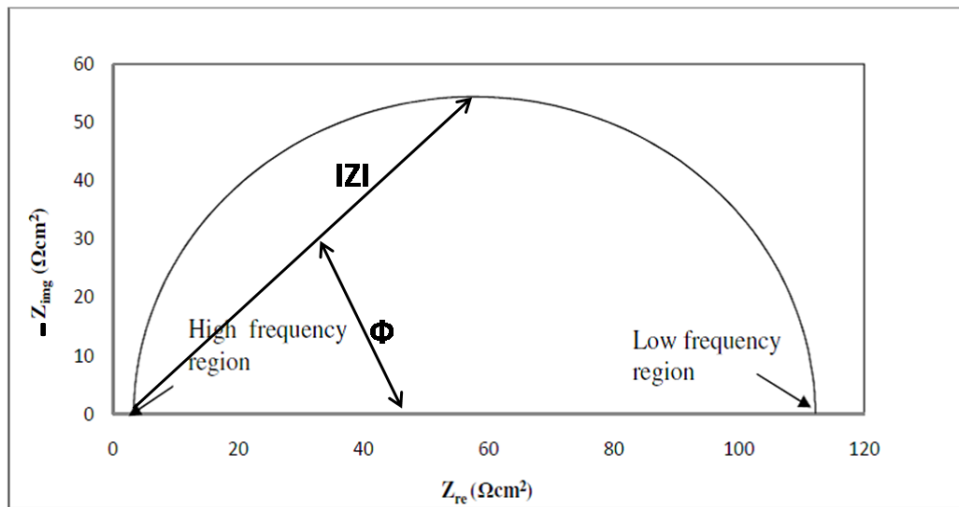
Fig. 1.6: Nyquist plot.
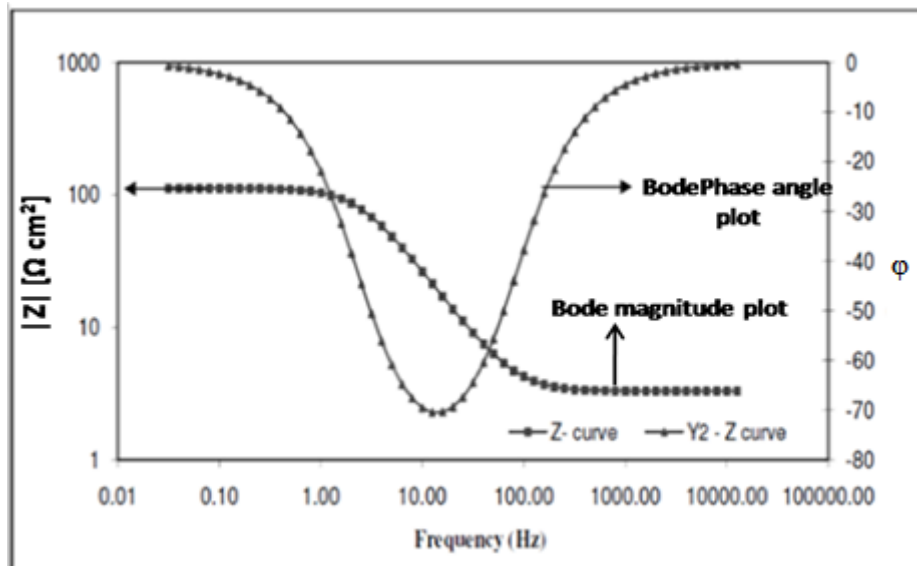
Fig.1.7: Bode plot.

EIS data is commonly analyzed by fitting it to an equivalent electrical circuit model. Most of the circuit elements in the model are common electrical elements such as resistors, capacitors, and inductors. EIS models usually consist of a number of these elements in network. To be useful, the elements in the model should have a basis in the physical electrochemistry of the system. As an example, most models contain a resistor that models the cell's solution resistance. The physical behaviour of the corrosion system can be simulated and quantified with equivalent circuit to gain insight into the important processes in the corrosion system. It is worthy to note that EIS cannot give

all the answers. It is a complementary technique and other methods must also be used to elucidate the interfacial processes (Lasia 1999).

Some benefits of EIS method include,

- Estimation of corrosion rates in slowly changing systems.
- Estimation of corrosion rate in low conductive medium [organic liquids, soil and concrete].
- Prediction of quality of coatings on metal surface. [Excellent coating, failed coating, etc].

Limitations of EIS method are listed below.

- Interpretation of results is relatively complex compared other methods.
- It is a complementary technique and requires benchmarking with other corrosion monitoring techniques.

1.10 CORROSION CONTROL

The corrosion types are so numerous, the mechanisms of corrosion are so different and conditions under which corrosion takes place are so varied that no single method can be used to control all possible corrosion cases. The choice of a control method depends on factors such as the type of metallic structure, the application for which it is designed, form of corrosion, residual stress in the fabricated articles and the nature of the prevailing environment. Some of the important methods are given below (Davis 2000).

- **Material selection:** The selected material should be such that it should be the most economic material exhibiting best corrosion resistance against given environment of exposure. Pure metal or nonmetallics should be used whenever possible without compromising the desired output.

- **Alteration of the environment:** Altering the environment provides versatile means for reducing the corrosion rate. Typical changes in the medium that are often employed include, lowering temperature, decreasing velocity, removing oxygen, oxidizers and changing the concentration of corrosive. Addition of corrosion inhibitors is also grouped under this category.

- **Mechanical design:** Metallic structures should be designed such that there is a minimum scope for any form of corrosion to occur, at the same time without

compromising any mechanical output requirements. There are many design rules, avoiding heterogeneity and excess mechanical stress are among the prominent ones.

- **Cathodic protection:** Cathodic protection is achieved by supplying electrons to the metal surface, making it cathodic to surrounding. Some measures include galvanic coupling with a sacrificial anode and impressed current method using external power supply with an inert anode. The greatest advantage of cathodic protection is that corrosion rate of cathodically protected structure is not just minimized but reduced to zero.

- **Anodic protection:** This method is applicable only for metals exhibiting active-passive transition. The metallic structure is protected as an anode using a potentiostat, by maintaining the potential of the metal well within the range where it exhibit passivity.

- **Surface coatings:** Any coating on the surface of the metal, capable of acting as a physical barrier between the metal and the corrosive is helpful in metal protection. Metallic, inorganic and organic coatings have been employed for several metals. To be effective as a physical barrier, a surface coating should be continuous, uniform, impervious and chemically inert to corrosive and should have reasonably long life.

1.11 CORROSION INHIBITORS

A corrosion inhibitor is defined as a chemical substance which, when added in small concentrations to an environment, decreases the corrosion rate. A good inhibitor must fulfill the following requirements.

- It should be chemically inert and thermally stable.

- It should be effective even when added in minute concentrations.

- It should be cost effective and ecofriendly.

- It should also inhibit the diffusion of hydrogen into metal.

The most common and widely known use of inhibitors is their application in automobile cooling systems and boiler feed waters (Schweitzer 2010).

1.11.1 Evaluation of corrosion inhibition efficiency

Because there may be more than one inhibitor suitable for a specific application, it is necessary to have a means of comparing the performance of each. This can be done by determining the inhibitor efficiency according to the following correlation:

$$\eta(\%) = \left[\frac{\upsilon_{corr_{(uninh)}} - \upsilon_{corr_{(inh)}}}{\upsilon_{corr_{(uninh)}}} \right] \times 100$$

(1.25)

where, $\upsilon_{corr(uninh)}$ and $\upsilon_{corr(inh)}$ are corrosion rates in uninhibited and inhibited conditions respectively. The corrosion rates $\upsilon_{corr(uninh)}$ and $\upsilon_{corr(inh)}$ can be determined by any of the standard corrosion testing techniques. The corrosion rate can be measured in any unit, such as weight loss (mpy), as long as the units are consistent across both tests. (Sastri. et al.2007).

1.11.2 Classification of corrosion inhibitors

A corrosion inhibitor can function in two ways. In some situations the added inhibitors can alter the corrosive environment into a noncorrosive or less corrosive environment through its interaction with the corrosive species. In other cases the corrosion inhibitor interacts with the metal surface and as a consequence inhibits the corrosion of the metal. Thus, based on the mode of interaction, there are two broad classes of inhibitors (Papavinasam 2011).

- **Environment modifiers:** In the case of environment modifiers, the action and mechanism of inhibition is a simple interaction with the aggressive species in the environment, and thus reduce the attack of the metal by the aggressive species. This is exemplified by oxygen scavengers such as hydrazine or sodium sulfite along with cobaltous nitrate and biocides used in inhibiting microbiological corrosion. In the case of corrosion in neutral and alkaline solutions, oxygen reduction is the cathodic reaction which can be countered by the oxygen scavengers and thus inhibit the corrosion.

- **Adsorption inhibitors:** Adsorption inhibitors reduce the corrosion rate due to polarization of the metal by extremely thin layer of their molecules adsorbed on the surface and inhibit the corrosion. There are two steps involved in the process:
  - Transport of inhibitor to the metal surface
  - Metal–inhibitor interactions

1.12 TYPES OF INHIBITORS

The mechanism of inhibition is the important criterion in classification of corrosion inhibitors and according to this criterion; inhibitors are classified into following categories.

- Anodic

- Cathodic
- Mixed
- Precipitation
- Vapour phase

1.12.1 Anodic (passivating) inhibitors

Oxidation of metal is the reaction that occurs at the anodic sites during corrosion. Anodic inhibitors are the substances which inhibit the anodic reactions and thereby reduce the corrosion rate. These inhibitors combine with metal ions formed at the anodic region, forming the sparingly soluble metal salts. These compounds formed are deposited on the anodic sites forming the protective films, which act as barriers between the fresh metal surface and the corrosive medium, thereby preventing further anodic reaction. Protection is rendered only when sufficient amount of inhibitor is added and conversely corrosion will be accelerated when inhibitor amount added is insufficient. Oxyanions such as chromates, molybdates, tungstates and also sodium nitrite are very effective anodic inhibitors. The effect of anodic inhibitor on polarization curves is represented in Fig.1.8 (a).

1.12.2 Cathodic inhibitors

Cathodic inhibitors are the substances which inhibit the cathodic reactions and thereby reduce the corrosion rate of the metal. The two important types of cathodic reactions are liberation of hydrogen and oxygen adsorption. Therefore there are two distinct approaches in achieving inhibition of cathodic reactions.

Inhibition of hydrogen liberation: This can be achieved by either retarding the diffusion of H^+ ions to cathode or by increasing the hydrogen overvoltage on the metal surface.

- Film impervious to H^+ ions: Some organic compounds acting as cathodic inhibitors like urea, thiourea, mercaptants get adsorbed to cathodic sites forming a protective film impervious to H^+ ions, thus prevent H^+ ions from coming in contact with the cathodic surface.

- Hydrogen evolution poisons: The cathodic inhibitors like oxides of arsenic, antimony, salts like sodium metarsenite, when added to system, deposit over cathode as adherent metallic film and retard the hydrogen evolution as hydrogen overvoltage on these metals is very high.

29

Inhibition of oxygen adsorption: These include inhibitors like zinc sulphate, magnesium sulphate etc. These salts when added to the system, cations of the salts migrate towards cathode surface and react with cathodically formed alkali to form metal hydroxides, which deposit over cathodic sites as films impervious to oxygen. (Gadag and Shetty 2010).

The effect of cathodic inhibitors on polarization curves is shown in Fig.1.8 (b).

1.12.3 Mixed type inhibitors

These are substances which affect both the cathodic and anodic reactions. They are typically film forming compounds that cause the formation of precipitates on the surface blocking both anodic and cathodic sites indirectly. Majority of organic inhibitors that cannot be designated specifically as anodic or cathodic inhibitors and are known as mixed inhibitors, which are adsorbed on the electrode surface and suppress the metal dissolution at the anode and reduction reactions at the cathode. The effect of mixed type inhibitor on polarization curves is shown in Fig.1.8 (c).

Mixed inhibitors protect the metal in three possible ways:
  a) Physical adsorption
  b) Chemisorption
  c) Film formation
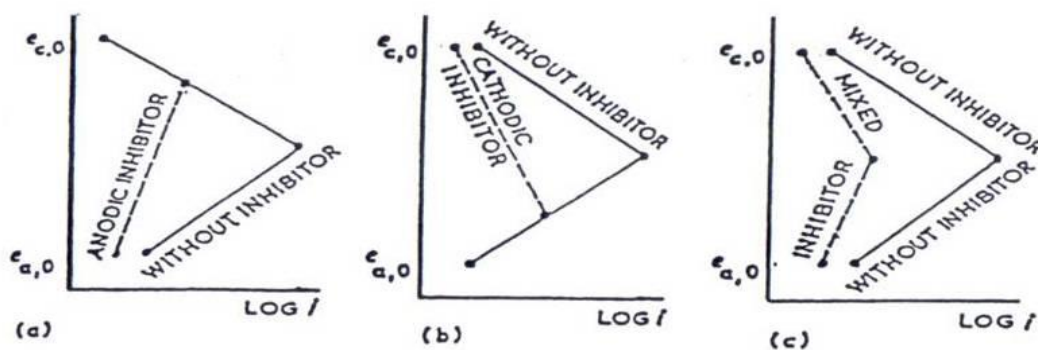
Fig. 1.8: Evans diagrams showing the effect of addition of a) anodic inhibitor b) cathodic inhibitor c) mixed inhibitor.

1.12.3.1 Physical adsorption

Physical adsorption is the result of the electrostatic attractive forces between organic ions or inhibitory dipoles and electrically charged surface of the metal.

30

Inhibitory species that undergo physical adsorption interact rapidly with the surface; however they can also be removed easily from the surface. The inhibition efficiency during physical adsorption depends on following factors.

- Structural parameters, such as hydrocarbon chain length and the nature and position of substituent in the aromatic ring.
- Electrical characteristics of inhibitors i.e. charge of the hydrophilic group.
- Type of ions present in the solution.
- Potential of the metal.

1.12.3.2 Chemical adsorption

This process involves charge sharing or charge transfer from the inhibitor molecules to the metal surface in order to form a coordinate type of bond. The chemisorption process takes place more slowly than electrostatic adsorption and with higher activation energy. It depends on the temperature, and higher degrees of inhibition should be expected at higher temperatures. Chemisorption is specific for certain metals and is not completely reversible. The bonding occurring with electron transfer clearly depends on the nature of the metal and the nature of the organic inhibitor. In fact, electron transfer is typical for metals having vacant, low-energy electron orbitals. Concerning inhibitors, the electron transfer can be expected with compounds having relatively loosely bound electrons.

1.12.3.3 Film formation

During the chemical adsorption, adsorbed inhibitor molecules can undergo surface reactions producing films. The properties of films are dependent upon its thickness, composition, solubility, temperature and other physical forces. Corrosion protection increases markedly as the films grow from nearly two-dimensional adsorbed layers to three-dimension films up to several hundred angstroms thick. Inhibition is effective only when the films are adherent, insoluble and impervious to corrosive.

1.12.4 Precipitation inhibitors

Precipitation inhibitors are film forming compounds that have a general action on the metal surface, blocking both anodic and cathodic sites indirectly. Precipitation

inhibitors are compounds that cause the formation of precipitates on the surface of the metal, thus providing a protective film. Example: silicates, phosphates etc.

1.12.5 Vapour-phase inhibitors

Vapor phase inhibitors (VPI) are also called volatile corrosion inhibitors (VCI) and are compounds transported in a closed environment to the site of corrosion by volatilization from a source. When these inhibitors come in contact with the metal surface, the vapours of these salts condense and are hydrolyzed by any moisture to liberate the protective ions. It is desirable, for an efficient VCI, to provide inhibition rapidly while lasting for long periods. Both qualities depend on the volatility of these compounds; fast action wanting high volatility while enduring protection requires low volatility. Vapour-phase inhibitors are used to protect metal surfaces in storage or transport, as well as to protect electronic materials, such as circuit boards.

1.12.6 Some examples of corrosion inhibitors

Organic substances have been used extensively as corrosion inhibitors and usually designated as 'film-forming', protect the metal by forming a hydrophobic film on the metal surface. The effectiveness of these inhibitors depends on the chemical composition, their molecular structure, and their affinities for the metal surface. Commercial inhibitor packages contain, in addition to active inhibitor other chemicals like surfactants, deemulsifiers, carriers (e. g. solvents) and biocides. The active ingredient of organic inhibitors invariably contain one or more functional groups containing one or more heteroatoms, N, O, S, P or Se, through which the inhibitors anchor to the metal surface. Some common anchoring groups are given in the Table 1.1 (Papavinasam 2011).

These groups are attached to a parent chain (backbone), which increases the ability of the inhibitor molecule to cover a large surface area. Common repeating units of the parent chain are methyl and phenyl groups. The backbone may contain additional molecules, or substituent groups, to enhance the electronic bonding strength of the anchoring group on the metal and/or to enhance the surface coverage. The outline of the constitution of an organic inhibitor is presented in Table 1.2.

Table 1.1: Common anchoring (functional) groups in organic inhibitors.

Structure	Name	Structure	Name
-OH	Hydroxyl	-SH	Thiol
$-C\equiv C-$	-yne	-S-	Sulfide
-C-O-C-	Epoxy	$-S=O$	Sulfoxide
-COOH	Carboxy	$-C=S-$	Thio
$-CONH_2$	Amide	$-P=O$	Phosphonium
$-NH_2$	Amino	-P-	Phosphor
-NH	Imino	-As-	Arsano
$-NO_2$	Nitro	-Se-	Seleno

Table 1.2: Constitution of an organic corrosion inhibitor.

Anchoring group	Backbone	Substituent groups
Binds onto the metal surface	Bear anchoring and substituent groups. Provides surface coverage	Supplements electronic strength and surface coverage

1.13 MECHANISM OF CORROSION INHIBITION

Corrosion inhibitors function by interfering with either the anodic or cathodic reactions or both. The mechanism of inhibition of different inhibitors varies and can be grouped into following general categories (Papavinasam 2011).

1.13.1 Adsorption mechanism

According to well accepted model, the adsorption of organic inhibitor molecules on the metal surface is a displacement process where, adsorbed water molecules on the metal surface are replaced by organic molecules in the solution.

$$Org_{(sol)} + xH_2O_{(ads)} \rightarrow Org_{(ads)} + xH_2O_{(sol)} \qquad (1.26)$$
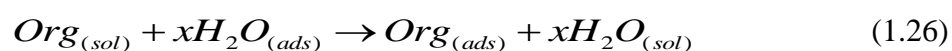
where, Org $_{(sol)}$ and Org $_{(ads)}$ are the organic molecules in the aqueous solution and adsorbed on the metal surface, respectively, $H_2O_{(ads)}$ is the water molecules adsorbed

on the metal surface and x is the size ratio representing the number of water molecules displaced by one molecule of organic inhibitor. The adsorbed inhibitor molecules may retard either anodic or cathodic or both reaction(s) depending upon the electrode on which they are adsorbed.

1.13.2 Physical barrier film

Inhibitors are able to form a multimolecular layer on the metal surface. The resulting barrier action is independent of the nature of the adsorption forces between inhibitor molecules and the metal surface. The formed layer prevents interaction of the corrosive species with the metal surface. The hindering of the mass transport causes inhibition of the corrosion reaction.

1.13.3 Blocking of active reaction sites

The adsorbed inhibitors can also inhibit the corrosion by blocking the active sites of the metals. The blockage of active sites at anode or cathode or both electrode surfaces results in reduced ratee of respective electrode reactions.

1.13.4 Participation in electrode reactions

The nature of the inhibitor initially present in the electrolyte may change with time as a consequence of electrochemical reactions at the electrodes. The inhibition due to the reaction products is called the secondary inhibition. Depending on the effectiveness of the reaction products, secondary inhibition may be higher or lower than primary inhibition. For example, diphenyl sulfoxide undergoes electrochemical reaction at the metal surface to produce diphenyl sulfide, which is more effective than the primary compound. On the contrary, the reduction of thiourea and its alkyl derivatives gives rise to HS^-, which accelerates corrosion.

1.14 MAGNESIUM AND ITS ALLOYS

Magnesium is an alkaline earth metal and eighth most abundant element in the earth's crust and ninth in the known universe as a whole. Magnesium in its elemental form has a very high chemical reactivity and hence exists in its ores as magnesium compounds. Although magnesium is present in more than sixty minerals, the most common and commercially viable are magnesite ($MgCO_3$), dolomite ($MgCO_3.CaCO_3$), carnallite ($KCl.MgCl_2.6H_2O$), brucite ($Mg(OH)_2$), etc. Due to magnesium ion's high

solubility in water, it is the second most abundant element dissolved in seawater. Magnesium is the lightest of all the engineering metals, having a density of 1.7 g/cm^3. It is 35% lighter than aluminum (2.7 g/cm^3) and over four times lighter than steel (7.86 g/cm^3). Magnesium in its metallic form is obtained by metallurgical extraction of its ores and by the electrolysis of molten magnesium chloride derived from seawater (Gupta and Sharon 2011).

Magnesium and its alloys are nonferrous metals with low density, good ductility, moderate strength and good corrosion resistance. Magnesium alloys with other metals, often aluminum, zinc, manganese, silicon, copper, rare earths and zirconium. Magnesium is the lightest structural metal. Magnesium alloys have hexagonal lattice structure, which affects the fundamental properties of these alloys. Plastic deformation of the hexagonal lattice is more complicated than in cubic latticed metals like aluminum, copper and steel. Therefore magnesium alloys are typically used as cast alloys, but research of wrought alloys has been more extensive since 2003. Cast magnesium alloys are used for many components of modern cars, and magnesium block engines have been used in some high-performance vehicles; die-cast magnesium is also used for camera bodies and components in lenses.

Magnesium alloys provide advantages when used as structural materials, because of their high strength-to-weight ratio, specific rigidity, good damping characteristics, and castability, which makes them applicable in various fields of modern engineering. Magnesium and its alloys are non-magnetic, have relatively high thermal and electrical conductivity, and good vibration and shock adsorption ability. Because of their low density and good mechanical properties, magnesium alloys are of particular interest to the aerospace and transport industry; for example, thorium-containing alloys have found applications in missiles and spacecrafts.

1.14.1 Applications of magnesium alloys

Magnesium alloys are in great demand as structural materials, especially in weight-critical applications. Some of the remarkable applications are summarized below.

1.14.1.1 Applications in transport industry

Many automobile parts are made of magnesium alloy, such as gearbox housing,

steering wheels, fuel tank cover and even in interior parts such as seat frame, driver's air bag housing. Although these were first experimented in race cars, magnesium alloy parts have also been introduced in domestic automobiles. As of today almost all clite automobile manufacturers such as Audi, Volkswagen, Mercedes-Benz, Toyota, Ford, BMW, Jagur, Fiat, Hyundai, etc, employ magnesium alloy parts in their products (Luo 2002, Balwert et al. 2004, Rosen et al.2005, Logan 2007).

1.14.1.2 Millitary applications

The technology used in armed forces is not too late to exploit the benefits of the light-weight nature of magnesium alloys. The aircrafts fitted with magnesium alloy parts were used during World War II. The H-19 Chickasaw helicopter, a US Army helicopter built in 1951, contains 17% (by weight) of magnesium, a record level during its time. Falcon GAR-1 a first air-to-air missile launched in 1956, contains 90% of magnesium in its structure. Some other historically prominent examples of 'military magnesium' include M-274 light cargo-personnel and weapon carrier, M-116 husky amphibious personnel carrier, military aircrafts like Eurofighter Typhoon, Tornado and F16 and intercontinental ballistic missiles like Titan, Agena and Atlas (Mathaudhu and Nyberg 2010).

1.14.1.3 Medical Applications

Magnesium alloys are explored as bio-implant materials. The density of magnesium alloys ($1.7 - 2.0$ g/cm^3) is close to that of natural bone ($1.8 - 2.1$ g/cm^3) and is lower than the competing near titanium alloys ($4.4 - 4.5$ g/cm^3). Magnesium alloys have a high mechanical strength compared to ceramic or polymeric biomaterials and possess greater fracture toughness. Magnesium ion participates naturally in human metabolism, it is the fourth most abundant cation in human body; hence magnesium is biocompatible and nontoxic at moderate levels.

1.14.1.4 Applications in electronics

For the user, portability is highly anticipated of the electronic devices. As compared to plastic electronic materials, magnesium alloys are not only light-weight but also have better heat transfer and the ability to protect against electromagnetic and radiofrequency interferences. The magnesium components currently found in

electronic devices include the housing of cell phones, digital cameras, computers, laptops, digital projectors, media players.

1.14.1.5 Applications in sports

The popularity of magnesium alloys as structural materials for sports equipment's is not surprising considering their enviable properties such as low density, their ease of machining which facilitates the creation of complex shapes, good properties of cushioning and shock absorption and vibration absorption. The handles of archery bows, tennis rackets, golf club head, chassis of in-line skates and mountain bike bicycle frames are some notable examples of magnesium parts in sports equipments.

1.14.1.6 Other applications

Magnesium alloys find applications in consumer products that must be lightweight for easy portability. Some examples include spectacle frames, binocular parts and hand-held working tools for mechanical operations.

1.14.2 GA9 Magnesium alloy

GA9 alloy, used for the development is a material made of magnesium with 9% aluminum (Al) and 1% zinc (Zn) content. GA9 alloy is one of the most commonly used Mg alloy in automotive field. GA9 magnesium alloy is a dual phase alloy with a typical microstructure of having a primary α-phase and a divorced eutectic β-phase ($Mg_{17}Al_{12}$) and the eutectic β-phase distributed along α-phase grain boundaries (Froes et al. 1998). The α-Mg matrix is an α-Mg-Al-Zn solid solution with the same crystal structure as pure magnesium and the β-phase is with a composition of $Mg_{17}Al_{12}$. The α-Mg matrix corrodes due to its very negative free corrosion potential. The β-phase of $Mg_{17}Al_{12}$ is cathodic to the α-Mg matrix and tends to accelerate the corrosion rate by micro galvanic coupling between anodic α-Mg phase and cathodic β-$Mg_{17}Al_{12}$ phase (Song et al. 1999, Zhao et al. 2008). However, the β-$Mg_{17}Al_{12}$ phase may act as a barrier against corrosion propagation if it is in the form of a continuous network (Zhao et al. 2008). GA9 has exhibits improved corrosion resistance compared pure magnesium (Badaway et al. 2010). This is due to the relatively fine β-phase network and the aluminum enrichment produced on the corroded surface (Guohua et al. 2005, Yu et al. 2006).

1.14.2.1 Properties of GA9 alloy

Like most of the magnesium alloys, GA9 also has low density, high strength, good castability and good weld ability under controlled atmosphere. Some of the prominent physical and mechanical properties are listed below in Table 1.3.

Table 1.3: Physical and mechanical properties of GA9 magnesium alloy

Parameter	Value
Density	1.792 gcm^{-3}
Melting point	559 °C
Specific heat	1.05 KJkg^{-1}K^{-1}
Thermal conductivity	72 Wm^{-1}K^{-1}
Latent heat of fusion	373 KJKg^{-1}

1.14.2.2 Uses

- It is used as structural material in aircraft fuselages, engine parts, and wheels.
- Used in jet-engine parts, rockets and missiles, luggage frames, portable power tools, cameras and optical instruments.
- It is used for various wrought manufactures including sheet, forgings and extrusions.
- Alloys of magnesium are used extensively for making airplanes and missiles parts, and wheels of cars and trucks.
- Alloys of aluminum-magnesium are used for making beverage cans.

1.15 LITERATURE REVIEW

1.15.1 Corrosion behaviour of pure magnesium and magnesium alloys

Cao et al. (2007) have investigated the corrosion behaviour of cast Mg, GA9 and cast GA9 in 0.1M NaCl solution by measuring open-circuit potential (OCP), steady-state current potential and electrochemical impedance spectra (EIS). Similar electrochemical behaviours were found for the three metal alloys.

Wang et al. (2010) have studied the corrosion behaviour of GA9 magnesium alloy in neutral solutions containing different concentrations of chloride ions using electrochemical measurements. GA9 alloy exhibited the corrosion and passivation zones in neutral solutions containing chloride ions. The passivation zone became

narrow with increasing concentration of chloride ions in the solution. XRD patterns showed the presence of $Mg(OH)_2$, $Mg_5(CO_3)_4.8H_2O$ and MgO phases in the corrosion product, whereas the latter two phases found in the passive film.

Baghni, et al. (2004) have presented the comparison of corrosion behaviour of pure magnesium and few selected magnesium alloys in industrial and marine environments. The effect of microstructure and additive alloying elements on corrosion rate of magnesium had been reported. The review has shown that elements like Zn, Cd, Ca, Ag have a moderate accelerating effect, whereas impurities of elements like Cu, Ni, Co, Fe, Zr have extremely degrading effect and elements like Mn, Na, Sn, Th, Be, Ce, Pr, Y have negligible effect on corrosion rate of magnesium. Data supporting the phenomenon of negative difference effect (NDE) and two step anodic dissolution of magnesium had been made available.

Chao et al. (2012) have investigated the corrosion behaviour of pure Mg in 1.0% NaCl solution at different immersion times by electrochemical impedance spectroscopy (EIS). The corrosion process and EIS evolution are divided into three stages. In the initial stage, EIS is composed of two overlapped capacitive arcs, the polarization resistance and charge transfer resistance increase rapidly with immersion time and the corrosion rate decreases. Then, two well defined capacitive arcs appear and the charge transfer resistance and corrosion rate remain same. After a long immersion time, inductive component appears in a low frequency range, the charge transfer resistance decreases and corrosion rate increases with the immersion time.

Baril and Pebere (2001) have investigated the corrosion behaviour of pure magnesium in aerated and deaerated 0.01M and 0.1M sodium sulphate solutions by polarization and impedance measurements. Additional study of corrosion rate measurements in deareted media with increased concentrations of sodium bicarbonate collectively showed that the anodic current densities increased with increased concentrations of sodium sulphate, and the current densities in deaerated media. The study presented conclusion that O_2 does not influence corrosion of pure magnesium.

Zhao et al. (2008) have investigated the influence of pH and chloride ion concentration on the corrosion behaviour of ZE41 using immersion tests and electrochemical measurements. The corrosion of ZE41 in NaCl solutions depended on the pH and the chloride ion concentration, a higher corrosion rate correlated with a

39

higher chloride ion concentration at each pH and correlated with a lower pH for each chloride ion concentration. The result is consistent with the known tendency of chloride ions to cause film breakdown, and the known instability of $Mg(OH)_2$ in solutions with pH less than 10.5. The electrochemical measurements of the corrosion rate, based on the corrosion current at the free corrosion potential, did not agree with direct measurements evaluated from the evolved hydrogen, in agreement with other observations for Mg.

Badaway et al. (2010) have studied the corrosion behaviour of Mg, Mg-Al-Zn and Mg-Al-Zn-Mn alloys in aqueous acidic, neutral and basic solutions by open circuit potential, polarization and electrochemical impedance spectroscopy (EIS). The results have shown that the rate of corrosion in acidic solution is relatively high compared to that in neutral or basic solutions. The presence of Al, Zn and Mn as alloying elements decreased the rate of corrosion of the alloy. The activation energy of the corrosion process occurring at the surface of Mg or Mg alloys in aqueous solutions was less than 40 KJ mol^{-1}. The value indicate a one electron transfer electrode reaction as a rate controlling process.

Altum and Sen (2004) have studied the influence of chloride ion concentration and pH on the corrosion behaviour of AZ63 magnesium alloy in NaCl solution by potentiodynamic polarization tests. The corrosion rate was high in highly acidic solutions (pH2) as compared to that in other solutions. The corrosion rate usually increased with the decrease in pH and the increase in chloride ion concentration. But the quantity of the increase in corrosion rate was different at separate pH and concentration regions. The corrosion potential usually shifted to more negative values with the increase in the concentration of chloride ions and the decrease in pH of the solution.

Qu et al. (2010) have studied corrosion behaviour of AZ31B magnesium alloy in different concentrations of NaCl solution saturated with CO_2 by electrochemical techniques, Fourier transform infrared spectroscopy, scanning electron microscopy and energy dispersive X-ray. The corrosion rate increased with increasing NaCl concentration both in the presence and absence of CO_2. The corrosion rate in NaCl solution saturated with CO_2 was bigger than that in single NaCl solution. The inhibitive

effect of CO_2 was also observed with immersion time showing that CO_2 reduces the average corrosion rate due to the formation of insoluble products.

Wang et al. (2010) have studied corrosion of AZ61 magnesium alloy using electrochemical measurements, in which the alloy exhibited the corrosion and passivation zones in dilute NaCl solutions. The results were compared to those obtained on AZ31 and GA9 alloys, in which the passivation zone of AZ61 alloy was broader than that of AZ31 alloy and gave a similar range to that of GA9 alloy. The values of open-circuit potential on AZ61 alloy were in the passivation zone when chloride ion concentration was less than 0.3mol/L. The potentiostatic polarization of specimens depended on the chloride ion concentration and exhibited the corrosion and passivation states at various applied potentials. The current densities increased as the films flake off and were dissolved, and then droped to the low values as the new films are formed in the corrosion state.

Yang et al. (2010) have studied the corrosion behaviour of die-cast AZ91D magnesium alloys in sulphate solutions by SEM, FTIR and polarization measurements. For immersion times less than 48 h, no pitting corrosion occurred and only generalized corrosion was apparent. According to the polarization curves, the corrosion rate order of the die-cast AZ91D Mg alloy in three aqueous solutions was: $NaCl > MgSO_4 > Na_2SO_4$. The main corrosion products were $Mg(OH)_2$ and $MgAl_2(SO_4)_4.22H_2O$ in the sulphate solutions and the product film was compact. Precipitation of $MgAl_2(SO_4)_4.22H_2O$ required a threshold immersion time.

Chen et al. (2007) have investigated corrosion behaviour of GA9 magnesium alloy in 0.1M sodium sulphate solution by using electrochemical impedance spectroscopy (EIS), environmental scanning electron microscopy (ESEM), energy dispersive X-ray spectroscopy (EDS), and X-ray photoelectron spectroscopy (XPS). The results showed that when the immersion time was less than 18 h, general corrosion occurred on the surface and the main corrosion products were hydroxides and sulphates. The film coverage effect was the main mechanism for the corrosion process of GA9 alloy. With the increasing immersion time, pitting occurred on the surface.

Helal (2011) studied corrosion behaviour of Mg-Al-Zn alloy in neutral solutions containing chloride ions at different concentrations using polarization and impedance techniques and reported that corrosion behaviour of magnesium alloys is governed by

41

partially protective surface film, with the corrosion reactions occurring predominantly at the imperfections of the partially protective film. The fraction of film-free surface increased with increasing chloride ion concentration, which is consistent with the known tendency of chloride ions to cause film breakdown.

1.15.2 Corrosion inhibitors for magnesium and magnesium alloys

A large number of investigations have been carried out using chemical compounds as corrosion inhibitors for pure magnesium and magnesium alloys in variety of media. This broad class of magnesium corrosion inhibitors includes both inorganic and organic chemicals and even the combination of the two. Some efficient magnesium inhibitors reported in literature along with certain essential details are listed in Table 1.4.

Table 1.4: Prominent corrosion inhibitors for magnesium and magnesium alloys.

Inhibitor used	Material	Medium	Reference
Sodium undecanoate	Mg-Al-Zn alloy	Aqueous salt solutions	Daloz et al. 1998
Potassium fluoride	Pure Mg	Ethylene glycol	Song and St John 2004
Sodium decanoate and sodium heptanoate	Pure mg	ASTM D1384-87	Mesbah et al. 2007
Cerium nitrate and lanthanum nitrate	AZ31 alloy	NaCl	Montemor and Ferreira 2008
Sodium dodecylbenzenesulfonate (SDBS)	AZ31 alloy	NaCl	Li et al. 2009
Sodium dodecyl sulphate (SDS), phytic acid, stearic acid, ethylenediamine tetraacetic acid (EDTA)	AZ61 alloy	Alkaline medium	Yang et al. 2009
8-Hydroxyquinoline and SDBS	AZ91D alloy	ASTM D1384-87	Gao et al. 2010

1,2,4-Triazole, salts of F^- and Ce^{3+}	AZ31 alloy	NaCl	Karavai et al. 2010
Phosphate and chromate	Pure Mg	NaCl	Williams et al. 2010
Cerium nitrate	AZ91D alloy	Na_2SO_4	Correa et al. 2011
Sodium silicate	AZ91D alloy	ASTM D1384-87	Gao et al. 2011
Amino acid methionine	Mg-Al-Zn alloy	NaCl	Helal 2011
Amino acids	Mg-Al-Zn alloy	Chloride free neutral solutions	Helal and Badaway 2011
Sodium aminopropyltriethoxysilicate and zinc nitrate	GW 103	ASTM D1384-87	Hu et al. 2011
Sodium phosphate and SDBS	GW103 alloy	Ethylene glycol	Huang et al. 2011
5-(3-Aminophenyl)-tetrazole	Mg-Mn alloy	NaCl	Sherif and Almajid 2011
Sodium lauryl sulphate (SLS), SDBS, sodium salts of N-lauroylsacrosine (NLS) and N-lauroyl-N-methyltaurine (NLT)	AZ31 alloy	Na_2SO_4 and NaCl	Frignani et al. 2012
Cerium nitrate	AM 60 alloy	NaCl	Heakal et al. 2012
Tetraphenylporphyrin	AZ91D alloy	NaCl	Hu et al. 2012
2-Hydroxy-4-methoxy-acetophenone (paeanol)	AZ91D alloy	NaCl	Hu et al. 2013

Alkyl carboxylates	ZE41 alloy	Aqueous salt solution	Dinodi and Shetty 2014
Zeolite coating	AZ91D alloy	NaCl	Banerjee et al. 2014
N,N[1]-bis(2-pyridylmethyllidene)-1,2-diiminoethane	AZ91D alloy	HCl	Seifzadeh et al. 2014
N-Acetyl-cysteine	Mg-Al-Zn alloy	Chloride free neutral solutions	Badaway et al. 2014
Sodium stearate	ZE41 alloy	Aqueous salt solution	Dinodi and Shetty 2014
Polyaspartic acid	WE43 alloy	NaCl	Yang et al. 2015
Magnesium fluoride-polydopamine-stearic acid composite	AZ31 alloy	NaCl	Zhang et al. 2016
Trichoderma harzianum	AZ31B alloy	Artificial sea water	Qu et al. 2017

1.15.3 Surfactants as corrosion inhibitors

Surfactants are amphiphilic molecules comprising of both hydrophilic (head) and hydrophobic (tail) groups. True to their name surfactants are surface-active agents and exhibit a tendency to accumulate at interfaces. Metal corrosion being a surface phenomenon, this tendency of surfactant to aggregate at interfaces comes in handy while inhibiting corrosion. For convenience the surfactants are grouped on the basis of chemical nature of the head group, as non-ionic (or molecular), cationic, anionic and zwitter-ionic. The hydrophilic head of the surfactants is known to facilitate interaction with metal surface which leads to physical or chemical adsorption depending upon the charge of the hydrophilic group and that on the metal. The hydrophobic tail is credited for water-repellent nature of inhibited metal surfaces which is an icing on the cake, considering so many other advantages of surfactants as corrosion inhibitors, like easy preparation, cost-effectiveness and low toxicity (Migahed and Al-Sabagh 2009, Malik

et al 2011). There are more works in literature than one quote, where the anti-corrosion property of the surfactants has been focused for various metal types. Among the magnesium inhibitors specified in Table 1.5, the following are surfactants; sodium undeconate, sodium deconate, sodium heptanoate, SDBS, SDS, sodium stearate, sodium lauryl sulphate and sodium salts of N-lauroylsarcosine and N-lauroyl-N-methyltaurine.

1.16 SCOPE AND OBJECTIVES OF THE PRESENT WORK
1.16.1 Scope of the work

Nowadays, the study of magnesium alloys is a topic of great relevance; owing to their wide spectrum of applications in various fields of modern engineering. Environmental conservation has given impulse to magnesium alloys research and development, because it depends, to a great extent, on transportation industry, particularly CO_2 emissions produced by transport vehicles. As CO_2 emission is in direct proportion to fuel consumption, car weight has become a very important criterion of design efficiency assessments. As the lightest structural metal available, magnesium's combination of low density and good mechanical strength results in a high strength-to-weight ratio and very easy for hot work metal. Magnesium alloys can absorb energy elastically because of their low modulus of elasticity. Combined with moderate strength, this provides excellent dent resistance and high damping capacity. Despite these advantages usage of magnesium alloys as a structural material has found disadvantages due to the poor corrosion resistance. Thus significant research is still needed on processing, surface treatment, corrosion resistance, new alloy development and mechanical properties improvement of these alloys.

A great number of investigations have been devoted to the protection of magnesium alloys, which include,

- Conversion surface treatments, as chromating, phosphating, etc.
- Surface coatings.

However, a very little work has been seldom involved on the use of corrosion inhibitors. The use of corrosion inhibitors is one of the most important methods for the protection of metals and alloys against corrosion in harsh environments. For the metals widely employed in the industry such as iron, copper and aluminum, adding corrosion

inhibitors is an effective and convenient method to decrease the corrosion rate, which has been widely perused. For magnesium and its alloys, there are very few publications on their corrosion inhibitors and few developed inhibitors such as the salts of fluoride ions and salts of dichromate pollute the environment seriously. Hence it is quite necessary to pay more attention to develop the environmental friendly corrosion inhibitors for magnesium and its alloys.

1.16.2 Objectives

1. To study the corrosion behaviour of GA9 magnesium alloy specimen in media of chloride and sulphate ions of different concentrations.

2. To investigate the influence of pH and temperature of chloride and sulphate media on the corrosion behaviour of GA9 magnesium alloy.

3. To investigate the corrosion inhibition effect of some surfactants on GA9 magnesium alloy in chloride and sulphate media.

4. To study the effect of temperature on the corrosion reaction and to evaluate the activation parameters for the corrosion in the presence and in the absence of the inhibitor.

5. To investigate the surface morphology of the metal alloy in chloride and sulphate solutions in the presence and in the absence of inhibitors using scanning electron microscopy (SEM).

6. To assign mechanisms for the inhibitive action of corrosion inhibitors in the chloride and sulphate media.

1.17 OUTLINE OF THE THESIS

The present thesis has been suitably divide into four chapters. The contents pertaining to each chapter as follows.

Chapter 1 presents some of the fundamental aspects of corrosion and some measures to monitor and combat the same. This chapter also emphasizes magnesium alloys as the futuristic structural materials for weight-sensitive applications. In addition, the appropriate works in the literature that focus upon the corrosion and the inhibition of pure magnesium and its alloys: have been reviewed. The chapter towards the end recognizes the scope of the present work, affirming the importance of magnesium alloys

and identifying the flaiure in the corrosion mitigation measures currently employed. The chapter eventually lays down the objectives of the current work.

C**hapter 2** is composed of descriptions about the experimentation part. The specific procedures adopted for the preparation of the test specimen and the electrolyte solutions has been elucidated. The chapter also presents the operative specifications related to the electrochemical techniques used together with the calculations that have allowed to deduce the numerical results of the current work.

C**hapter 3** offers a detailed description of the full results obtained in the study. The chapter also provides the interpretation of the graphical and the numerical results. This chapter basically is an attempt to explicate the electrochemical behaviour and corrosion inhibition of GA9 on the basis of the study.

C**hapter 4** summarises the work included in the thesis and also lists the conclusions drawn on the basis of experimental evidences and discussions.

CHAPTER 2

MATERIALS AND METHODS

2.1 MATERIALS

2.1.1 GA9 magnesium alloy

The experiments were performed with specimen of GA9 magnesium alloy. Percentage composition of GA9 magnesium alloy sample is given in Table 2.1.

Table 2.1: Composition of specimen (% by weight).

Element	% Composition
Aluminium	8.30
Zinc	0.60
Manganese	0.35
Copper	0.12
Iron	0.20
Silicon	0.20
Magnesium	90.23

2.1.2 Preparation of test coupons

Cylindrical test coupons were cut from the plate and sealed with epoxy resin in such a way that, the area exposed to the medium was 0.64 cm^2. These coupons were polished as per standard metallographic practice, belt grinding followed by polishing on emery papers, finally on polishing wheel using legated alumina to obtain mirror finish, degreased with acetone, washed with double distilled water and dried before immersing in the corrosion medium.

2.2 MEDIA

The media used for the investigation were sodium chloride and sodium sulphate at five different concentrations.

2.2.1 Preparation of standard sodium chloride solution

Standard solutions of sodium chloride having concentration 0.1 M, 0.5 M, 1.0 M, 1.5 M and 2.0 M were prepared by analytical grade sodium chloride in double distilled water.

2.2.1 Preparation of standard sodium sulphate solution

Standard solutions of sodium sulphate having concentration 0.1 M, 0.5 M, 1.0 M, 1.5 M and 2.0 M were prepared by dissolving analytical grade sodium sulphate in double distilled water.

2.2.3 Preparation of chloride and sulphate media with varying pH

A part of the study dealt with understanding the influence of solution pH on corrosion of GA9. For this particular investigation the chloride and sulphate media of concentrations 0.1M, 0.5 M, 1.0 M, 1.5 M and 2.0 M were prepared by dissolving analytical grade sodium chloride and sodium sulphate in double distilled water. The pH of the solutions were adjusted to desired value (pH = 3, 5, 7, 9, 12 for each chloride and sulphate concentration) with HCl, H_2SO_4 and NaOH using calibrated pH meter.

2.3 INHIBITORS

Four different anionic surfactants were tested for their inhibition effect. The studied inhibitors are sodium dodecylbenzenesulfonate (SDBS), sodium 4-n-octylbenzenesulfonate (SOBS), sodium xylenesulfonate (SXS) and sodium benzenesulfonate (SBS). The skeletal structures of the inhibitors are shown below.
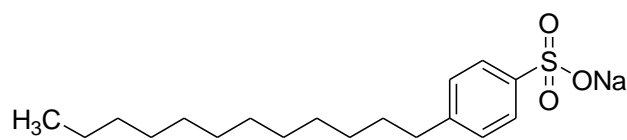
Fig. 2.1. Structure of SDBS.
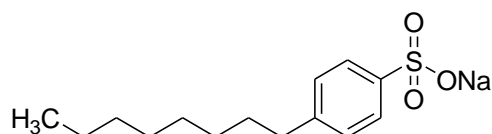
Fig. 2.2. Structure of SOBS.
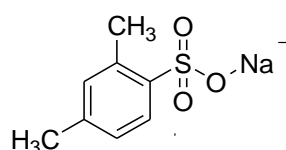
Fig. 2.3. Structure of SDMBS.
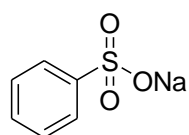
Fig. 2.4. Structure of SBS.

2.4 METHODS

2.4.1 Electrochemical measurements

The electrochemical measurements were carried out using an electrochemical work station, Gill AC having ACM instrument Version 5 software. A three electrode cell was used for the electrochemical measurements. The working electrode was made of GA9 magnesium alloy. A saturated calomel electrode (SCE) and a platinum electrode were used as the reference and the counter electrode, respectively. Electrode potentials were measured with respect to saturated calomel electrode (SCE). The working electrode was allowed to immerse in the electrolytic medium to establish a steady-state and the achievement of the steady-state was monitored by monitoring the change in potential of the working electrode with respect to time. The polarization and impedance measurements were initiated only after reaching steady-state with an equilibrium electrode potential corresponding to the open circuit potential (OCP). Polarization studies were performed immediately after the EIS studies on the same electrode without any additional surface treatment. A minimum of three trials were carried out to ensure the reproducibility of the results and mean values were documented.

2.4.1.1 Potentiodynamic polarization studies

Finely polished GA9 magnesium alloy of 0.64 cm^2 surface area was exposed to the corrosion media of sodium chloride and sodium sulphate (0.1 M to 2.0 M) in the presence and absence of studied inhibitors at different temperatures (30 ℃ - 50 ℃) and allowed to establish a steady state open circuit potential (OCP). The potentiodynamic current potential curves were recorded by polarizing the specimen to -250 mV cathodically and +250 mV anodically from the OCP at a scaning rate of 1 mV s^{-1}.

2.4.1.2 Electrochemical impedance spectroscopy (EIS) studies

The corrosion behaviour of the GA9 magnesium alloy was also obtained from EIS technique. In EIS technique, a small amplitude ac signal of 10 mV was applied to the electrochemical system over a wide range of frequencies (10 kHz to 0.01 Hz) at the OCP and the response to the input signal was measured. The polarization resistance (R_p) was extracted from the Nyquist plot. The impedance data points were simulated

with an appropriate theoretical model corresponding to an equivalent circuit using ZsimpWin version 3.21 software.

2.4.2 Surface analysis

The morphology and composition of the specimen surface were examined by recording the SEM images and EDX spectra of different samples using JEOL JSM-6380LA analytical scanning electron microscope.

2.5 CALCULATIONS

2.5.1 Computation of corrosion rate

The corrosion current density values (i_{corr}) were deduced from the extrapolation of cathodic Tafel branches to the corrosion potential. The experimentally determined i_{corr} values were used in the calculation of corrosion rate (υ_{corr}) using the equation mentioned below.

$$Corrosion\ rate\ (\upsilon_{corr})\ =\ K\frac{i_{corr}}{\rho}EW \qquad (2.1)$$

where, K is 3.27×10^{-3}, a constant that defines the unit for the corrosion rate, i_{corr} is the current density in A cm^{-2}, ρ is the density in g cm^{-3} and EW is equivalent weight of the alloy. Equivalent weight for the alloy was calculated from the following equation (Dean 1999).

$$EW = \frac{1}{\Sigma\dfrac{n_i f_i}{W_i}} \qquad (2.2)$$

where, f_i is the mass fraction of the ith element in the alloy, W_i is the atomic weight of the ith element in the alloy and n_i is the valence of the ith element of the alloy.

2.5.2 Calculation of inhibition efficiency

The inhibition efficiency (η) was evaluated as a function of surface coverage (θ) and relation between the two is presented in following equation.

$$\eta(\%) = \theta \times 100 \qquad (2.3)$$

The value of θ was deduced from the results of electrochemical measurements. The i_{corr} values obtained from the Tafel polarization studies and values of R_p acquired fom EIS

measurements were used separately in the evaluation of θ, as per the equations presented below.

$$\theta = \frac{i_{corr(b)} - i_{corr(inh)}}{i_{corr(b)}} \tag{2.4}$$

where, i_{corr} and $i_{corr(inh)}$ signify the corrosion current densities in the absence and presence of inhibitors, respectively.

$$\theta = \frac{R_{p(inh)} - R_{p(b)}}{R_{p(inh)}} \tag{2.5}$$

where, $R_{p(inh)}$ and R_p are the polarization resistances obtained in inhibited and uninhibited solutions, respectively.

2.5.3 Evaluation of activation energy

The apparent activation energy (E_a) for the corrosion process in the presence and absence of the inhibitor was calculated using Arrhenius law equation (Bouklah et al. 2004).

$$\ln(\upsilon_{corr}) = B - \frac{E_a}{RT} \tag{2.6}$$

where, B is a constant which depends on the metal type and R is the universal gas constant, υ_{corr} is the corrosion rate, E_a is the activation energy, T is absolute temperature. The plot of $ln(\upsilon_{corr})$ versus reciprocal of absolute temperature ($1/T$) gives a straight line with slope $= - E_a / R$, from which, the activation energy values for the corrosion process were calculated (Atta et al. 2011).

The entropy of activation ($\Delta H^{\#}$) and enthalpy of activation ($\Delta S^{\#}$) for the corrosion of alloy were calculated from the transition state theory equation (Abd EL-Rehim et al. 1999).

$$\upsilon_{corr} = \frac{RT}{Nh} \exp\left(\frac{\Delta S^{\#}}{R}\right) \exp\left(\frac{-\Delta H^{\#}}{R}\right) \tag{2.7}$$

where, h is Plank's constant, N is Avagadro's number. A plot of $ln(\upsilon_{corr}/T)$ vs $1/T$ gives straight line with the slope being given by equation (2.8) and intercept given by equation (2.9).

$$\text{Slope} = \frac{-\Delta H^{\#}}{R} \tag{2.8}$$

$$\text{Intercept} \; = \; \ln(\frac{R}{Nh}) + \frac{\Delta S^{\#}}{R} \tag{2.9}$$

2.5.4 Calculation of thermodynamic parameters

The calculation of the thermodynamic parameter for the adsorption of inhibitor were based on a suitable adsorption isotherm model with which the system under the study showed best agreement. An adsorption isotherm is defined as a graphical representation showing the variation of extent of adsorption with pressure at a given constant temperature. For the adsorption occurring at solution/solid interface, the concentration of the adsorbate (inhibitor) can be considered as the equivalent of pressure. The mathematical expression for the adsorption isotherms highlights an equilibrium relation between inhibitor concentrations on the metal surface and that in bulk solution. Hence the adsorption isotherms are applicable to the systems where the inhibition is the consequence of surface coverage brought about by the inhibitor on adsorption. Some adsorption isotherm are commonly verified to explain corrosion inhibition, their mathematical expressions and verification plots are presented in Table 2.2.

Table 2.2: List of adsorption isotherms.

Name	Isotherm	Verification Plot
Langmuir	$\theta/(1-\theta) = \beta.C$	C/θ vs C
Frumkin	$[\theta/(1-\theta)]e^{f\theta} = \beta.C$	θ vs log C
Bockris-Swinkels	$\theta/(1-\theta)^n.[\,\theta + n(1-\theta)]^{n-1}/n^n = C.e^{-\beta}/55.4$	$\theta/(1-\theta)$ vs log C
Temkin	$\theta = (1/f)\ln K.C$	θ vs log C
Virial Parson	$\theta.e^{2f\theta} = \beta.C$	θ vs log(θ/C)
Flory Huggins	$\log(\theta/C) = \log nK + n\log(1-\theta)$	$\log(\theta/C)$ vs log(1-θ)
El – Awady	$\log[\theta/(1-\theta)] = \log K + y \log C$	$\log[\theta/(1-\theta)]$ vs log C.

where, θ is the surface coverage; $\beta = \Delta G/2.303RT$, ΔG is free energy of adsorption; R is gas constant; T is temperature; C is bulk inhibitor concentration; n is number of water molecules; f is inhibitor interaction parameter (0, no interaction; +, attraction; -, repulsion); and K is constant.

The C and θ values from the current study involving sulfonates as inhibitors showed best agreements with the Langmuir adsorption isotherm. The standard free energy of adsorption of the inhibitor molecules on the alloy surface, ΔG°_{ads} was calculated using the relation:

$$K_{ads} = \frac{1}{55.5} \exp(\frac{-\Delta G^0_{ads}}{RT}) \qquad (2.10)$$

where, the value 55.5 is the concentration of water in solution in mol dm^{-3}, R is the universal gas constant and T is absolute temperature in K.

Standard enthalpy of adsorption (ΔH°_{ads}) and standard entropy of adsorption (ΔS°_{ads}) were calculated from Gibbs–Helmholtz equation:

$$\Delta G^0_{ads} = \Delta H^0_{ads} - T\Delta S^0_{ads} \qquad (2.11)$$

The variation of ΔG^0_{ads} with T gives a straight line with slope equals to ΔS^0_{ads} and an intercept equals to ΔH^0_{ads}.

CHAPTER 3

RESULTSS AND
DISCUSSION

3.1 CORROSION BEHAVIOUR OF GA9 MAGNESIUM ALLOY IN SODIUM CHLORIDE MEDIUM

3.1.1 Potentiodynamic polarization studies

The corrosion behaviour of GA9 magnesium alloy in sodium chloride solution was established by exposing the alloy to sodium chloride medium at different temperatures and ionic concentrations, followed by the electrochemical monitoring. Fig. 3.1 represents potentiodynamic polarization curves for the corrosion of GA9 magnesium alloy in different concentrations of NaCl at 40 °C. Similar plots were obtained at other temperatures also. It is observed from the Fig. 3.1 that the polarization curves are shifted to the higher current density region as the concentration of chloride ion is increased, indicating the increase in the corrosion rate with the increase in chloride ion concentration of the solutions.
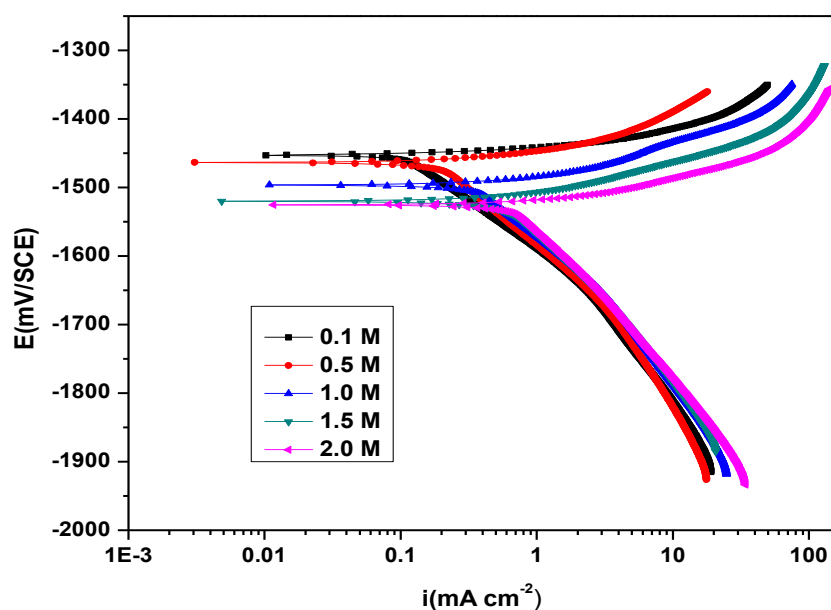
Fig. 3.1: Potentiodynamic polarization curves for the corrosion of GA9 magnesium alloy in different concentrations of NaCl at 40 °C.

The anodic polarization curves represent anodic oxidation of magnesium. It is seen from Fig. 3.1 that the anodic polarization curves do not possess a distinct Tafel region. However, the cathodic branch of polarization curves showed linear behaviour in the Tafel region and represent the cathodic hydrogen evolution through the reduction

of water. Therefore the corrosion current density (i_{corr}) is obtained by extrapolating the cathodic Tafel slope to the rest potential. The potentiodynamic polarization parameters like corrosion potential (E_{corr}), corrosion current (i_{corr}), cathodic slope (b_c) and corrosion rate (υ_{corr}) were calculated from the plots and are tabulated in Table 3.1. It is clear from the data presented in Table 3.1 that the corrosion rate of GA9 magnesium alloy specimen increases with the increase in the concentration of sodium chloride in the solution, indicating the strong influence of the corrosive strength of the media on the rate of alloy corrosion. Chloride has been reported to be a strong corrosive, possessing appreciable influence on the electrochemical behaviour of pure magnesium and some of its alloys (Song et al. 1997, Baril and Pebere 2001, Wang et al. 2010). The corrosiveness of chloride ions towards magnesium and its alloys arises from their tendency to cause surface film breakdown by transforming the deposited corrosion product, $Mg(OH)_2$, to easily soluble $MgCl_2$. The corrosion potential (E_{corr}), shifts towards more negative (more active) values with the increase in the concentration of chloride ions in the corrosion media. Similar trend of a more negative E_{corr} associated with a higher corrosion rate had been reported by Baril and Pebere (2001) for pure magnesium corrosion in sulphate medium and by Zhao et al. (2008) for the corrosion of magnesium zinc alloy in chloride medium. However, this behaviour cannot be concluded as a phenomenon, as in majority of studies no such direct relation between E_{corr} and corrosion rate had been reported (Dinodi and Shetty 2013). The slopes of the Tafel branches change with the change in the chloride ion concentration of the medium, without any modifications in overall shape. This fact indicates that the strength of the corrosive medium strongly influences kinetics of the cathodic hydrogen evolution and the anodic metal dissolution reactions without altering the mechanism of alloy corrosion.

The corrosion of magnesium alloy normally proceeds by an electrochemical reaction with water to produce magnesium hydroxide and molecular hydrogen (H_2) (Wang et al. 2010, Liu et al. 2009). The overall reaction is

$$Mg + 2H_2O \rightarrow Mg(OH)_2 + H_2 \qquad (3.1)$$

The anodic dissolution of magnesium has been proposed to be consisting of oxidation of magnesium into monovalent Mg^+ ions and divalent Mg^{2+} ions as represented by the following reactions (Bhagni et al. 2004).

$$Mg \rightarrow Mg^+ + e^- \qquad (3.2)$$

$$Mg \rightarrow Mg^{2+} + 2e^- \qquad (3.3)$$

The standard electrode potential of magnesium is -2.38 V (/SCE), but the steady state working potential is about -1.5 V (/SCE). The difference in potential has been attributed to the formation of $Mg(OH)_2$ film on the metal surface (Udhayan and Bhat 1996). As represented in the equation 3.2 and 3.3, the anodic dissolution of magnesium and its alloys involves two oxidation processes. At more active potentials around -2.78V (vs SCE), magnesium is oxidized to monovalent magnesium ion and at slightly higher potentials of -1.56V (vs SCE), oxidation of magnesium to divalent magnesium ion takes place. Monovalent magnesium, being unstable, undergoes oxidation to divalent magnesium ion through a series of reactions involving unstable intermediates like magnesium hydride as shown in equations below.
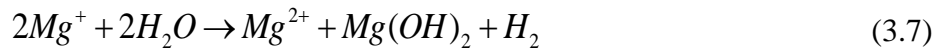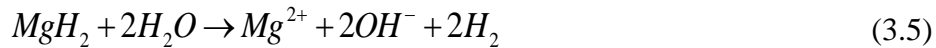
$$Mg^+ + 2H^+ + 3e^- \rightarrow MgH_2 \qquad (3.4)$$

$$MgH_2 + 2H_2O \rightarrow Mg^{2+} + 2OH^- + 2H_2 \qquad (3.5)$$

$$Mg^{2+} + 2OH^- \rightarrow Mg(OH)_2 \qquad (3.6)$$

$$2Mg^+ + 2H_2O \rightarrow Mg^{2+} + Mg(OH)_2 + H_2 \qquad (3.7)$$

GA9 magnesium alloy is a dual phase alloy with a typical microstructure of having a primary α-phase and a divorced eutectic β-phase, distributed along the boundaries (Froes et al. 1998). The α-Mg matrix is an α-Mg-Al-Zn solid solution with the same crystal structure as pure magnesium and the β-phase is with a composition of $Mg_{17}Al_{12}$. The α-Mg matrix corrodes due to its very negative free corrosion potential. The β-phase of $Mg_{17}Al_{12}$ is cathodic to the α-Mg matrix and tends to accelerate the corrosion rate by micro galvanic coupling between anodic α-Mg phase and cathodic β-$Mg_{17}Al_{12}$ (Song et al. 1999, Zhao et al. 2008). However, the β-$Mg_{17}Al_{12}$ phase may act as a barrier against corrosion propagation if it is in the form of a continuous network

(Zhao et al. 2008). The corrosion of the alloy in the chloride media indicates the discontinuities in the β-phase. According to the reports in the literature, magnesium alloys exhibit higher corrosion resistance than pure magnesium (Badaway et al. 2010). The improvement of the corrosion behaviour of Mg alloys elements has been attributed to a number of factors such as refining of β-phase formation by forming another intermetallic, which is less harmful to the α-Mg matrix, and added elements may incorporate into the protective film and thus increasing its stability (Guohua et al. 2005, Yu et al. 2006). Small additions of Mn have been reported to increase the corrosion resistance of magnesium alloys and reduce the effects of metallic impurities (Carlson et al. 1993, Polmer et al. 1992).

The increase in the corrosion rate with the increase in the chloride ion concentration can be attributed to the participation of chloride ions in the reaction. Chloride ions are harmful to both magnesium and aluminum. The adsorption of chloride ions to oxide covered magnesium surface transforms $Mg(OH)_2$ to easily soluble $MgCl_2$.

3.1.2 Electrochemical impedance spectroscopy (EIS) studies

The corrosion behaviour of GA9 magnesium alloy specimen was also investigated by EIS method in different concentrations of sodium chloride at different temperatures. The impedance spectra recorded are displayed as Nyquist plots and Fig. 3.2 represents the Nyquist plots for the corrosion of GA9 magnesium alloy in different concentrations of NaCl at 40 °C. Similar plots were obtained at other temperatures also.

The Nyquist plots are characterized by a capacitive loop, extended from high frequency(HF) to low frequency(LF) range, an inductive loop in the low frequency region(LF) range and a tail at the medium frequency(MF) range (Arrabal et al. 2012, Chen et al. 2007, Baril et al. 2001). The HF capacitive loop is usually due to the charge transfer resistance and double layer capacitance at the metal-solution interface. The inductive behaviour at low frequencies is typically associated with the high concentration of Mg ions on relatively film-free areas (Chen et al. 2007, Baril et al. 2001) or due to the presence of adsorbed surface species such as $Mg(OH)^+$, $Mg(OH)_2$ and Mg^+ (Song et al. 1998, Song et al. 1997, Qu et al. 2011). Also tail in the Nyquist plot, in the lower frequency range correlates with the breakage of native corrosion product film (Song et al. 2010). The charge transfer resistance (R_{ct}) and the double layer

60

capacitance (C_{dl}) are deduced from the analysis of a higher frequency capacitive loop (Song et al. 2004). R_{ct} is inversely proportional to the corrosion current and was used to calculate the corrosion rate.
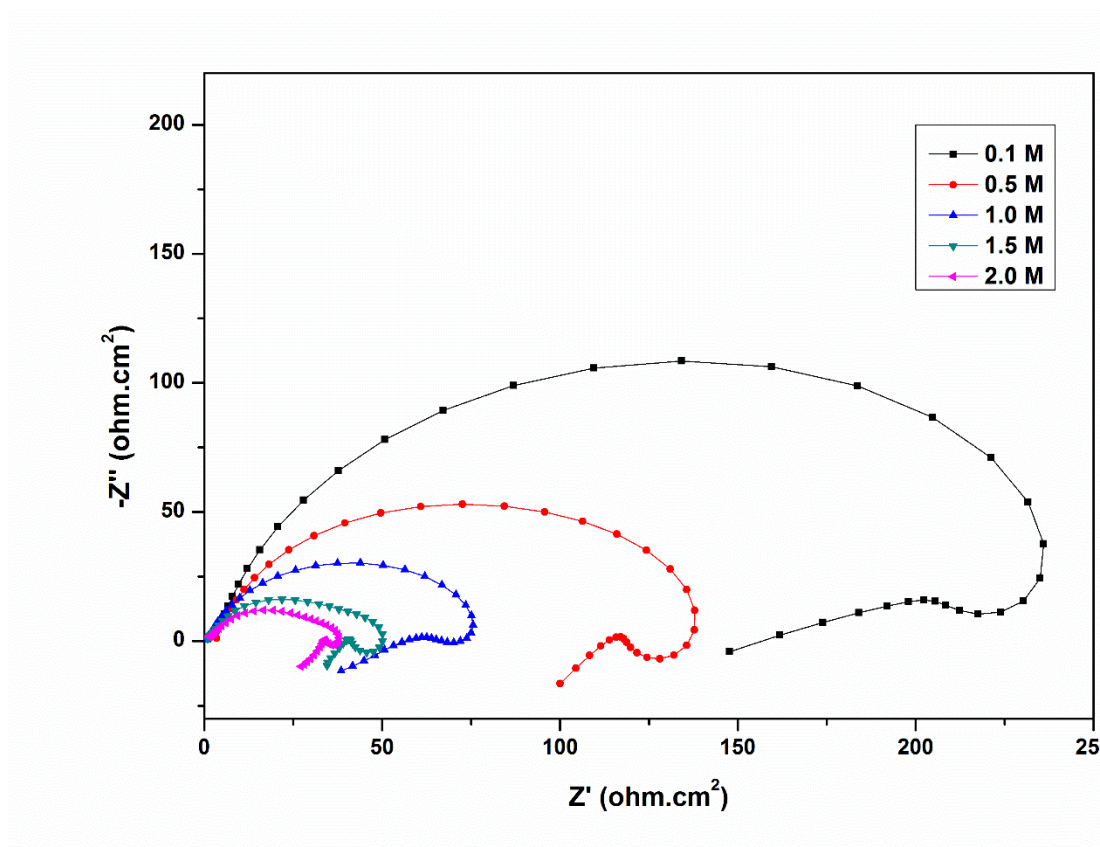
Fig. 3.2: Nyquist plots for the corrosion of GA9 magnesium alloy in different concentrations of NaCl at 40 °C.

From the Fig. 3.2 it is clear that the diameter of the capacitive loop decreases with the increase in the concentration of the chloride ions, indicating the decrease in R_{ct} value and an increase in the corrosion rate. The results are well in agreement with the results obtained from potentiodynamic polarization measurements.

The impedance results are analyzed using equivalent circuit models. The circuit fitment was done by ZSimpWin software of version 3.21. Fig. 3.3 shows the simulation of the impedance data points. The equivalent circuit model for the electrochemical behaviour of the interface, as shown at the inset of Fig. 3.3 comprises of five circuit elements, R_e stands for the electrolyte resistance, R_{ct} stands for the charge transfer resistance. The capacitive loop appears as depressed semicircle, as a result of frequency

dispersion arising due to the inhomogeneity of the alloy surface (Liu et al. 2009). The constant phase element (CPE) is substituted for the ideal capacitive element to account for the unevenness and porosity of the electrode surface. The impedance of the constant phase is described by the expression (Mansfeld et al. 1992).

$$Z_Q = Y_0^{-1}(j\omega)^{-n} \tag{3.8}$$

where Y_0 is the CPE constant, ω is the angular frequency (in rad s^{-1}), $j^2 = -1$, is the imaginary number and n is a CPE exponent that is a measure of the heterogeneity or roughness of the surface. The value of n falls in the range from -1 to $+1$. CPE simulates an ideal capacitor when $n = 1$, an ideal inductor for $n = -1$, and an ideal resistor for $n = 0$. The actual capacitance after taking into consideration of the frequency dispersion, is calculated using the following expression (Mansfeld et al. 1992).

$$C = Y_0(\omega_{max})^{n-1} \tag{3.9}$$

where ω_{max} is the frequency at which the imaginary part of the impedance (Z") has a maximum.
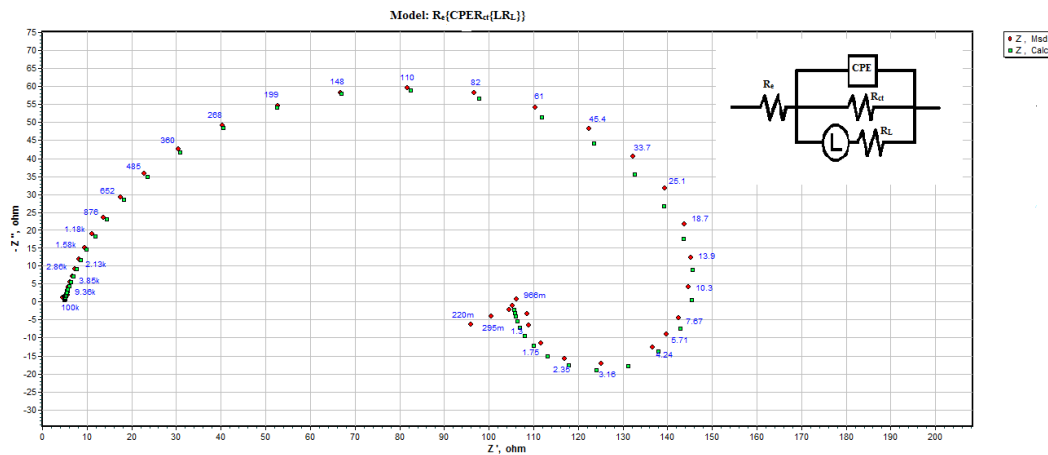
Fig. 3.3: The equivalent circuit model used to fit the experimental data for the corrosion of the specimen in 0.5 M NaCl solution at 35 °C.

The results show that the charge transfer resistance (R_{ct}) value decreases and double layer capacitance (C_{dl}) increases with the increase in the concentration of sodium chloride. The increase in the C_{dl} value may be due to the desorption of the chloride ions at the metal surface causing a change in the double layer structure (Abd Ei-Rehim et al. 1999). The Nyquist plots obtained in the real system represent a general

behaviour where the double layer on the interface of metal/solution does not behave as a real capacitor. On the metal side electrons control the charge distribution whereas on the solution side it is controlled by ions. As ions are much larger than the electrons, the equivalent ions to the charge on the metal will occupy quite a large volume on the solution side of the double layer. Increase in the capacitance, which can result from an increase in local dielectric constant and/or a decrease in the thickness of the electrical double layer, suggests that the chloride ions get desorbed from the metal surface (Prabhu et al. 2007).

3.1.3 Effect of temperature

The effect of temperature on the corrosion rate of GA9 magnesium alloy was studied by measuring the corrosion rate at different temperatures between 30 °C – 50 °C. Figures 3.4 and 3.5 represent the potentiodynamic polarization curves and Nyquist plots respectively, at different temperatures for the corrosion of GA9 magnesium alloy sample in 1.0 M NaCl solution. Similar plots were obtained in other concentrations of the solutions also.
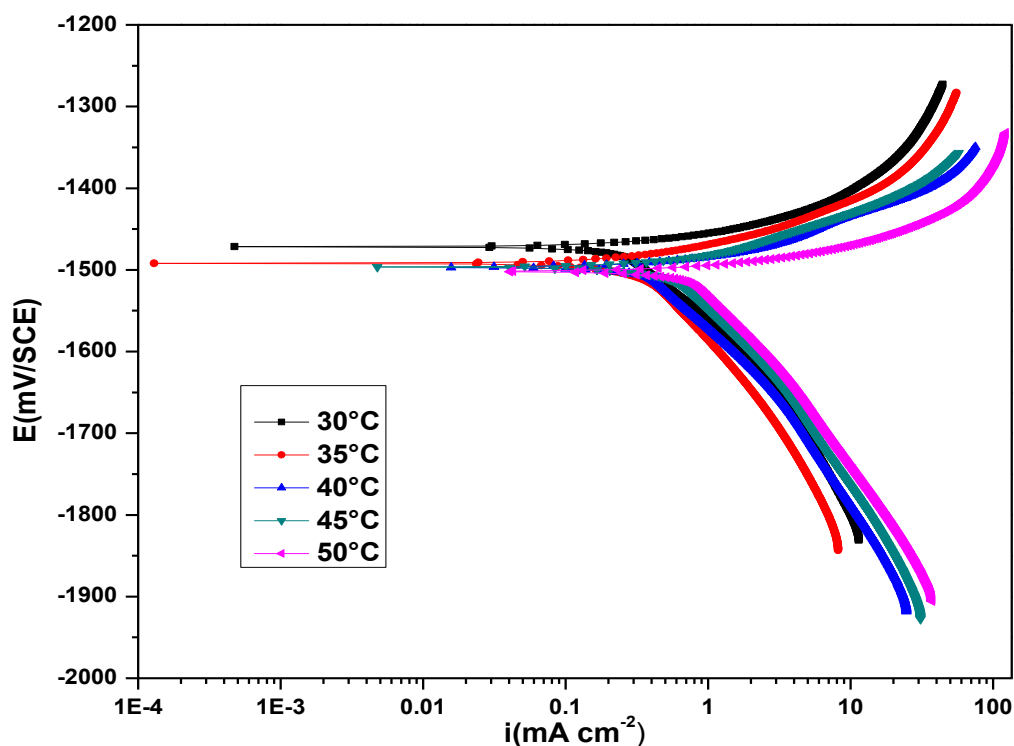
Fig. 3.4: Potentiodynamic polarization curves for the corrosion of GA9 magnesium alloy in 1.0 M NaCl solution at different temperatures.
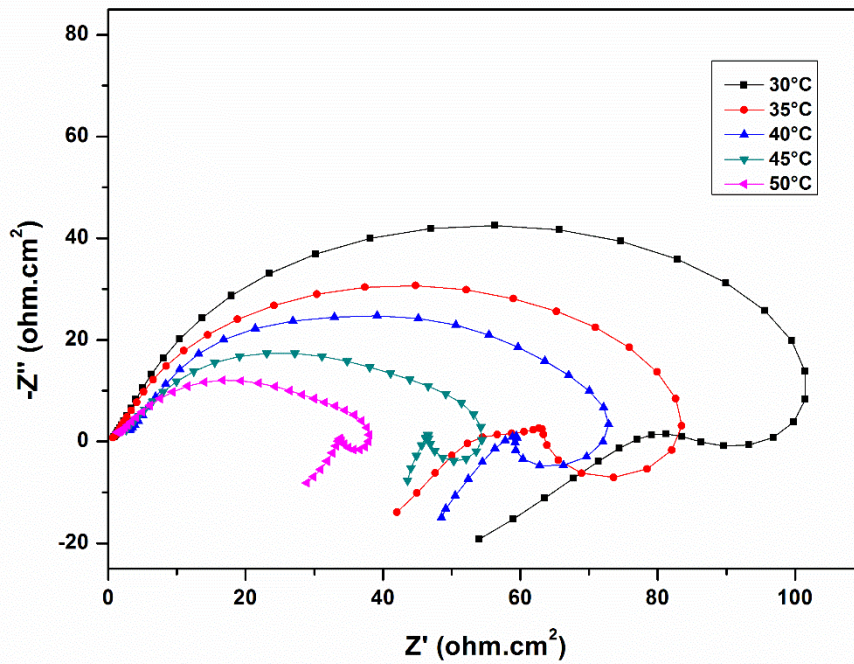
Fig. 3.5: Nyquist plots for the corrosion of GA9 magnesium alloy in 1.0 M NaCl solution at different temperatures.
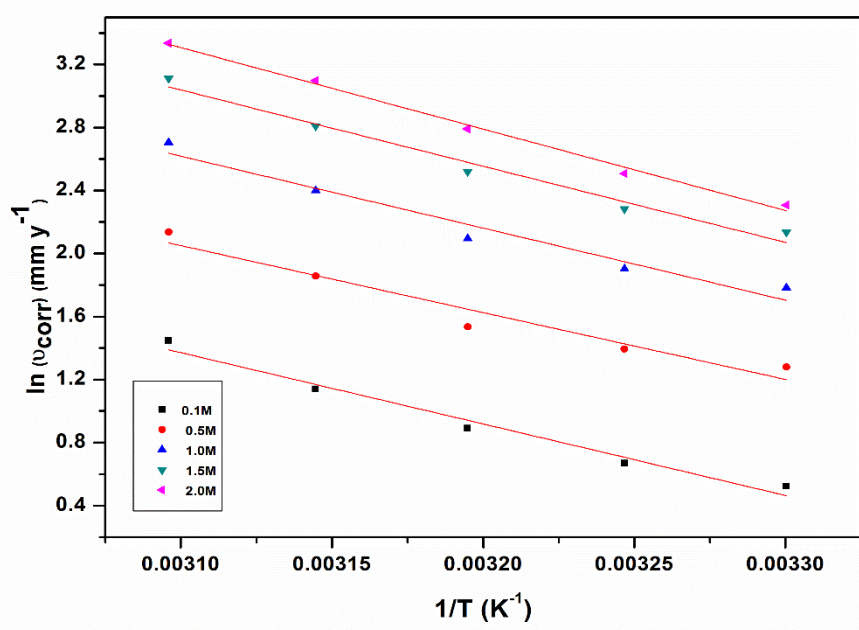
Fig. 3.6: Arrhenius plots for the corrosion of GA9 magnesium alloy in NaCl solution of different concentrations.
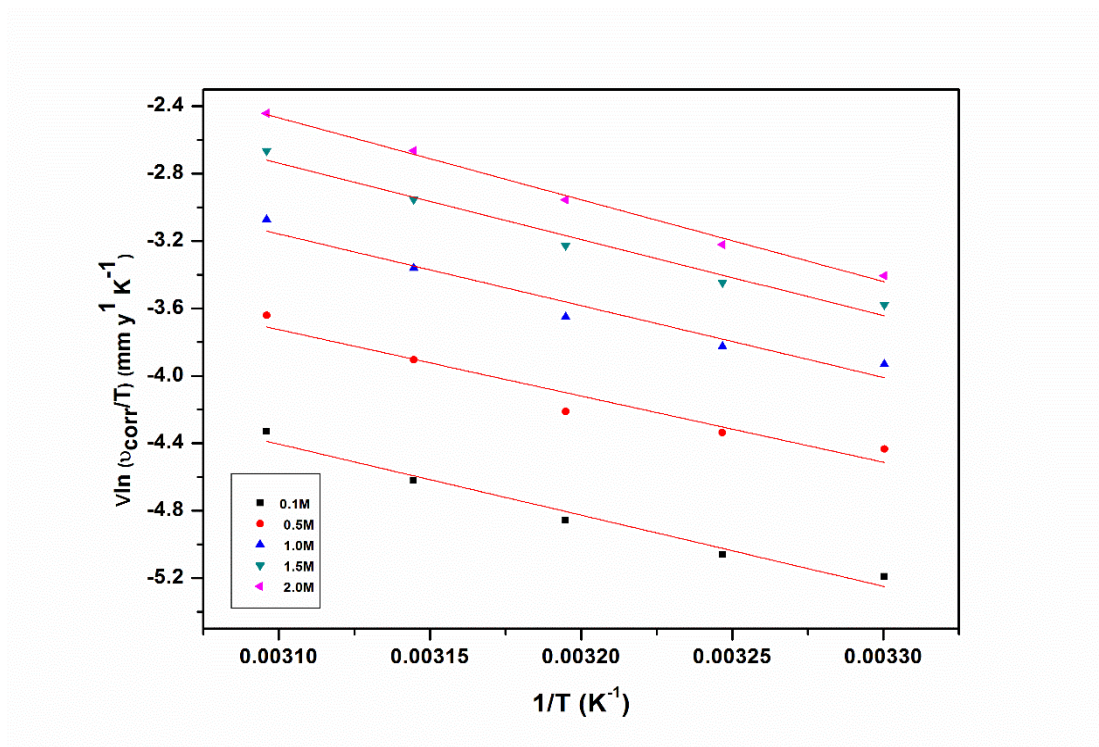
Fig. 3.7: Plots of ln(υcorr/T) vs 1/T for the corrosion of GA9 magnesium alloy in NaCl solution of different concentrations.

The Tafel polarization results and EIS results at different temperatures are listed in Tables 3.1 and 3.2, respectively. From the Figures 3.4 and 3.5, and also from the results presented in Tables 3.1 and 3.2, it is seen that the corrosion rate increases with the increase in temperature. The values of b_c and R_{ct} change with the change in temperature, which indicative of the fact that temperature play an influential role in the kinetics of the corrosion reactions. However, the basic shape of polarization curves and Nyquist plots remain unaltered, which illustrates that temperature modifies only the rate of the alloy corrosion but not the mechanism.

The variation of corrosion rate with temperature follows Arrhenius equation (Eqn. 2.6), which was utilized to calculate the activation energy (E_a). Enthalpy of activation ($\Delta H^{\#}$) and entropy of activation ($\Delta S^{\#}$) were calculated using transition state equation (Eqn. 2.7) from the plots of ln(υ_{corr}/T) vs 1/T. The Arrhenius plots for the corrosion of GA9 magnesium alloy in sodium chloride media are shown in Fig.3.6. The plots of ln(υ_{corr}/T) vs 1/T are shown in the Fig. 3.7. The activation parameters calculated are listed in Table 3.3. The activation energy values indicate that the

corrosion of the alloy is controlled by a surface reaction, since the values of the activation energy for the corrosion process is greater than 20 kJmol^{-1} (Bouklah et al. 2005). The entropy of activation is negative. This implies that in the rate-determining step, the activated complex represents association rather than dissociation, indicating a decrease of randomness taking place on going from the reactants to the activated complex (Prabhu et al. 2007).

3.1.4 Effect of concentration

It is clear from the Table 3.1 and 3.2 as well as from the polarisation curves (Fig .3.1) and Nyquist plots (Fig. 3.2) that the corrosion rate of GA9 magnesium alloy increases with increase in sodium chloride concentration. The E_{corr} value slightly shift to more negative side as the concentration of chloride ion increases. There is no significant change in the values of b_c for the alloy specimen with change in concentration of sodium chloride, which implies that, there is no change in corrosion reaction mechanism with change in chloride ion concentration. This fact is supported by similar shapes of polarisation curves at different concentrations of sodium chloride.

3.1.5 Scanning electron microscopy (SEM)/EDX studies

The scanning electron microscope images were recorded to establish the interaction of sodium chloride solution with the metal surface. The SEM image of a freshly polished surface of GA9 magnesium alloy sample is given in Fig.3.8 (a), which shows the uncorroded surface with a few scratches due to polishing. Fig.3.8 (b) shows the SEM image of GA9 magnesium alloy surface after immersed in 2.0 M NaCl. The SEM images reveal that the specimen not immersed in the chloride solutions is in a better condition having a smooth surface while the metal surface immersed in 2.0 M NaCl is deteriorated due to the chloride action with metal surface.

EDX survey spectra were used to determine the surface composition of the specimens before and after exposure to the sodium chloride solution. Fig. 3.9(a) reveals the fresh surface of the GA9 alloy specimen with an intense peak of Mg. The Fig. 3.9(b) shows that the Mg peaks is considerably suppressed relative to the fresh specimen. Also, a peak for chlorine is observed in Fig. 3.9(b), indicating the presence of chloride ions on the metal surface as part of the corrosion product.
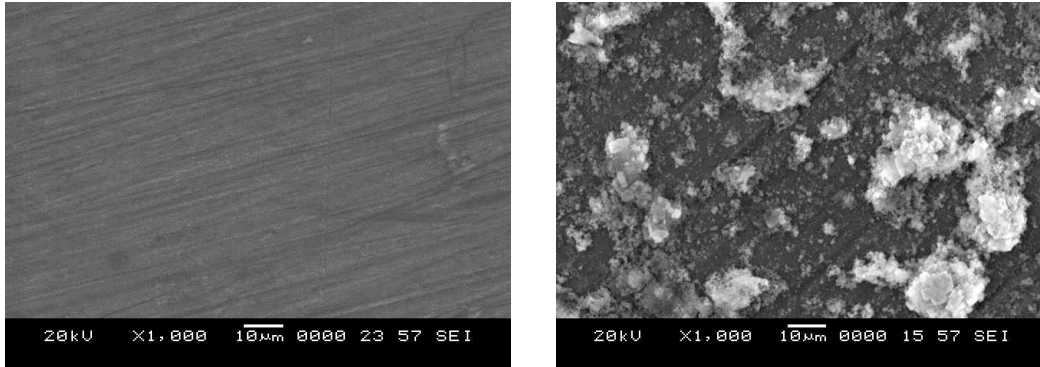
Fig. 3.8: SEM images of (a) Freshly polished surface (b) Corroded surface
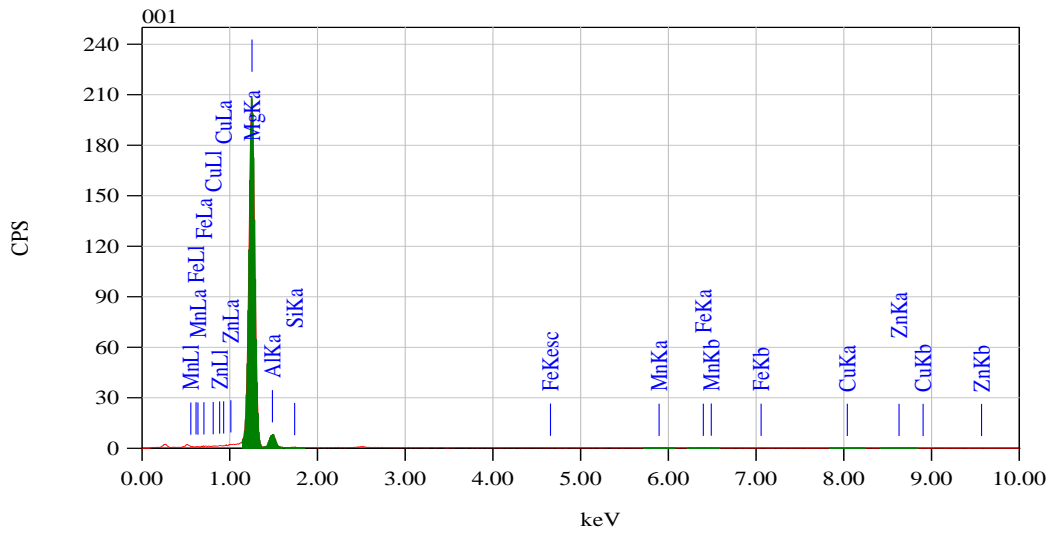
Figure 3.9 (a): EDX spectra of the freshly polished surface.
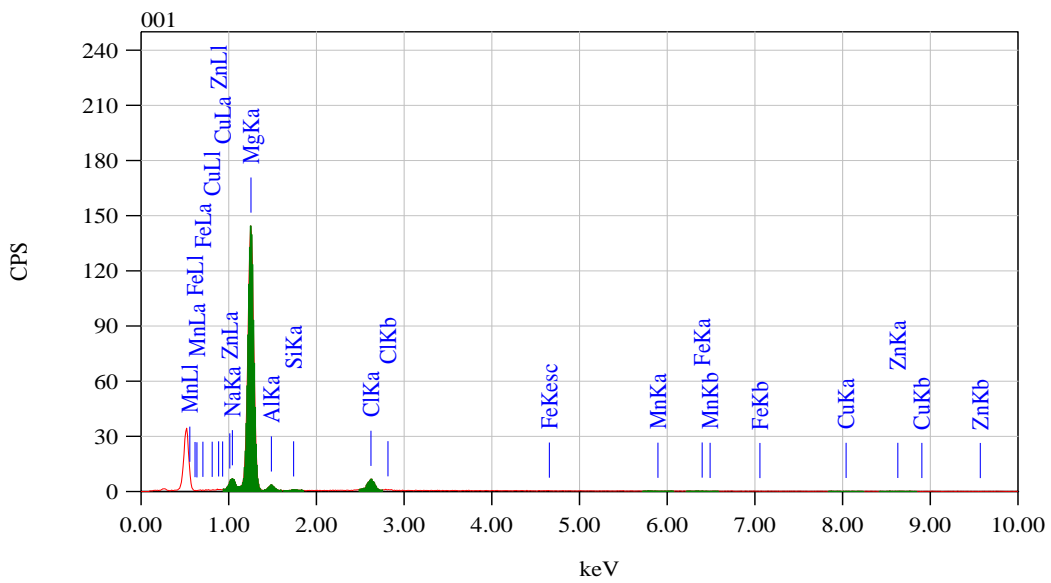
Figure 3.9 (b): EDX spectra of the corroded surface.

Table 3.1: Electrochemical polarization parameters for the corrosion of GA9 magnesium alloy in different concentrations of NaCl at different temperatures.

Molarity of NaCl	Temperature K	$-E_{corr}$ (mV vs SCE)	$-b_c$ (mV dec^{-1})	i_{corr} (μA cm^{-2})	υ_{corr} (mm y^{-1})
0.1M	303	1449	149	75.1	1.687
	308	1445	156	86.9	1.952
	313	1450	164	108.4	2.435
	318	1465	169	139.1	3.126
	323	1472	173	189.3	4.254
0.5M	303	1451	152	160.0	3.595
	308	1473	158	179.3	4.029
	313	1466	167	206.6	4.641
	318	1490	171	285.1	6.405
	323	1497	175	377.1	8.473
1.0M	303	1474	156	264.5	5.942
	308	1495	162	298.9	6.716
	313	1496	169	361.5	8.122
	318	1496	177	491.0	11.031
	323	1501	179	665.6	14.955
1.5M	303	1497	169	376.5	8.458
	308	1499	173	436.5	9.802
	313	1519	181	552.6	12.416
	318	1520	195	738.2	16.585
	323	1529	210	999.6	22.458
2.0M	303	1524	192	447.5	10.055
	308	1525	195	546.9	12.286
	313	1529	206	726.0	16.310
	318	1530	213	986.2	22.157
	323	1535	222	1249.8	28.078

Table 3.2: Impedance parameters for the corrosion of GA9 magnesium alloy in different concentrations of NaCl at different temperatures.

Molarity of NaCl	Temperature K	R_{ct} (Ω cm^2)	C_{dl} (μF cm^{-2})	υ_{corr} (mm y^{-1})
0.1M	303	361.5	11.29	1.619
	308	302.5	11.41	1.935
	313	245.4	15.20	2.385
	318	184.5	23.51	3.172
	323	132.8	28.95	4.409
0.5M	303	162.9	26.17	3.592
	308	147.0	27.21	3.982
	313	127.3	28.63	4.597
	318	91.0	35.08	6.429
	323	70.8	40.33	8.272
1.0M	303	99.7	33.50	5.869
	308	87.4	34.93	6.697
	313	72.8	39.91	8.042
	318	52.7	66.70	11.097
	323	39.0	77.59	15.021
1.5M	303	67.9	41.61	8.617
	308	60.2	61.15	9.730
	313	47.5	69.81	12.337
	318	35.5	89.49	16.487
	323	26.3	107.44	22.279
2.0M	303	58.5	58.01	10.012
	308	48.2	65.11	12.144
	313	36.2	83.99	16.192
	318	26.4	109.41	22.207
	323	21.1	123.26	27.818

Table 3.3: Activation parameters for the corrosion of GA9 magnesium alloy in NaCl media.

Molarity of NaCl	Ea (KJ mol^{-1})	$\Delta H^{\#}$ (kJ mol^{-1})	$\Delta S^{\#}$(J mol^{-1} K^{-1})
0.1M	37.67	35.07	-125.49
0.5M	35.31	32.71	-127.16
1.0M	37.98	35.38	-114.14
1.5M	40.24	37.64	-103.66
2.0M	42.98	40.39	-92.91

3.2 CORROSION BEHAVIOUR OF GA9 MAGNESIUM ALLOY IN SODIUM SULPHATE MEDIUM

3.2.1 Potentiodynamic polarization studies

Fig. 3.10 represents the potentiodynamic polarization curves for the corrosion of GA9 magnesium alloy in sodium sulphate solutions of different concentrations at 40℃. Similar plots were obtained at other temperatures also. The potentiodynamic polarization parameters are summarised in the Table 3.4. The corrosion current density (i_{corr}) increases with the increase in the concentration of sodium sulphate in the solution. The values of b_c change with the increase in sodium sulphate concentration, indicating the influence of sodium sulphate concentration on the kinetics of hydrogen evolution.
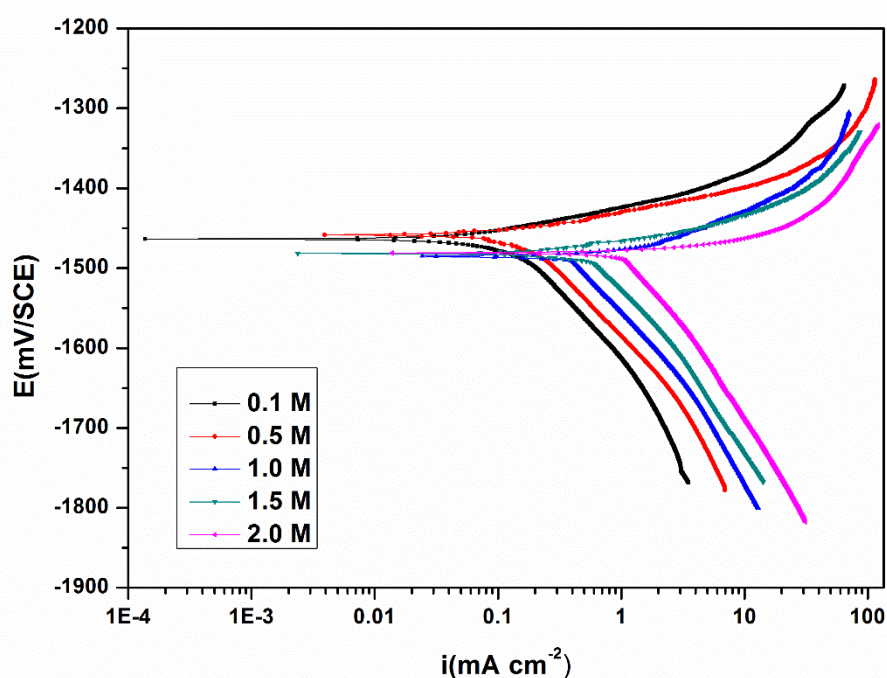
Fig. 3.10: Potentiodynamic polarisation curves for the corrosion of GA9 magnesium alloy in different concentrations of Na$_2$SO$_4$ at 40 °C.

From the data summarized in Table 3.4 it is observed that the corrosion rate of GA9 magnesium alloy increases with the increase in the concentration of sulphate ion in the solution. It is also observed from the results that the corrosion potential is shifted towards more negative values as the concentration of sulphate ion is increased. The polarisation curves did not exhibit Tafel behaviour in the anodic branch. Even though

sulphate is regarded as a mild corrosive compared to chloride, sulphate has been reported to possess an appreciable influence on the electrochemical behaviour of pure magnesium and some of its alloys (Song et al. 1997, Baril et al. 2001). The corrosiveness of these ions towards magnesium and its alloys arises from their tendency to cause surface film breakdown by the dissolution of the deposited corrosion product.

3.2.2 Electrochemical impedance spectroscopy (EIS) studies

Nyquist plots for the corrosion of GA9 magnesium alloy in different concentrations of Na_2SO_4 at 40 °C are shown in Fig. 3.11. Similar results were obtained at other four temperatures also.The graphs obtained by EIS were characterized by a capacitive loop, extended from high frequency (HF) to low frequency (LF) range, an inductive loop in the low frequency region (LF) range and a tail at the medium frequency (MF) range (Arrabal et al. 2012, Chen et al. 2007, Baril et al. 2001). The plots are similar in their shape to the one obtained for the corrosion of the alloy in chloride medium. The enlargement of capacitive loops reflects reduced rate corrosion (Pebere et al. 1994). It is evident from Fig.3.10 that the capacitive loops enlarge with reduced concentrations of sulphate ions; implying that the corrosion rate decreases with the reduction in these ion concentrations.
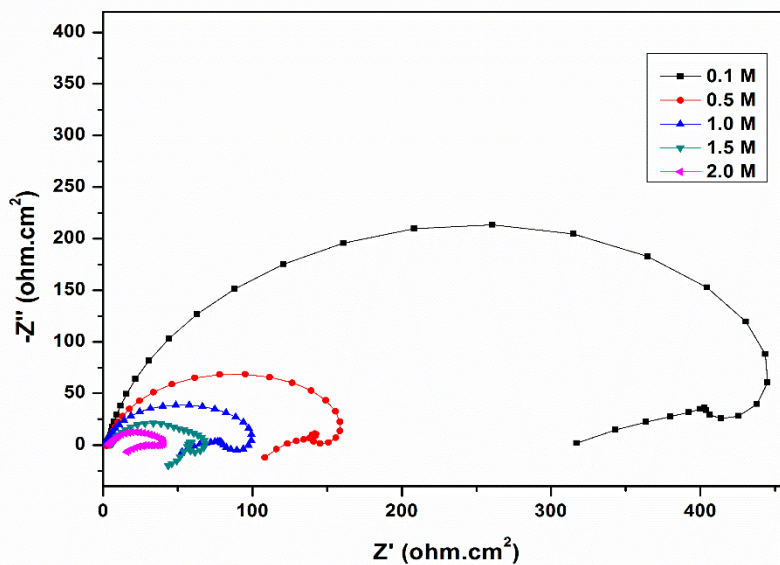
Fig. 3.11: Nyquist plots for the corrosion of GA9 magnesium alloy in different concentrations of Na_2SO_4 at 40 ^{0}C.

The equivalent circuit used for the corrosion of the alloy in NaCl medium shown in the Fig. 3.3 is used to fit the experimental data in the sodium sulphate medium also. The calculated values of $R_{ct,}$ C_{dl} and corrosion rate (υ_{corr}) are listed in Table 3.5. The values of charge transfer resistance (R_{ct}) decreases and that of the double layer capacitance (C_{dl}) increases with the increase in the concentrations of sodium sulphate, indicating an increase in the corrosion rate with the increase in the concentration of sodium sulphate. This is in agreement with the results of potentiodynamic polarization studies.

3.2.3 Effect of temperature

Fig. 3.12 and Fig.3.13 represent the potentiodynamic polarization curves and Nyquist plots, respectively, at different temperatures, for the corrosion of GA9 magnesium alloy specimen in 1.0 M Na_2SO_4 solution. Similar plots were obtained in other concentrations of the solutions also. It is clear from the data presented in the Tables 3.4 and 3.5 that the corrosion rate of GA9 magnesium alloy increases with the increase in the temperature of sodium sulphate medium. The values of b_c and R_{ct} change with the varying temperature, which indicate that temperature play an influential role in the kinetics of the corrosion reactions. However the basic shape of polarization curves and Nyquist plots remain unaltered, which illustrates that temperature modifies only the rate of the alloy corrosion but not the mechanism.
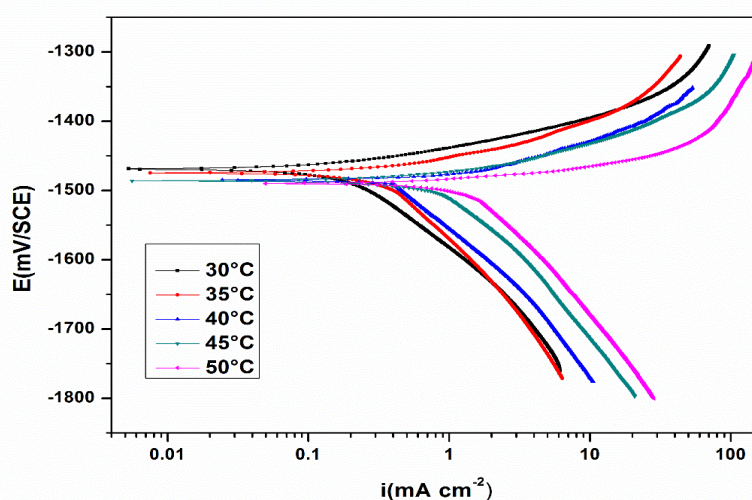
Fig. 3.12: Potentiodynamic polaristion curves for the corrosion of GA9 magnesium alloy in 1.0 M Na₂SO₄ solution at different temperatures.
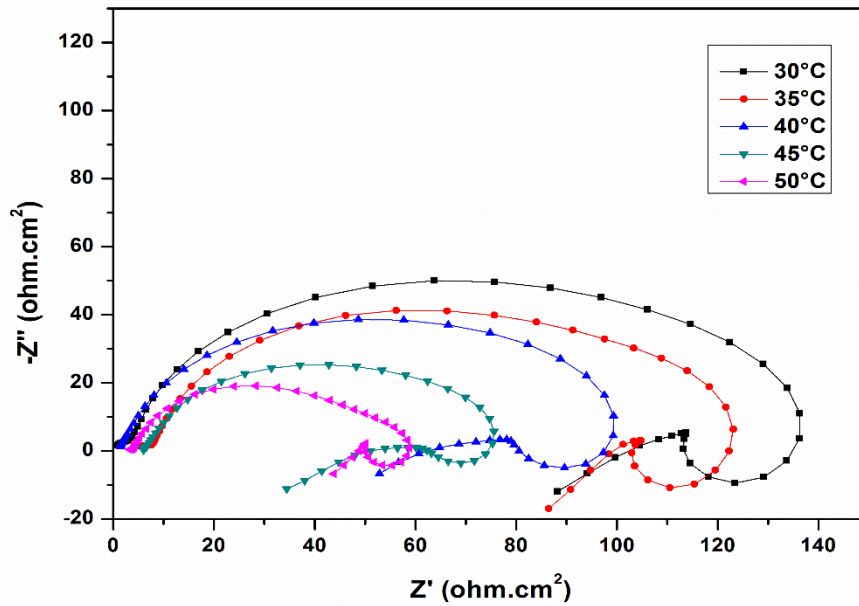
Fig. 3.13: Nyquist plots for the corrosion of GA9 magnesium alloy in 1.0 M Na₂SO₄ solution at different temperatures.

The Arrhenius plots for the corrosion of GA9 magnesium alloy in sodium sulphate solutions of different concentrations are shown in Fig.3.14. The plots of ln(v_{corr}/T) versus *1/T* for the GA9 magnesium alloy in different concentrations of sodium sulphate are shown in Fig. 3.15.
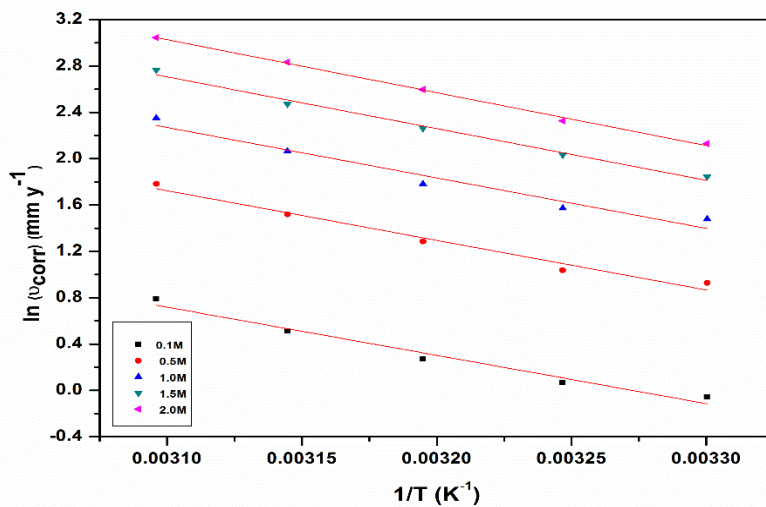
Fig. 3.14: Arrhenius plots for the corrosion of GA9 magnesium alloy in Na₂SO₄ solutions of different concentrations.

74
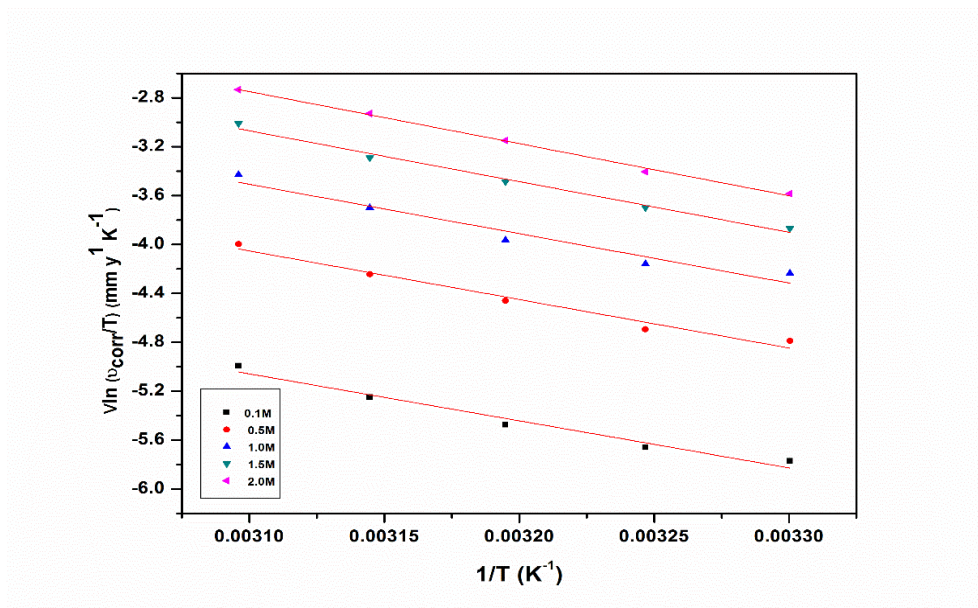
Fig. 3.15: Plots of ln(υ_{corr} / T) vs 1/ T for the corrosion of GA9 magnesium alloy in Na$_2$SO$_4$ solutions of different concentrations.

The activation parameters calculated are listed in Table 3.6. The E_a value for the occurrence of corrosion reaction increases with the increased sulphate concentrations. The entropy of activation $\Delta S^{\#}$ is negative; implying that the activated complex in the rate-determining step represents association rather than dissociation, indicating that a decrease in randomness takes place on going from the reactants to the activated complex (Bentiss et al. 2005).

3.2.4 Effect of concentration

It is clear from the Table 3.3 and 3.4 as well as from the polarisation curves (Fig .3.10) and Nyquist plots (Fig. 3.11) that the corrosion rate of GA9 magnesium alloy increases with increase in sodium sulphate concentration. The E_{corr} value slightly shift to more negative side as the concentration of sulphate ion increases. There is no significant change in the values of b_c for the alloy specimen with change in concentration of sodium sulphate, which implies that, there is no change in corrosion reaction mechanism with change in sulphate ion concentration.

3.2.5 Scanning electron microscopy (SEM)/EDX studies

The surface morphology of GA9 magnesium alloy specimen immersed in 2.0 M sodium sulphate solution was compared with that of the non-corroded element by

recording their SEM images. The SEM image of a freshly polished surface of the GA9 magnesium alloy sample is given in Fig.3.16 (a), which shows the non-corroded surface with few scratches due to polishing. Fig.3.16 (b) shows the SEM image of GA9 magnesium alloy surface after immersion in 2.0 M sodium sulphate. The SEM images reveal that the specimen not immersed in the sodium sulphate solution is in a better condition having a smooth surface while the metal surface immersed in sodium sulphate is deteriorated due to the sulphate ion action.
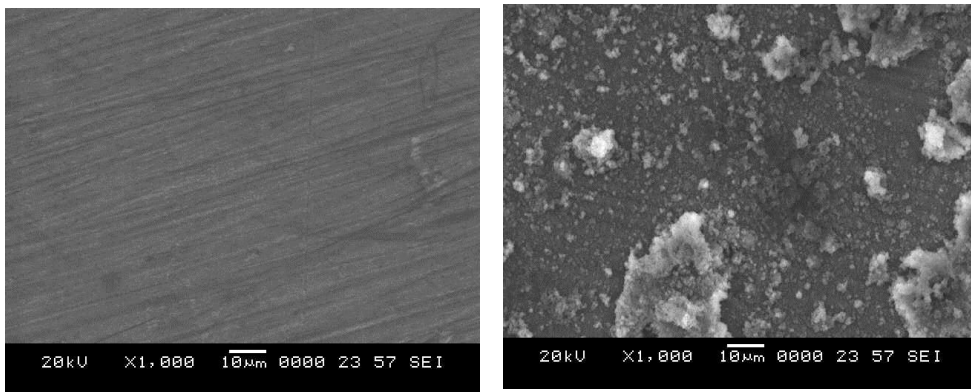
Fig. 3.16: SEM images of (a) Freshly polished surface (b) Corroded surface.

EDX survey spectra were used to determine the surface composition of the specimens before and after exposure to the sodium sulphate solution. The Fig. 3.17 shows that the Mg peaks are considerably suppressed relative to the fresh specimen. Also, a peak for sulphur is observed in Fig. 3.17, indicating the presence of sulphate on the metal surface as part of the corrosion product.
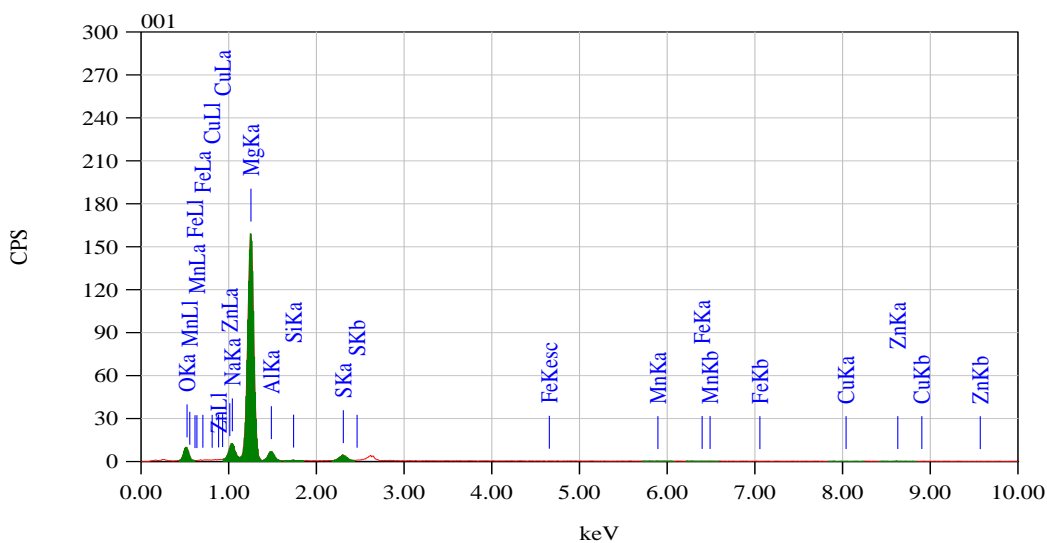
Fig. 3.17: EDX spectra of the corroded surface.

Table 3.4: Electrochemical polarization parameters for the corrosion of GA9 magnesium alloy in different concentrations of Na₂SO₄ at different temperatures.

Molarity of Na$_2$SO$_4$	Temperature K	-E$_{corr}$ (mV vs SCE)	-b$_c$ (mV dec^{-1})	i$_{corr}$ (μA cm^{-2})	υ$_{corr}$ (mm y^{-1})
0.1M	303	1456	139	42.1	0.946
	308	1461	144	47.7	1.071
	313	1463	151	58.4	1.311
	318	1468	159	74.4	1.671
	323	1469	167	97.8	2.197
0.5M	303	1461	144	112.4	2.526
	308	1462	149	125.5	2.819
	313	1459	156	161.1	3.619
	318	1475	164	203.3	4.568
	323	1487	173	264.3	5.939
1.0M	303	1472	151	195.2	4.386
	308	1477	156	214.2	4.813
	313	1486	160	264.3	5.938
	318	1487	171	350.4	7.872
	323	1490	181	466.3	10.477
1.5M	303	1477	158	281.7	6.328
	308	1483	165	339.2	7.621
	313	1482	173	426.8	9.589
	318	1486	182	527.1	11.843
	323	1492	194	707.4	15.894
2.0M	303	1488	169	374.6	8.417
	308	1483	176	455.4	10.232
	313	1481	185	597.1	13.415
	318	1489	197	755.8	16.981
	323	1499	209	927.7	20.842

Table 3.5: Impedance parameters for the corrosion of GA9 magnesium alloy in different concentrations of Na₂SO₄ at different temperatures.

Molarity of Na$_2$SO$_4$	Temperature K	R_{ct} (Ω cm^2)	C_{dl} (μF cm^{-2})	υ_{corr} (mm y^{-1})
0.1M	303	604.7	10.53	0.968
	308	545.5	10.98	1.073
	313	447.8	11.35	1.307
	318	356.5	16.50	1.642
	323	273.0	25.71	2.144
0.5M	303	219.1	18.29	2.672
	308	200.4	22.81	2.921
	313	165.0	26.11	3.547
	318	128.8	30.77	4.545
	323	97.8	34.19	5.984
1.0M	303	139.0	30.91	4.212
	308	122.6	32.17	4.775
	313	97.4	40.62	6.012
	318	72.1	45.05	8.122
	323	55.5	56.30	10.539
1.5M	303	91.6	34.56	6.389
	308	77.7	40.12	7.537
	313	62.4	54.17	9.381
	318	48.7	71.38	12.015
	323	37.5	88.74	15.621
2.0M	303	67.5	42.55	8.674
	308	57.4	50.87	10.198
	313	43.2	69.58	13.552
	318	34.0	85.41	17.212
	323	27.8	102.33	21.059

Table 3.6: Activation parameters for the corrosion of GA9 magnesium alloy in Na$_2$SO$_4$ media.

Molarity of Na$_2$SO$_4$	Ea (KJ mol^{-1})	$\Delta H^{\#}$ (kJ mol^{-1})	$\Delta S^{\#}$(J mol^{-1} K^{-1})
0.1M	34.57	31.97	-140.53
0.5M	35.60	32.99	-128.98
1.0M	36.22	33.62	-122.51
1.5M	37.09	34.49	-116.19
2.0M	37.75	35.15	-111.50

3.3 INFLUENCE OF pH ON THE CORROSION OF GA9 MAGNESIUM ALLOY IN SODIUM CHLORIDE MEDIUM

The effect of pH on the corrosion and electrochemical behaviour of GA9 alloy was studied in NaCl solutions of different concentrations (0.1, 0.5, 1.0, 1.5 and 2.0 M) and pH values (3, 5, 7, 9 and 12). Fig. 3.18 and Fig. 3.19 represent the potentiodynamic polarization curves and Nyquist plots, respectively, for the corrosion of GA9 magnesium in 2.0 M in NaCl with varying pH, at 30 ^{0}C. Similar plots were obtained in NaCl solutions of other concentrations and at other temperatures also. The results confirm the influential role of the medium pH on GA9 alloy corrosion.
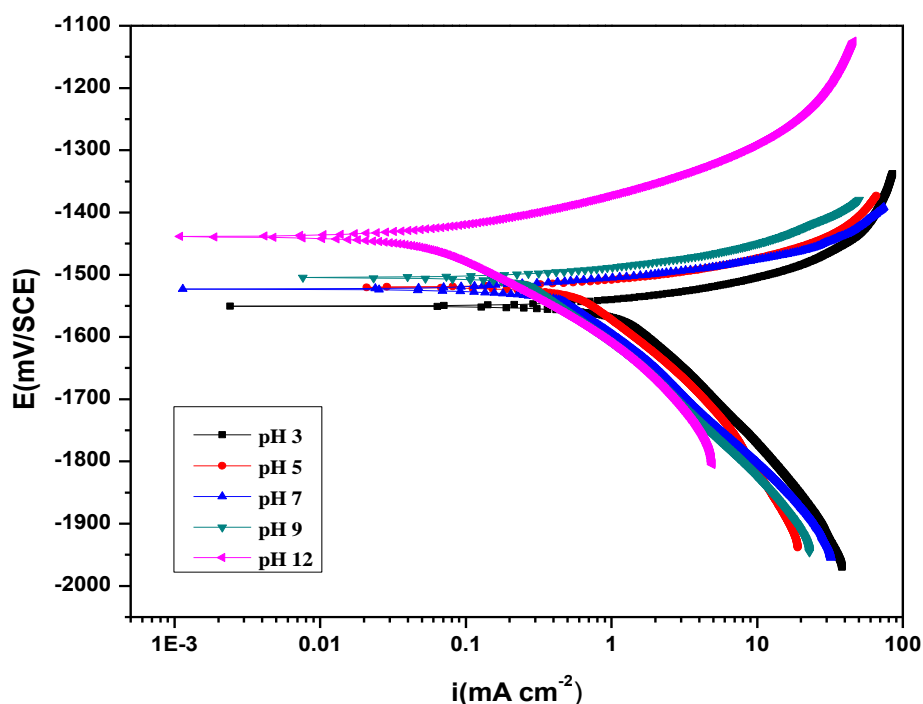
Fig. 3.18: Potentiodynamic polarization curves for the corrosion of GA9 magnesium alloy in 2.0 M NaCl solution of different pH at 30 ℃.

As seen from Fig. 3.18 polarization curves shift to the higher current density region, implying an increased corrosion rate as the medium pH decreases from highly alkaline (pH = 12) to highly acidic (pH = 3) conditions. A similar trend of a higher corrosion rate associated with a lower medium pH was observed at other chloride ion concentrations. The potentiodynamic polarization parameters like corrosion potential

(E_{corr}), corrosion current density (i_{corr}), cathodic slopes (b_c) and corrosion rate (v_{corr}) calculated at different pH in 2.0 M NaCl solution from Tafel plots are tabulated in Table 3.7. The corresponding impedance parameters are tabulated in Table 3.8.
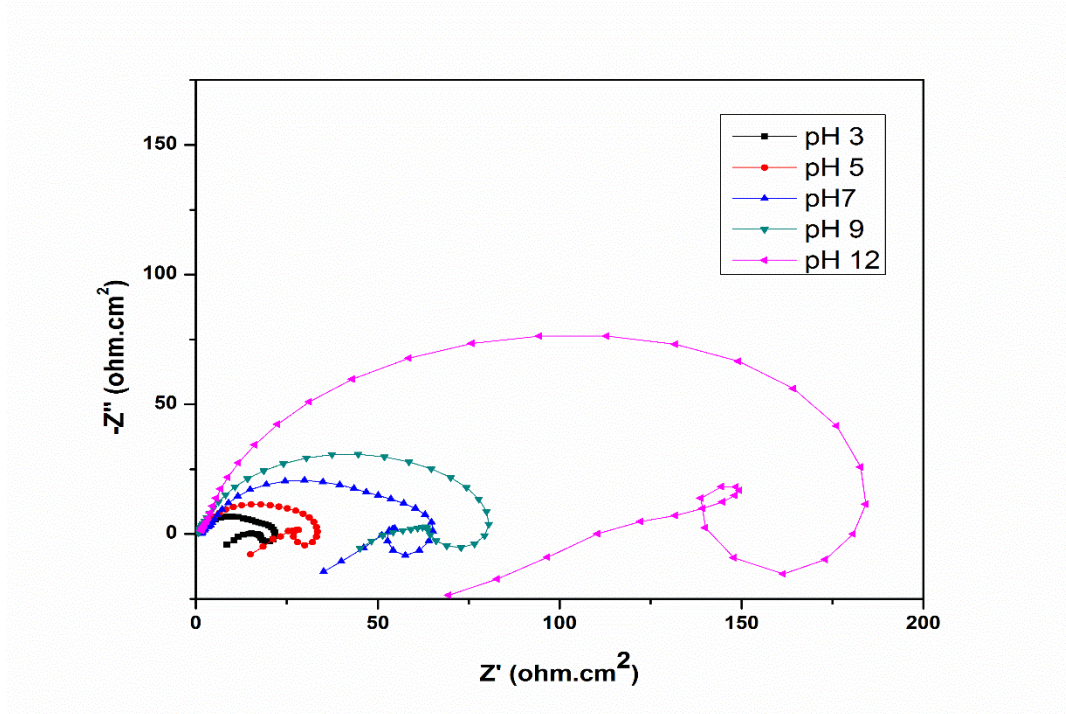
Fig. 3.19: Nyquist plot for GA9 magnesium alloy in 2.0 M NaCl solution of different pH at 30 ℃.

The Pourbaix diagram for pure magnesium as shown in Fig. 3.20, best explains the corrosion behaviour of magnesium and its alloys in a wide range of pH. This potential–pH plot represents the stability of metallic magnesium and its corrosion product magnesium hydroxide (Mg(OH)$_2$) as a function of the potential and pH (acidity or alkalinity) of aqueous solutions (Pourbaix 1974).

The corrosion reactions of magnesium can be summarized in following reactions:

$$Mg \rightarrow Mg^{2+} + 2e^- \tag{3.10}$$

$$2H_2O + 2e^- \rightarrow H_2 + 2OH^- \tag{3.11}$$

$$Mg^{2+} + 2OH^- \rightarrow Mg(OH)_2 \tag{3.12}$$

The anodic reaction involves dissolution of magnesium, the cathodic reaction is hydrogen evolution by the reduction of water. Due to the low solubility, Mg(OH)$_2$ precipitates forming a surface layer on the corroding metal. The Pourbaix diagram indicates the corrosion product, Mg(OH)$_2$, to be stable only in alkaline conditions, with

pH above 10.5. Even though Mg(OH)$_2$ is thermodynamically unstable at pH below 10.5, metallic magnesium can readily develop Mg(OH)$_2$ surface film even at acidic pH values, if the dissolution rate of Mg(OH)$_2$ is lower than the rate of its formation. Moreover, as a result of the cathodic reaction of hydroxyl ion generation, an alkaline pH zone develops at the electrode interface, which facilitates Mg(OH)$_2$ precipitation and film formation, even when bulk pH is acidic (Zhao et al. 2008).
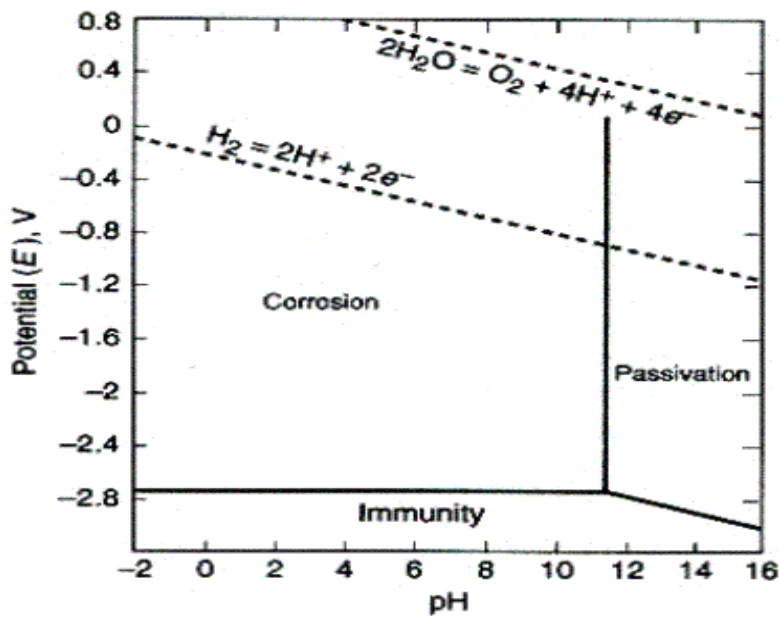
Fig. 3.20: Pourbaix diagram for pure magnesium.

With the understanding of the mechanism, it is safe to justify the observed trend of the increased corrosion rate of GA9 alloy with the decrease of pH at every medium concentration tested. At alkaline conditions the Mg(OH)$_2$ surface film is highly stable and protective, resulting in a reduced corrosive attack. Lowering the medium pH increases the solubility of the surface film, which accounts for high corrosion rates in acidic media. However, the corrosion rate observed in alkaline media is significant although small; this is because the Mg(OH)$_2$ surface film is thin with a Pilling-Bedworth ratio ~ 0.81 (Guo 2010) and the film is partially protective, hence incapable of imparting complete passivity to the underlying metal. Thus the corrosion reactions take place predominantly at the breaks and imperfections of the film (Song and Atrens 2003, 2007, 2010). Also, both E_{corr} and b_c, gradually change with varying pH, indicating

the influence of pH in the kinetics of cathodic hydrogen evolution and anodic metal dissolution reactions.

Figures 3.21(a), 3.21(b) and 3.22(c) are SEM images of the GA9 alloy surface after 3 hour of immersion in an acidic medium 2.0 M NaCl with pH 3, in neutral 2.0 M NaCl and alkaline 2.0 M NaCl with pH 12, respectively. From the figure, it can be seen that, at lower pH values, surface of the GA9 alloy was completely corroded, with the corrosion pits distributed all the over entire surface. The specimen immersed in a alkaline medium showed least deterioration of the surface, as presumed due to reduced dissolution of $Mg(OH)_2$. The EDX images of the corroded surface are shown in Figures 3.22(a), 3.22(b) and 3.22(c) for specimens immersed in an acidic, neutral and alkaline NaCl, respectively.
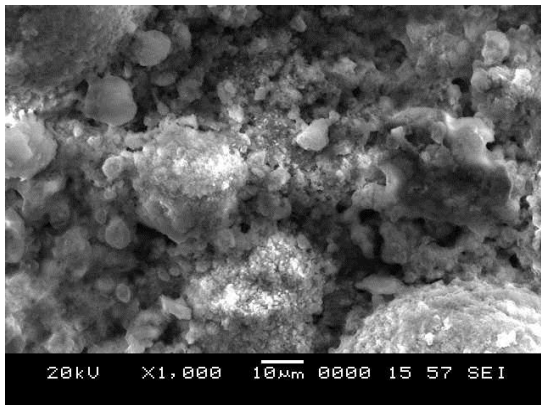
3.21(a)
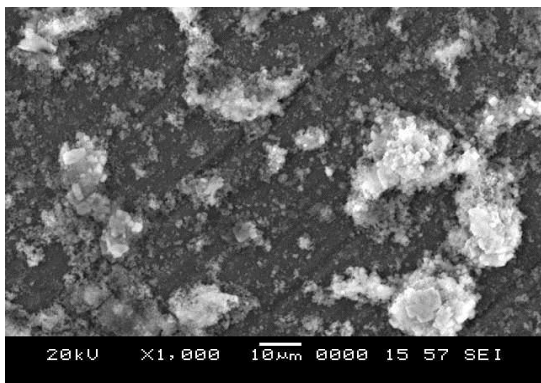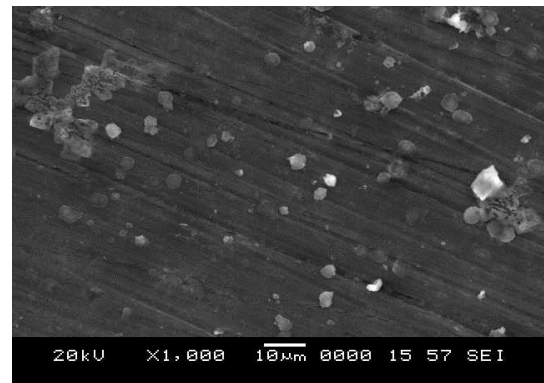
3.21(b)   **3.21(c)**

Fig. 3.21: SEM images of the corroded surfaces in (a) Acidic 2.0 M NaCl with pH 3 (b) Neutral 2.0 M NaCl (c) Alkaline 2.0 M NaCl with pH 12.
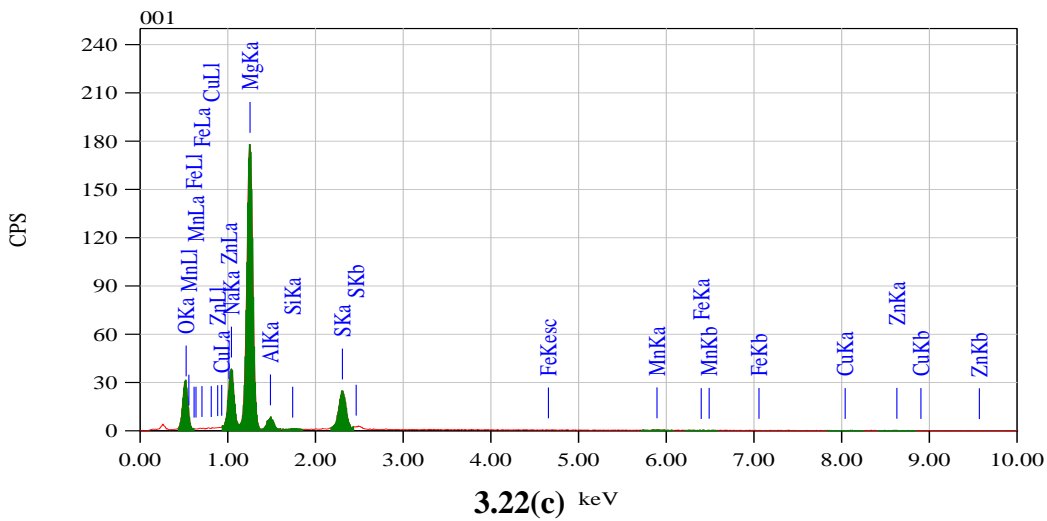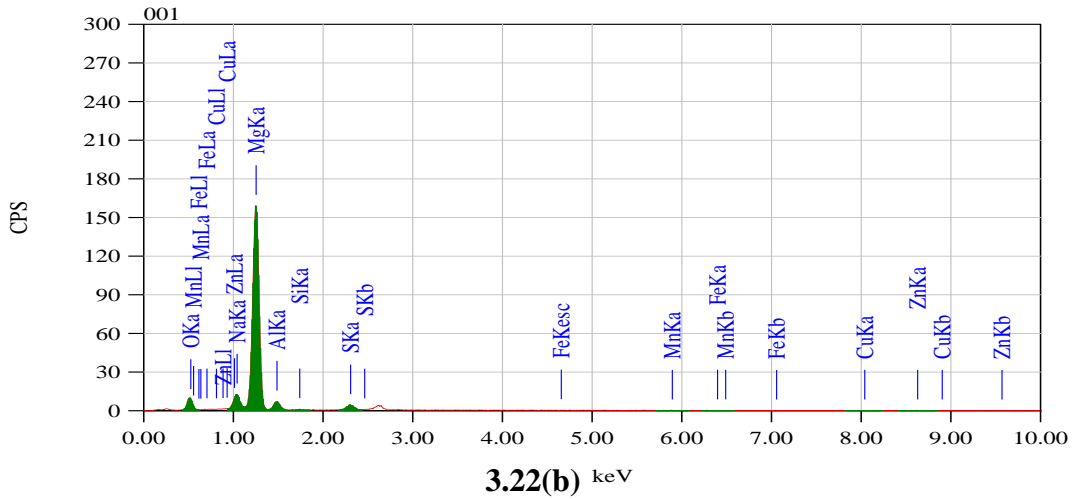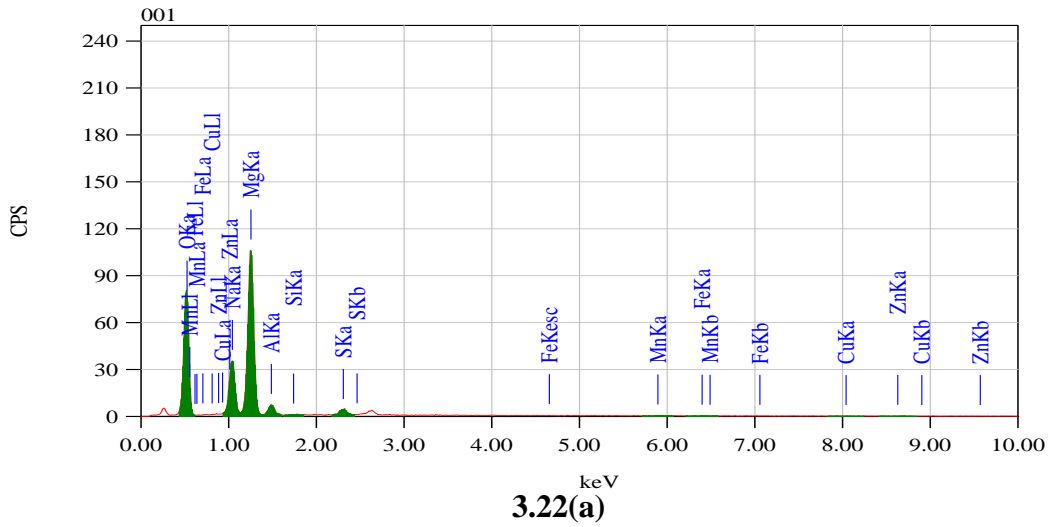
Fig. 3.22: EDX spectra of the corroded surfaces in (a) Acidic 2.0 M NaCl with pH 3 (b) Neutral 2.0 M NaCl (c) Alkaline 2.0 M NaCl with pH 12.

Table 3.7: Electrochemical polarization parameters for the corrosion of GA9 magnesium alloy in NaCl solutions of different concentrations at different pH at 30 °C.

Molarity of NaCl	pH	$-E_{corr}$ (mV vs SCE)	$-b_c$ (mV dec^{-1})	i_{corr} (μA cm^{-2})	υ_{corr} (mm y^{-1})
0.1M	3	1478	178	310.2	6.970
	5	1468	159	89.4	2.009
	7	1449	149	75.1	1.687
	9	1445	141	51.5	1.157
	12	1319	129	3.9	0.088
0.5M	3	1500	197	494.9	11.118
	5	1472	163	228.4	5.131
	7	1451	152	160.0	3.595
	9	1453	145	118.1	2.652
	12	1356	133	24.0	0.539
1.0M	3	1518	222	818.4	18.386
	5	1475	169	376.3	8.454
	7	1474	156	264.5	5.942
	9	1461	150	199.0	4.470
	12	1380	138	45.7	1.027
1.5M	3	1539	235	1082.2	24.314
	5	1501	185	556.1	12.494
	7	1497	169	376.5	8.458
	9	1474	161	301.7	6.779
	12	1426	145	96.8	2.175
2.0M	3	1548	253	1401.7	31.492
	5	1521	204	785.3	17.642
	7	1524	192	447.5	10.055
	9	1503	174	368.3	8.275
	12	1447	149	137.7	3.094

Table 3.8: Impedance parameters for the corrosion of GA9 Magnesium Alloy in NaCl solutions of different concentrations at different pH at 30 °C.

Molarity of NaCl	pH	R_{ct} (Ω cm^2)	C_{dl} (μF cm^{-2})	υ_{corr} (mm y^{-1})
0.1M	3	82.5	38.23	7.092
	5	279.8	12.87	2.092
	7	361.5	11.29	1.619
	9	496.9	10.51	1.178
	12	6727.0	8.01	0.087
0.5M	3	52.4	47.26	11.160
	5	117.7	30.52	4.972
	7	162.9	26.17	3.592
	9	217.2	18.36	2.695
	12	1062.0	9.92	0.551
1.0M	3	32.0	66.32	18.292
	5	67.4	45.09	8.684
	7	99.7	33.50	5.869
	9	129.6	29.98	4.515
	12	558.5	10.29	1.048
1.5M	3	23.8	87.96	24.547
	5	47.0	65.76	12.464
	7	67.9	41.61	8.617
	9	84.2	34.56	6.952
	12	264.1	16.33	2.216
2.0M	3	18.6	102.36	31.477
	5	34.0	88.12	17.211
	7	58.5	58.01	10.012
	9	69.0	42.65	8.482
	12	187.2	24.01	3.127

3.4 INFLUENCE OF pH ON THE CORROSION OF GA9 MAGNESIUM ALLOY IN SODIUM SULPHATE MEDIUM

The effect of pH on the corrosion and electrochemical behaviour of GA9 alloy was studied in Na_2SO_4 solutions of different concentrations (0.1, 0.5, 1.0, 1.5 and 2.0 M) and pH values (3, 5, 7, 9 and 12). Fig. 3.23 and Fig. 3.24 represent the potentiodynamic polarization curves and Nyquist plots, respectively, for the corrosion of GA9 magnesium in 2.0 M in Na_2SO_4 with gradually varying pH, at 30 ^{0}C. Similar plots were obtained in Na_2SO_4 solutions of other concentrations and at other temperatures also. The results confirm the influential role of the medium pH on GA9 alloy corrosion.
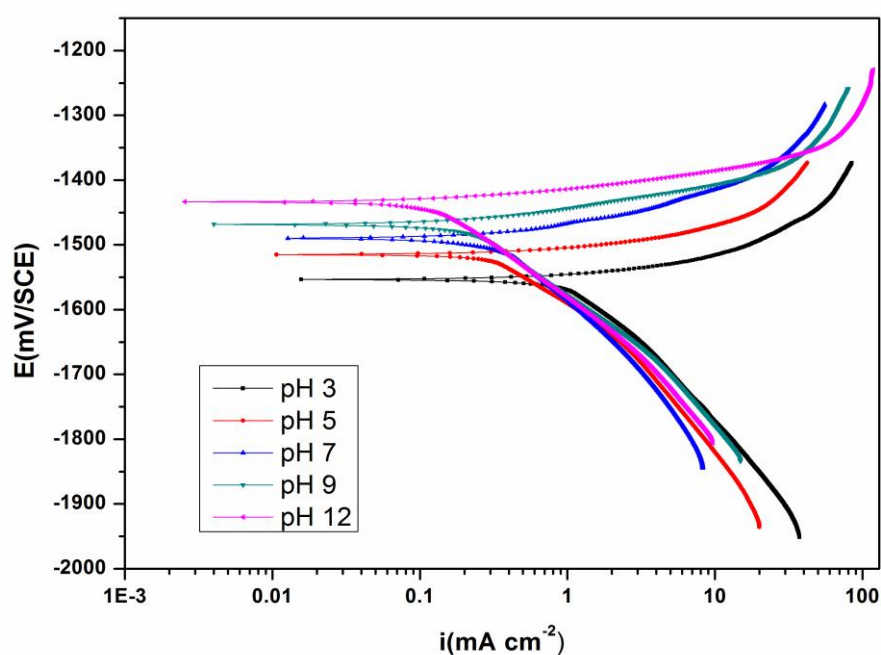
Fig. 3.23: Potentiodynamic polarization curves for the corrosion of GA9 magnesium alloy in 2.0 M Na_2SO_4 solution of different pH at 30 ℃.

As seen from Fig. 3.23 polarization curves shift to the higher current density region, implying an increased corrosion rate as the medium pH decreases from highly alkaline (pH=12) to highly acidic (pH=3) conditions. A similar trend of a higher corrosion rate associated with a lower medium pH was observed at other sulphate ion concentrations. The potentiodynamic polarization parameters like corrosion potential (E_{corr}), corrosion current density (i_{corr}), cathodic slopes (b_c) and corrosion rate (v_{corr})

calculated at different pH in Na_2SO_4 solutions of different concentrations from Tafel plots are tabulated in Table 3.9. The corresponding impedance parameters are tabulated in Table 3.10.
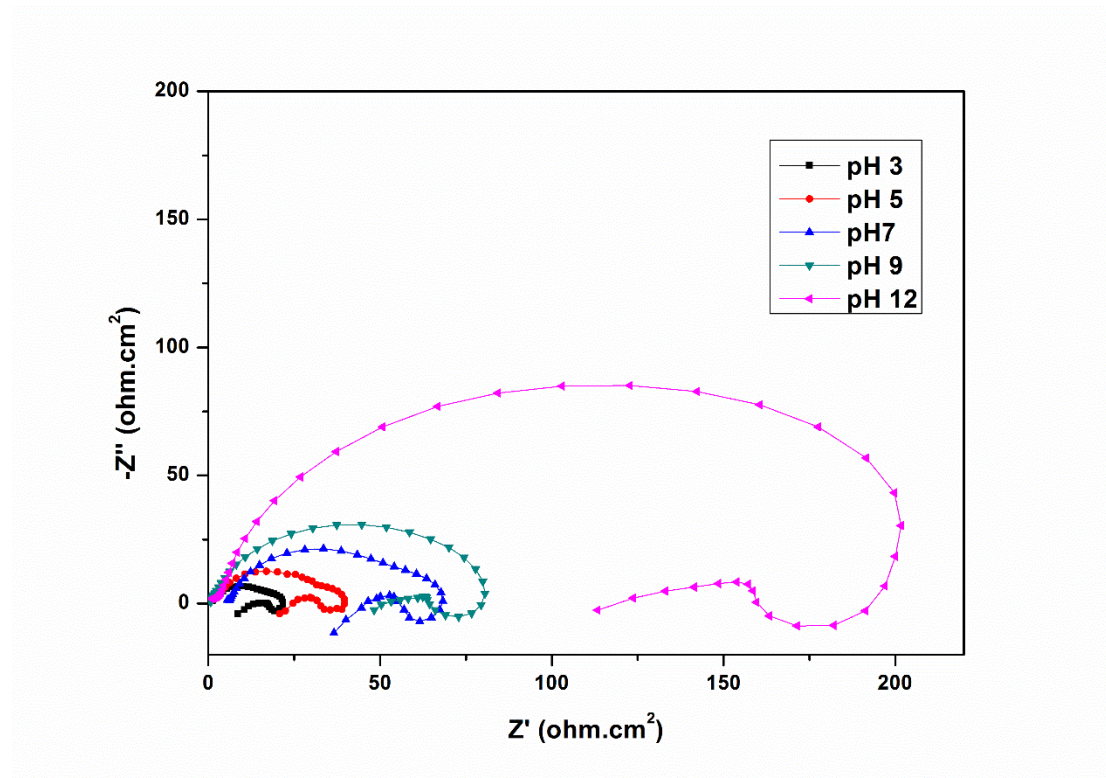
Fig. 3.24: Nyquist plots for the corrosion of GA9 magnesium alloy in 2.0 M Na_2SO_4 solution of different pH at 30 °C.

Figures 3.25(a), 3.25(b) and 3.25(c) are SEM images of the GA9 alloy surface after 3 hour of immersion in an acidic medium 2.0 M Na_2SO_4 with pH 3, in neutral 2.0 M Na_2SO_4 and alkaline 2.0 M Na_2SO_4 with pH 12 respectively. From the figures, it can be seen that, at lower pH values, surface of the GA9 alloy was completely corroded, with the corrosion pits distributed on the entire surface. The specimen immersed in a alkaline medium showed the least deterioration of the surface, as presumed due to reduced dissolution of $Mg(OH)_2$. The EDX images of the corroded surface are shown in figures 3.26(a), 3.26(b) and 3.26(c) for specimens immersed in an acidic, neutral and alkaline Na_2SO_4, respectively.
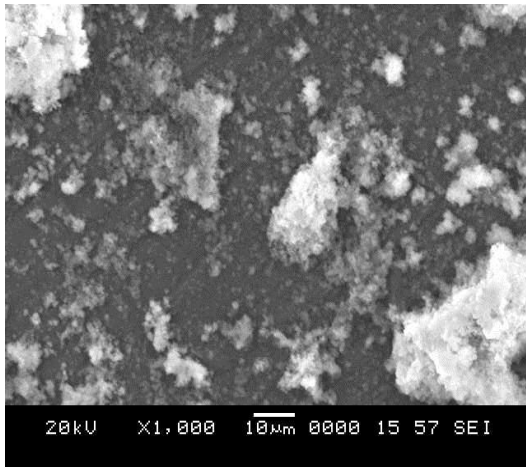
3.25(a)
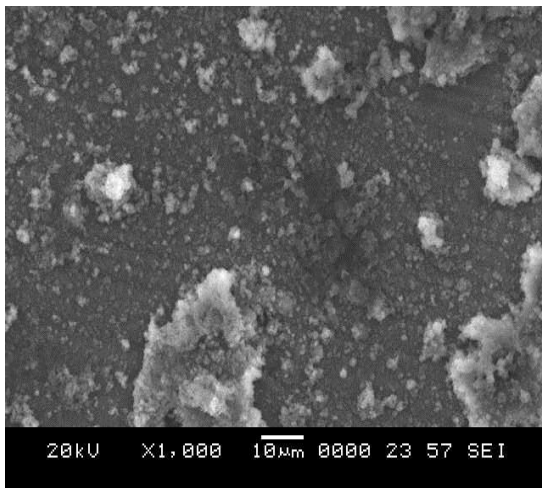
3.25(b)
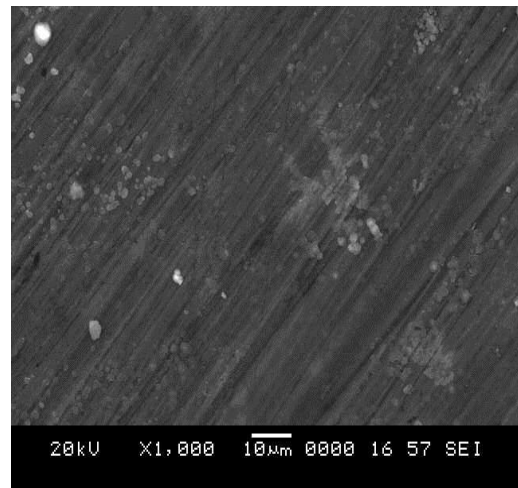
3.25(c)

Fig. 3.25: SEM images of the corroded surfaces in (a) Acidic 2.0 M Na$_2$SO$_4$ with pH 3 (b) Neutral 2.0 M Na$_2$SO$_4$ (c) Alkaline 2.0 M Na$_2$SO$_4$ with pH 12.
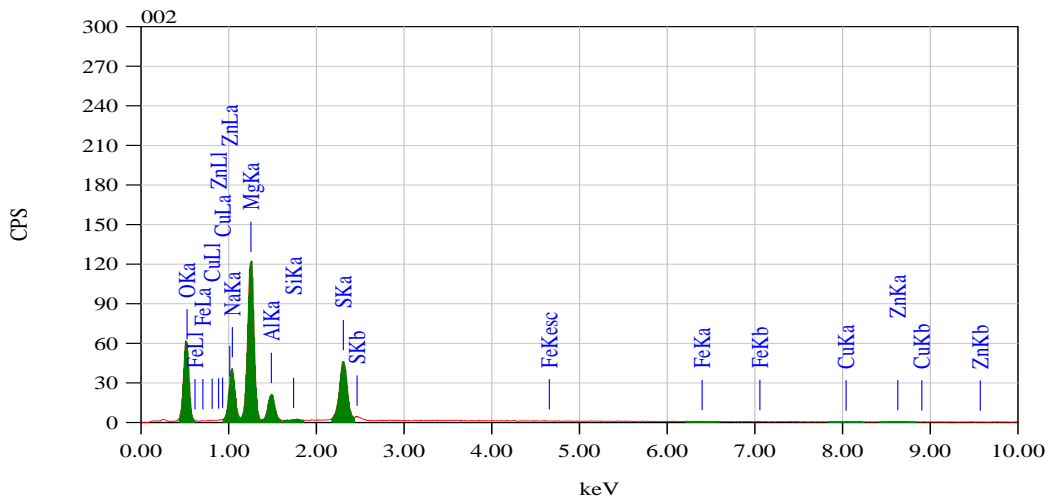
3.26(a)
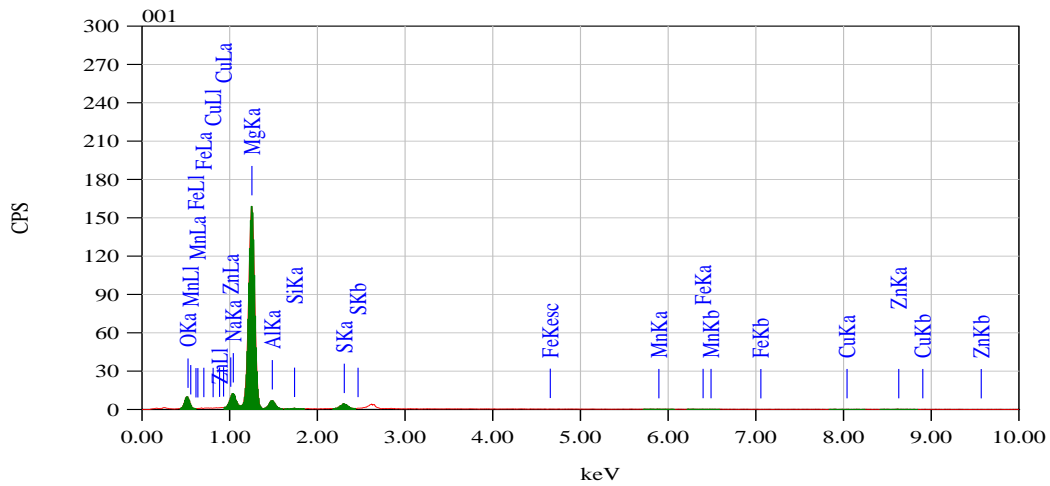
3.26(b)
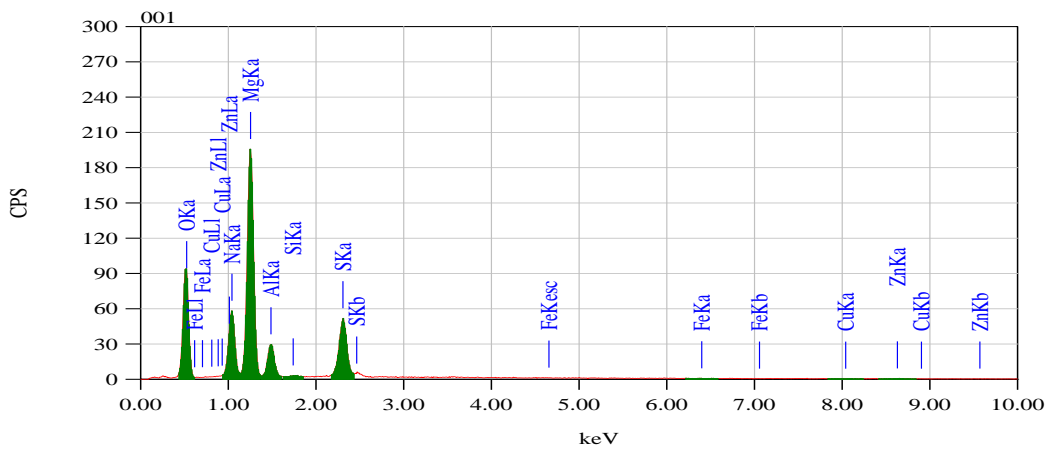
3.26(c)

Fig. 3.26: EDX spectra of the corroded surfaces in (a) Acidic 2.0 M Na₂SO₄ with pH 3 (b) Neutral 2.0 M Na₂SO₄ (c) Alkaline 2.0 M Na₂SO₄ with pH 12.

Table 3.9: Electrochemical polarization parameters for the corrosion of GA9 magnesium alloy in Na₂SO₄ solutions of different concentrations at different pH at 30 °C.

Molarity of NaCl	pH	$-E_{corr}$ (mV vs SCE)	$-b_c$ (mV dec^{-1})	i_{corr} (μA cm^{-2})	υ_{corr} (mm y^{-1})
0.1M	3	1472	167	179.2	4.027
	5	1462	148	75.1	1.687
	7	1456	139	42.1	0.946
	9	1445	131	26.2	0.589
	12	1315	118	2.5	0.055
0.5M	3	1492	183	406.6	9.135
	5	1472	155	176.3	3.960
	7	1461	144	112.4	2.526
	9	1456	139	69.1	1.552
	12	1354	122	21.0	0.472
1.0M	3	1505	208	666.0	14.962
	5	1488	161	277.4	6.232
	7	1478	149	195.2	4.386
	9	1469	144	142.5	3.201
	12	1375	132	48.0	1.079
1.5M	3	1528	220	893.3	20.069
	5	1497	172	456.6	10.259
	7	1477	158	281.7	6.328
	9	1465	153	231.3	5.197
	12	1418	138	82.1	1.844
2.0M	3	1552	239	1239.8	27.854
	5	1514	187	664.9	14.939
	7	1488	169	374.6	8.417
	9	1470	159	321.5	7.222
	12	1434	141	122.2	2.745

Table 3.10: Impedance parameters for the corrosion of GA9 Magnesium Alloy in Na$_2$SO$_4$ solutions of different concentrations at different pH at 30 °C.

Molarity of NaCl	pH	R_{ct} (Ω cm^2)	C_{dl} (μF cm^{-2})	υ_{corr} (mm y^{-1})
0.1M	3	147.0	22.17	3.982
	5	346.7	12.78	1.688
	7	604.7	10.53	0.968
	9	929.1	9.79	0.630
	12	10452.0	7.48	0.056
0.5M	3	63.8	40.13	9.180
	5	147.1	22.12	3.979
	7	219.1	18.35	2.672
	9	371.6	13.59	1.575
	12	1184.0	9.52	0.494
1.0M	3	39.1	62.12	14.984
	5	93.3	35.36	6.277
	7	139.0	30.91	4.212
	9	188.7	22.76	3.102
	12	542.0	14.14	1.080
1.5M	3	29.1	81.32	20.115
	5	56.8	53.29	10.306
	7	91.6	34.56	6.389
	9	113.1	27.56	5.175
	12	309.9	18.55	1.889
2.0M	3	20.9	99.76	27.940
	5	39.0	61.44	15.022
	7	67.5	42.55	8.674
	9	80.8	34.57	7.244
	12	209.8	22.31	2.789

3.5 SODIUM DODECYLBENZENESULFONATE (SDBS) AS CORROSION INHIBITOR ON GA9 MAGNESIUM ALLOY IN SODIUM CHLORIDE MEDIUM

3.5.1 Potentiodynamic polarization measurements

Potentiodynamic polarization curves for the corrosion of GA9 magnesium alloy in 1.0 M NaCl solution in the presence of different concentrations of SDBS, at 40 °C are shown in Fig. 3.27. Similar plots were obtained at other temperatures and also in the other concentrations of NaCl at the different temperatures studied.

Fig. 3.27: Potentiodynamic polarization curves for the corrosion of GA9 magnesium alloy in 1.0 M NaCl solution containing different concentrations of SDBS at 40 °C.

The potentiodynamic polarization parameters such as corrosion potential (E_{corr}), corrosion current density (i_{corr}), cathodic Tafel slope (b_c) were calculated from Tafel plots in the presence of different concentrations of SDBS at different temperatures and are summarized in Tables 3.11 to 3.15.

In general, according to the results presented in Tables 3.11 to 3.15 and also from polarization curves in Fig. 3.27, the corrosion current density (i_{corr}) decreases significantly even on the addition of small concentration of SDBS and the inhibition efficiency ($\eta\%$) increases with the increase in the inhibitor concentration for the Ga9 magnesium alloy. The maximum quantity of the inhibitor reported corresponds to the optimum concentration of the inhibitor. It can be observed that both the cathodic and anodic reactions are suppressed with the addition of SDBS, which suggested that the inhibitor exerted an efficient inhibitory effect both on anodic dissolution of metal and on cathodic hydrogen liberation reaction (Tao et al. 2010). Inhibition efficiency increases with the increase in the inhibitor concentration up to an optimum value. Thereafter the increase in the inhibitor concentration resulted in negligible increase in inhibition efficiency.

In comparison with the blank the polarization plots for the SDBS containing solutions consistently appeared at lower current density regions symbolizing the reduction in the rate of GA9 alloy dissolution. The basic shape of the Tafel curves is displayed as a consequence of the various electrochemical reactions occurring at the surface of the working electrode (Song et al. 2004). The introduction of SDBS does not seem to affect the shape of the polarization curves, which implies that the added SDBS does not alter the corrosion mechanism or participate in any of the electrode reactions, but only decreases the rate of corrosion, most likely by blocking the active electrode sites of reaction on the alloy surface through adsorption. Due to the non-linear nature of anodic branches, the values of corrosion current density were determined from the cathodic Tafel extrapolation. The inhibition efficiency ($\eta\%$) values were computed as per the previously stated equations 2.3 and 2.4.

It is seen from Tables, that the value of b_c does not change significantly with the increase in SDBS concentration, which indicates that the addition of SDBS does not alter the mechanism of cathodic hydrogen evolution reaction. Hydrogen evolution reaction has been reported to be generally the dominant local cathodic process in the corrosion of GA9 magnesium alloy in aqueous chloride solutions, via H^+ ion or H_2O molecule reduction, respectively.

It can also be seen from Tables 3.11 to 3.15 that there is no appreciable shift in the corrosion potential value (E_{corr}) on the addition of SDBS to the corrosion medium

and also on increasing the concentration of SDBS. If the displacement in corrosion potential is more than ±85 mV with respect to corrosion potential of the blank, then the inhibitor can be considered exclusively as a cathodic or anodic type. However, the maximum displacement in the present study is 20 mV, which indicates that SDBS is a mixed type inhibitor, affecting both the metal dissolution and the hydrogen evolution reactions. Therefore, the added SDBS functions as a mixed type corrosion inhibitor by hindering both the anodic reaction of metal oxidation and cathodic reaction of hydrogen evolution. This indicates that the inhibitive action of SDBS may be considered due to the adsorption and formation of barrier film on the electrode surface. The protective film formed on the surface of the metal reduces the likelihood of both the anodic and cathodic reactions, as a result of the decrease in the corrosion rate (Dinodi et al. 2014, Li et al. 2008).

The increase in the inhibition efficiency with the increase in inhibitor concentration is attributed to the increased surface coverage by the inhibitor molecules as the concentration is increased (El- Sayed et al. 1997).

3.5.2 Electrochemical impedance spectroscopy (EIS) studies

Nyquist plots for the corrosion of GA9 magnesium alloy in 1.0 M NaCl solution in the presence of different concentrations of SDBS are shown in Fig. 3.28. Similar plots were obtained in other concentrations of NaCl and also at other temperatures. The results of EIS studies for the corrosion of GA9 magnesium alloy in 1.0 M NaCl are summarised in Tables 3.16 to 3.20. It can be observed from the figure that the diameter of the semicircle increases with the increase in the concentration of SDBS, indicating a decrease in the corrosion rate of the alloy sample.

The Nyquist plots are characterized by a capacitive loop, extended from high frequency (HF) to low frequency (LF) range, an inductive loop in the low frequency region (LF) range and a tail at the medium frequency (MF) range. Similar plots have been reported in the literature for the corrosion of magnesium alloys in NaCl media (Arrabal et al. 2012, Chen et al. 2007, Baril et al. 2001). The HF capacitive loop is usually due to the charge transfer resistance and double layer capacitance at the metal-solution interface. The inductive behaviour at low frequencies typically associated with high concentration of Mg ions on relatively film-free areas (Chen et al. 2007, Baril et

al. 2001) or due to the presence of adsorbed surface species such as $Mg(OH)^+$, $Mg(OH)_2$ and Mg^+ (Song et al. 1998, Song et al. 1997, Qu et al. 2011). Also tail in the Nyquist plot in the lower frequency range, which correlates with the breakage of native corrosion product film (Song et al. 2010). The charge transfer resistance (R_{ct}) and the double layer capacitance (C_{dl}) are deduced from the analysis of a higher frequency capacitive loop (Song et al. 2004). When compared with the blank the capacitive semicircles appear enlarged in the presence of SDBS. This is indicative of improved corrosion resistance of GA9 in SDBS containing solutions. Also seen in the Fig. 3.28, even after introduction of SDBS the primary shape of the Nyquist plots remain unaffected and the capacitive loops enlarged in diameter with an increase in diameter with the increase in the concentration of SDBS added. This implies a decrease in the rate of dissolution of GA9 achieved without disturbing the mechanism of corrosion (Huang et al. 2011). The impedance data were simulated using the same equivalent electrical circuit as shown in Fig. 3.3. The inhibition efficiency ($\eta\%$) values were computed as per the previously stated equations 2.3 and 2.5.
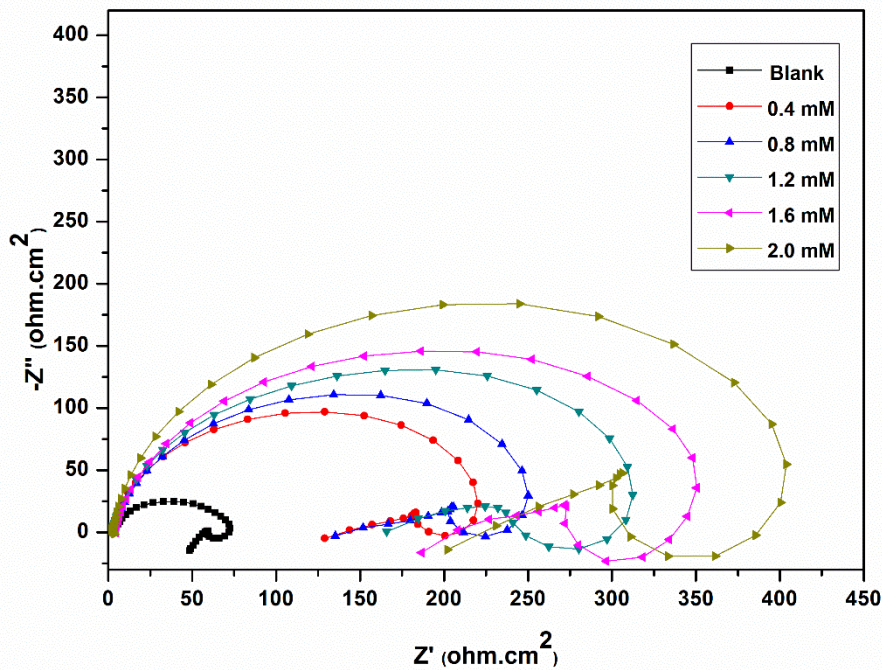
Fig. 3.28: Nyquist plots for the corrosion of GA9 magnesium alloy specimen in 1.0 M NaCl solution containing different concentrations of SDBS at 40 °C.

The results show that the values of C_{dl} decreases, while the values of R_{ct} increase with the increase in the concentration of SDBS, suggesting that the amount of the inhibitor molecules adsorbed on the electrode surface increases as the concentration of SDBS increases (Amin et al. 2007). The value of the double layer capacitance decreases as the inhibitor concentration increases either by the reduction of the local dielectric constant or by the increase of the electrical double layer thickness. This fact suggests that the studied inhibitor molecule acts by adsorption at the metal/solution interface with the gradual replacement of adsorbed water molecules by the inhibitor molecules on the metal surface (Seifzadeh et al. 2014, Wang et al. 2010). Thus, when the inhibitor concentration increases, more inhibitor molecules adsorb along the interface by replacing previously adsorbed water molecules (Dinodi et al. 2014).
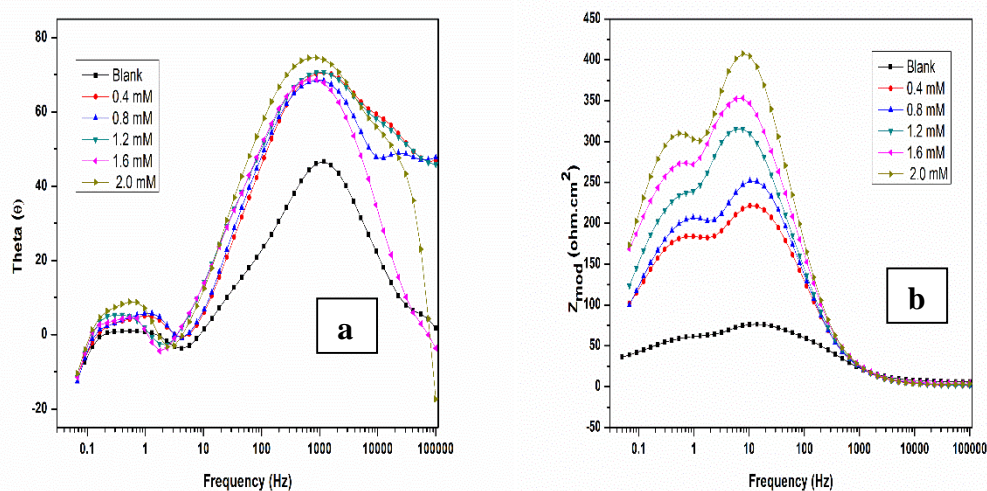
Fig. 3.29: Bode (a) phase angle plots and (b) amplitude plots for the corrosion of GA9 magnesium alloy in 1.0 M NaCl solution containing different concentrations of SDBS at 40 ℃.

The Bode plots of phase angle and amplitude for the corrosion of the GA9 magnesium alloy immersed in 1.0 M NaCl at 40 °C in the presence of different concentration of SDBS, are shown in Fig. 3.29 (a) and Fig. 3.29 (b), respectively. As seen from the Bode plots, both the impedance modulus (Z_{mod}) at low frequency and the phase maximum (θ_{max}) at intermediate frequency increase with the increase in SDBS concentration, which collectively point out the presence of highly protective surface film, able enough to oppose corrosive penetration.

3.5.3 Effect of temperature

The results in Tables 3.11 to 3.20 indicate that the inhibition efficiency of SDBS decreases with increase in temperature. It is also seen from the data in the above mentioned Tables, that the increase in solution temperature, does not alter the corrosion potential (E_{corr}) and cathodic Tafel slope (b_c) values significantly. This indicates that the increase in temperature does not change the mechanism of corrosion reaction (Poornima et al 2011). However, i_{corr} and hence the corrosion rate of the specimen increases with the increase in temperature in both the blank and the inhibited solutions. The decrease in inhibition efficiency with the increase in temperature may be attributed to the higher dissolution rates of GA9 magnesium alloy at elevated temperature and also a possible desorption of adsorbed inhibitor due to the increased solution agitation resulting from higher rates of hydrogen gas evolution (Antropov 1967). The higher rate of hydrogen gas evolution may also reduce the ability of the inhibitor to be adsorbed on the metal surface. The decrease in inhibition efficiency with the increase in temperature is also suggestive of physisorption of the inhibitor molecules on the metal surface (Dinodi and Shetty 2014). The apparent activation energy (E_a) for the corrosion process in the presence and absence of the inhibitor was calculated using Arrhenius law Equation (Eqn. 2.6) (Bouklah et al. 2004).

The Arrhenius plots for the corrosion of GA9 magnesium alloy in the presence of different concentrations of SDBS in 1.0 M sodium chloride are shown in Fig. 3.30. The plots of $\ln(\upsilon_{corr}/T)$ versus $1/T$ for the corrosion of GA9 magnesium alloy in the presence of different concentrations of SDBS in 1.0 M sodium chloride are shown in Fig. 3.31. The calculated values of activation parameters are recorded in Table 3.21. The data in the Table 3.21 show that the values of E_a for the corrosion of GA9 magnesium alloy in the presence of SDBS are higher than those in the uninhibited medium. The increase in the E_a values, with increasing inhibitor concentration indicates the increase in energy barrier for the corrosion reaction, with the increasing concentrations of the inhibitor (Schorr et al. 1972). It is also indicated that the whole process is controlled by surface reaction, since the activation energies of the corrosion process are above 20 kJ mol^{-1}. The adsorption of the inhibitor on the electrode surface leads to the formation of a physical barrier between the metal surface and the corrosion medium, blocking the

charge transfer, and thereby reducing the metal reactivity in the electrochemical reactions of corrosion (Antropov et al. 1967).
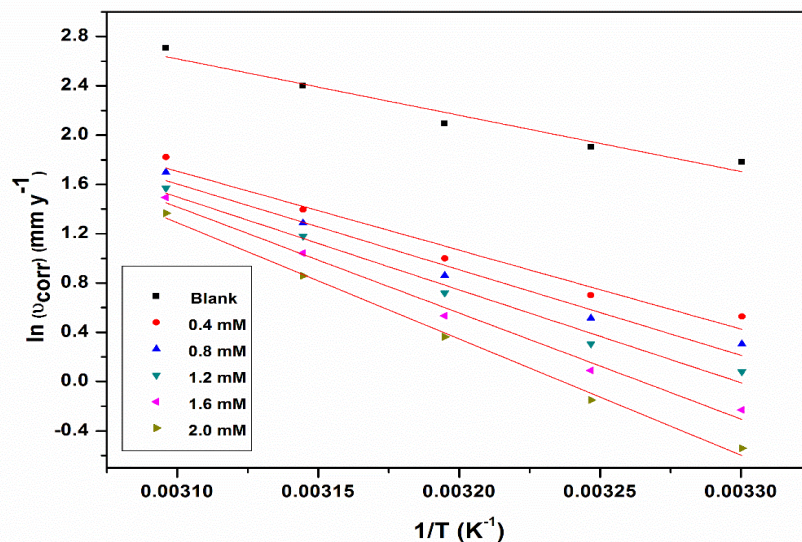
3.30: Arrhenius plots for the corrosion of GA9 magnesium alloy in 1.0 M NaCl solution containing different concentrations of SDBS.
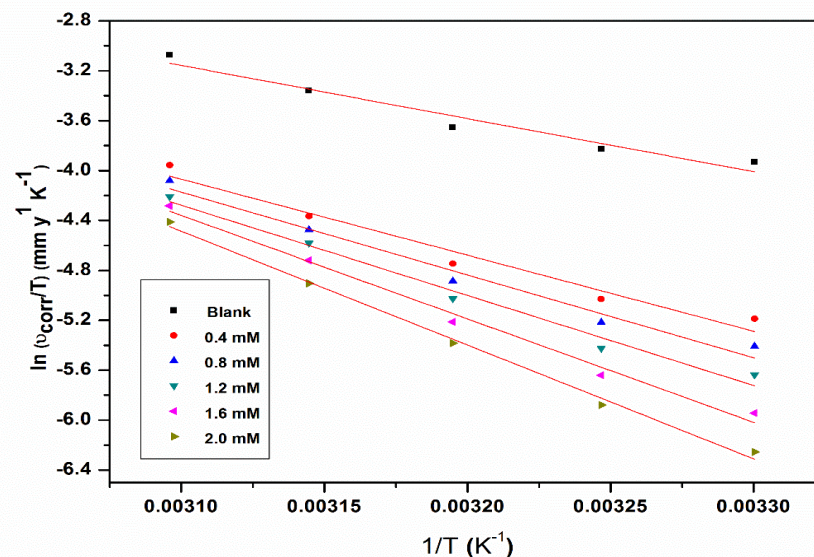
Fig. 3.31: Plots of ln(υ_{corr}/T) versus 1/T for the corrosion of GA9 magnesium alloy in 1.0 M NaCl solution containing different concentrations of SDBS.

The large negative values of entropy of activation ($\Delta S^{\#}$) in the absence and presence of inhibitor imply that the activated complex in the rate determining step

represents an association rather than dissociation, resulting in a decrease in randomness on going from the reactants to the activated complex (Sahin et al .2003, Satpati et al. 2008).

3.5.4 Effect of sodium chloride concentration

Table 3.22 summarises the maximum inhibition efficiencies exhibited by SDBS in the NaCl solutions of different concentrations at different temperatures. It is evident from both polarization and EIS experimental results that, for a particular concentration of inhibitor, the inhibition efficiency decreases with the increase in sodium chloride concentration on the GA9 magnesium alloy. The highest inhibition efficiency is observed in sodium chloride of 0.1 M concentration. The decreased inhibition efficiency in higher concentration of sodium chloride can be attributed to the higher corrosivity of the medium.

3.5.5 Adsorption isotherms

The information on the interaction between the inhibitor molecules and the metal surface can be provided by adsorption isotherms (Fekry et al. 2010). An adsorption isotherm is a graphical representation of variation of extent of adsorption with pressure or concentration of adsorbate at a given constant temperature. The phenomenon of adsorption plays a vital role during the action of corrosion inhibitors. Hence a thorough knowledge about the adsorption isotherm is a prerequisite in understanding the nature of interactions prevailing between the inhibitor molecules and the metal surface. A metal/electrolyte interface has water molecules adsorbed all along. During inhibitor adsorption, the inhibitor molecules in solution ($Inh_{(sol)}$) replace previously adsorbed water molecules ($H_2O_{(ads)}$) through a process similar to substitution, as shown below (Tao et al. 2010).

$$Inh_{(sol)} + \chi H_2O_{(abs)} \leftrightarrow Inh_{(ads)} + \chi H_2O_{(sol)} \qquad (3.13)$$
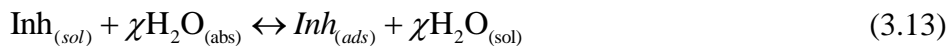
where χ, the size ratio, is the number of water molecules displaced by one molecule of organic inhibitor. χ is assumed to be independent of coverage or charge on the electrode (Tao et al. 2010, Oguzie et al. 2008).

The surface coverage (θ) was calculated from potentiodynamic polarization data using the equation:

$$\theta = \frac{\eta(\%)}{100} \tag{3.14}$$

where η (%) is the percentage inhibition efficiency. The values of θ at different concentrations of inhibitor in the solution (C_{inh}) were applied to various isotherms including Langmuir, Temkin, Frumkin and Florye - Huggins isotherms. It was found that the data fitted best with the Langmuir adsorption isotherm, which is given by the relation (Wang et al. 2010).

$$\frac{C_{inh}}{\theta} = C_{inh} + \frac{1}{K} \tag{3.15}$$

where K is the adsorption/desorption equilibrium constant, C_{inh} is the corrosion inhibitor concentration in the solution, and θ is the surface coverage. The plot of C_{inh}/θ versus C_{inh} gives a straight line with an intercept of $1/K$. The Langmuir adsorption isotherms for the adsorption of SDBS on the GA9 magnesium alloy are shown in Fig. 3.32. Similar plots were obtained in other NaCl solutions also. The linear regression coefficients are close to unity and the slopes of the straight lines are nearly unity, suggesting that the adsorption of SDBS obeys Langmuir's adsorption isotherm with a litttle interaction between the adsorbed molecules.

The standard free energy of adsorption ($\Delta G°_{ads}$) was calculated using the relation

$$K = \frac{1}{55.5} \exp\left(\frac{-\Delta G^0_{ads}}{RT}\right) \tag{3.16}$$

where, the value 55.5 is the concentration of water in solution in mol dm^{-3}, R is the universal gas constant and T is absolute temperature.

The standard enthalpy of adsorption ($\Delta H°_{ads}$) and standard enthalpy of adsorption ($\Delta S°_{ads}$) were calculated by the expression

$$\Delta G^0_{ads} = \Delta H^0_{ads} - T\Delta S^0_{ads} \tag{3.17}$$

The plot of ΔG°_{ads} Vs T gives a straight line and the ΔH°_{ads} and ΔS°_{ads} values are calculated from the slope and intercept. The plot of ΔG°_{ads} Vs T is shown in Fig. 3.33. The thermodynamic data obtained for the adsorption of SDBS on the alloy surface are tabulated in Table 3.23.
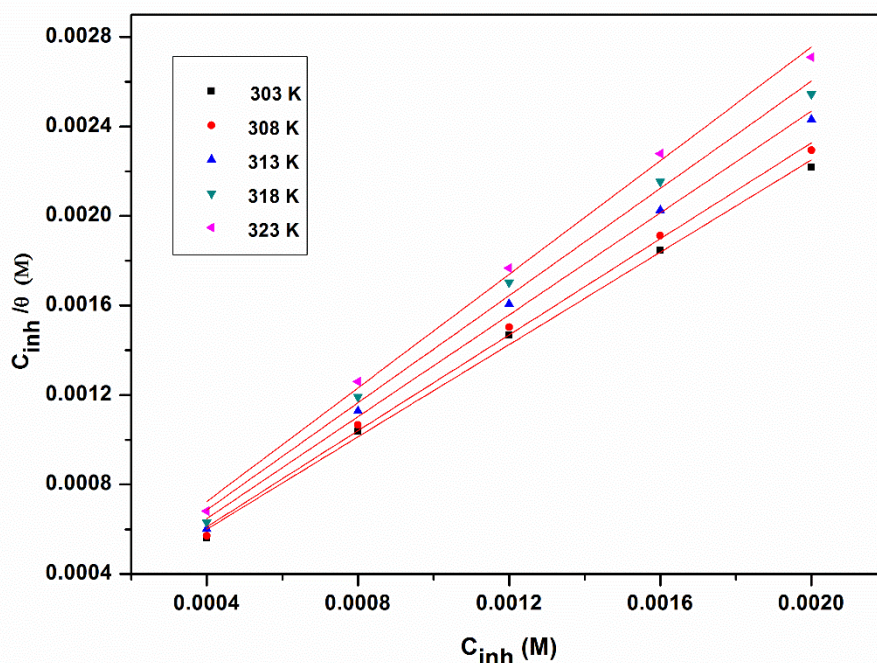
Fig. 3.32: Langmuir adsorption isotherms for the adsorption of SDBS on GA9 magnesium alloy in 1.0 M NaCl solution at different temperatures.

The negative ΔG°_{ads} values are consistent with the spontaneity of the adsorption process and the stability of the adsorbed layer on the alloy surface. When the value of ΔG°_{ads} is less negative than -20 kJ mol^{-1}, the adsorption processes are associated with an electrostatic interaction between charged molecules and charged metal surface, resulting in physisorption and more negative than -40 kJ mol^{-1} involve charge transfer or sharing from the inhibitor molecules to the metal surface to form a coordinate covalent bond, resulting in chemisorption (Hosseini et al. 2003). In the present case, the value of ΔG°_{ads} is -31 to -34 kJ mol^{-1}, indicating that the adsorption of SDBS is mixed adsorption, involving both physisorption and chemisorption. The decrease in inhibition efficiency with the increase in temperature also hints at physisorption of SDBS on the

102

alloy surface. Therefore it can be concluded that the adsorption of SDBS as mixed adsorption with predominant physical mode of adsorption.

The negative sign of ΔH°_{ads} in NaCl solution indicates that the adsorption of inhibitor molecules is an exothermic process. Generally, an exothermic adsorption process signifies either physisorption or chemisorption while endothermic process is attributable unequivocally to chemisorption. Typically, the standard enthalpy of physisorption process is less negative than 41.86 kJ mol^{-1}, while that of chemisorption process approaches to -100 kJ mol^{-1} (Martinez et al. 2002). In the present study the value of ΔH°_{ads} is -3.64 to -11.93 kJ mol^{-1}, which shows that the adsorption of SDBS on GA9 magnesium alloy involves physisorption phenomenon (Ashish Kumar et al. 2010).
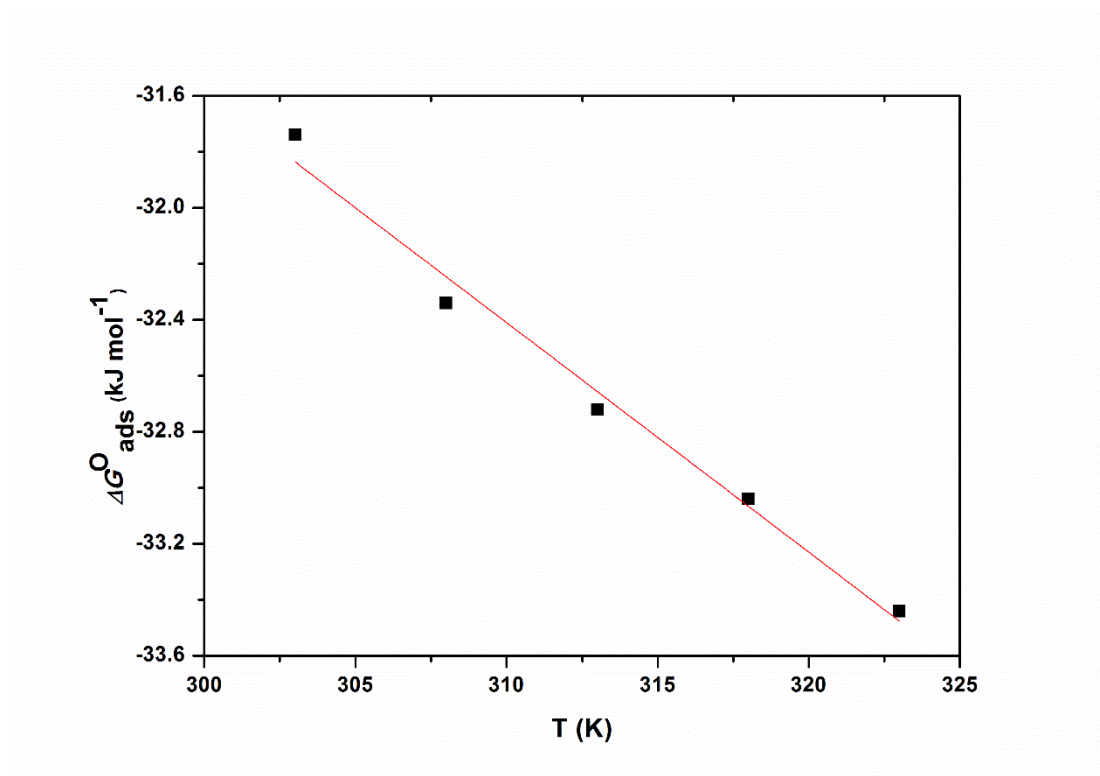
Fig. 3.33: The plot of ΔG°_{ads} vs T for the adsorption of SDBS on GA9 magnesium alloy in 1.0 M NaCl solution.

The ΔS^0_{ads} value is positive indicating that increase in randomness involved in the adsorption of SDBS molecules on the alloy surface. This could be the result of the adsorption of the inhibitor molecules, which could be regarded as a quasi-substitution

process between the inhibitor molecule in the aqueous phase and water molecules at electrode surface. In the present case, the increase in entropy is caused by the displacement of previously adsorbed water molecules, which inturn is moving freely in electrolyte bulk.

3.5.6 Mechanism of corrosion inhibition

GA9 magnesium alloy is a dual phase alloy, consisting of a primary α-phase and a divorced eutectic β-phase, distributed along the grain boundaries of primary phase. The α-phase is an Mg-Al-Zn solid solution with the same crystal structure as pure magnesium and the β-phase is the discontinuous precipitate of inter-metallic compound $Mg_{17}Al_{12}$. The α-Mg matrix corrodes due to its very negative free corrosion potential and there is the tendency for the corrosion rate of the α-Mg matrix to be accelerated by micro-galvanic coupling between the α-phase and the β-phase. The β-phase has a relatively low corrosion rate and it is more efficient site for the cathodic reactions.

Magnesium dissolution in wet environments generally proceeds by an electrochemical reaction with water to produce magnesium hydroxide and molecular hydrogen (H_2), thus magnesium corrosion is relatively insensitive to oxygen concentration.

The overall corrosion reaction is:

$$Mg + 2H_2O \rightarrow Mg(OH)_2 + H_2 \quad\quad\quad (3.17)$$

The overall corrosion reaction (3.16) may be expressed as the sum of the following partial reactions:

Anodic reaction: $\quad\quad Mg \rightarrow Mg^{2+} + 2e^- \quad\quad\quad\quad\quad (3.18)$

Cathodic reaction: $\quad 2H_2O + 2e^- \rightarrow H_2 + 2OH^- \quad\quad\quad (3.19)$

Product formation: $\quad Mg^{2+} + 2OH^- \rightarrow Mg(OH)_2 \quad\quad\quad (3.20)$
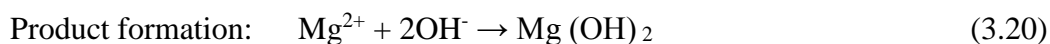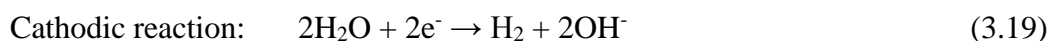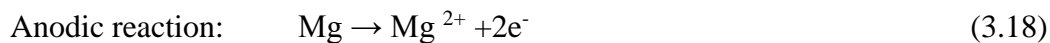
Generally the inhibition brought about by chemical inhibitors is attributed to adsorption and barrier film formation at the metal surface. The SDBS is anionic surfactant with the sulfonate polar head and long alkyl hydrophobic tail. The SDBS might physically adsorb through the electrostatic interactions between their anionic

head and Mg^{2+} ions trapped within the imperfections of surface film developed over the α-Mg matrix. There certainly is a scope for chemisorption as well, at the cathodic phases which are rich in Mn and Zn elements (Hu et al. 2011). Strong covalent bonds might develop from donor–accepter interactions between unshared electron pairs of oxygen of sulfonate and vacant d orbitals of Mn metal atom, leading to chemisorption of inhibitors. The SDBS, chemisorbed along cathodic intermetallic phases are likely to inhibit cathodic hydrogen evolution by blocking the active cathodic reaction sites. The physisorbed surfactant on the other hand, might precipitate as their sparingly soluble magnesium salts within the pores of the film over the α-Mg matrix. The precipitation is favoured due to very low solubility product of magnesium salt of the surfactant and the presence of sufficiently high amounts of dissolved Mg^{2+} ions. The precipitates fill-up the pores and densify the surface film. As an overall result the electrolyte ingress is reduced on the addition of the surfactant. In all likelihood van der Waals interactions exists between the long alkyl chains of adsorbed surfactant molecules, this causes the adsorption behaviour to slightly deviate from ideal Langmuir behaviour. Such mutual interactions further improve the compactness of the modified film. As an added advantage, the modified film even attains certain hydrophobicity which repels the aqueous corrosive (Cao et al. 2010).

3.5.7 SEM/EDX studies

In order to differentiate between the surface morphology and to identify the composition of the species formed on the metal surface after its immersion in 2.0 M NaCl in the absence and in the presence of SDBS, SEM/EDX investigations were carried out. Fig. 3.34 (a) represents SEM image of the corroded GA9 magnesium alloy sample. The corroded surface shows detachment of particles from the surface. The corrosion of the alloy may be predominantly attributed to the galvanic effect between the precipitates and the matrix. Fig. 3.34 (b) represents SEM image of GA9 magnesium alloy after the corrosion tests in a medium of 2.0 M NaCl containing 2.0 mM of SDBS. The image clearly shows an undeteriorated surface due to the adsorbed layer of inhibitor molecules on the alloy surface, thus protecting the metal from corrosion.
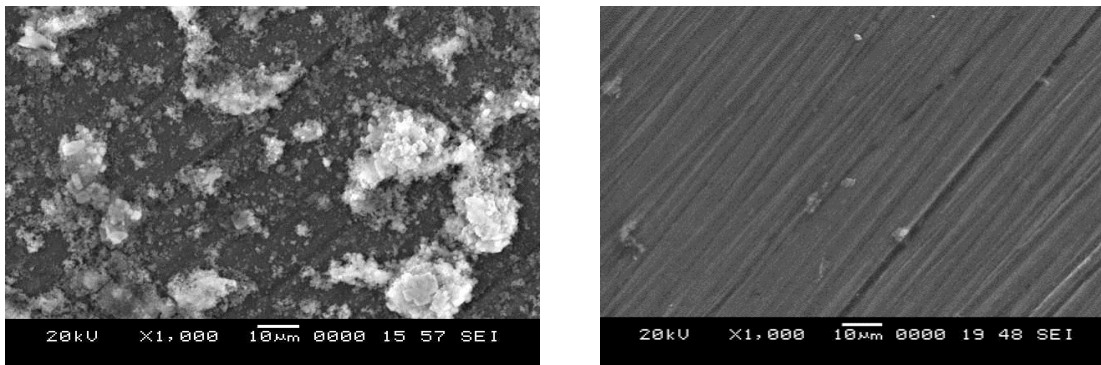
Fig. 3.34: SEM images of GA9 after immersion in 2.0 M NaCl solution a) in the absence and b) in the presence of SDBS.

EDX investigations were carried out in order to identify the composition of the species formed on the metal surface in NaCl media in the absence and in the presence of SDBS. The EDX profile analyses for the selected areas on the SEM images of Fig. 3.34 (a) and (b) are shown in Fig. 3.35 (a) and 3.35 (b). In the EDX spectra (Fig. 3.35 (b)), apart from the peaks for Mg, Al, Zn and Cl, an additional small peak for carbon and oxygen is obtained, which indicates the presence of some organic moieties on the alloy surface, which possibly are the surface adsorbed SDBS molecules.
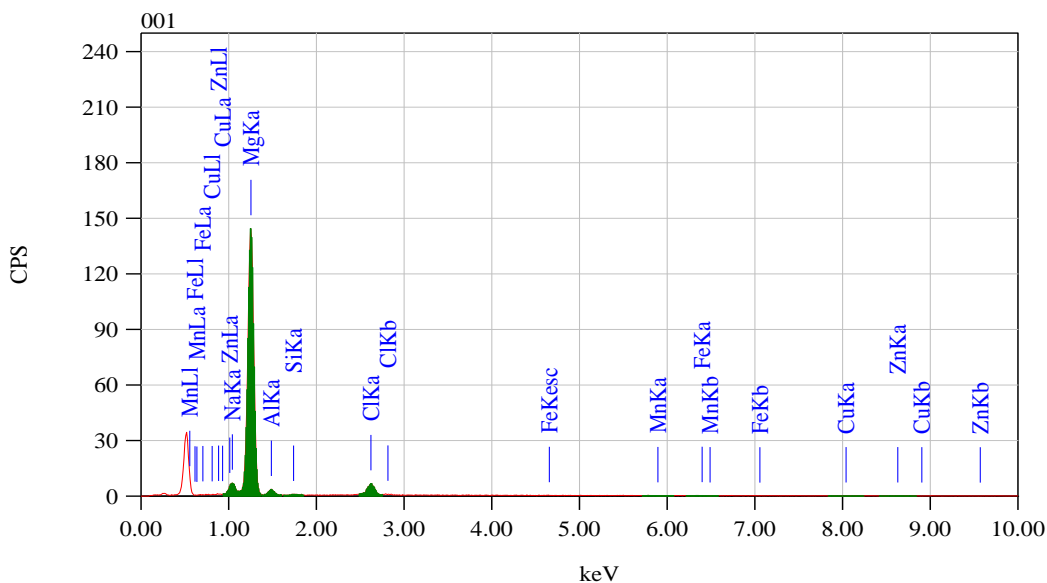
Fig. 3.35 (a): EDX spectra of GA9 magnesium alloy after immersion in 2.0 M NaCl solution in the absence of SDBS.
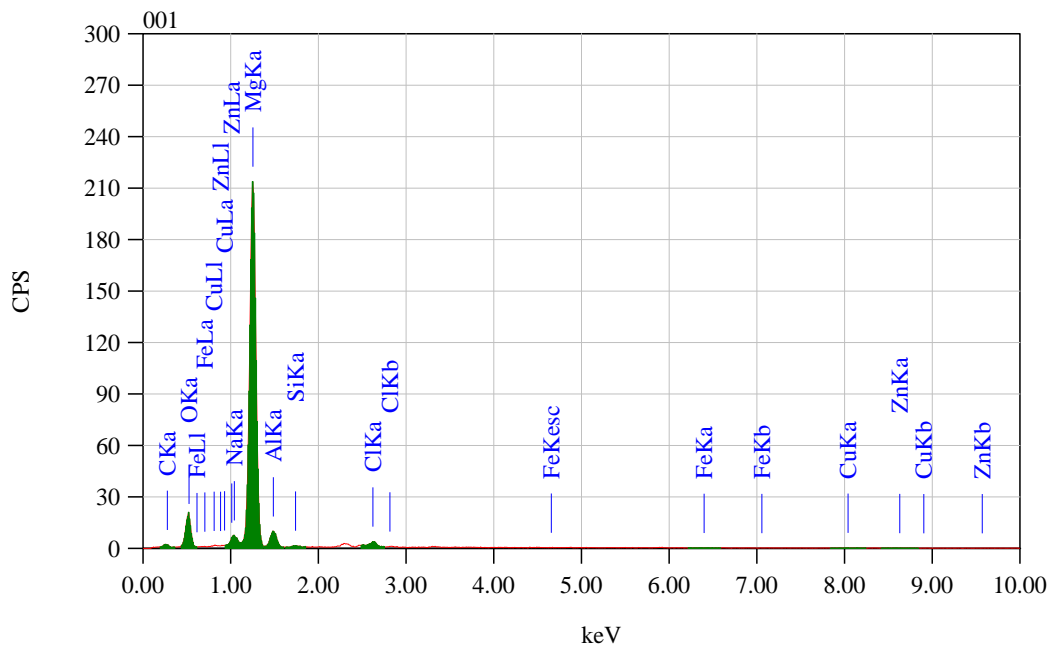
Fig. 3.35 (b): EDX spectra of GA9 magnesium alloy after immersion in 2.0 M NaCl solution in the presence of SDBS.
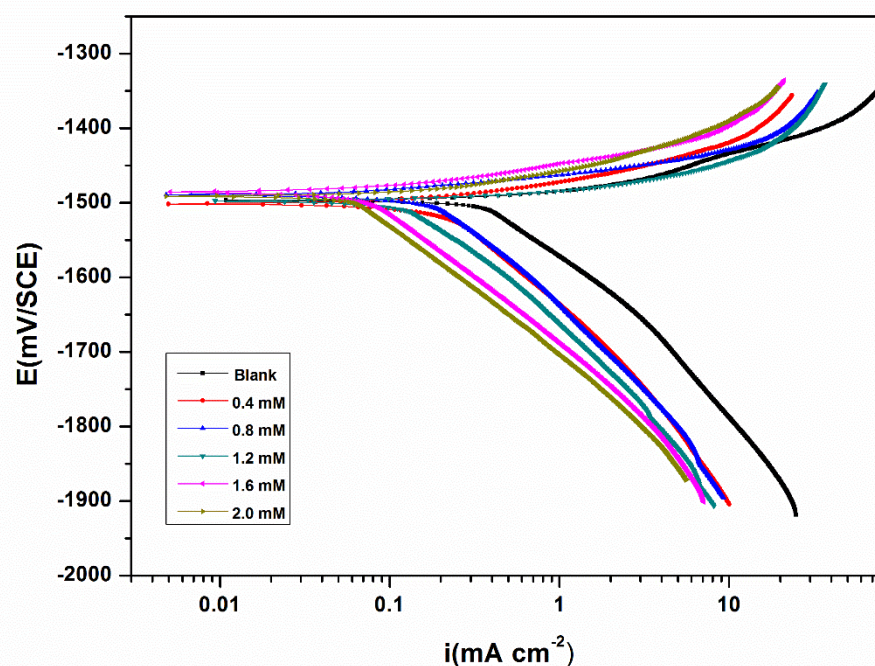
Table 3.11: Results of potentiodynamic polarization studies for the corrosion of GA9 magnesium alloy in 0.1 M sodium chloride solution containing different concentrations of SDBS.

Temperature (℃)	Conc. of inhibitor (mM)	$-E_{corr}$ (mV /SCE)	$-b_c$ (mV dec^{-1})	i_{corr} (µA cm^{-2})	υ_{corr} (mm y^{-1})	η (%)
30	Blank	1449	149	75.1	1.687	
	0.4	1455	121	18.2	0.409	75.8
	0.8	1452	119	13.7	0.308	80.1
	1.2	1451	115	10.4	0.234	84.8
	1.6	1442	112	7.1	0.159	88.7
	2.0	1447	110	4.7	0.106	92.5
35	Blank	1445	157	86.9	1.952	
	0.4	1458	133	21.7	0.488	75.0
	0.8	1452	130	18.1	0.407	79.2
	1.2	1454	127	14.3	0.321	83.6
	1.6	1449	123	10.5	0.236	87.9
	2.0	1444	119	7.8	0.175	91.0
40	Blank	1450	164	108.4	2.435	
	0.4	1459	140	28.5	0.640	73.7
	0.8	1457	137	25.0	0.562	76.9
	1.2	1450	133	20.1	0.452	81.5
	1.6	1454	131	15.1	0.339	86.1
	2.0	1446	126	11.4	0.256	89.5
45	Blank	1465	169	139.1	3.126	
	0.4	1467	149	42.6	0.957	69.4
	0.8	1469	146	37.8	0.849	72.8
	1.2	1464	144	32.1	0.721	76.9
	1.6	1456	141	25.9	0.582	81.4
	2.0	1460	138	20.6	0.463	85.2
50	Blank	1472	173	189.3	4.254	
	0.4	1478	153	67.6	1.519	64.3
	0.8	1471	151	60.6	1.361	68.0
	1.2	1475	146	54.0	1.213	71.5
	1.6	1468	145	47.9	1.076	74.7
	2.0	1463	140	43.3	0.973	77.1

Table 3.12: Results of potentiodynamic polarization studies for the corrosion of GA9 magnesium alloy in 0.5 M sodium chloride solution containing different concentrations of SDBS.

Temperature (℃)	Conc. of inhibitor (mM)	$-E_{corr}$ (mV /SCE)	$-b_c$ (mV dec^{-1})	i_{corr} (µA cm^{-2})	υ_{corr} (mm y^{-1})	η (%)
	Blank	1451	152	160.0	3.595	
	0.4	1455	130	42.2	0.948	73.6
30	0.8	1453	127	34.6	0.777	78.4
	1.2	1450	122	27.4	0.616	82.9
	1.6	1446	117	19.8	0.445	87.6
	2.0	1449	114	14.2	0.319	91.1
	Blank	1473	158	179.3	4.029	
	0.4	1469	137	49.5	1.112	72.4
	0.8	1467	135	41.2	0.926	77.0
35	1.2	1461	132	33.9	0.762	81.1
	1.6	1464	129	25.5	0.573	85.8
	2.0	1457	126	18.8	0.422	89.5
	Blank	1466	167	206.6	4.641	
	0.4	1472	147	61.2	1.375	70.4
	0.8	1467	143	51.9	1.166	74.9
40	1.2	1469	140	43.8	0.984	78.8
	1.6	1462	137	35.7	0.802	82.7
	2.0	1459	133	27.7	0.622	86.6
	Blank	1490	171	285.1	6.405	
	0.4	1491	153	90.9	2.042	68.1
	0.8	1494	151	80.1	1.800	71.9
45	1.2	1486	146	69.8	1.568	75.5
	1.6	1485	144	62.7	1.409	78.0
	2.0	1481	139	53.6	1.204	81.2
	Blank	1497	175	377.1	8.473	
	0.4	1502	159	140.3	3.152	62.8
	0.8	1498	156	127.8	2.871	66.1
50	1.2	1495	153	114.3	2.568	69.7
	1.6	1489	150	101.8	2.287	73.0
	2.0	1492	146	89.7	2.015	76.2

Table 3.13: Results of potentiodynamic polarization studies for the corrosion of GA9 magnesium alloy in 1.0 M sodium chloride solution containing different concentrations of SDBS.

Temperature (°C)	Conc. of inhibitor (mM)	$-E_{corr}$ (mV /SCE)	$-b_c$ (mV dec^{-1})	i_{corr} (μA cm^{-2})	υ_{corr} (mm y^{-1})	η (%)
30	Blank	1474	156	264.5	5.942	
	0.4	1480	139	75.4	1.694	71.5
	0.8	1476	136	60.3	1.355	77.2
	1.2	1470	134	48.1	1.081	81.8
	1.6	1475	131	35.4	0.795	86.6
	2.0	1467	128	25.9	0.582	90.2
35	Blank	1495	162	298.9	6.716	
	0.4	1492	146	89.7	2.015	70.0
	0.8	1497	143	74.4	1.672	75.1
	1.2	1488	140	60.4	1.357	79.8
	1.6	1482	138	48.7	1.094	83.7
	2.0	1485	135	38.3	0.861	87.2
40	Blank	1496	169	361.5	8.122	
	0.4	1501	154	121.1	2.721	66.5
	0.8	1489	152	105.2	2.364	70.9
	1.2	1497	149	91.5	2.056	74.7
	1.6	1485	146	75.9	1.705	79.0
	2.0	1492	144	64.0	1.438	82.3
45	Blank	1496	177	491.0	11.031	
	0.4	1506	161	179.7	4.038	63.4
	0.8	1499	158	161.1	3.620	67.2
	1.2	1502	156	144.9	3.256	70.5
	1.6	1491	153	126.2	2.836	74.3
	2.0	1494	151	105.1	2.361	78.6
50	Blank	1501	179	665.6	14.955	
	0.4	1504	165	274.9	6.177	58.7
	0.8	1511	163	242.9	5.458	63.5
	1.2	1508	160	213.7	4.801	67.9
	1.6	1494	157	198.4	4.458	70.2
	2.0	1499	154	174.4	3.919	73.8

Table 3.14: Results of potentiodynamic polarization studies for the corrosion of GA9 magnesium alloy in 1.5 M sodium chloride solution containing different concentrations of SDBS.

Temperature (°C)	Conc. of inhibitor (mM)	$-E_{corr}$ (mV /SCE)	$-b_c$ (mV dec^{-1})	i_{corr} (μA cm^{-2})	υ_{corr} (mm y^{-1})	η (%)
30	Blank	1497	169	376.5	8.458	
	0.4	1500	154	112.6	2.530	70.1
	0.8	1502	152	94.1	2.114	75.0
	1.2	1496	149	79.1	1.777	79.0
	1.6	1492	146	62.1	1.395	83.5
	2.0	1488	142	49.3	1.108	86.9
35	Blank	1499	173	436.5	9.802	
	0.4	1508	159	140.6	3.159	67.8
	0.8	1504	157	112.2	2.521	74.3
	1.2	1495	154	99.5	2.236	77.2
	1.6	1491	151	73.8	1.658	83.1
	2.0	1499	147	65.5	1.472	85.0
40	Blank	1519	181	552.6	12.416	
	0.4	1523	168	198.9	4.469	64.0
	0.8	1526	165	171.8	3.860	68.9
	1.2	1516	163	146.4	3.289	73.5
	1.6	1518	159	121.0	2.719	78.1
	2.0	1511	155	102.8	2.310	81.4
45	Blank	1520	195	738.2	16.585	
	0.4	1532	183	289.4	6.503	60.8
	0.8	1521	180	259.1	5.822	64.9
	1.2	1526	177	230.3	5.174	68.8
	1.6	1517	173	207.4	4.660	71.9
	2.0	1513	169	157.2	3.532	78.7
50	Blank	1529	210	999.6	22.458	
	0.4	1537	199	416.8	9.365	58.1
	0.8	1538	195	373.9	8.401	62.6
	1.2	1531	192	340.9	7.660	66.7
	1.6	1524	190	315.9	7.098	69.8
	2.0	1528	186	290.9	6.536	73.1

Table 3.15: Results of potentiodynamic polarization studies for the corrosion of GA9 magnesium alloy in 2.0 M sodium chloride solution containing different concentrations of SDBS.

Temperature (°C)	Conc. of inhibitor (mM)	$-E_{corr}$ (mV /SCE)	$-b_c$ (mV dec^{-1})	i_{corr} (μA cm^{-2})	υ_{corr} (mm y^{-1})	η (%)
30	Blank	1524	192	447.5	10.055	
	0.4	1537	179	147.2	3.307	67.1
	0.8	1538	177	118.6	2.665	73.5
	1.2	1531	174	102.9	2.312	77.0
	1.6	1524	168	88.1	1.979	80.3
	2.0	1528	165	74.3	1.669	83.4
35	Blank	1525	195	546.9	12.286	
	0.4	1534	183	192.0	4.314	64.9
	0.8	1530	180	166.8	3.748	69.5
	1.2	1525	177	147.7	3.319	73.0
	1.6	1522	173	126.9	2.851	76.8
	2.0	1517	170	105.0	2.359	80.8
40	Blank	1529	206	726.0	16.310	
	0.4	1535	195	275.9	6.199	62.0
	0.8	1533	192	236.7	5.318	67.4
	1.2	1528	188	208.4	4.682	71.3
	1.6	1523	184	175.0	3.932	75.9
	2.0	1520	177	152.5	3.426	79.0
45	Blank	1530	213	986.2	22.157	
	0.4	1539	203	402.4	9.041	59.2
	0.8	1531	200	365.9	8.221	62.9
	1.2	1536	196	338.3	7.601	65.7
	1.6	1522	193	305.7	6.869	69.0
	2.0	1527	188	275.2	6.183	72.1
50	Blank	1535	222	1249.8	28.078	
	0.4	1548	210	561.2	12.609	55.1
	0.8	1543	207	518.7	11.654	58.5
	1.2	1532	204	462.4	10.389	63.0
	1.6	1537	200	427.4	9.603	65.8
	2.0	1529	197	392.4	8.817	68.6

Table 3.16: EIS data for the corrosion of GA9 magnesium alloy in 0.1 M sodium chloride solution containing different concentrations of SDBS.

Temperature (°C)	Conc. of inhibitor (mM)	R_{ct} (ohm. cm^2)	C_{dl} (μF cm^{-2})	η (%)
30	Blank	361.5	11.29	
	0.4	1506.0	8.50	76.0
	0.8	1853.0	8.44	80.5
	1.2	2426.0	8.08	85.1
	1.6	3347.0	7.83	89.2
	2.0	4885.0	7.05	92.6
35	Blank	302.5	11.41	
	0.4	1229.0	8.77	75.4
	0.8	1447.0	8.61	79.1
	1.2	1811.0	8.38	83.3
	1.6	2420.0	8.01	87.5
	2.0	3437.0	7.89	91.2
40	Blank	245.4	15.20	
	0.4	947.5	10.22	74.1
	0.8	1076.0	9.81	77.2
	1.2	1334.0	9.52	81.6
	1.6	1888.0	9.27	87.0
	2.0	2504.0	8.82	90.2
45	Blank	184.5	23.51	
	0.4	613.0	13.21	69.9
	0.8	691.0	12.96	73.3
	1.2	809.2	12.62	77.2
	1.6	1025.0	12.34	82.0
	2.0	1272.0	11.95	85.5
50	Blank	132.8	28.95	
	0.4	380.5	16.90	65.1
	0.8	432.6	16.72	69.3
	1.2	464.3	16.48	71.4
	1.6	527.0	16.28	74.8
	2.0	603.6	16.07	78.0

Table 3.17: EIS data for the corrosion of GA9 magnesium alloy in 0.5 M sodium chloride solution containing different concentrations of SDBS.

Temperature (°C)	Conc. of inhibitor (mM)	R_{ct} (ohm. cm^2)	C_{dl} (µF cm^{-2})	η (%)
	Blank	162.9	26.17	
	0.4	656.9	10.81	74.0
30	0.8	757.7	10.63	78.5
	1.2	952.6	10.48	82.9
	1.6	1392.3	10.02	88.3
	2.0	1916.5	9.72	91.5
	Blank	147.0	27.21	
	0.4	542.4	10.96	72.9
35	0.8	650.4	10.77	77.4
	1.2	807.7	10.62	81.8
	1.6	1050.0	10.09	86.0
	2.0	1485.0	9.81	90.1
	Blank	127.3	28.63	
	0.4	425.8	11.55	70.1
40	0.8	515.4	11.44	75.3
	1.2	609.1	11.22	79.1
	1.6	753.3	10.90	83.1
	2.0	971.8	10.63	86.9
	Blank	91.0	35.08	
	0.4	290.7	14.21	68.7
45	0.8	325.0	13.98	72.0
	1.2	361.1	13.49	74.8
	1.6	419.4	13.08	78.3
	2.0	491.9	12.55	81.5
	Blank	70.8	40.33	
	0.4	191.4	17.21	63.0
50	0.8	213.3	16.99	66.8
	1.2	235.2	16.47	69.9
	1.6	262.2	16.10	73.0
	2.0	297.5	15.71	76.4

Table 3.18: EIS data for the corrosion of GA9 magnesium alloy in 1.0 M sodium chloride solution containing different concentrations of SDBS.

Temperature (°C)	Conc. of inhibitor (mM)	R_{ct} (ohm. cm^2)	C_{dl} (μF cm^{-2})	η (%)
	Blank	99.7	33.50	
	0.4	357.3	11.13	72.1
30	0.8	418.9	10.97	76.2
	1.2	550.8	10.62	81.9
	1.6	791.3	10.12	87.4
	2.0	1083.0	9.77	90.8
	Blank	87.4	34.93	
	0.4	294.3	16.45	70.3
35	0.8	356.7	15.51	75.5
	1.2	441.4	14.17	80.2
	1.6	546.3	13.73	84.0
	2.0	734.5	12.45	88.1
	Blank	72.8	39.91	
	0.4	220.6	18.57	67.0
40	0.8	255.4	18.08	71.5
	1.2	294.7	17.51	75.3
	1.6	365.8	16.93	80.1
	2.0	413.6	16.38	82.4
	Blank	52.7	66.70	
	0.4	143.2	28.49	63.2
45	0.8	160.2	27.63	67.1
	1.2	179.3	26.64	70.6
	1.6	206.7	25.17	74.5
	2.0	249.8	23.01	78.9
	Blank	39.0	77.59	
	0.4	95.6	38.39	59.2
50	0.8	107.7	37.05	63.8
	1.2	121.9	35.10	68.0
	1.6	131.8	33.89	70.4
	2.0	150.6	32.54	74.1

Table 3.19: EIS data for the corrosion of GA9 magnesium alloy in 1.5 M sodium chloride solution containing different concentrations of SDBS.

Temperature (°C)	Conc. of inhibitor (mM)	R_{ct} (ohm. cm²)	C_{dl} (µF cm⁻²)	η (%)
30	Blank	67.9	41.61	
	0.4	233.3	24.56	70.9
	0.8	273.8	24.12	75.2
	1.2	332.8	23.38	79.6
	1.6	424.4	21.68	84.0
	2.0	543.2	20.01	87.5
35	Blank	60.2	61.15	
	0.4	189.3	35.59	68.2
	0.8	230.7	34.12	73.9
	1.2	267.6	33.31	77.5
	1.6	373.9	31.75	83.9
	2.0	406.8	30.12	85.2
40	Blank	47.5	69.71	
	0.4	133.8	39.81	64.5
	0.8	154.2	38.23	69.2
	1.2	180.6	36.42	73.7
	1.6	216.9	35.01	78.1
	2.0	248.7	32.53	80.9
45	Blank	35.5	89.49	
	0.4	91.3	45.23	61.1
	0.8	100.0	43.02	64.5
	1.2	113.1	40.18	68.6
	1.6	126.8	38.56	72.0
	2.0	14.4	35.54	78.4
50	Blank	26.3	107.44	
	0.4	62.4	49.41	57.9
	0.8	69.0	47.35	61.9
	1.2	80.2	45.51	67.2
	1.6	89.8	42.68	70.7
	2.0	98.1	40.55	73.2

Table 3.20: EIS data for the corrosion of GA9 magnesium alloy in 2.0 M sodium chloride solution containing different concentrations of SDBS.

Temperature (℃)	Conc. of inhibitor (mM)	R_{ct} (ohm. cm^2)	C_{dl} (μF cm^{-2})	η (%)
	Blank	58.5	58.01	
	0.4	180.0	35.63	67.5
30	0.8	223.3	34.18	73.8
	1.2	256.6	33.98	77.2
	1.6	300.0	32.94	80.5
	2.0	365.6	31.53	84.0
	Blank	48.2	65.11	
	0.4	137.8	37.44	65.0
35	0.8	156.0	36.10	69.1
	1.2	177.2	34.58	72.8
	1.6	212.3	33.02	77.3
	2.0	257.8	31.37	81.3
	Blank	36.2	83.99	
	0.4	94.5	42.78	61.7
40	0.8	109.7	41.45	67.0
	1.2	126.1	39.98	71.3
	1.6	149.6	37.44	75.8
	2.0	178.3	35.02	79.7
	Blank	26.4	109.41	
	0.4	65.5	58.20	59.7
45	0.8	71.2	56.01	62.9
	1.2	78.3	53.49	66.3
	1.6	85.7	51.71	69.2
	2.0	98.9	48.56	73.3
	Blank	21.1	123.26	
	0.4	47.3	62.55	55.4
50	0.8	51.3	60.42	58.9
	1.2	56.1	58.47	62.4
	1.6	62.4	55.56	66.2
	2.0	67.0	53.31	68.5

Table 3.21: Activation parameters for the corrosion of GA9 magnesium alloy in NaCl solutions containing different concentrations of SDBS.

Concentration of NaCl	Conc. of inhibitor (mM)	E_a (kJ mol^{-1})	$\Delta H^{\#}$ (kJ mol^{-1})	$\Delta S^{\#}$ (J mol^{-1} K^{-1})
	Blank	37.67	35.07	-125.49
	0.4	53.47	50.87	-85.53
0.1	0.8	57.29	54.69	-74.41
	1.2	66.57	63.97	-46.70
	1.6	76.75	74.15	-16.37
	2.0	87.79	85.19	15.04
	Blank	35.31	32.71	-127.16
	0.4	48.79	46.19	-93.97
0.5	0.8	53.14	50.54	-81.36
	1.2	57.99	55.39	-67.24
	1.6	67.73	65.13	-37.87
	2.0	76.84	74.24	-10.68
	Blank	37.98	35.38	-114.14
	0.4	53.25	50.65	-74.38
1.0	0.8	57.78	55.18	-61.21
	1.2	62.66	60.06	-46.96
	1.6	71.52	68.92	-20.18
	2.0	78.42	75.82	0.15
	Blank	40.24	37.64	-103.66
	0.4	54.25	51.65	-67.46
1.5	0.8	58.42	55.82	-50.43
	1.2	61.09	58.49	-47.98
	1.6	69.61	67.01	-22.27
	2.0	71.83	69.23	-16.64
	Blank	42.98	40.39	-92.91
	0.4	55.55	52.95	-60.76
2.0	0.8	60.76	58.16	-45.23
	1.2	62.37	59.77	-41.08
	1.6	65.66	63.06	-31.66
	2.0	69.78	67.18	-19.64

Table 3.22: Maximum inhibition efficiencies attained by SDBS in sodium chloride solutions of different concentrations at different temperatures.

Temperature (ºC)	Sodium chloride concentration (M)	Concentration of SDBS (mM)	GA9 magnesium alloy η (%)	
			Potentiodynamic polarization method	EIS method
30	0.1	2.0	92.5	92.6
	0.5		91.1	91.5
	1.0		90.2	90.8
	1.5		86.9	87.5
	2.0		83.4	84.0
35	0.1	2.0	91.0	91.2
	0.5		89.5	90.1
	1.0		87.2	88.1
	1.5		85.0	85.2
	2.0		80.8	81.3
40	0.1	2.0	89.5	90.2
	0.5		86.6	86.9
	1.0		82.3	82.4
	1.5		81.4	80.9
	2.0		79.0	79.7
45	0.1	2.0	85.2	85.5
	0.5		81.2	81.5
	1.0		78.6	78.9
	1.5		78.7	78.4
	2.0		72.1	73.3
50	0.1	2.0	77.1	78.0
	0.5		76.2	76.4
	1.0		73.8	74.1
	1.5		73.1	73.2
	2.0		68.6	68.5

Table 3.23: Thermodynamic parameters for the adsorption of SDBS on GA9 magnesium alloy surface in sodium chloride solutions at different temperatures.

Molarity of NaCl (M)	Temperature (° C)	$-\Delta G^o_{ads}$ (kJ mol^{-1})	ΔH^o_{ads} (kJ mol^{-1})	ΔS^o_{ads} (J mol^{-1} K^{-1})	R^2	Slope
0.1	30	32.15			0.996	1.02
	35	32.70			0.997	1.03
	40	33.05	-4.95	89.84	0.995	1.05
	45	33.31			0.994	1.10
	50	34.09			0.997	1.23
0.5	30	31.93			0.996	1.03
	35	32.41			0.995	1.05
	40	32.93	-3.64	93.44	0.995	1.05
	45	33.36			0.997	1.17
	50	33.79			0.996	1.24
1.0	30	31.74			0.996	1.03
	35	32.34			0.997	1.07
	40	32.72	-6.99	82.02	0.996	1.14
	45	33.04			0.994	1.20
	50	33.44			0.997	1.27
1.5	30	31.82			0.997	1.08
	35	32.26			0.997	1.09
	40	32.37	-11.93	65.63	0.995	1.14
	45	32.52			0.987	1.19
	50	33.33			0.996	1.28
2.0	30	31.92			0.998	1.13
	35	32.11			0.995	1.16
	40	32.28	-9.99	72.15	0.996	1.17
	45	33.13			0.996	1.31
	50	33.21			0.996	1.36

3.6 SODIUM DODECYLBENZENESULFONATE (SDBS) AS CORROSION INHIBITOR ON GA9 MAGNESIUM ALLOY IN SODIUM SULPHATE MEDIUM

3.6.1 Potentiodynamic polarization measurement

The Tafel plots for the corrosion of GA9 magnesium alloy in 1.0 M sodium sulphate solution in the presence of different concentrations of SDBS, at 30 °C are shown in Fig. 3.36. Similar plots were obtained at other temperatures and also in the other five concentrations of sodium sulphate at the different temperatures studied. The potentiodynamic polarization parameters were calculated from Tafel plots in the presence of different concentrations of SDBS at different temperatures and are summarized in Tables 3.24 to 3.29. As seen from the data, in the absence of inhibitor, GA9 magnesium alloy corrodes severely in 1.0 M sodium sulphate. The presence of inhibitor brings down the corrosion rate considerably. Polarization curves are shifted to a lower current density region indicating a decrease in corrosion rate (Li et al. 2008). Inhibition efficiency increases with the increase in SDBS.
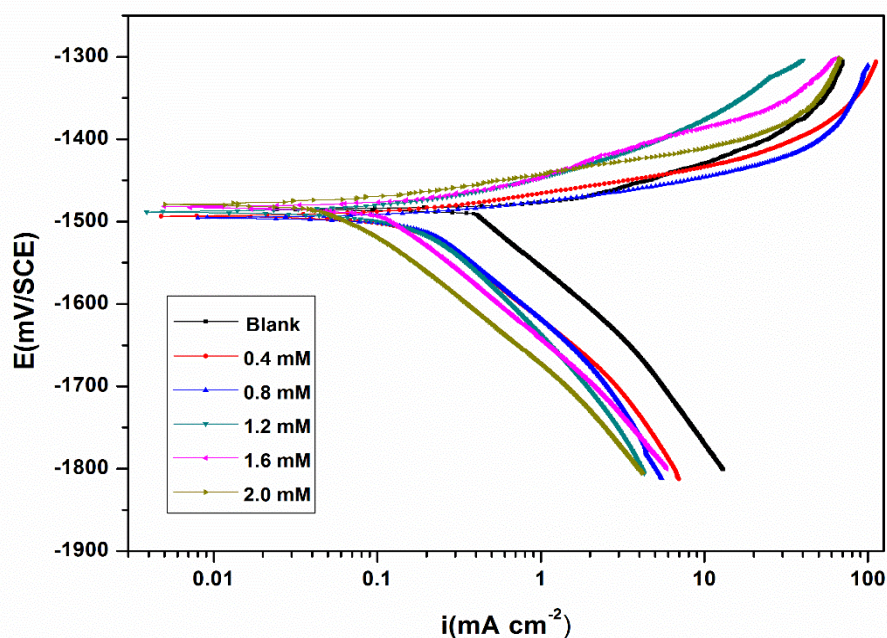
Fig. 3.36: Potentiodynamic polarization curves for the corrosion of GA9 magnesium alloy in 1.0 M Na$_2$SO$_4$ solution containing different concentrations of SDBS at 40 °C.

No definite trend is observed in the shift of E_{corr} values; both anodic and cathodic polarization profiles are influenced simultaneously, almost to the same extent, which indicate the influence of SDBS on both the anodic and the cathodic reactions; metal dissolution and hydrogen evolution. The maximum displacement of E_{corr} is 20 mV, which indicates that SDBS is a mixed type inhibitor (Ferreira et al. 2004 and Li et al. 2008). The data in Tables 3.24 to 3.28 show that there is no significant change in the values of cathodic Tafel slope b_c with the increase in the concentration of the inhibitor. This suggests that the reduction mechanism at the cathode and the oxidation mechanism at the anode are not affected by the presence of inhibitor and hence the corrosion reaction is slowed down by the surface-blocking effect of the inhibitor (Ehteshamzadeh et al. 2009 and Ateya et al. 1976). Thus, the inhibitor, SDBS, can be regarded as a mixed type inhibitor. The inhibition efficiency increases with the increase in inhibitor concentration, reaching a maximum value of 91.1 % at 2.0 mM of SDBS in 1.0 M sodium sulphate solution.

3.6.2 Electrochemical impedance spectroscopy (EIS)

Nyquist plots for the corrosion of GA9 magnesium alloy in 1.0 M sodium sulphate solution in the presence of different concentrations of SDBS are shown in Fig. 3.37. Similar plots were obtained in other concentrations of sulphuric acid and also at other temperatures. The experimental results of EIS measurements obtained for the corrosion of GA9 magnesium alloy in sodium sulphate solution of different concentrations at different temperatures are summarized in Tables 3.29 to 3.33.

The Nyquist plots are characterized by a capacitive loop, extended from high frequency (HF) to low frequency (LF) range, an inductive loop in the low frequency region (LF) range and a tail at the medium frequency (MF) range in the presence as well as in the absence of inhibitor. This indicates that the corrosion of GA9 magnesium alloy is controlled by a charge transfer process and the addition of SDBS does not change the reaction mechanism of the corrosion of sample in sodium sulphate solution (Amin et al. 2007). SDBS inhibits the corrosion primarily through its adsorption and subsequent formation of a barrier film on the metal surface (El Hosary et al. 1972, Sanaa T. 2008). This is in accordance with the observations of Tafel polarization measurements.
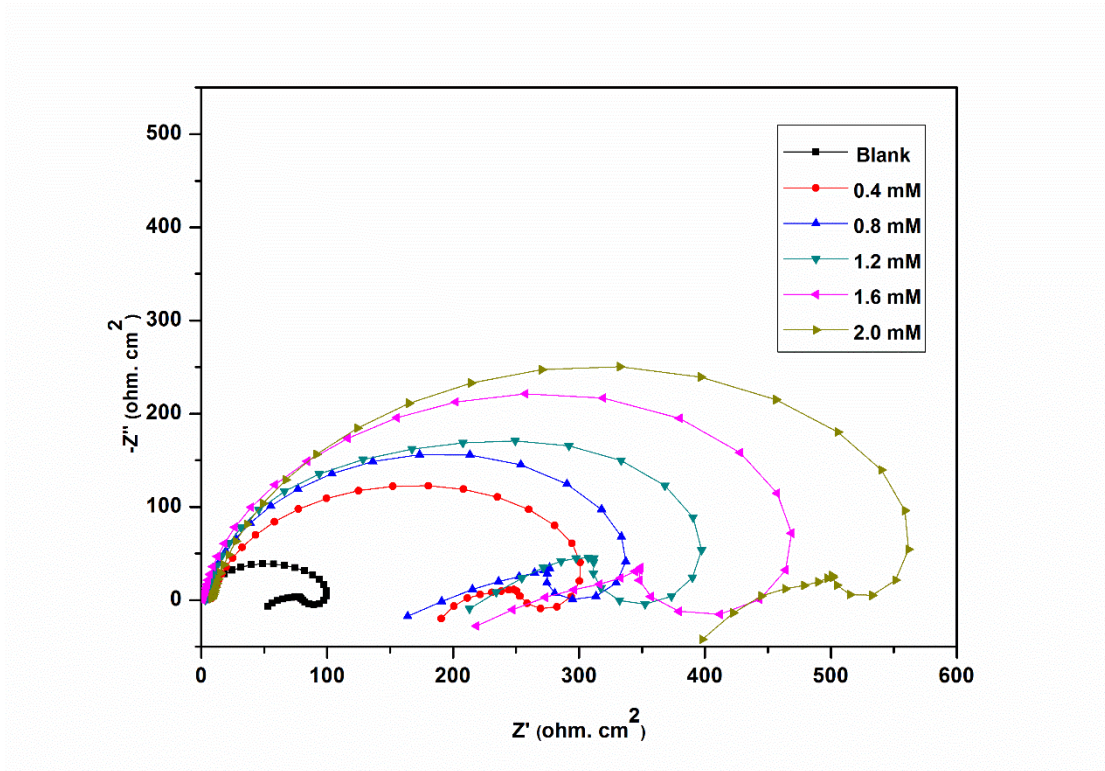
Fig. 3.37: Nyquist plots for the corrosion of GA9 magnesium alloy in 1.0 M Na$_2$SO$_4$ solution containing different concentrations of SDBS at 40 ℃.
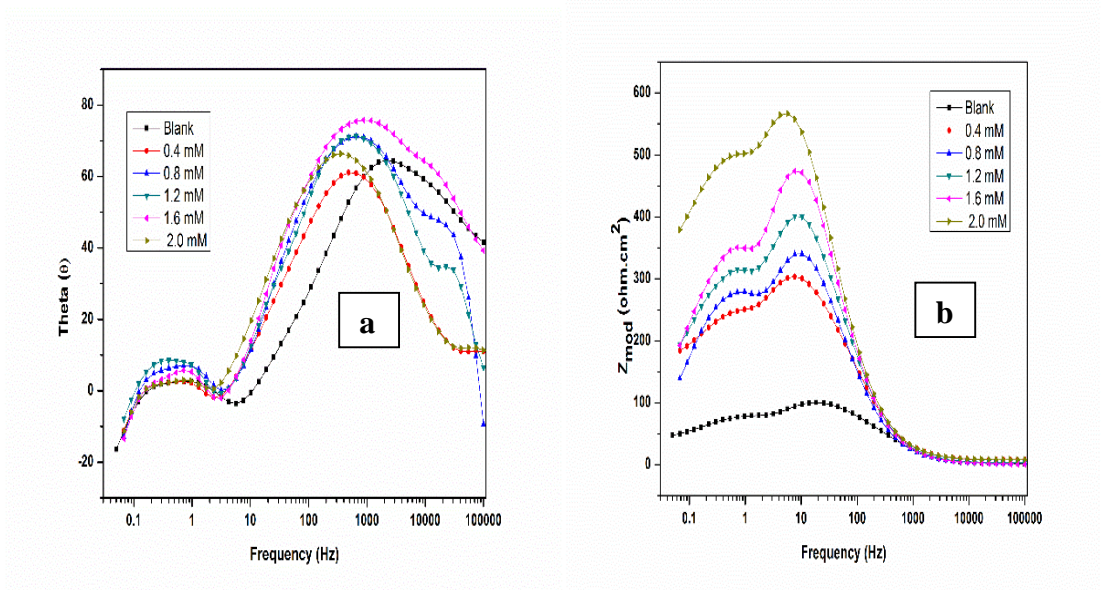
Fig. 3.38: Bode (a) phase angle plots and (b) amplitude plots for the corrosion of GA9 magnesium alloy in 1.0 M Na$_2$SO$_4$ solution containing different concentrations of SDBS at 40 °C.

123

The equivalent circuit models shown in Fig. 3.3 is used for the interpretation of the Nyquist plots in the presence and absence of SDBS.

The Bode plots of phase angle and amplitude for the corrosion of the GA9 magnesium alloy immersed in 1.0 M Na_2SO_4 solution at 40 °C varying amounts of SDBS, are shown in Fig. 3.38 (a) and Fig. 3.38 (b), respectively. As seen from the Bode plots, both the impedance modulus (Z_{mod}) at low frequency and the phase maximum (θ_{max}) at intermediate frequency increase with the increase in SDBS concentration, which suggests the presence of highly protective surface film, opposing the corrosive penetration.

3.6.3 Effect of temperature

The results in Tables 3.24 to 3.33 shows that corrosion rate increases and the inhibition efficiency of SDBS decreases with the increase in temperature. The decrease in inhibition efficiency with the increase in temperature indicates desorption of the inhibitor molecules from the metal surface on increasing the temperature (Frignani et al. 2012). This fact is also suggestive of physisorption of the inhibitor molecules on the metal surface. Corrosion reactions are usually regarded as Arrhenius processes and the apparent activation energy (E_a) of the corrosion reaction was calculated from Arrhenius equation as discussed in the section 3.5.3. The plot of $ln(v_{corr})$ versus reciprocal of absolute temperature ($1/T$) gives a straight line with slope $= -E_a / R$, from which, the activation energy values for the corrosion process were calculated. The Arrhenius plots for the corrosion of GA9 magnesium alloy in the presence of different concentrations of SDBS in 1.0 M Na_2SO_4 acid are shown in Fig. 3.39. The plots of $ln(v_{corr}/T)$ versus $1/T$ in 1.0 M Na_2SO_4 in the presence of different concentrations of SDBS are shown in Fig. 3.40.

The calculated values of E_a, $\Delta H^{\#}$ and $\Delta S^{\#}$ are given in Table 3.34. The proportionate increase in the activation energy on the addition of SDBS can be attributed to the adsorption of SDBS providing a barrier on the alloy surface (Avci et al. 2008). The values of entropy of activation indicates that the activated complex in the rate determining step represents an association rather than dissociation, resulting in a decrease in randomness on going from the reactants to the activated complex.
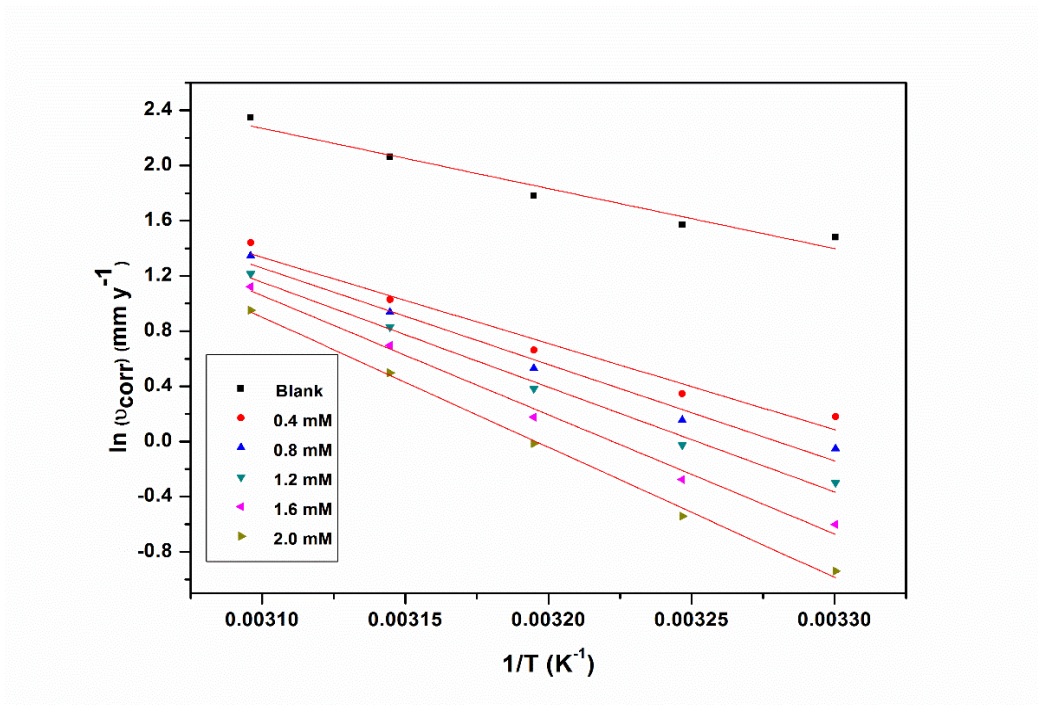
Fig. 3.39: Arrhenius plots for the corrosion of GA9 magnesium alloy in 1.0 M Na₂SO₄ solution containing different concentrations of SDBS.
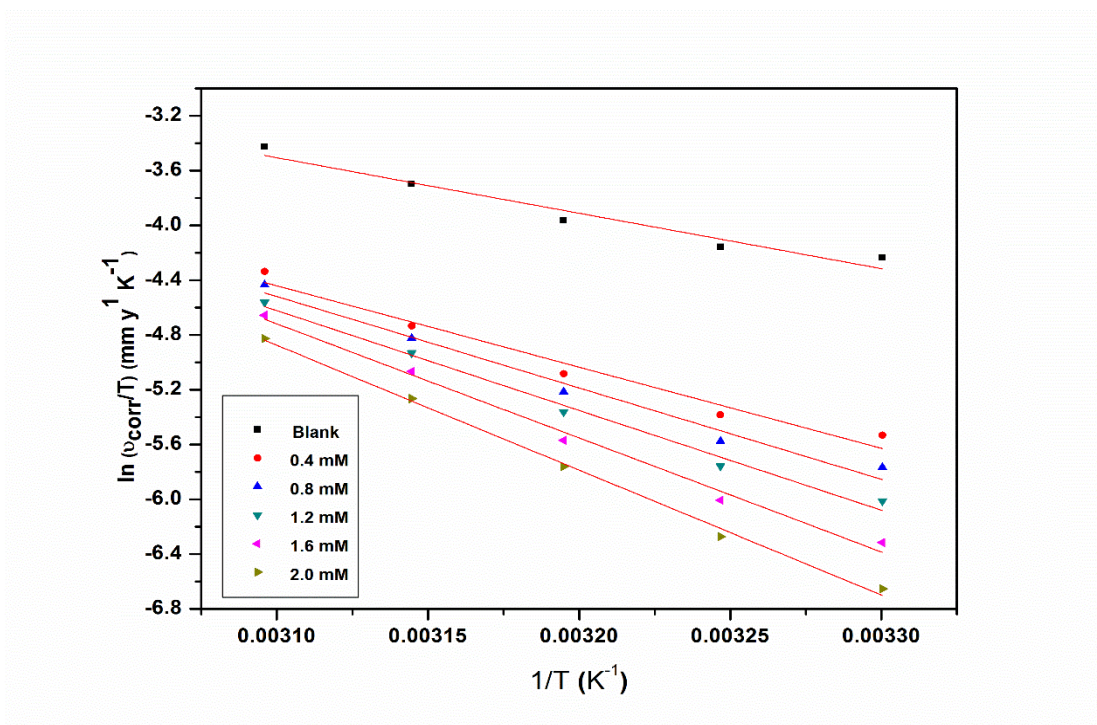
Fig. 3.40: Plots of ln(υ_{corr}/T) versus 1/T for the corrosion of GA9 magnesium alloy in 1.0 M Na₂SO₄ solution containing different concentrations of SDBS.

3.6.4 Effect of sodium sulphate concentration

Tables 3.25 summarises the maximum inhibition efficiencies exhibited by SDBS in the sodium sulphate solutions of different concentrations at different temperatures. It is evident from both polarization and EIS experimental results that, for a particular concentration of inhibitor, the inhibition efficiency decreases with the increase in sodium sulphate concentration on GA9 magnesium alloy. The highest inhibition efficiency is observed in sodium sulphate of 0.1 M concentration.

3.6.5 Adsorption isotherms

The adsorption of SDBS on the surface of GA9 magnesium alloy was found to obey Langmuir adsorption isotherm. The Langmuir adsorption isotherms for the adsorption of SDBS on GA9 magnesium alloy in 1.0 M Na_2SO_4 are shown in Fig. 3.41. The linear regression coefficients are close to unity and the slopes of the straight lines are nearly unity, suggesting that the adsorption of SDBS obeys Langmuir's adsorption isotherm with negligible interaction between the adsorbed molecules. The plot of ΔG°_{ads} Vs T is shown in Fig. 3.42.
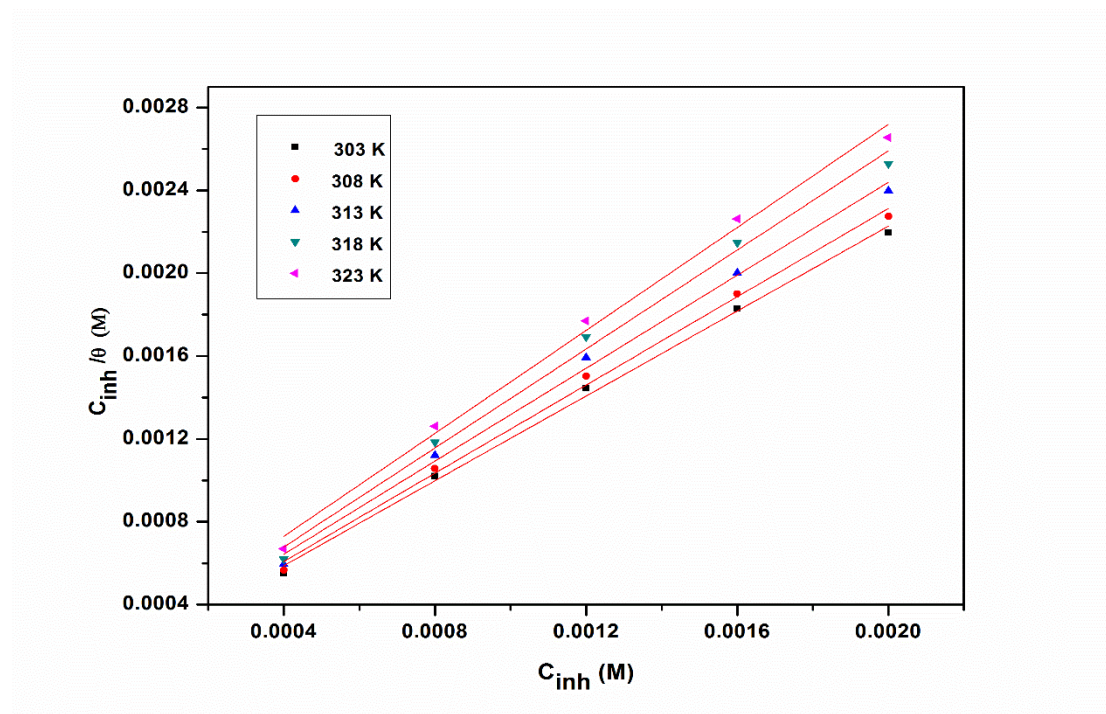
Fig. 3.41: Langmuir adsorption isotherms for the adsorption of SDBS on GA9 magnesium alloy in 1.0 M Na_2SO_4 solution at different temperatures.
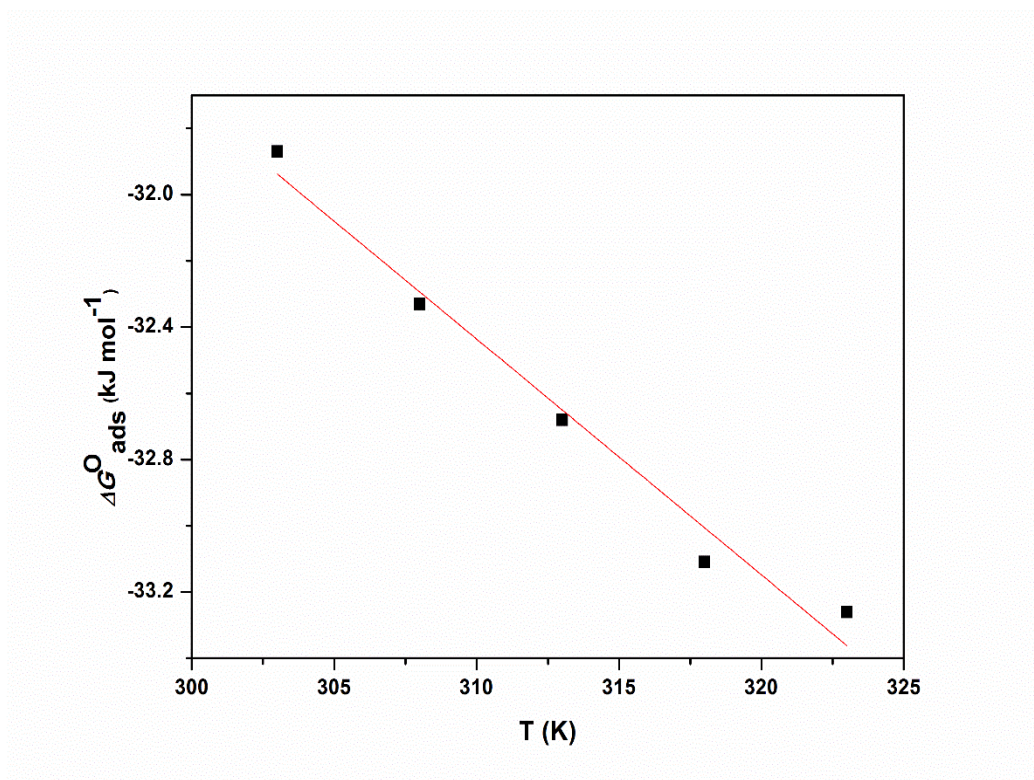
Fig. 3.42: The plot of ΔG°_{ads} Vs *T* for the adsorption of SDBS on GA9 magnesium alloy in 1.0 M Na$_2$SO$_4$ solution.

The thermodynamic data obtained for the adsorption of SDBS on GA9 magnesium alloy are tabulated in Table 3.26. The linear regression coefficients are close to unity and the slopes of the straight lines are nearly unity, suggesting that the adsorption of SDBS obeys Langmuir's adsorption isotherm with negligible interaction between the adsorbed molecules. The exothermic ΔH°_{ads} values of less than 41.86 kJ mol^{-1} predict physisorption of SDBS on the alloy surfaces (Martinez et al. 2002). The ΔG°_{ads} values predict both physisorption and chemisorption of SDBS. Therefore it can be concluded that the adsorption of SDBS on the GA9 magnesium alloy is predominantly through physisorption. These facts are also supported by the variation of inhibition efficiencies with temperature on the alloy surface as discussed under section 3.6.3.

3.6.6 Mechanism of corrosion inhibition

The corrosion inhibition mechanism of SDBS in sodium sulphate solution can be explained in the same lines as that of SDBS in the section 3.5.6. The inhibitor SDBS

127

protects the alloy surface through predominant physisorption mode in which the SDBS gets adsorbed on the alloy surface through electrostatic attraction.

3.6.7 SEM/EDX studies

Fig. 3.43 (a) represents SEM image of the corroded GA9 magnesium alloy sample. The corroded surface shows detachment of particles from the surface. The corrosion of the alloy may be predominantly attributed to the galvanic effect between the precipitates and the matrix. Fig. 3.43 (b) represents SEM image of GA9 magnesium alloy after the corrosion tests in a medium of 2.0 M sodium sulphate containing 2.0 mM of SDBS. The image clearly shows a less deteriorated surface due to the adsorbed layer of inhibitor molecules on the alloy surface, thus protecting the metal from corrosion.

(a)   (b)
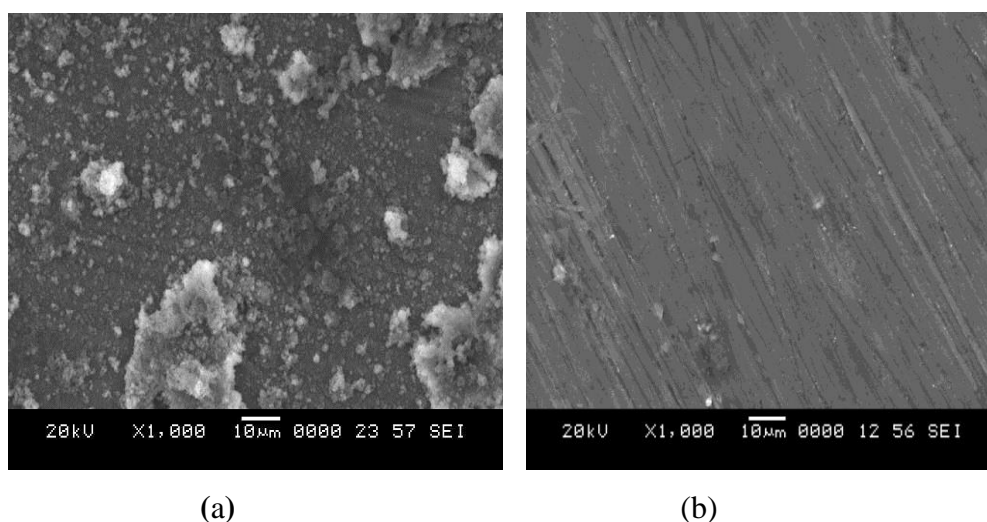
Fig.3.43: SEM images of GA9 magnesium alloy after immersion in 2.0 M Na$_2$SO$_4$ solution a) in the absence and b) in the presence of SDBS.

The EDX profile analyses for the selected areas on the SEM images of Fig. 3.43 (a) and (b) are shown in Fig. 3.44 (a) and 3.44 (b), respectively. In the EDX spectra Fig. 3.44(b), apart from the peaks for Mg, Al, Zn and S, an additional small peak for carbon and oxygen is obtained, which indicates the presence of some organic moieties on the alloy surface, which possibly are the surface adsorbed SDBS molecules.
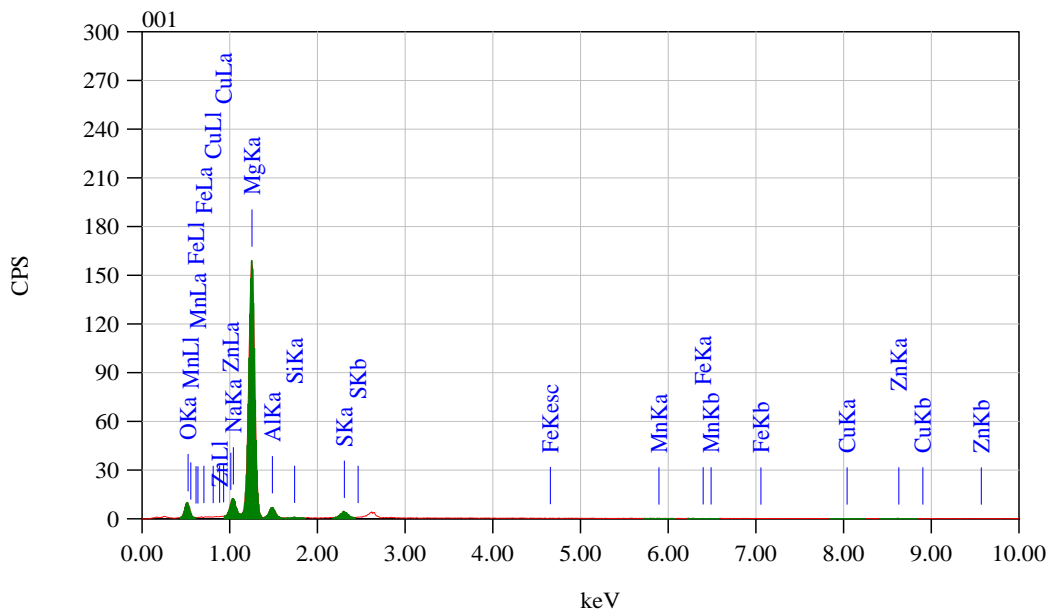
Fig. 3.44 (a): EDX spectra of GA9 magnesium alloy after immersion in 1.0 M Na₂SO₄ solution in the absence of SDBS.
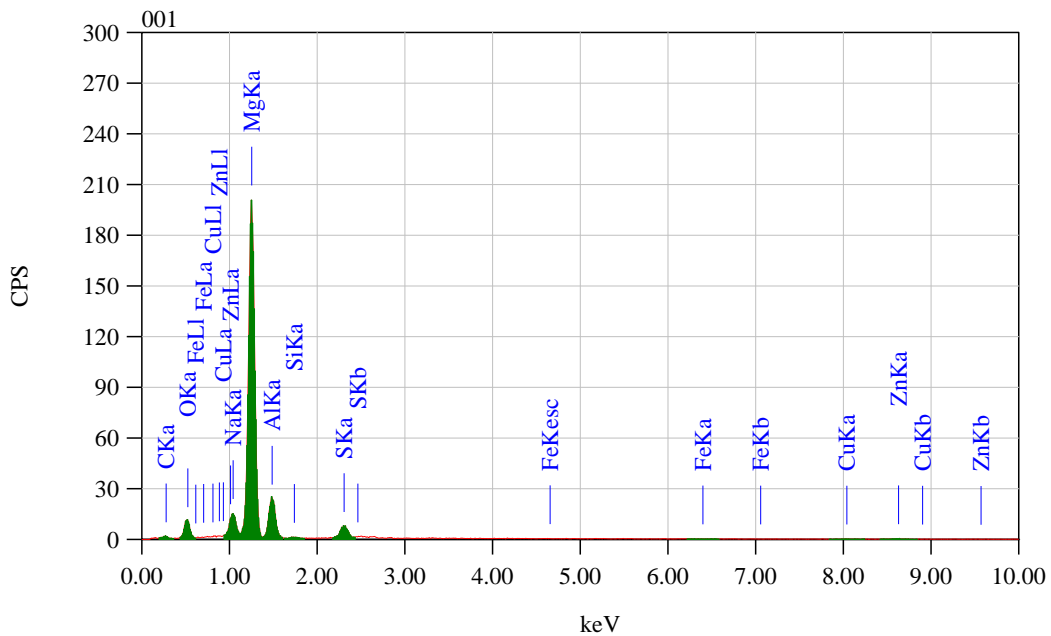
Fig. 3.44 (b): EDX spectra of GA9 magnesium alloy after immersion in 1.0 M Na₂SO₄ solution in the presence of SDBS.

Table 3.24: Results of potentiodynamic polarization studies for the corrosion of GA9 magnesium alloy in 0.1 M sodium sulphate solution containing different concentrations of SDBS.

Temperature (℃)	Conc. of inhibitor (mM)	$-E_{corr}$ (mV /SCE)	$-b_c$ (mV dec^{-1})	i_{corr} (μA cm^{-2})	υ_{corr} (mm y^{-1})	η (%)
	Blank	1456	139	42.1	0.946	
	0.4	1462	114	9.9	0.222	76.4
30	0.8	1457	112	8.2	0.184	80.5
	1.2	1459	109	6.3	0.142	85.1
	1.6	1453	107	4.3	0.097	89.7
	2.0	1451	104	2.9	0.065	93.1
	Blank	1461	144	47.7	1.071	
	0.4	1468	118	11.6	0.261	75.7
	0.8	1465	115	9.9	0.222	79.3
35	1.2	1462	112	7.6	0.171	84.1
	1.6	1455	110	5.6	0.126	88.2
	2.0	1458	107	4.1	0.092	91.4
	Blank	1463	151	58.4	1.311	
	0.4	1469	127	15.0	0.337	74.3
	0.8	1462	124	13.1	0.294	77.5
40	1.2	1466	121	10.3	0.231	82.4
	1.6	1459	118	7.9	0.177	86.5
	2.0	1457	114	6.0	0.135	89.8
	Blank	1468	159	74.4	1.671	
	0.4	1474	136	22.2	0.499	70.1
	0.8	1472	133	19.7	0.443	73.5
45	1.2	1465	130	17.0	0.382	77.1
	1.6	1469	127	12.8	0.288	82.8
	2.0	1462	123	10.1	0.227	86.4
	Blank	1469	167	97.8	2.197	
	0.4	1473	146	33.5	0.753	65.7
	0.8	1476	143	31.1	0.699	68.2
50	1.2	1468	141	28.0	0.629	71.4
	1.6	1463	139	24.7	0.555	74.7
	2.0	1466	136	20.5	0.461	79.0

Table 3.25: Results of potentiodynamic polarization studies for the corrosion of GA9 magnesium alloy in 0.5 M sodium sulphate solution containing different concentrations of SDBS.

Temperature (℃)	Conc. of inhibitor (mM)	$-E_{corr}$ (mV /SCE)	$-b_c$ (mV dec^{-1})	i_{corr} (μA cm^{-2})	υ_{corr} (mm y^{-1})	η (%)
	Blank	1461	144	112.4	2.526	
	0.4	1468	122	29.0	0.652	74.2
30	0.8	1465	120	23.3	0.524	79.3
	1.2	1462	118	18.4	0.413	83.6
	1.6	1457	116	13.4	0.301	88.1
	2.0	1459	113	9.0	0.202	92.0
	Blank	1462	149	125.5	2.819	
	0.4	1468	127	33.2	0.746	73.5
	0.8	1465	124	27.5	0.618	78.1
35	1.2	1461	122	22.8	0.512	81.8
	1.6	1466	119	16.9	0.380	86.5
	2.0	1459	115	12.2	0.274	90.3
	Blank	1459	156	161.1	3.619	
	0.4	1465	134	44.9	1.009	72.1
	0.8	1461	132	39.5	0.888	75.5
40	1.2	1463	129	32.4	0.728	79.9
	1.6	1458	126	26.6	0.598	83.5
	2.0	1457	123	20.3	0.456	87.4
	Blank	1475	164	203.3	4.568	
	0.4	1479	143	63.0	1.416	69.0
	0.8	1476	141	56.3	1.265	72.3
45	1.2	1472	138	48.4	1.087	76.2
	1.6	1469	136	43.7	0.982	78.5
	2.0	1467	133	36.2	0.813	82.2
	Blank	1487	173	264.3	5.939	
	0.4	1495	153	96.5	2.168	63.5
	0.8	1492	151	87.5	1.966	66.9
50	1.2	1489	149	77.2	1.735	70.8
	1.6	1482	146	69.0	1.550	73.9
	2.0	1485	143	60.5	1.359	77.1

Table 3.26: Results of potentiodynamic polarization studies for the corrosion of GA9 magnesium alloy in 1.0 M sodium sulphate solution containing different concentrations of SDBS.

Temperature (℃)	Conc. of inhibitor (mM)	$-E_{corr}$ (mV /SCE)	$-b_c$ (mV dec^{-1})	i_{corr} (μA cm^{-2})	υ_{corr} (mm y^{-1})	η (%)
30	Blank	1472	151	195.2	4.386	
	0.4	1476	134	53.3	1.198	72.7
	0.8	1473	131	42.2	0.948	78.4
	1.2	1471	127	33.0	0.741	83.1
	1.6	1463	124	24.4	0.548	87.5
	2.0	1465	122	17.4	0.391	91.1
35	Blank	1477	156	214.2	4.813	
	0.4	1485	140	63.0	1.416	70.6
	0.8	1476	137	52.0	1.168	75.7
	1.2	1479	134	43.3	0.973	79.8
	1.6	1474	132	33.8	0.759	84.2
	2.0	1472	129	25.9	0.582	87.9
40	Blank	1486	160	264.3	5.938	
	0.4	1492	146	86.4	1.941	67.3
	0.8	1496	143	75.6	1.699	71.4
	1.2	1486	141	5.3	1.467	75.3
	1.6	1482	137	53.1	1.193	79.9
	2.0	1479	134	43.9	0.986	83.4
45	Blank	1487	171	350.4	7.872	
	0.4	1494	153	124.4	2.795	64.5
	0.8	1490	150	113.5	2.550	67.6
	1.2	1482	147	102.0	2.292	70.9
	1.6	1487	144	89.3	2.006	74.5
	2.0	1479	142	73.2	1.645	79.1
50	Blank	1490	181	466.3	10.477	
	0.4	1494	165	187.9	4.222	59.7
	0.8	1498	163	170.7	3.835	63.4
	1.2	1491	160	150.1	3.372	67.8
	1.6	1482	158	136.6	3.069	70.7
	2.0	1486	156	115.2	2.588	75.3

Table 3.27: Results of potentiodynamic polarization studies for the corrosion of GA9 magnesium alloy in 1.5 M sodium sulphate solution containing different concentrations of SDBS.

Temperature (℃)	Conc. of inhibitor (mM)	$-E_{corr}$ (mV /SCE)	$-b_c$ (mV dec^{-1})	i_{corr} (μA cm^{-2})	υ_{corr} (mm y^{-1})	η (%)
	Blank	1477	158	281.7	6.328	
	0.4	1485	141	83.1	1.867	70.5
30	0.8	1482	138	68.2	1.532	75.8
	1.2	1479	135	56.3	1.265	80.0
	1.6	1472	132	44.8	1.007	84.1
	2.0	1475	128	34.4	0.773	87.8
	Blank	1483	165	339.2	7.621	
	0.4	1490	148	106.8	2.400	68.5
	0.8	1483	145	85.1	1.912	74.9
35	1.2	1486	143	73.6	1.654	78.3
	1.6	1480	141	56.0	1.258	83.5
	2.0	1478	139	49.5	1.112	85.4
	Blank	1482	173	426.8	9.589	
	0.4	1485	160	149.8	3.366	64.9
	0.8	1486	157	128.9	2.896	69.8
40	1.2	1482	154	110.5	2.483	74.1
	1.6	1479	151	91.3	2.051	78.6
	2.0	1475	146	73.4	1.650	82.8
	Blank	1486	182	527.1	11.843	
	0.4	1492	170	202.9	4.559	61.5
	0.8	1482	167	182.9	4.109	65.3
45	1.2	1489	163	160.8	3.613	69.5
	1.6	1480	160	142.8	3.208	72.9
	2.0	1485	158	123.9	2.784	76.5
	Blank	1492	194	707.4	15.894	
	0.4	1494	184	299.9	6.738	57.6
	0.8	1490	181	275.2	6.183	61.1
50	1.2	1496	177	245.5	5.516	65.3
	1.6	1487	174	218.6	4.912	69.1
	2.0	1485	172	189.6	4.260	73.2

Table 3.28: Results of potentiodynamic polarization studies for the corrosion of GA9 magnesium alloy in 2.0 M sodium sulphate solution containing different concentrations of SDBS.

Temperature (℃)	Conc. of inhibitor (mM)	$-E_{corr}$ (mV /SCE)	$-b_c$ (mV dec^{-1})	i_{corr} (µA cm^{-2})	υ_{corr} (mm y^{-1})	η (%)
30	Blank	1488	169	374.6	8.417	
	0.4	1491	158	121.0	2.719	67.7
	0.8	1493	155	96.6	2.170	74.2
	1.2	1485	153	82.8	1.860	77.9
	1.6	1489	149	73.0	1.640	80.5
	2.0	1483	145	60.3	1.354	83.9
35	Blank	1483	176	455.4	10.232	
	0.4	1486	164	158.5	3.561	65.2
	0.8	1489	161	137.5	3.089	69.8
	1.2	1483	158	120.7	2.712	73.5
	1.6	1481	154	104.3	2.343	77.1
	2.0	1478	152	85.2	1.914	81.3
40	Blank	1481	185	597.1	13.415	
	0.4	1482	173	221.5	4.977	62.9
	0.8	1488	171	192.3	4.320	67.8
	1.2	1484	167	164.2	3.689	72.5
	1.6	1478	164	140.9	3.166	76.4
	2.0	1479	159	120.0	2.696	79.9
45	Blank	1489	197	755.8	16.981	
	0.4	1495	187	306.0	6.875	59.5
	0.8	1492	184	278.1	6.248	63.2
	1.2	1488	181	254.7	5.722	66.3
	1.6	1483	177	231.3	5.197	69.4
	2.0	1486	172	204.8	4.601	72.9
50	Blank	1499	209	927.7	20.842	
	0.4	1505	197	413.8	9.297	55.4
	0.8	1502	194	381.3	8.567	58.9
	1.2	1498	190	341.4	7.671	63.2
	1.6	1493	187	314.5	7.066	66.1
	2.0	1499	183	282.9	6.356	69.5

Table 3.29: EIS data for the corrosion of GA9 magnesium alloy in 0.1 M sodium sulphate solution containing different concentrations of SDBS.

Temperature (℃)	Conc. of inhibitor (mM)	R_{ct} (ohm. cm^2)	C_{dl} (µF cm^{-2})	η (%)
	Blank	604.7	10.53	
	0.4	2509.0	6.95	75.9
30	0.8	3149.0	6.72	80.8
	1.2	4085.0	6.53	85.2
	1.6	5987.0	6.46	89.9
	2.0	8892.0	6.14	93.2
	Blank	545.5	10.98	
	0.4	2190.0	7.91	75.1
35	0.8	2700.0	7.69	79.8
	1.2	3565.0	7.53	84.7
	1.6	4870.0	7.31	88.8
	2.0	6129.0	7.09	91.1
	Blank	447.8	11.35	
	0.4	1777.0	8.47	74.5
40	0.8	2044.0	8.32	78.1
	1.2	2515.0	8.16	82.2
	1.6	3269.0	8.04	86.3
	2.0	4224.0	7.75	89.4
	Blank	356.5	16.50	
	0.4	1217.0	10.16	70.7
45	0.8	1381.0	9.98	74.2
	1.2	1658.0	9.69	78.5
	1.6	2109.0	9.47	83.1
	2.0	2763.0	9.31	87.1
	Blank	273.0	25.71	
	0.4	800.6	15.53	65.9
50	0.8	875.1	15.04	68.8
	1.2	951.2	14.91	71.3
	1.6	1092.0	14.52	75.0
	2.0	1312.0	14.19	79.2

Table 3.30: EIS data for the corrosion of GA9 magnesium alloy in 0.5 M sodium sulphate solution containing different concentrations of SDBS.

Temperature (℃)	Conc. of inhibitor (mM)	R_{ct} (ohm. cm^2)	C_{dl} (µF cm^{-2})	η (%)
30	Blank	219.1	18.29	
	0.4	839.5	9.29	73.9
	0.8	1074.0	8.95	79.6
	1.2	1328.0	8.72	83.5
	1.6	1857.0	8.57	88.2
	2.0	2845.0	8.40	92.3
35	Blank	200.4	22.81	
	0.4	762.0	10.61	73.7
	0.8	945.3	10.28	78.8
	1.2	1119.0	9.79	82.1
	1.6	1578.0	9.32	87.3
	2.0	2109.0	9.01	90.5
40	Blank	165.0	26.11	
	0.4	608.9	12.77	72.9
	0.8	696.2	12.62	76.3
	1.2	812.8	12.35	79.7
	1.6	937.5	11.88	82.4
	2.0	1320.0	11.44	87.5
45	Blank	128.8	30.77	
	0.4	419.5	14.32	69.3
	0.8	461.6	13.96	72.1
	1.2	567.4	13.73	77.3
	1.6	625.2	13.09	79.4
	2.0	736.0	12.57	82.5
50	Blank	97.8	34.19	
	0.4	265.8	17.54	63.2
	0.8	297.3	16.91	67.1
	1.2	328.2	16.52	70.2
	1.6	380.5	16.23	74.3
	2.0	436.6	15.89	77.6

Table 3.31: EIS data for the corrosion of GA9 magnesium alloy in 1.0 M sodium sulphate solution containing different concentrations of SDBS.

Temperature (°C)	Conc. of inhibitor (mM)	R_{ct} (ohm. cm^2)	C_{dl} (μF cm^{-2})	η (%)
	Blank	139.0	30.91	
	0.4	512.9	10.67	72.9
30	0.8	646.5	10.15	78.5
	1.2	827.4	9.75	83.2
	1.6	1112.0	9.43	87.5
	2.0	1544.0	9.04	91.0
	Blank	122.6	32.17	
	0.4	414.2	12.45	70.4
35	0.8	515.1	12.01	76.2
	1.2	609.9	11.66	79.9
	1.6	780.9	11.18	84.3
	2.0	973.0	10.73	87.4
	Blank	97.4	40.62	
	0.4	296.0	19.11	67.1
40	0.8	344.2	18.69	71.7
	1.2	402.5	18.01	75.8
	1.6	470.5	17.16	79.3
	2.0	556.5	16.09	82.5
	Blank	72.1	45.05	
	0.4	204.8	22.53	64.8
45	0.8	228.9	22.19	68.5
	1.2	250.3	21.39	71.2
	1.6	286.1	20.30	74.8
	2.0	350.0	19.22	79.4
	Blank	55.5	56.30	
	0.4	136.4	26.18	59.3
50	0.8	149.6	25.27	62.9
	1.2	174.0	24.38	68.1
	1.6	192.0	23.10	71.1
	2.0	229.4	22.01	75.8

Table 3.32: EIS data for the corrosion of GA9 magnesium alloy in 1.5 M sodium sulphate solution containing different concentrations of SDBS.

Temperature (℃)	Conc. of inhibitor (mM)	R_{ct} (ohm. cm^2)	C_{dl} (μF cm^{-2})	η (%)
	Blank	91.6	34.56	
	0.4	306.4	12.44	70.1
30	0.8	370.9	12.21	75.3
	1.2	469.7	11.85	80.5
	1.6	591.0	11.69	84.5
	2.0	727.0	11.40	87.4
	Blank	77.7	40.12	
	0.4	243.6	18.57	68.1
35	0.8	313.3	18.02	75.2
	1.2	361.4	17.55	78.5
	1.6	473.8	16.61	83.6
	2.0	514.6	15.90	84.9
	Blank	62.4	54.17	
	0.4	178.8	28.49	65.1
40	0.8	205.3	27.68	69.6
	1.2	241.9	26.71	74.2
	1.6	290.2	24.65	78.5
	2.0	358.6	23.72	82.6
	Blank	48.7	71.38	
	0.4	125.5	33.50	61.2
45	0.8	142.4	32.01	65.8
	1.2	161.8	31.39	69.9
	1.6	181.0	30.53	73.1
	2.0	204.6	29.05	76.2
	Blank	37.5	88.74	
	0.4	88.9	40.02	57.8
50	0.8	97.7	38.43	61.6
	1.2	108.1	37.86	65.3
	1.6	123.8	35.79	69.7
	2.0	141.5	33.42	73.5

Table 3.33: EIS data for the corrosion of GA9 magnesium alloy in 2.0 M sodium sulphate solution containing different concentrations of SDBS.

Temperature (℃)	Conc. of inhibitor (mM)	R_{ct} (ohm. cm^2)	C_{dl} (μF cm^{-2})	η (%)
30	Blank	67.5	42.55	
	0.4	206.4	18.76	67.3
	0.8	261.6	18.02	74.2
	1.2	297.4	17.54	77.3
	1.6	339.2	16.77	80.1
	2.0	409.1	15.69	83.5
35	Blank	57.4	50.87	
	0.4	167.8	24.31	65.8
	0.8	193.3	22.20	70.3
	1.2	216.6	21.75	73.5
	1.6	249.5	20.58	77.0
	2.0	305.3	19.60	81.2
40	Blank	43.2	69.58	
	0.4	118.4	32.53	63.5
	0.8	135.8	30.31	68.2
	1.2	157.1	28.44	72.5
	1.6	182.3	26.53	76.3
	2.0	217.1	24.00	80.1
45	Blank	34.0	85.41	
	0.4	84.2	42.49	59.6
	0.8	90.4	40.21	62.4
	1.2	100.3	38.47	66.1
	1.6	113.0	35.74	69.9
	2.0	127.8	33.27	73.4
50	Blank	27.8	102.33	
	0.4	62.2	48.06	55.3
	0.8	67.8	46.33	59.0
	1.2	77.0	44.01	63.9
	1.6	81.3	41.55	65.8
	2.0	90.8	38.23	69.4

Table 3.34: Activation parameters for the corrosion of GA9 magnesium alloy in sodium sulphate solutions containing different concentrations of SDBS.

Concentration of Na_2SO_4	Conc. of inhibitor (mM)	E_a (kJ mol^{-1})	$\Delta H^{\#}$ (kJ mol^{-1})	$\Delta S^{\#}$ (J mol^{-1} K^{-1})
	Blank	34.57	31.97	-140.53
	0.4	50.12	47.52	-101.61
0.1	0.8	54.50	51.90	-88.75
	1.2	61.29	58.69	-68.73
	1.6	69.97	67.37	-43.26
	2.0	78.22	75.62	-19.22
	Blank	35.60	32.99	-128.98
	0.4	49.36	46.76	-95.18
0.5	0.8	54.54	51.94	-79.87
	1.2	58.81	56.21	-67.72
	1.6	68.65	66.05	-37.98
	2.0	79.60	77.00	-13.44
	Blank	36.22	33.62	-122.51
	0.4	51.91	49.31	-81.63
1.0	0.8	58.07	55.47	-63.20
	1.2	63.18	60.58	-48.21
	1.6	71.80	69.20	-22.28
	2.0	78.38	75.78	-3.19
	Blank	37.09	34.49	-116.19
	0.4	52.14	49.54	-76.78
1.5	0.8	57.77	55.17	-60.07
	1.2	60.56	57.96	-52.37
	1.6	66.70	64.10	-34.27
	2.0	70.40	67.80	-23.92
	Blank	37.75	35.15	-111.50
	0.4	50.70	48.10	-78.25
2.0	0.8	56.17	53.56	-61.94
	1.2	58.26	55.66	-56.27
	1.6	60.47	57.86	-50.23
	2.0	64.55	61.95	-38.48

Table 3.35: Maximum inhibition efficiencies attained in different concentrations of sodium sulphate solutions at different temperatures for SDBS.

Temperature (ºC)	Sodium sulphate concentration (M)	Concentration of SDBS (mM)	GA9 magnesium alloy η (%)	
			Potentiodynamic polarization method	EIS method
30	0.1		93.1	93.2
	0.5		92.0	92.3
	1.0	2.0	91.1	91.0
	1.5		87.8	87.4
	2.0		83.9	83.5
35	0.1		91.4	91.1
	0.5		90.3	90.5
	1.0	2.0	87.9	87.4
	1.5		85.4	84.9
	2.0		81.3	81.2
40	0.1		89.8	89.4
	0.5		87.4	87.5
	1.0	2.0	83.4	82.5
	1.5		82.8	82.6
	2.0		79.9	80.1
45	0.1		86.4	87.1
	0.5		82.2	82.5
	1.0	2.0	79.1	79.4
	1.5		76.5	76.2
	2.0		72.9	73.4
50	0.1		79.0	65.9
	0.5		77.1	77.6
	1.0	2.0	75.3	75.8
	1.5		73.2	73.5
	2.0		69.5	69.4

Table 3.36: Thermodynamic parameters for the adsorption of SDBS on GA9 magnesium alloy surface in sodium sulphate solutions at different temperatures.

Molarity of Na$_2$SO$_4$ (M)	Temperature (°C)	$-\Delta G^o_{ads}$ (kJ mol^{-1})	ΔH^o_{ads} (kJ mol^{-1})	ΔS^o_{ads} (J mol^{-1} K^{-1})	R^2	Slope
	30	32.13			0.996	1.01
	35	32.73			0.997	1.03
0.1	40	33.16	-7.74	80.84	0.996	1.05
	45	33.23			0.992	1.08
	50	33.90			0.994	1.20
	30	31.96			0.996	1.02
	35	32.51			0.995	1.04
0.5	40	33.08	-1.36	101.23	0.996	1.08
	45	33.81			0.997	1.16
	50	33.84			0.996	1.22
	30	31.87			0.997	1.02
	35	32.33			0.996	1.07
1.0	40	32.68	-10.36	71.21	0.995	1.12
	45	33.11			0.993	1.19
	50	33.26			0.993	1.24
	30	31.84			0.996	1.07
	35	32.37			0.997	1.09
1.5	40	32.36	-13.98	59.20	0.994	1.12
	45	32.97			0.995	1.22
	50	33.02			0.993	1.27
	30	32.02			0.998	1.12
	35	32.17			0.995	1.16
2.0	40	32.38	-13.02	62.45	0.996	1.16
	45	33.07			0.995	1.30
	50	33.13			0.995	1.34

3.7 SODIUM 4-n-OCTYLBENZENESULFONATE (SOBS) AS CORROSION INHIBITOR ON GA9 MAGNESIUM ALLOY IN SODIUM CHLORIDE MEDIUM

3.7.1 Potentiodynamic polarization measurements

Potentiodynamic polarization curves for the corrosion of GA9 magnesium alloy in 1.0 M NaCl solution in the presence of different concentrations of SOBS, at 40 °C are shown in Fig. 3.45. Similar plots were obtained at other temperatures and also in the other concentrations of NaCl. The potentiodynamic polarization parameters are summarized in Tables 3.37 to 3.41.
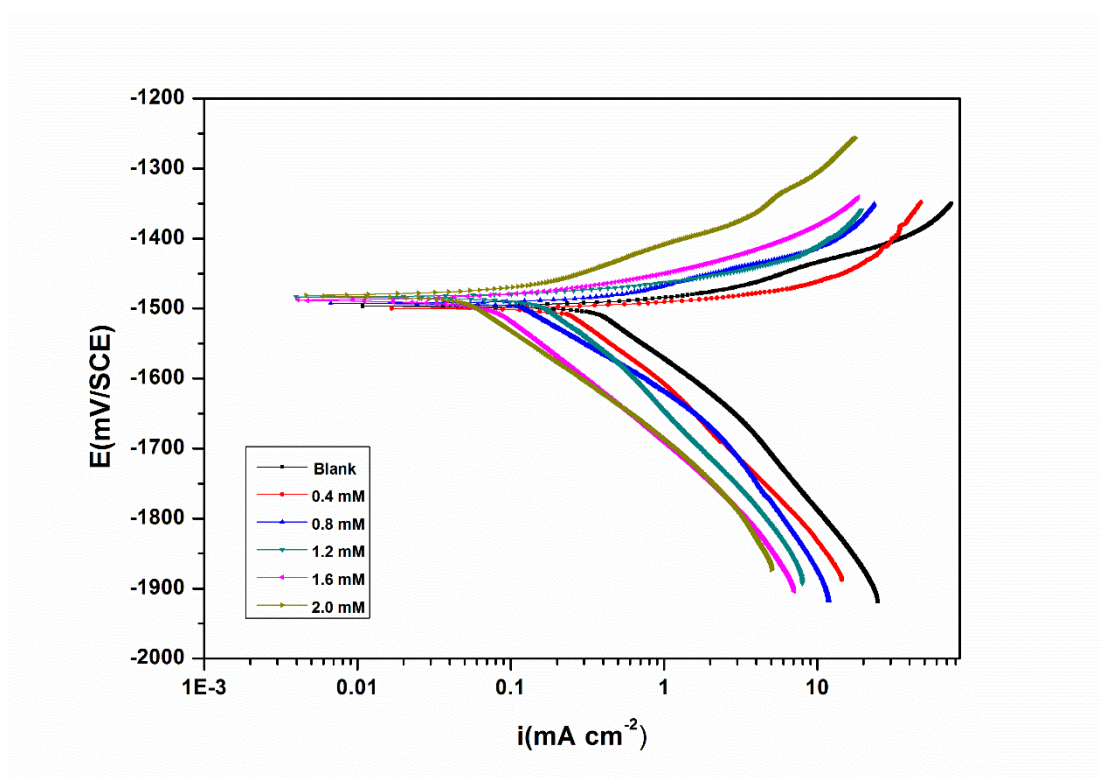
Fig. 3.45: Potentiodynamic polarization curves for the corrosion of GA9 magnesium alloy in 1.0 M NaCl solution containing different concentrations of SOBS at 40 °C.

The polarization curves in Fig. 3.45, appear to have been shifted towards the lower current density region on the introduction of SOBS into the blank solution. Such a shift along with no evident alteration in shape of the Tafel curves symbolizes that SOBS inhibits alloy dissolution without interfering with the mechanism of corrosion. The anodic branches of the polarization curves do not show Tafel regions and hence

cathodic Tafel extrapolation is used for the deduction of corrosion current density values.

It could be observed that both the anodic and cathodic reactions were suppressed with the addition of inhibitor, which suggested that the inhibitor exerted an efficient inhibitory effect both on the anodic dissolution of metal and on cathodic hydrogen evolutin reaction (Tao et al. 2010). In general, according to the results presented in Tables 3.37 to 3.41 and also from polarization curves in Fig. 3.45, the corrosion current density (i_{corr}) decreased significantly even on the addition of small concentration of SOBS and the inhibition efficiency ($\eta\%$) increases with the increase in the inhibitor concentration of SOBS. In the presence of SOBS the maximum displacement of E_{corr} is not more than 20 mV vs. SCE. Therefore it can be concluded that SOBS acts as a mixed type inhibitor on GA9 magnesium alloy. The rest of the discussion is similar to the discussion regarding the inhibition behaviour of SDBS for the corrosion of GA9 magnesium alloy in sodium chloride medium, under the section 3.5.1.

3.7.2 Electrochemical impedance spectroscopy (EIS) studies

Nyquist plots for the corrosion of GA9 magnesium alloy in 1.0 M NaCl solution in the presence of different concentrations of SOBS are given in Fig. 3.46. Similar results were obtained in other concentrations of sodium chloride and also at other temperatures. The capacitive loops of the Nyquist plots are enlarged successively with the increase in the concentration of SOBS, while the nature remains the same, suggesting an inhibition achieved without the participation of the inhibitor in the electrode reactions. The impedance plots on simulation with equivalent electrical circuit as represented in Fig. 3.3, yielded impedance parameters like R_{ct} and C_{dl} for the corrosion of GA9 magnesium alloy in the presence of different concentrations of SOBS in sodium chloride medium which are presented in Tables 3.42 to 3.46.

The inhibition efficiency values for SOBS calculated from the impedance analyses are close to those obtained from the polarization measurements and, SOBS at higher concentrations appear to favour the formation of a thick and highly protective surface film as reflected by the higher charge transfer resistance values, which are observed exclusively at higher SOBS concentrations at any particular temperature. The

formation of such an effective surface film justifies the increase in efficiency with the increased concentration of SOBS.
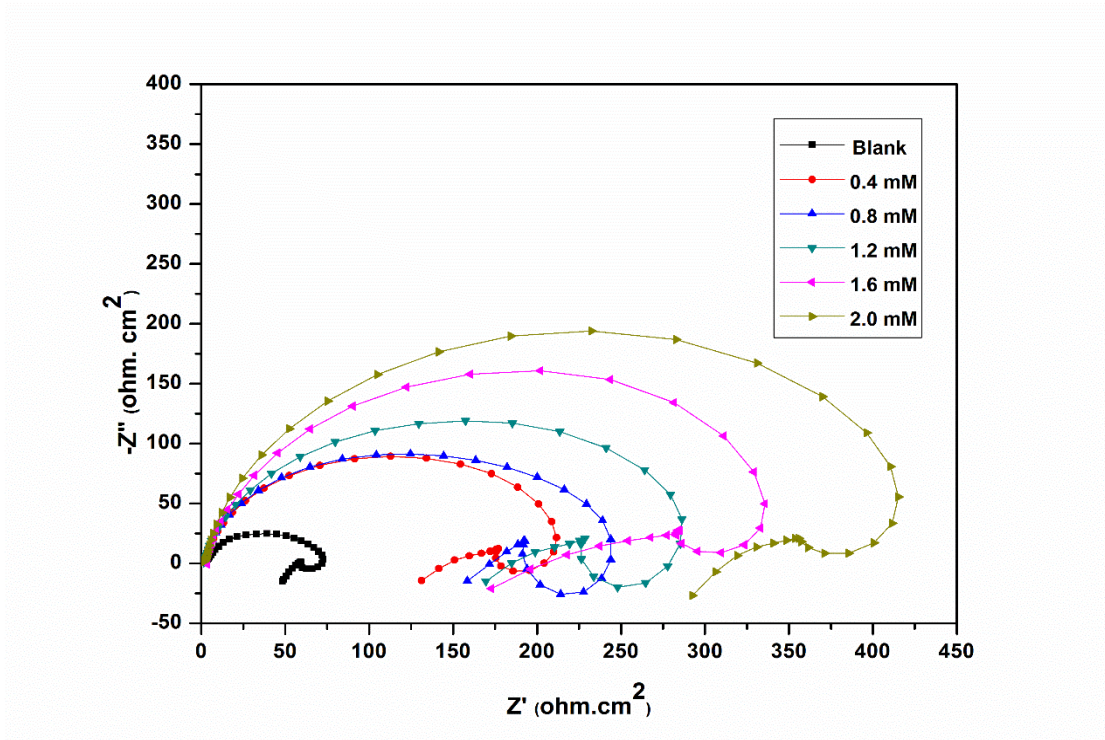
Fig. 3.46: Nyquist plots for the corrosion of GA9 magnesium alloy specimen in 1.0 M NaCl solution containing different concentrations of SOBS at 40 °C.
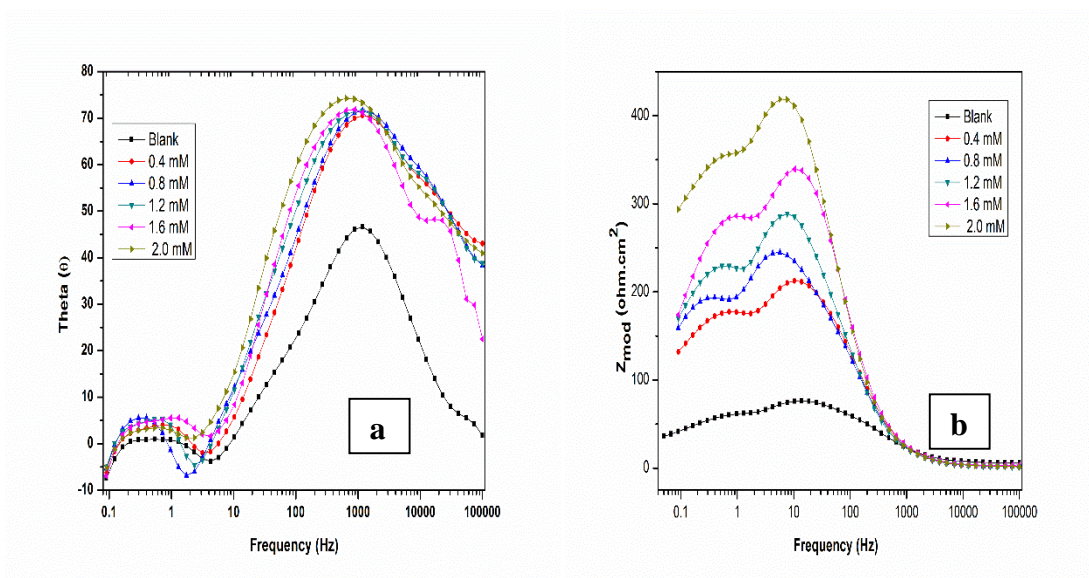
Fig. 3.47: Bode (a) phase angle plots and (b) amplitude plots for the corrosion of GA9 magnesium alloy in 1.0 M NaCl solution containing different concentrations of SOBS at 40 °C.

The Bode plots of phase angle and amplitude for the corrosion of the GA9 magnesium alloy immersed in 1.0 M NaCl at 40 °C in the presence of varying amounts of SOBS, are shown in Fig. 3.47 (a) and Fig. 3.47 (b), respectively. As seen from the Bode plots, both the impedance modulus (Z_{mod}) at low frequency and the phase maximum (θ_{max}) at intermediate frequency increase with the increase in SOBS concentration, which collectively point out the presence of highly protective surface film, able enough to oppose corrosive penetration.

3.7.3 Effect of temperature

The increase in the temperature of the solution is unfavourable for the inhibition by SOBS, as indicated by the inhibition efficiency values tabulated in Tables 3.37 to 3.46, which decrease with the increase in temperature. The decrease in inhibition efficiency with the increase in temperature may be attributed to the higher dissolution rates of GA9 magnesium alloy at elevated temperature and also a possible desorption of adsorbed inhibitor due to the increased solution agitation resulting from higher rates of hydrogen gas evolution (Poornima et al. 2011). The decrease in inhibition efficiency with the increase in temperature is also suggestive of physisorption of the inhibitor molecules on the metal surface (Geetha et al. 2011).

The Arrhenius plots and the plots of $\ln(v_{corr}/T)$ versus $1/T$ for the corrosion of GA9 magnesium alloy in the presence of different concentrations of SOBS in 1.0 M sodium chloride solution are shown in Fig. 3.48 and Fig. 3.49 respectively. The calculated values of activation parameters are recorded in Table 3.47.

The increased addition of SOBS increasingly hinders the appearance of corrosion of the GA9 magnesium alloy, as indicated by the increase in the activation energy values. . It is also indicated that the whole process is controlled by surface reaction (Fouda et al. 2009), since the activation energies of the corrosion process are above 20 kJ mol^{-1}. The pattern of change in $\Delta H^{\#}$ values is identical to that of E_a.

The values of $\Delta S^{\#}$ are negative for both the blank and the electrolyte containing SOBS, which suggests the non-involvement of added SOBS in electrode reactions, to be precise, even in the presence of SOBS, the activated complex in the rate-determining step of GA9 corrosion continue to form from the association of the reactants resulting in a decrease in entropy during activation (Abd EI Rehim et al. 2003). It is also seen

from the Table 3.47 that entropy of activation increases with the increase in the concentration of SOBS.
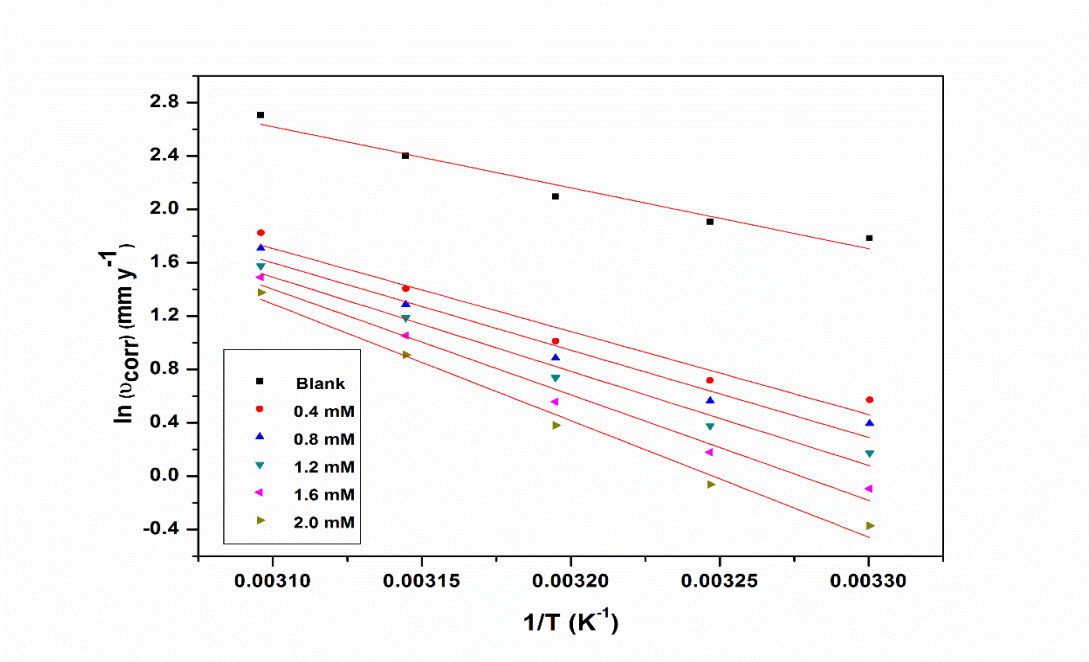
3.48: Arrhenius plots for the corrosion of GA9 magnesium alloy in 1.0 M NaCl solution containing different concentrations of SOBS.

Fig. 3.49: Plots of ln(υ_{corr}/T) versus 1/T for the corrosion of GA9 magnesium alloy in 1.0 M NaCl solution containing different concentrations of SOBS.

3.7.4 Effect of sodium chloride concentration

Table 3.48 summarises the maximum inhibition efficiencies exhibited by SOBS in NaCl solutions of different concentrations. It is evident from both polarization and EIS experimental results that, for a particular concentration of inhibitor, the inhibition efficiency decreases with the increase in sodium chloride concentration. The highest inhibition efficiency is observed in sodium chloride of 0.1 M concentration.

3.7.5 Adsorption isotherm

With graphical attempts of trial and error of substitution of the values of surface coverage (θ) and concentration of SOBS (C_{inh}) in the mathematical relations describing Langmuir, Temkin, Frumkin and Flory-Huggins isotherms, it was recognised that the interfacial adsorption of SOBS can be best expressed using Langmuir adsorption isotherm. The linear regression coefficients are close to unity and the slopes of the straight lines are nearly unity, suggesting that the adsorption of SOBS obeys Langmuir's adsorption isotherm with negligible interaction between the adsorbed molecules. The Langmuir adsorption isotherms for adsorption of SOBS on GA9 magnesium alloy surface at different temperatures in 1.0 M NaCl are shown in Fig. 3.50.

The thermodynamic data obtained for the adsorption of SOBS on GA9 magnesium alloy are tabulated in Table 3.49. The plot of ΔG°_{ads} Vs T gives a straight line and the ΔH°_{ads} and ΔS°_{ads} values are calculated from the slope and intercept. The plot of ΔG°_{ads} Vs T is shown in Fig. 3.51. The exothermic ΔH°_{ads} values of less than -41.86 kJ mol^{-1} predict physisorption of SOBS on the alloy surfaces (Ashish Kumar et al. 2010). The ΔG°_{ads} values predict both physisorption and chemisorption of SOBS. Therefore it can be concluded that the adsorption of SOBS on GA9 magnesium alloy is predominantly through physisorption. The spontaneity of SOBS adsorption is ascertained from the negative values of ΔG°_{ads}.

The ΔS^{0}_{ads} value is positive, indicating the increase in randomness involved in the adsorption of SOBS molecules on the alloy surface. In the present case, the increase in entropy is caused by the displacement of previously adsorbed water molecules, which inturn is moving freely in electrolyte bulk.
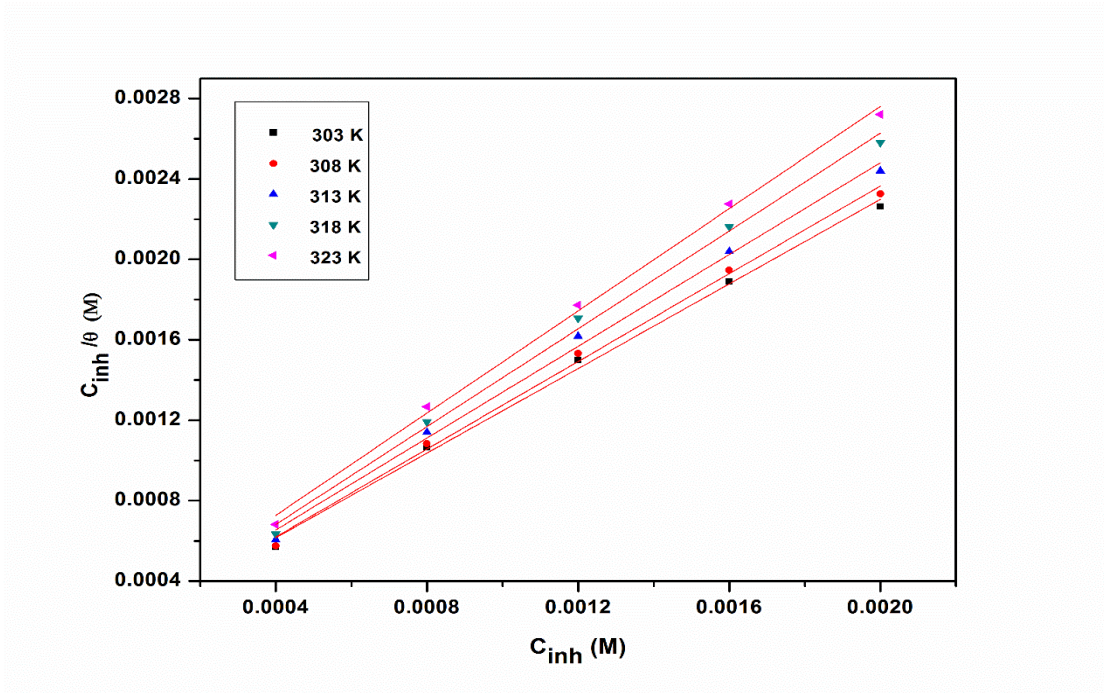
Fig. 3.50: Langmuir adsorption isotherms for the adsorption of SOBS on GA9 magnesium alloy in 1.0 M NaCl solution at different temperatures.
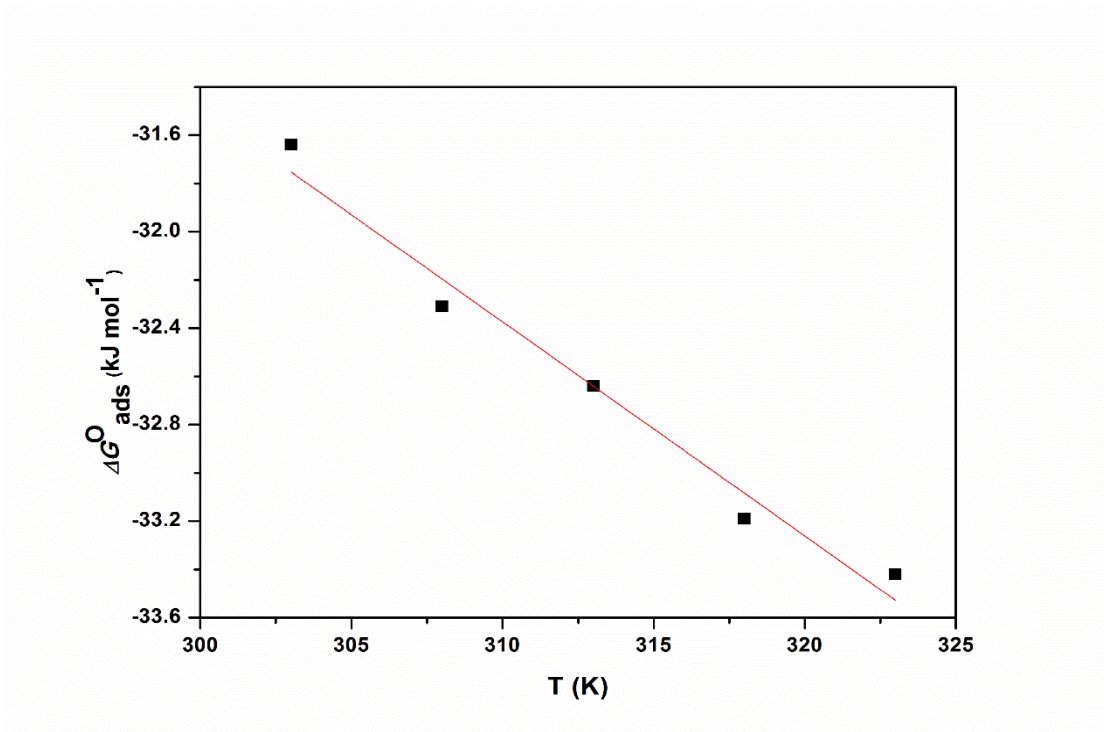
Fig. 3.51: The plot of ΔG°ads vs T for the adsorption of SOBS on GA9 magnesium alloy in 1.0 M NaCl solution.

3.7.6 Mechanism of corrosion inhibition

The inhibitive effect of SOBS on the corrosion of GA9 magnesium alloy can be accounted for on the basis of its adsorption on the alloy surface. The SOBS is anionic surfactant with the sulfonate polar head and long alkyl hydrophobic tail. The SOBS might physically adsorb through the electrostatic interactions between their anionic head and Mg^{2+} ions trapped within the imperfections of surface film developed over the α-Mg matrix (Hu et al. 2011). The physisorbed surfactant on the other hand, might precipitate as their sparingly soluble magnesium salts within the pores of the film over the α-Mg matrix. The precipitation is favoured due to very low solubility product of magnesium salt of the surfactant and the presence of sufficiently high amounts of dissolved Mg^{2+} ions. The precipitates fill-up the pores and densify the surface film. As an overall result the electrolyte ingress is reduced on the addition of the surfactant.

3.7.7 SEM/EDX studies

Fig. 3.52 represents SEM image of GA9 magnesium alloy after the corrosion tests in a medium of 2.0 M sodium chloride containing 2.0 mM of SOBS. The image clearly shows a relatively smooth, undeteriorated surface due to the presence of adsorbed inhibitor layer on the surface of the alloy.
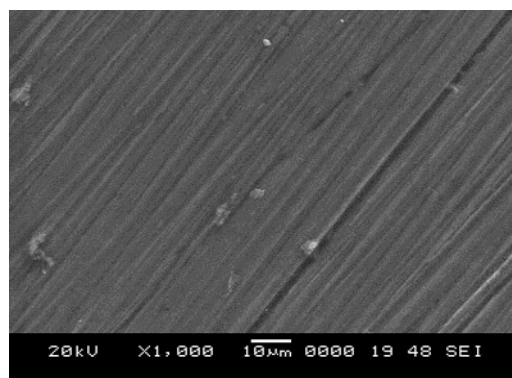
Fig. 3.52: SEM image of the GA9 magnesium alloy after immersion in 2.0 M NaCl solution in the presence of SOBS.

EDX investigations were carried out in order to identify the composition of the species formed on the metal surface in NaCl media in the absence and in the presence of SOBS. The EDX profile analyses for the selected areas on the SEM images of Fig. 3.52 is shown in Fig. 3.53. In the EDX spectra Fig. 3.53, apart from the peaks for Mg, Al and Na, an additional small peak for carbon, oxygen and sulphur is obtained, which

indicates the presence of some organic moieties on the alloy surface, which possibly are the surface adsorbed SOBS molecules.
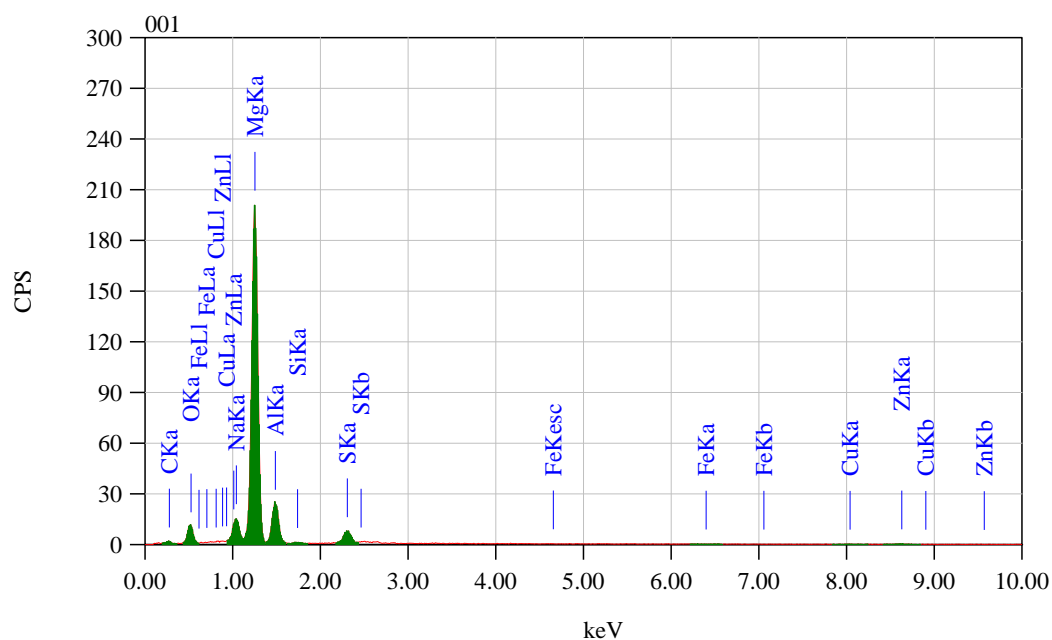
Fig. 3.53: EDX spectra of GA9 magnesium alloy after immersion in 2.0 M NaCl solution in the presence of SOBS.

Table 3.37: Results of potentiodynamic polarization studies for the corrosion of GA9 magnesium alloy in 0.1 M sodium chloride solution containing different concentrations of SOBS.

Temperature (°C)	Conc. of inhibitor (mM)	$-E_{corr}$ (mV /SCE)	$-b_c$ (mV dec^{-1})	i_{corr} (μA cm^{-2})	υ_{corr} (mm y^{-1})	η (%)
30	Blank	1449	149	75.1	1.687	
	0.4	1453	122	18.8	0.422	75.0
	0.8	1450	118	15.5	0.348	79.4
	1.2	1444	116	12.2	0.274	83.7
	1.6	1448	114	9.3	0.209	87.6
	2.0	1438	111	6.5	0.146	91.3
35	Blank	1445	157	86.9	1.952	
	0.4	1455	136	22.3	0.501	74.3
	0.8	1459	133	18.6	0.418	78.6
	1.2	1450	129	14.9	0.335	82.9
	1.6	1437	125	11.3	0.254	87.0
	2.0	1444	122	8.5	0.191	90.2
40	Blank	1450	164	108.4	2.435	
	0.4	1457	144	29.4	0.661	72.9
	0.8	1455	141	26.0	0.584	76.0
	1.2	1459	138	21.0	0.472	80.6
	1.6	1447	135	16.0	0.359	85.2
	2.0	1448	131	12.1	0.272	88.8
45	Blank	1465	169	139.1	3.126	
	0.4	1468	152	43.1	0.968	69.0
	0.8	1460	149	38.4	0.863	72.4
	1.2	1467	147	33.0	0.741	76.3
	1.6	1452	144	27.1	0.609	80.5
	2.0	1458	141	21.6	0.485	84.5
50	Blank	1472	173	189.3	4.254	
	0.4	1474	155	68.1	1.530	64.0
	0.8	1476	153	61.1	1.373	67.7
	1.2	1470	149	55.1	1.238	70.9
	1.6	1465	147	49.2	1.105	74.0
	2.0	1466	144	44.3	0.995	76.6

Table 3.38: Results of potentiodynamic polarization studies for the corrosion of GA9 magnesium alloy in 0.5 M sodium chloride solution containing different concentrations of SOBS.

Temperature (℃)	Conc. of inhibitor (mM)	$-E_{corr}$ (mV /SCE)	$-b_c$ (mV dec^{-1})	i_{corr} (µA cm^{-2})	υ_{corr} (mm y^{-1})	η (%)
30	Blank	1451	152	160.0	3.595	
	0.4	1451	132	44.0	0.989	72.5
	0.8	1445	129	36.5	0.820	77.2
	1.2	1446	125	29.0	0.652	81.9
	1.6	1442	120	21.6	0.485	86.5
	2.0	1449	117	15.7	0.353	90.2
35	Blank	1473	158	179.3	4.029	
	0.4	1461	140	50.9	1.144	71.6
	0.8	1463	137	42.1	0.946	76.5
	1.2	1460	135	35.1	0.789	80.4
	1.6	1458	131	27.1	0.609	84.9
	2.0	1455	129	20.8	0.467	88.4
40	Blank	1466	167	206.6	4.641	
	0.4	1474	150	63.4	1.425	69.3
	0.8	1465	148	53.7	1.207	74.0
	1.2	1463	144	46.1	1.036	77.7
	1.6	1467	140	37.6	0.845	81.8
	2.0	1457	137	30.8	0.692	85.1
45	Blank	1490	171	285.1	6.405	
	0.4	1491	156	94.1	2.114	67.0
	0.8	1488	153	83.5	1.876	70.7
	1.2	1485	149	73.3	1.647	74.3
	1.6	1489	147	63.0	1.416	77.9
	2.0	1478	141	55.6	1.249	80.5
50	Blank	1497	175	377.1	8.473	
	0.4	1494	161	145.9	3.278	61.3
	0.8	1492	158	130.1	2.923	65.5
	1.2	1489	155	116.9	2.627	69.0
	1.6	1498	153	106.3	2.388	71.8
	2.0	1485	149	94.3	2.119	75.0

Table 3.39: Results of potentiodynamic polarization studies for the corrosion of GA9 magnesium alloy in 1.0 M sodium chloride solution containing different concentrations of SOBS.

| Temperature (℃)	Conc. of inhibitor (mM)	$-E_{corr}$ (mV /SCE)	$-b_c$ (mV dec^{-1})	i_{corr} (µA cm^{-2})	υ_{corr} (mm y^{-1})	η (%)
30	Blank	1474	156	264.5	5.942	
	0.4	1474	142	78.8	1.771	70.2
	0.8	1475	139	65.9	1.481	75.1
	1.2	1471	136	52.9	1.189	80.0
	1.6	1478	133	40.5	0.910	84.7
	2.0	1467	130	30.7	0.690	88.4
35	Blank	1495	162	298.9	6.716	
	0.4	1489	148	91.2	2.049	69.5
	0.8	1493	145	78.3	1.759	73.8
	1.2	1483	142	64.9	1.458	78.3
	1.6	1489	140	53.2	1.195	82.2
	2.0	1487	138	41.8	0.939	86.0
40	Blank	1496	169	361.5	8.122	
	0.4	1500	157	122.5	2.752	66.1
	0.8	1494	155	107.7	2.420	70.2
	1.2	1483	152	93.3	2.096	74.2
	1.6	1488	149	77.7	1.746	78.5
	2.0	1481	147	65.1	1.463	82.0
45	Blank	1496	177	491.0	11.031	
	0.4	1503	164	181.2	4.071	63.1
	0.8	1495	161	161.0	3.617	67.2
	1.2	1497	158	145.8	3.276	70.3
	1.6	1489	155	127.7	2.869	74.0
	2.0	1491	153	110.5	2.483	77.5
50	Blank	1501	179	665.6	14.955	
	0.4	1511	167	275.6	6.192	58.6
	0.8	1502	165	245.6	5.518	63.1
	1.2	1505	162	215.0	4.831	67.7
	1.6	1497	159	197.7	4.442	70.3
	2.0	1496	157	176.4	3.963	73.5

Table 3.40: Results of potentiodynamic polarization studies for the corrosion of GA9 magnesium alloy in 1.5 M sodium chloride solution containing different concentrations of SOBS.

Temperature (℃)	Conc. of inhibitor (mM)	$-E_{corr}$ (mV /SCE)	$-b_c$ (mV dec^{-1})	i_{corr} (μA cm^{-2})	υ_{corr} (mm y^{-1})	η (%)
30	Blank	1497	169	376.5	8.458	
	0.4	1500	156	117.5	2.640	68.8
	0.8	1502	154	99.8	2.242	73.5
	1.2	1491	151	83.2	1.869	77.9
	1.6	1490	148	68.9	1.548	81.7
	2.0	1493	144	54.6	1.227	85.5
35	Blank	1499	173	436.5	9.802	
	0.4	1500	160	144.0	3.235	67.0
	0.8	1502	158	123.1	2.766	71.8
	1.2	1497	155	103.9	2.334	76.2
	1.6	1490	153	81.6	1.833	81.3
	2.0	1489	149	72.5	1.629	83.4
40	Blank	1519	181	552.6	12.416	
	0.4	1521	168	198.4	4.458	64.1
	0.8	1522	166	173.5	3.898	68.6
	1.2	1518	164	149.8	3.366	72.9
	1.6	1507	160	128.8	2.894	76.7
	2.0	1511	157	109.4	2.458	80.2
45	Blank	1520	195	738.2	16.585	
	0.4	1531	183	290.1	6.518	60.7
	0.8	1527	180	260.6	5.855	64.7
	1.2	1529	178	232.5	5.224	68.5
	1.6	1515	173	211.1	4.743	71.4
	2.0	1507	171	177.2	3.981	76.0
50	Blank	1529	210	999.6	22.458	
	0.4	1531	199	421.8	9.477	57.8
	0.8	1527	196	382.8	8.601	61.7
	1.2	1530	193	345.9	7.774	65.4
	1.6	1521	191	309.9	6.963	69.0
	2.0	1519	188	284.9	6.401	71.5

Table 3.41: Results of potentiodynamic polarization studies for the corrosion of GA9 magnesium alloy in 2.0 M sodium chloride solution containing different concentrations of SOBS.

Temperature (°C)	Conc. of inhibitor (mM)	$-E_{corr}$ (mV /SCE)	$-b_c$ (mV dec^{-1})	i_{corr} (μA cm^{-2})	υ_{corr} (mm y^{-1})	η (%)
30	Blank	1524	192	447.5	10.055	
	0.4	1530	180	155.3	3.489	65.3
	0.8	1533	178	138.7	3.116	69.0
	1.2	1528	176	121.7	2.734	72.8
	1.6	1529	172	105.2	2.364	76.5
	2.0	1518	169	88.6	1.991	80.2
35	Blank	1525	195	546.9	12.286	
	0.4	1535	185	199.1	4.473	63.6
	0.8	1529	184	178.8	4.017	67.3
	1.2	1519	179	159.7	3.588	70.8
	1.6	1524	176	137.3	3.085	74.9
	2.0	1515	172	118.7	2.667	78.3
40	Blank	1529	206	726.0	16.310	
	0.4	1528	196	281.7	6.329	61.2
	0.8	1532	194	250.5	5.628	65.5
	1.2	1521	190	219.3	4.927	69.8
	1.6	1527	185	192.4	4.323	73.5
	2.0	1517	179	164.1	3.687	77.4
45	Blank	1530	213	986.2	22.157	
	0.4	1537	205	410.3	9.219	58.4
	0.8	1533	202	374.8	8.421	62.0
	1.2	1535	198	342.2	7.689	65.3
	1.6	1525	195	313.6	7.046	68.2
	2.0	1518	189	286.0	6.426	71.0
50	Blank	1535	222	1249.8	28.078	
	0.4	1544	211	584.9	13.142	53.2
	0.8	1538	209	539.9	12.131	56.8
	1.2	1542	205	498.7	11.205	60.1
	1.6	1530	202	462.4	10.389	63.0
	2.0	1527	200	426.2	9.576	65.9

Table 3.42: EIS data for the corrosion of GA9 magnesium alloy in 0.1 M sodium chloride solution containing different concentrations of SOBS.

Temperature (℃)	Conc. of inhibitor (mM)	R_{ct} (ohm. cm^2)	C_{dl} (µF cm^{-2})	η (%)
30	Blank	361.5	11.29	
	0.4	1470.0	8.62	75.4
	0.8	1781.0	8.55	79.7
	1.2	2231.0	8.24	83.8
	1.6	2988.0	7.89	87.9
	2.0	4253.0	7.42	91.5
35	Blank	302.5	11.41	
	0.4	1186.0	9.01	74.5
	0.8	1427.0	8.71	78.8
	1.2	1779.0	8.53	83.0
	1.6	2363.0	8.17	87.2
	2.0	3119.0	7.99	90.3
40	Blank	245.4	15.20	
	0.4	898.9	10.48	72.7
	0.8	1018.0	10.17	75.9
	1.2	1259.0	10.01	80.5
	1.6	1681.0	9.64	85.4
	2.0	2231.0	9.15	89.0
45	Blank	184.5	23.51	
	0.4	605.0	13.71	69.5
	0.8	675.8	13.30	72.7
	1.2	788.5	12.88	76.6
	1.6	941.3	12.55	80.4
	2.0	1206.0	12.29	84.7
50	Blank	132.8	28.95	
	0.4	370.9	17.39	64.2
	0.8	411.1	17.17	67.7
	1.2	450.2	16.96	70.5
	1.6	516.7	16.52	74.3
	2.0	574.9	16.27	76.9

Table 3.43: EIS data for the corrosion of GA9 magnesium alloy in 0.5 M sodium chloride solution containing different concentrations of SOBS.

Temperature (°C)	Conc. of inhibitor (mM)	R_{ct} (ohm. cm^2)	C_{dl} (µF cm^{-2})	η (%)
	Blank	162.9	26.17	
	0.4	590.2	11.15	72.4
30	0.8	717.6	10.98	77.3
	1.2	895.1	10.77	81.8
	1.6	1253.0	10.41	87.0
	2.0	1697.0	10.08	90.4
	Blank	147.0	27.21	
	0.4	521.3	11.44	71.8
35	0.8	625.5	11.31	76.5
	1.2	757.7	11.02	80.6
	1.6	986.6	10.59	85.1
	2.0	1324.0	10.15	88.9
	Blank	127.3	28.63	
	0.4	417.4	12.02	69.5
40	0.8	493.4	11.89	74.2
	1.2	578.6	11.67	78.0
	1.6	711.2	11.28	82.1
	2.0	878.0	10.94	85.5
	Blank	91.0	35.08	
	0.4	277.4	15.52	67.2
45	0.8	312.7	15.17	70.9
	1.2	356.9	14.75	74.5
	1.6	413.6	14.31	78.0
	2.0	471.5	13.89	80.7
	Blank	70.8	40.33	
	0.4	183.9	18.74	61.5
50	0.8	207.0	18.39	65.8
	1.2	230.6	17.95	69.3
	1.6	250.2	17.41	71.7
	2.0	281.0	16.73	74.8

Table 3.44: EIS data for the corrosion of GA9 magnesium alloy in 1.0 M sodium chloride solution containing different concentrations of SOBS.

Temperature (℃)	Conc. of inhibitor (mM)	R_{ct} (ohm. cm^2)	C_{dl} (μF cm^{-2})	η (%)
30	Blank	99.7	33.50	
	0.4	336.8	11.55	70.4
	0.8	403.6	11.37	75.3
	1.2	511.3	11.03	80.5
	1.6	655.9	10.51	84.8
	2.0	867.0	10.19	88.5
35	Blank	87.4	34.93	
	0.4	289.4	17.00	69.8
	0.8	336.2	16.52	74.0
	1.2	406.5	16.02	78.5
	1.6	493.8	15.41	82.3
	2.0	628.8	14.66	86.1
40	Blank	72.8	39.91	
	0.4	216.7	19.71	66.4
	0.8	244.3	19.31	70.2
	1.2	285.5	18.74	74.5
	1.6	340.2	18.02	78.6
	2.0	411.3	17.41	82.3
45	Blank	52.7	66.70	
	0.4	144.0	29.91	63.4
	0.8	159.7	29.10	67.0
	1.2	175.7	28.17	70.6
	1.6	204.3	27.03	74.2
	2.0	236.3	25.87	77.7
50	Blank	39.0	77.59	
	0.4	94.0	40.02	58.5
	0.8	104.8	39.11	62.8
	1.2	120.0	37.95	67.5
	1.6	130.9	36.49	70.2
	2.0	147.7	34.04	73.6

Table 3.45: EIS data for the corrosion of GA9 magnesium alloy in 1.5 M sodium chloride solution containing different concentrations of SOBS.

Temperature (℃)	Conc. of inhibitor (mM)	R_{ct} (ohm. cm^2)	C_{dl} (µF cm^{-2})	η (%)
	Blank	67.9	41.61	
	0.4	219.0	25.01	69.0
30	0.8	258.2	24.71	73.7
	1.2	308.6	24.01	78.0
	1.6	373.1	22.98	81.8
	2.0	478.2	21.70	85.8
	Blank	60.2	61.15	
	0.4	183.5	37.25	67.2
35	0.8	212.7	36.24	71.7
	1.2	254.0	35.01	76.3
	1.6	325.4	33.75	81.5
	2.0	373.9	31.89	83.9
	Blank	47.5	69.71	
	0.4	133.1	41.11	64.3
40	0.8	150.8	40.00	68.5
	1.2	174.0	38.62	72.7
	1.6	202.1	37.71	76.5
	2.0	238.7	34.85	80.1
	Blank	35.5	89.49	
	0.4	90.1	48.25	60.6
45	0.8	100.9	46.51	64.8
	1.2	114.1	44.61	68.9
	1.6	125.4	42.03	71.7
	2.0	148.5	38.55	76.1
	Blank	26.3	107.44	
	0.4	61.9	52.10	57.5
50	0.8	68.1	50.54	61.4
	1.2	76.2	47.95	65.5
	1.6	85.4	45.13	69.2
	2.0	92.9	42.99	71.7

Table 3.46: EIS data for the corrosion of GA9 magnesium alloy in 2.0 M sodium chloride solution containing different concentrations of SOBS.

Temperature (℃)	Conc. of inhibitor (mM)	R_{ct} (ohm. cm^2)	C_{dl} (μF cm^{-2})	η (%)
30	Blank	58.5	58.01	
	0.4	168.1	36.51	65.2
	0.8	187.5	35.92	68.8
	1.2	212.7	35.03	72.5
	1.6	247.9	33.95	76.4
	2.0	297.0	32.51	80.3
35	Blank	48.2	65.11	
	0.4	132.8	39.01	63.7
	0.8	148.3	37.92	67.5
	1.2	162.8	36.77	70.4
	1.6	190.5	35.10	74.7
	2.0	223.1	33.47	78.4
40	Blank	36.2	83.99	
	0.4	93.5	44.58	61.3
	0.8	104.6	43.26	65.4
	1.2	120.3	41.74	69.9
	1.6	137.6	39.59	73.7
	2.0	161.6	37.44	77.6
45	Blank	26.4	109.41	
	0.4	63.6	60.25	58.5
	0.8	69.8	58.02	62.2
	1.2	76.3	55.87	65.4
	1.6	83.8	53.13	68.5
	2.0	91.3	50.55	71.1
50	Blank	21.1	123.26	
	0.4	45.3	64.23	53.4
	0.8	48.5	62.18	56.5
	1.2	52.8	59.91	60.0
	1.6	57.5	57.52	63.3
	2.0	62.2	54.77	66.1

Table 3.47: Activation parameters for the corrosion of GA9 magnesium alloy in NaCl solutions containing different concentrations of inhibitor SOBS.

Concentration of NaCl	Conc. of inhibitor (mM)	E_a (kJ mol^{-1})	$\Delta H^{\#}$ (kJ mol^{-1})	$\Delta S^{\#}$ (J mol^{-1} K^{-1})
	Blank	37.67	35.07	-125.49
	0.4	52.45	49.85	-88.61
0.1	0.8	56.30	64.17	-77.52
	1.2	61.80	59.20	-61.47
	1.6	68.16	65.56	-43.03
	2.0	77.32	74.72	-15.83
	Blank	35.31	32.71	-127.16
	0.4	48.79	46.19	-93.70
0.5	0.8	52.29	49.62	-83.78
	1.2	57.13	54.53	-69.66
	1.6	65.40	62.80	-44.90
	2.0	74.15	71.54	-18.64
	Blank	37.98	35.38	-114.14
	0.4	51.73	49.13	-79.10
1.0	0.8	54.38	51.78	-71.80
	1.2	58.67	56.07	-59.37
	1.6	65.72	63.12	-38.27
	2.0	75.60	69.99	-17.88
	Blank	40.24	37.64	-103.66
	0.4	52.88	50.28	-71.71
1.5	0.8	55.84	53.31	-63.34
	1.2	59.38	56.78	-53.22
	1.6	64.27	61.67	-38.89
	2.0	68.17	65.57	-27.71
	Blank	42.98	40.39	-92.91
	0.4	54.86	52.26	-62.69
2.0	0.8	56.20	53.60	-59.25
	1.2	58.21	55.61	-53.75
	1.6	61.51	58.91	-44.17
	2.0	65.30	62.70	-33.13

Table 3.48: Maximum inhibition efficiencies attained in different concentrations of sodium chloride solutions at different temperatures for SOBS.

Temperature (ºC)	Sodium chloride concentration (M)	Concentration of SOBS (mM)	GA9 magnesium alloy η (%)	
			Potentiodynamic polarization method	EIS method
30	0.1	2.0	91.3	91.5
	0.5		90.2	90.4
	1.0		88.4	88.5
	1.5		85.5	85.8
	2.0		80.2	80.3
35	0.1	2.0	90.2	90.3
	0.5		88.4	88.9
	1.0		86.0	86.1
	1.5		83.4	83.9
	2.0		78.3	78.4
40	0.1	2.0	88.8	89.0
	0.5		85.1	85.5
	1.0		82.0	82.3
	1.5		80.2	80.1
	2.0		77.4	77.6
45	0.1	2.0	84.5	84.7
	0.5		80.5	80.7
	1.0		77.5	77.7
	1.5		76.0	76.1
	2.0		71.0	71.1
50	0.1	2.0	76.6	76.9
	0.5		75.0	74.8
	1.0		73.5	73.6
	1.5		71.5	71.7
	2.0		65.9	66.1

Table 3.49: Thermodynamic parameters for the adsorption of SOBS on GA9 magnesium alloy surface in sodium chloride solutions at different temperatures.

Molarity of NaCl (M)	Temperature (° C)	$-\Delta G^o_{ads}$ (kJ mol^{-1})	ΔH^o_{ads} (kJ mol^{-1})	ΔS^o_{ads} (J mol^{-1} K^{-1})	R^2	Slope
	30	32.16			0.996	1.03
	35	32.69			0.997	1.04
0.1	40	32.97	-4.57	91.02	0.995	1.06
	45	33.34			0.994	1.11
	50	34.11			0.997	1.24
	30	31.83			0.996	1.04
	35	32.44			0.996	1.06
0.5	40	32.95	-1.18	101.41	0.996	1.11
	45	33.61			0.997	1.17
	50	33.78			0.997	1.26
	30	31.64			0.995	1.05
	35	32.31			0.996	1.09
1.0	40	32.64	-4.85	88.82	0.995	1.14
	45	33.19			0.995	1.22
	50	33.42			0.997	1.27
	30	31.76			0.995	1.10
	35	32.18			0.997	1.11
1.5	40	32.55	-7.33	80.63	0.996	1.16
	45	32.89			0.994	1.24
	50	33.42			0.997	1.31
	30	31.67			0.995	1.17
	35	32.08			0.995	1.20
2.0	40	32.29	-6.62	82.67	0.995	1.20
	45	33.15			0.997	1.33
	50	33.20			0.996	1.42

3.8 SODIUM 4-n-OCTYLBENZENESULFONATE (SOBS) AS CORROSION INHIBITOR FOR GA9 MAGNESIUM ALLOY IN SODIUM SULPHATE MEDIUM

3.8.1 Potentiodynamic polarization measurement

The Tafel plots for the corrosion of GA9 magnesium alloy in 1.0 M sodium sulphate solution in the presence of different concentrations of SOBS, at 40 °C are shown in Fig. 3.54. Similar plots were obtained at other temperatures and also in the other five concentrations of sodium sulphate at the different temperatures studied. The potentiodynamic polarization parameters were calculated from Tafel plots in the presence of different concentrations of SOBS at different temperatures and are summarized in Tables 3.50 to 3.54. As seen from the data, the presence of inhibitor brings down the corrosion rate considerably. Polarization curves are shifted to a lower current density region indicating a decrease in corrosion rate (Li et al. 2008). Inhibition efficiency increases with the increase in SOBS.
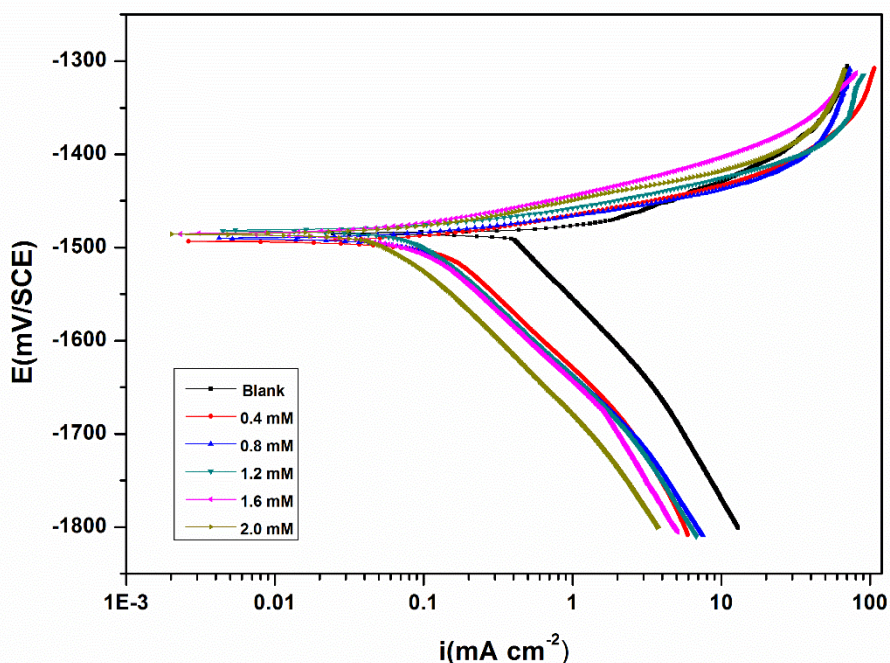
Fig. 3.54: Potentiodynamic polarization curves for the corrosion of GA9 magnesium alloy in 1.0 M Na$_2$SO$_4$ solution containing different concentrations of SOBS at 40 ℃.

No definite trend is observed in the shift of E_{corr} values; both anodic and cathodic polarization profiles are influenced simultaneously, almost to the same extent, which indicate the influence of SOBS on both the anodic and the cathodic reactions; metal dissolution and hydrogen evolution and acting acts as a mixed inhibitor. The data in Tables 3.50 to 3.54 show that there is no significant change in the values of cathodic Tafel slope b_c with the increase in the concentration of the inhibitor. This suggests that the corrosion reaction is slowed down by the surface-blocking effect of the inhibitor (Ehteshamzadeh et al. 2009 and Ateya et al. 1976).

3.8.2 Electrochemical impedance spectroscopy (EIS) studies

Nyquist plots for the corrosion of GA9 magnesium alloy in 1.0 M sodium sulphate solution in the presence of different concentrations of SOBS are shown in Fig. 3.55. Similar plots were obtained in other concentrations of sodium sulphate and also at other temperatures. The experimental results of EIS measurements obtained for the corrosion of GA9 magnesium alloy in 1.0 M sodium sulphate are summarized in Tables 3.55 to 3.59.

The Nyquist plots are characterized by a capacitive loop, extended from high frequency (HF) to low frequency (LF) range, an inductive loop in the low frequency region (LF) range and a tail at the medium frequency (MF) range in the presence as well as in the absence of inhibitor.

As seen from Fig. 3.55, the capacitive loops of the Nyquist plots are enlarged successively with the increase in the concentration of SOBS, while the nature remains the same, suggesting an inhibition achieved without participation in the electrode reactions. This indicates that the corrosion of GA9 magnesium alloy is controlled by a charge transfer process and the addition of SOBS does not change the reaction mechanism of the corrosion of sample in Na_2SO_4 solution (Amin et al. 2007). The charge transfer resistance (R_{ct}) increases and double layer capacitance decreases with the increase in the concentration of SOBS, indicating an increase in the inhibition efficiency. SOBS inhibits the corrosion primarily through its adsorption and subsequent formation of a barrier film on the metal surface (El Hosary et al. 1972, Sanaa T. 2008). This is in accordance with the observations of potentiodynamic polarization measurements.

The equivalent circuit models shown in Fig. 3.3 is used for the interpretation of the Nyquist plots in the presence and absence of SOBS.
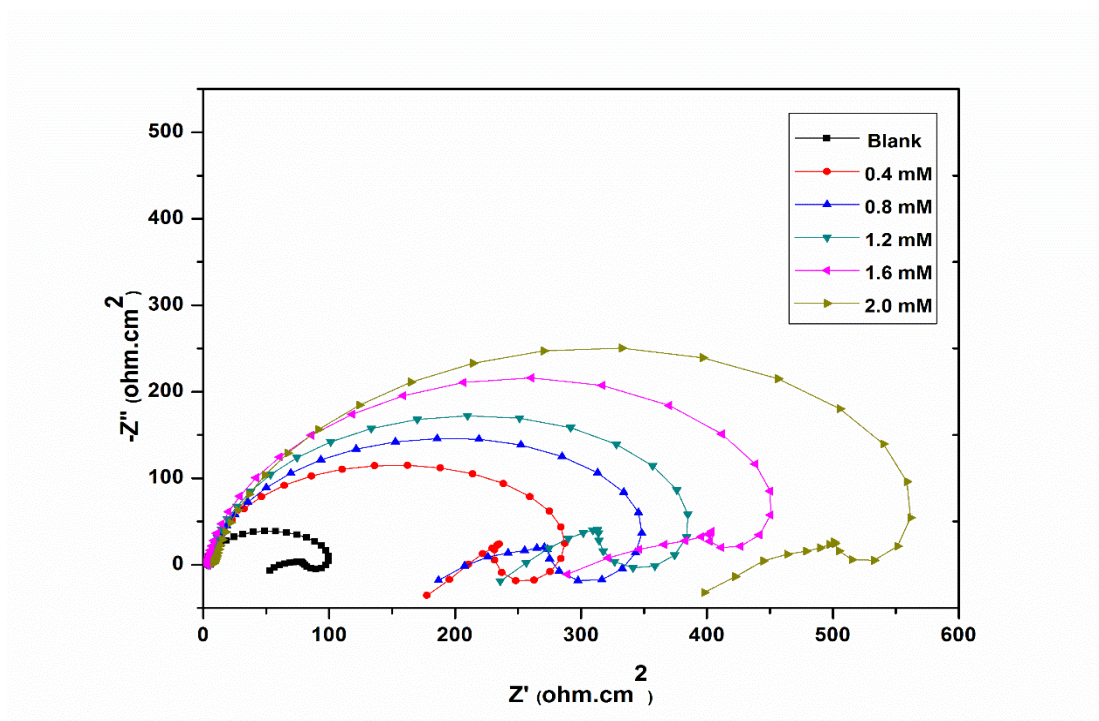
Fig. 3.55: Nyquist plots for the corrosion of GA9 magnesium alloy in 1.0 M Na₂SO₄ solution containing different concentrations of SOBS at 40 ℃.
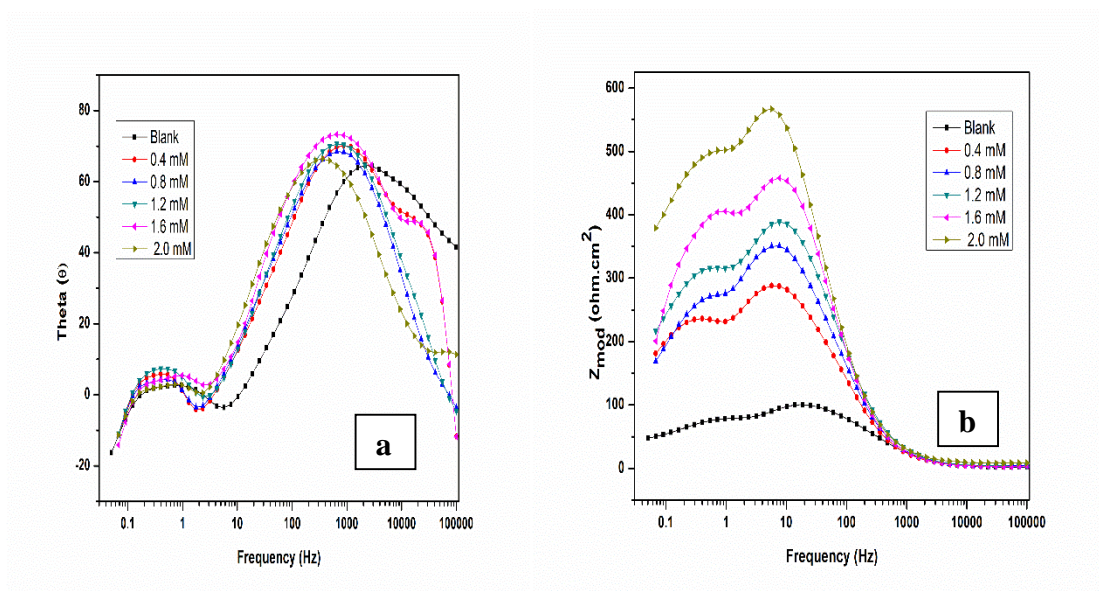
Fig. 3.56: Bode (a) phase angle plots and (b) amplitude plots for the corrosion of GA9 magnesium alloy in 1.0 M Na₂SO₄ solution containing different concentrations of SOBS at 40 °C.

The Bode plots of phase angle and amplitude for the corrosion of the GA9 magnesium alloy immersed in 1.0 M Na$_2$SO$_4$ solution at 40 °C in the presence of varying amounts of SOBS, are shown in Fig. 3.56 (a) and Fig. 3.56 (b), respectively. As seen from the Bode plots, both the impedance modulus (Z$_{mod}$) at low frequency and the phase maximum (θ$_{max}$) at intermediate frequency increase with the increase in SOBS concentration, which collectively point out the presence of highly protective surface film, able enough to oppose corrosive penetration.

3.8.3 Effect of temperature

The potentiodynamic polarization and EIS results pertaining to different temperatures in different concentrations of sodium sulphate have been listed in the Tables 3.50 to 3.59. The decrease in the efficiency of inhibition with the increase in temperature indicates the desorption of the inhibitor molecules of the metal surface when the temperature increases (Poornima et al. 2011). This fact is also suggestive of physisorption of the inhibitor molecules on the metal surface.

The Arrhenius plots for the corrosion of GA9 magnesium alloy in the presence of different concentrations of SOBS in 1.0 M Na$_2$SO$_4$ solution are shown in Fig. 3.57. The plots of ln(υ$_{corr}$ /T) versus 1/T in 1.0 M Na$_2$SO$_4$ solution in the presence of different concentrations of SOBS are shown in Fig. 3.58.
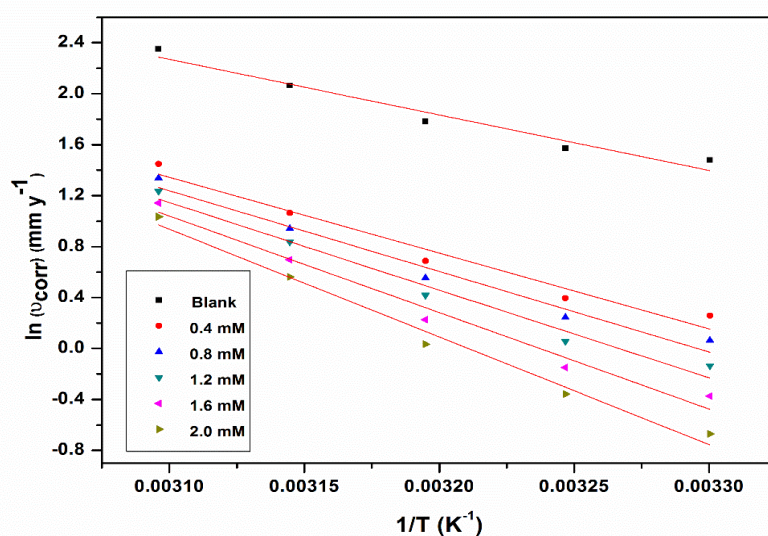
Fig. 3.57: Arrhenius plots for the corrosion of GA9 magnesium alloy in 1.0 M Na$_2$SO$_4$ solution containing different concentrations of SOBS.
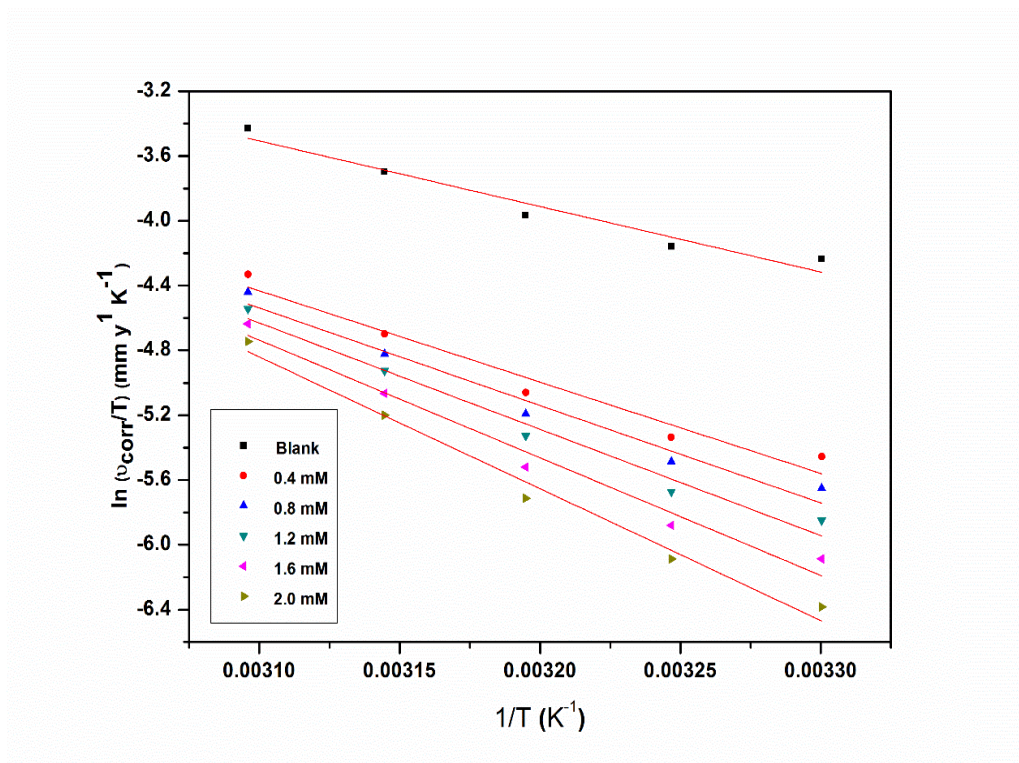
Fig. 3.58: Plots of ln(υ_{corr}/T) versus 1/T for the corrosion of GA9 magnesium alloy in 1.0 M Na₂SO₄ solution containing different concentrations of SOBS.

The calculated values of E_a, $\Delta H^{\#}$ and $\Delta S^{\#}$ are given in Table 3.60. The increase in the activation energy on the addition of SOBS can be attributed to the greater SOBS adsorption that provides a barrier on the surface of the alloy (Avci et al. 2008). The values of entropy of activation indicates that the activated complex in the rate determination step represents an association rather than dissociation, resulting in a decrease in randomness when moving from reactants to activated complex.

3.8.4 Effect of sodium sulphate concentration

Tables 3.61 summarises the maximum inhibition efficiencies exhibited by SOBS in the Na₂SO₄ solutions of different concentrations at different temperatures. The experimental results of the polarization and the EIS clearly show that, for a given inhibitor concentration, the effectiveness of the inhibition decreases with the increase of the concentration of sodium sulphate on the GA9 magnesium alloy. The highest inhibition efficiency is observed in sodium sulphate solution of 0.1 M concentration.

3.8.5 Adsorption isotherm

The adsorption of SOBS on the surface of GA9 magnesium alloy was found to obey Langmuir adsorption isotherm. The Langmuir adsorption isotherms for the adsorption of SOBS on GA9 magnesium alloy in 1.0 M Na_2SO_4 solution are shown in Fig. 3.59. The linear regression coefficients are close to unity and the slopes of the straight lines are nearly unity, suggesting that the adsorption of SOBS obeys Langmuir's adsorption isotherm with a little interaction between the adsorbed molecules. The thermodynamic data obtained for the adsorption of SOBS on GA9 magnesium alloy are tabulated in Table 3.62. The plot of $\Delta G°_{ads}$ Vs T gives a straight line and the $\Delta H°_{ads}$ and $\Delta S°_{ads}$ values are calculated from the slope and intercept. The plot of $\Delta G°_{ads}$ Vs T is shown in Fig. 3.60. The exothermic $\Delta H°_{ads}$ values of less than -41.86 kJ mol^{-1} predict physisorption of SOBS on the alloy surfaces (Ashish Kumar et al. 2010). The $\Delta G°_{ads}$ values predict both physisorption and chemisorption of SOBS. Therefore it can be concluded that the adsorption of SOBS on the GA9 magnesium alloy is predominantly through physisorption. These facts are also supported by the variation of inhibition efficiencies with temperature on the alloy surface as discussed under section 3.8.3.
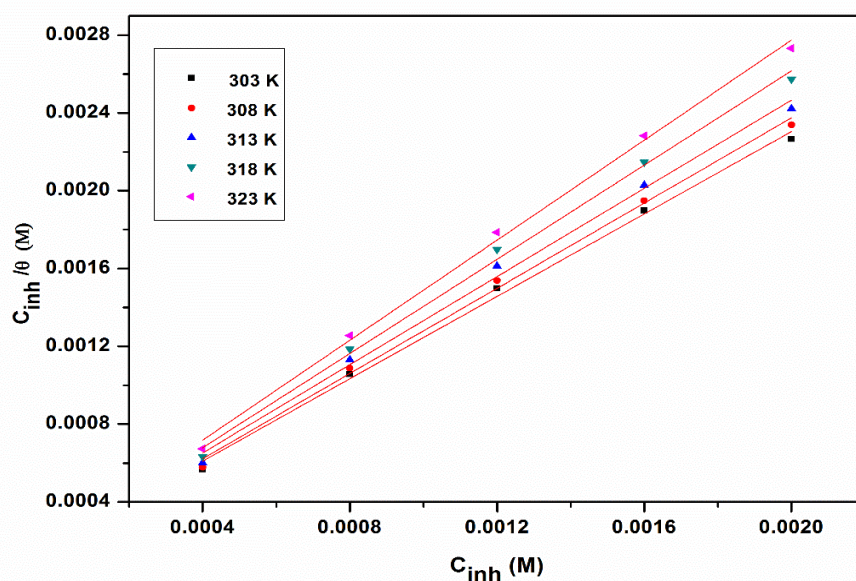
Fig. 3.59: Langmuir adsorption isotherms for the adsorption of SOBS on GA9 magnesium alloy in 1.0 M Na2SO4 solution at different temperatures.
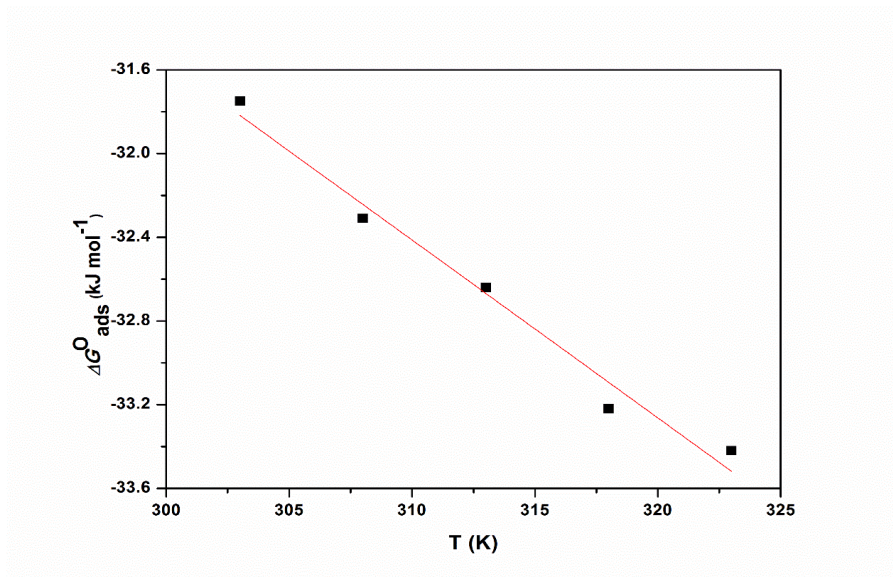
Fig. 3.60: The plot of ΔG°_{ads} Vs T for the adsorption of SOBS on GA9 magnesium alloy in 1.0 M Na$_2$SO$_4$ solution.

3.8.6 Mechanism of corrosion inhibition

The corrosion inhibition mechanism of SOBS in sodium sulphate solution can be explained in the same lines as that of SOBS in the section 3.7.6. The inhibitor SOBS protects the alloy surface through predominant physisorption mode in which the SOBS gets adsorbed on the alloy surface through electrostatic attraction.

3.8.7 SEM/EDX studies

Fig. 3.61 represents the SEM image of GA9 magnesium alloy after the corrosion tests in a medium of 2.0 M sodium sulphate containing 2.0 mM of SOBS. The image clearly shows an undeteriorated surface due to the adsorbed layer of inhibitor molecules on the alloy surface, thus protecting the metal from corrosion.
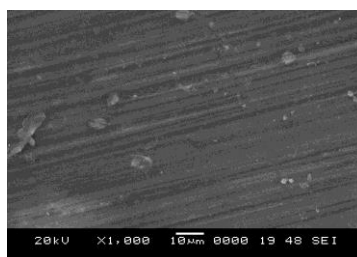
Fig. 3.61: SEM image of GA9 magnesium alloy after immersion in 1.0 M Na$_2$SO$_4$ solution in the presence of SOBS.

171

The EDX profile analyses for the selected areas on the SEM images of Fig. 3.61 is shown in Fig. 3.62, respectively. In the EDX spectra Fig. 3.62, apart from the peaks for Mg, Al and S, an additional small peak for carbon and oxygen is obtained, which indicates the presence of some organic moieties on the alloy surface, which possibly are the surface adsorbed SOBS molecules.
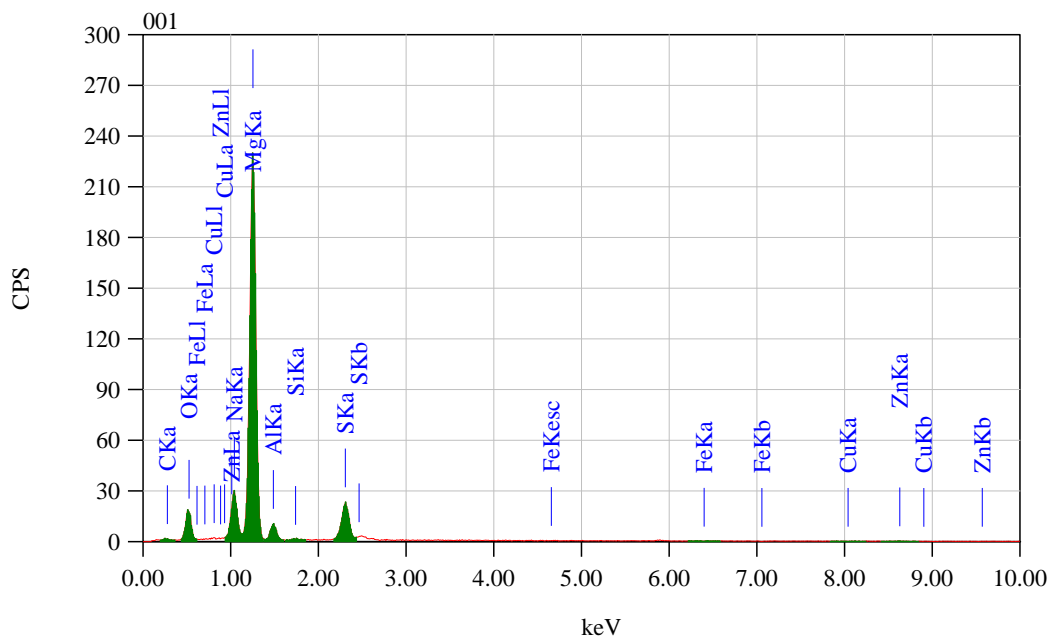
Fig. 3.62: EDX spectra of GA9 magnesium alloy after immersion in 2.0 M

Na₂SO₄ solution in the presence of SOBS.

Table 3.50: Results of potentiodynamic polarization studies for the corrosion of GA9 magnesium alloy in 0.1 M sodium sulphate solution containing different concentrations of SOBS.

Temperature (°C)	Conc. of inhibitor (mM)	$-E_{corr}$ (mV /SCE)	$-b_c$ (mV dec^{-1})	i_{corr} (μA cm^{-2})	υ_{corr} (mm y^{-1})	η (%)
30	Blank	1456	139	42.1	0.946	
	0.4	1455	116	10.4	0.234	75.3
	0.8	1459	114	8.5	0.191	79.7
	1.2	1454	112	6.7	0.151	84.0
	1.6	1451	109	5.0	0.112	88.1
	2.0	1449	107	3.5	0.079	91.7
35	Blank	1461	144	47.7	1.071	
	0.4	1464	121	12.2	0.274	74.5
	0.8	1467	118	10.0	0.225	79.0
	1.2	1458	115	8.0	0.180	83.3
	1.6	1455	111	6.1	0.137	87.2
	2.0	1457	109	4.5	0.101	90.5
40	Blank	1463	151	58.4	1.311	
	0.4	1461	129	15.7	0.353	73.2
	0.8	1464	127	13.6	0.306	76.7
	1.2	1460	124	11.2	0.252	80.9
	1.6	1459	122	8.3	0.186	85.8
	2.0	1452	118	6.3	0.142	89.2
45	Blank	1468	159	74.4	1.671	
	0.4	1470	139	22.9	0.515	69.2
	0.8	1475	136	20.5	0.461	72.5
	1.2	1467	133	17.3	0.389	76.7
	1.6	1464	131	14.2	0.319	80.9
	2.0	1455	127	11.3	0.254	84.8
50	Blank	1469	167	97.8	2.197	
	0.4	1473	149	34.7	0.780	64.5
	0.8	1477	147	31.3	0.703	68.0
	1.2	1468	144	28.3	0.636	71.1
	1.6	1465	141	25.2	0.566	74.2
	2.0	1459	138	22.1	0.497	77.4

Table 3.51: Results of potentiodynamic polarization studies for the corrosion of GA9 magnesium alloy in 0.5 M sodium sulphate solution containing different concentrations of SOBS.

Temperature (°C)	Conc. of inhibitor (mM)	$-E_{corr}$ (mV /SCE)	$-b_c$ (mV dec^{-1})	i_{corr} (μA cm^{-2})	υ_{corr} (mm y^{-1})	η (%)
30	Blank	1461	144	112.4	2.526	
	0.4	1466	123	30.6	0.688	72.8
	0.8	1464	121	25.9	0.582	77.0
	1.2	1469	119	20.8	0.467	81.5
	1.6	1460	117	15.5	0.348	86.2
	2.0	1455	115	11.1	0.249	90.1
35	Blank	1462	149	125.5	2.819	
	0.4	1467	129	35.3	0.793	71.9
	0.8	1469	127	28.7	0.645	77.1
	1.2	1461	123	23.8	0.535	81.0
	1.6	1458	121	18.6	0.418	85.2
	2.0	14560	117	14.4	0.324	88.5
40	Blank	1459	156	161.1	3.619	
	0.4	1463	137	48.0	1.078	70.2
	0.8	1458	135	40.6	0.912	74.8
	1.2	1460	131	34.6	0.777	78.5
	1.6	1451	128	28.4	0.638	82.4
	2.0	1455	126	23.2	0.521	85.6
45	Blank	1475	164	203.3	4.568	
	0.4	1471	145	66.1	1.485	67.5
	0.8	1475	142	58.6	1.317	71.2
	1.2	1473	139	51.4	1.155	74.7
	1.6	1467	137	44.3	0.995	78.2
	2.0	1468	135	38.6	0.867	81.0
50	Blank	1487	173	264.3	5.939	
	0.4	1494	156	98.3	2.209	62.8
	0.8	1491	153	89.9	2.020	66.0
	1.2	1480	151	78.8	1.771	70.2
	1.6	1484	149	70.3	1.580	73.4
	2.0	1479	146	62.4	1.402	76.4

Table 3.52: Results of potentiodynamic polarization studies for the corrosion of GA9 magnesium alloy in 1.0 M sodium sulphate solution containing different concentrations of SOBS.

| Temperature (℃)	Conc. of inhibitor (mM)	$-E_{corr}$ (mV /SCE)	$-b_c$ (mV dec^{-1})	i_{corr} (μA cm^{-2})	υ_{corr} (mm y^{-1})	η (%)
30	Blank	1472	151	195.2	4.386	
	0.4	1475	136	57.6	1.294	70.5
	0.8	1476	134	47.4	1.065	75.7
	1.2	1464	131	38.8	0.872	80.1
	1.6	1469	127	30.6	0.688	84.3
	2.0	1461	124	22.8	0.512	88.3
35	Blank	1477	156	214.2	4.813	
	0.4	1483	142	66.0	1.483	69.2
	0.8	1480	139	56.8	1.276	73.5
	1.2	1474	137	47.1	1.058	78.0
	1.6	1476	134	38.3	0.861	82.1
	2.0	1469	130	31.1	0.699	85.5
40	Blank	1486	160	264.3	5.938	
	0.4	1490	147	88.5	1.988	66.5
	0.8	1492	145	77.4	1.739	70.7
	1.2	1482	143	67.7	1.521	74.4
	1.6	1485	140	55.8	1.254	78.9
	2.0	1486	136	46.0	1.034	82.6
45	Blank	1487	171	350.4	7.872	
	0.4	1494	155	128.9	2.896	63.2
	0.8	1491	152	113.9	2.559	67.5
	1.2	1486	149	102.7	2.308	70.7
	1.6	1488	147	89.4	2.009	74.5
	2.0	1477	144	78.1	1.755	77.7
50	Blank	1490	181	466.3	10.477	
	0.4	1495	166	189.3	4.253	59.4
	0.8	1499	164	169.3	3.804	63.7
	1.2	1489	161	152.9	3.435	67.2
	1.6	1485	159	139.4	3.132	70.1
	2.0	1486	158	125.0	2.809	73.2

Table 3.53: Results of potentiodynamic polarization studies for the corrosion of GA9 magnesium alloy in 1.5 M sodium sulphate solution containing different concentrations of SOBS.

Temperature (℃)	Conc. of inhibitor (mM)	$-E_{corr}$ (mV /SCE)	$-b_c$ (mV dec^{-1})	i_{corr} (μA cm^{-2})	υ_{corr} (mm y^{-1})	η (%)
	Blank	1477	158	281.7	6.328	
	0.4	1483	143	87.3	1.961	69.0
30	0.8	1484	141	73.8	1.658	73.8
	1.2	1477	138	60.6	1.362	78.5
	1.6	1482	135	50.4	1.132	82.1
	2.0	1469	131	40.3	0.905	85.7
	Blank	1483	165	339.2	7.621	
	0.4	1488	149	111.3	2.501	67.2
	0.8	1487	147	95.0	2.135	72.0
35	1.2	1485	144	79.7	1.791	76.5
	1.6	1480	143	62.1	1.395	81.7
	2.0	1484	141	55.0	1.236	83.8
	Blank	1482	173	426.8	9.589	
	0.4	1485	161	154.5	3.471	63.8
	0.8	1484	159	135.7	3.049	68.2
40	1.2	1481	156	117.4	2.638	72.5
	1.6	1487	153	102.0	2.292	76.1
	2.0	1472	149	85.4	1.919	80.0
	Blank	1486	182	527.1	11.843	
	0.4	1490	171	207.7	4.667	60.6
	0.8	1499	169	188.2	4.229	64.3
45	1.2	1484	166	166.6	3.743	68.4
	1.6	1479	162	149.2	3.352	71.7
	2.0	1473	159	127.6	2.867	75.8
	Blank	1492	194	707.4	15.894	
	0.4	1493	184	300.6	6.754	57.5
	0.8	1492	181	273.1	6.136	61.4
50	1.2	1488	177	247.6	5.563	65.0
	1.6	1495	175	223.5	5.022	68.4
	2.0	1479	173	204.4	4.593	71.1

Table 3.54: Results of potentiodynamic polarization studies for the corrosion of GA9 magnesium alloy in 2.0 M sodium sulphate solution containing different concentrations of SOBS.

Temperature (℃)	Conc. of inhibitor (mM)	$-E_{corr}$ (mV /SCE)	$-b_c$ (mV dec^{-1})	i_{corr} (μA cm^{-2})	υ_{corr} (mm y^{-1})	η (%)
30	Blank	1488	169	374.6	8.417	
	0.4	1490	159	129.2	2.903	65.5
	0.8	1491	157	113.5	2.550	69.7
	1.2	1497	155	99.3	2.231	73.5
	1.6	1485	152	85.8	1.928	77.1
	2.0	1480	148	71.5	1.606	80.9
35	Blank	1483	176	455.4	10.232	
	0.4	1477	165	165.3	3.714	63.7
	0.8	1486	162	145.7	3.274	68.0
	1.2	1482	159	129.8	2.916	71.5
	1.6	1485	156	112.5	2.528	75.3
	2.0	1475	154	96.5	2.168	78.8
40	Blank	1481	185	597.1	13.415	
	0.4	1486	175	232.9	5.233	61.0
	0.8	1490	173	208.4	4.682	65.1
	1.2	1479	171	182.1	4.092	69.5
	1.6	1477	166	161.8	3.635	72.9
	2.0	1472	162	137.3	3.085	77.0
45	Blank	1489	197	755.8	16.981	
	0.4	1493	188	313.7	7.048	58.5
	0.8	1491	186	284.9	6.401	62.3
	1.2	1485	183	259.2	5.824	65.7
	1.6	1483	178	241.1	5.417	68.1
	2.0	1489	173	216.9	4.873	71.3
50	Blank	1499	209	927.7	20.842	
	0.4	1503	199	431.4	9.693	53.5
	0.8	1507	196	398.9	8.963	57.0
	1.2	1495	192	366.4	8.232	60.5
	1.6	1493	189	339.5	7.628	63.4
	2.0	1497	186	311.7	7.003	66.4

Table 3.55: EIS data for the corrosion of GA9 magnesium alloy in 0.1 M sodium sulphate solution containing different concentrations of SOBS.

Temperature (℃)	Conc. of inhibitor (mM)	R_{ct} (ohm. cm^2)	C_{dl} (µF cm^{-2})	η (%)
30	Blank	604.7	10.53	
	0.4	2429.0	7.12	75.1
	0.8	2950.0	6.88	79.5
	1.2	3665.0	6.65	83.5
	1.6	4916.0	6.57	87.7
	2.0	7031.0	6.31	91.4
35	Blank	545.5	10.98	
	0.4	2131.0	8.05	74.4
	0.8	2623.0	7.74	79.2
	1.2	3306.0	7.59	83.5
	1.6	4329.0	7.42	87.4
	2.0	5866.0	7.15	90.7
40	Blank	447.8	11.35	
	0.4	1684.0	8.55	73.4
	0.8	1930.0	8.39	76.8
	1.2	2357.0	8.22	81.0
	1.6	3245.0	8.07	86.2
	2.0	4265.0	7.71	89.5
45	Blank	356.5	16.50	
	0.4	1161.0	10.32	69.3
	0.8	1296.0	10.07	72.5
	1.2	1550.0	9.81	77.0
	1.6	1896.0	9.58	81.2
	2.0	2425.0	9.40	85.3
50	Blank	273.0	25.71	
	0.4	773.4	15.78	64.7
	0.8	858.5	15.11	68.2
	1.2	957.9	14.89	71.5
	1.6	1079.0	14.56	74.7
	2.0	1213.0	14.27	77.5

Table 3.56: EIS data for the corrosion of GA9 magnesium alloy in 0.5 M sodium sulphate solution containing different concentrations of SOBS.

Temperature (℃)	Conc. of inhibitor (mM)	R_{ct} (ohm. cm^2)	C_{dl} (μF cm^{-2})	η (%)
30	Blank	219.1	18.29	
	0.4	808.5	9.34	72.9
	0.8	952.6	9.13	77.0
	1.2	1178.0	8.85	81.4
	1.6	1599.0	8.67	86.3
	2.0	2236.0	8.51	90.2
35	Blank	200.4	22.81	
	0.4	718.3	10.75	72.1
	0.8	871.3	10.44	77.0
	1.2	1044.0	10.01	80.8
	1.6	1327.0	9.56	84.9
	2.0	1684.0	9.21	88.1
40	Blank	165.0	26.11	
	0.4	555.6	12.91	70.3
	0.8	657.4	12.70	74.9
	1.2	763.9	12.44	78.4
	1.6	921.8	11.97	82.1
	2.0	1138.0	11.55	85.5
45	Blank	128.8	30.77	
	0.4	397.5	14.41	67.6
	0.8	448.8	14.05	71.3
	1.2	511.1	13.80	74.8
	1.6	599.1	13.21	78.5
	2.0	685.1	12.69	81.2
50	Blank	97.8	34.19	
	0.4	264.3	17.56	63.0
	0.8	291.1	16.95	66.4
	1.2	331.5	16.49	70.5
	1.6	371.9	16.27	73.7
	2.0	416.2	15.94	76.5

Table 3.57: EIS data for the corrosion of GA9 magnesium alloy in 1.0 M sodium sulphate solution containing different concentrations of SOBS.

Temperature (℃)	Conc. of inhibitor (mM)	R_{ct} (ohm. cm^2)	C_{dl} (μF cm^{-2})	η (%)
	Blank	139.0	30.91	
	0.4	471.2	10.81	70.5
30	0.8	569.7	10.34	75.6
	1.2	702.0	10.01	80.2
	1.6	891.0	9.63	84.4
	2.0	1198.0	9.31	88.4
	Blank	122.6	32.17	
	0.4	395.5	12.59	69.0
35	0.8	452.4	12.19	72.9
	1.2	552.3	11.85	77.8
	1.6	688.8	11.36	82.2
	2.0	822.8	10.99	85.1
	Blank	97.4	40.62	
	0.4	291.6	19.15	66.6
40	0.8	335.4	18.77	70.9
	1.2	379.0	18.22	74.3
	1.6	457.3	17.31	78.7
	2.0	559.8	16.12	82.6
	Blank	72.1	45.05	
	0.4	197.5	22.71	63.5
45	0.8	223.2	22.32	67.7
	1.2	245.2	21.46	70.6
	1.6	286.1	20.30	74.8
	2.0	327.7	19.48	78.0
	Blank	55.5	56.30	
	0.4	137.0	26.11	59.5
50	0.8	152.5	25.21	63.6
	1.2	168.2	24.51	67.0
	1.6	186.9	23.23	70.3
	2.0	207.9	22.18	73.3

Table 3.58: EIS data for the corrosion of GA9 magnesium alloy in 1.5 M sodium sulphate solution containing different concentrations of SOBS.

Temperature (℃)	Conc. of inhibitor (mM)	R_{ct} (ohm. cm^2)	C_{dl} (μF cm^{-2})	η (%)
30	Blank	91.6	34.56	
	0.4	294.5	12.62	68.9
	0.8	345.7	12.31	73.5
	1.2	418.3	11.97	78.1
	1.6	508.9	11.75	82.0
	2.0	645.1	11.48	85.8
35	Blank	77.7	40.12	
	0.4	239.1	18.68	67.5
	0.8	280.5	18.14	72.3
	1.2	336.4	17.77	76.9
	1.6	431.7	16.89	82.0
	2.0	491.8	16.08	84.2
40	Blank	62.4	54.17	
	0.4	171.9	28.71	63.7
	0.8	196.2	27.92	68.2
	1.2	226.1	26.98	72.4
	1.6	262.2	25.04	76.2
	2.0	313.6	24.11	80.1
45	Blank	48.7	71.38	
	0.4	124.9	33.62	61.0
	0.8	138.4	32.41	64.8
	1.2	157.1	31.74	69.0
	1.6	175.2	30.83	72.2
	2.0	205.5	29.01	76.3
50	Blank	37.5	88.74	
	0.4	88.2	40.23	57.5
	0.8	96.9	38.62	61.3
	1.2	107.8	37.98	65.2
	1.6	119.4	36.07	68.6
	2.0	130.7	34.02	71.3

Table 3.59: EIS data for the corrosion of GA9 magnesium alloy in 2.0 M sodium sulphate solution containing different concentrations of SOBS.

Temperature (℃)	Conc. of inhibitor (mM)	R_{ct} (ohm. cm^2)	C_{dl} (µF cm^{-2})	η (%)
30	Blank	67.5	42.55	
	0.4	195.1	18.95	65.4
	0.8	224.3	18.31	69.9
	1.2	253.8	17.94	73.4
	1.6	300.0	17.04	77.5
	2.0	351.6	15.93	80.8
35	Blank	57.4	50.87	
	0.4	158.6	24.55	63.8
	0.8	179.9	23.31	68.1
	1.2	200.7	22.01	71.4
	1.6	234.3	20.95	75.5
	2.0	274.0	19.76	79.1
40	Blank	43.2	69.58	
	0.4	111.3	32.81	61.2
	0.8	124.1	30.88	65.2
	1.2	140.7	28.77	69.3
	1.6	160.6	27.02	73.1
	2.0	187.8	24.74	77.0
45	Blank	34.0	85.41	
	0.4	82.3	42.91	58.7
	0.8	90.4	40.21	62.4
	1.2	98.8	38.69	65.6
	1.6	106.3	36.04	68.0
	2.0	119.3	33.55	71.5
50	Blank	27.8	102.33	
	0.4	59.3	49.34	53.1
	0.8	64.2	47.02	56.7
	1.2	70.2	44.95	60.4
	1.6	76.2	41.98	63.5
	2.0	82.5	39.14	66.3

Table 3.60: Activation parameters for the corrosion of GA9 magnesium alloy in sodium sulphate solutions containing different concentrations of SOBS.

Concentration of Na_2SO_4	Conc. of inhibitor (mM)	E_a (kJ mol^{-1})	$\Delta H^{\#}$ (kJ mol^{-1})	$\Delta S^{\#}$ (J mol^{-1} K^{-1})
	Blank	34.57	31.97	-140.53
	0.4	49.28	46.68	-103.95
0.1	0.8	53.91	51.31	-90.40
	1.2	59.14	56.54	-75.23
	1.6	66.22	63.62	-54.58
	2.0	74.57	71.97	-30.02
	Blank	35.60	32.99	-128.98
	0.4	48.03	45.43	-99.04
0.5	0.8	51.93	49.33	-87.81
	1.2	55.74	53.14	-77.02
	1.6	63.19	60.59	-54.86
	2.0	72.13	69.53	-28.04
	Blank	36.22	33.62	-122.51
	0.4	49.46	46.86	-89.17
1.0	0.8	52.62	50.07	-80.25
	1.2	57.18	54.58	-66.87
	1.6	62.97	60.36	-49.82
	2.0	70.25	67.65	-28.09
	Blank	37.09	34.49	-116.19
	0.4	50.33	47.73	-82.31
1.5	0.8	53.65	51.05	-72.80
	1.2	57.73	55.13	-60.98
	1.6	62.67	60.07	-46.49
	2.0	66.47	63.87	-35.62
	Blank	37.75	35.15	-111.50
	0.4	49.63	47.03	-81.28
2.0	0.8	51.78	49.18	-75.32
	1.2	53.69	51.09	-70.13
	1.6	57.11	54.51	-60.15
	2.0	61.04	58.44	-48.74

Table 3.61: Maximum inhibition efficiencies attained in different concentrations of sodium sulphate solutions at different temperatures for SOBS.

Temperature (°C)	Sodium sulphate concentration (M)	Concentration of SOBS (mM)	GA9 magnesium alloy η (%)	
			Potentiodynamic polarization method	EIS method
30	0.1	2.0	91.7	91.4
	0.5		90.1	90.2
	1.0		88.3	88.4
	1.5		85.7	85.8
	2.0		80.9	80.8
35	0.1	2.0	90.5	90.7
	0.5		88.5	88.1
	1.0		85.5	85.1
	1.5		83.8	84.2
	2.0		78.8	79.1
40	0.1	2.0	89.2	89.5
	0.5		85.6	85.5
	1.0		82.6	82.6
	1.5		80.0	80.1
	2.0		77.0	77.0
45	0.1	2.0	84.8	85.3
	0.5		81.0	81.2
	1.0		77.7	78.0
	1.5		75.8	76.3
	2.0		71.3	71.5
50	0.1	2.0	77.4	77.5
	0.5		76.4	76.5
	1.0		73.2	73.3
	1.5		71.1	71.3
	2.0		66.4	66.3

Table 3.62: Thermodynamic parameters for the adsorption of SOBS on GA9 magnesium alloy surface in sodium sulphate solutions at different temperatures.

Molarity of Na$_2$SO$_4$ (M)	Temperature (° C)	$-\Delta G^o_{ads}$ (kJ mol^{-1})	ΔH^o_{ads} (kJ mol^{-1})	ΔS^o_{ads} (J mol^{-1} K^{-1})	R^2	Slope
	30	32.16			0.996	1.03
	35	32.72			0.997	1.04
0.1	40	33.01	-5.57	87.85	0.995	1.05
	45	33.33			0.995	1.11
	50	34.05			0.996	1.23
	30	31.84			0.995	1.04
	35	32.53			0.997	1.06
0.5	40	33.08	-1.92	99.21	0.997	1.10
	45	33.65			0.997	1.17
	50	33.76			0.996	1.23
	30	31.75			0.996	1.06
	35	32.31			0.996	1.10
1.0	40	32.64	-6.06	85.03	0.995	1.13
	45	33.22			0.996	1.21
	50	33.62			0.997	1.29
	30	31.79			0.996	1.09
	35	32.16			0.996	1.11
1.5	40	32.50	-7.76	79.22	0.995	1.17
	45	32.86			0.994	1.24
	50	33.42			0.997	1.32
	30	31.67			0.995	1.13
	35	32.11			0.996	1.19
2.0	40	32.30	-6.2	102.01	0.994	1.21
	45	33.17			0.997	1.33
	50	33.69			0.997	1.33

3.9 SODIUM 2,4-DIMETHYLBENZENESULFONATE (SDMBS) AS CORROSION INHIBITOR ON GA9 MAGNESIUM ALLOY IN SODIUM CHLORIDE MEDIUM

3.9.1 Potentiodynamic polarization measurements

Potentiodynamic polarization curves for the corrosion of GA9 magnesium alloy in 1.0 M NaCl solution in the presence of different concentrations of SDMBS, at 40 °C are shown in Fig. 3.63. Similar plots were obtained at other temperatures and also in the other concentrations of NaCl at the different temperatures studied. The potentiodynamic polarization parameters are summarized in Tables 3.63 to 3.67.
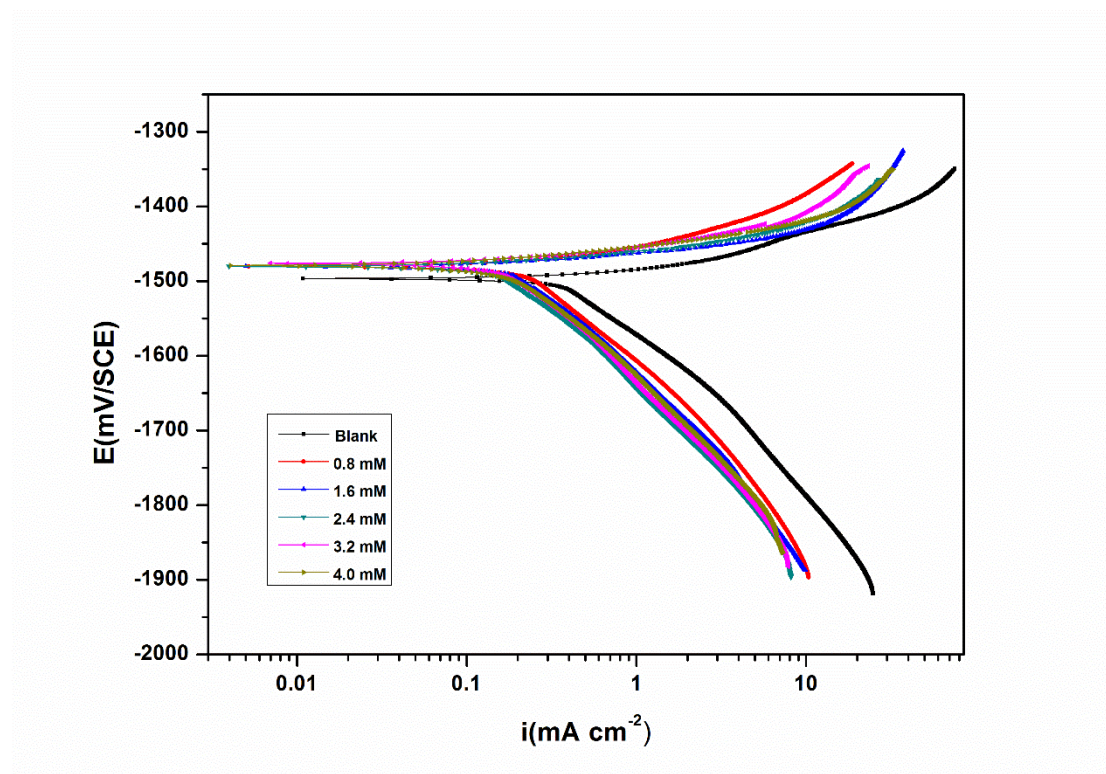
Fig. 3.63: Potentiodynamic polarization curves for the corrosion of GA9 magnesium alloy in 1.0 M NaCl solution containing different concentrations of SDMBS at 40 ℃.

The highlighted observations from Fig. 3.63 are the successive change of the polarization curves towards a region of lower current density with increasing SDMBS concentration, without apparent change in overall shape, the implication of this result is same as that explained for SDBS and SOBS. Once again the linear Tafel behaviour

is exclusive to cathodic branches and hence corrosion current density (i_{corr}) was deduced from cathodic extrapolation of Tafel plots at corrosion potential.

From Tables 3.63 to 3.67 it follows that SDMBS also functions as mixed type inhibitor, which for the most part limits the anodic reaction because the addition of SDMBS produces an anodic change in the corrosion potential (not more than 35 mV vs. SCE), together with slight variations in cathodic slopes. In addition, the increase in the addition of SDMBS improves the efficiency of inhibition.

3.9.2 Electrochemical impedance spectroscopy (EIS) studies

Nyquist plots for the corrosion of GA9 magnesium alloy in 1.0 M NaCl solution in the presence of different concentrations of SDMBS are given in Fig. 3.64. Similar plots were obtained in other concentrations of the sodium chloride and also at other temperatures. The impedance parameters are presented in Tables 3.64 to 3.68.
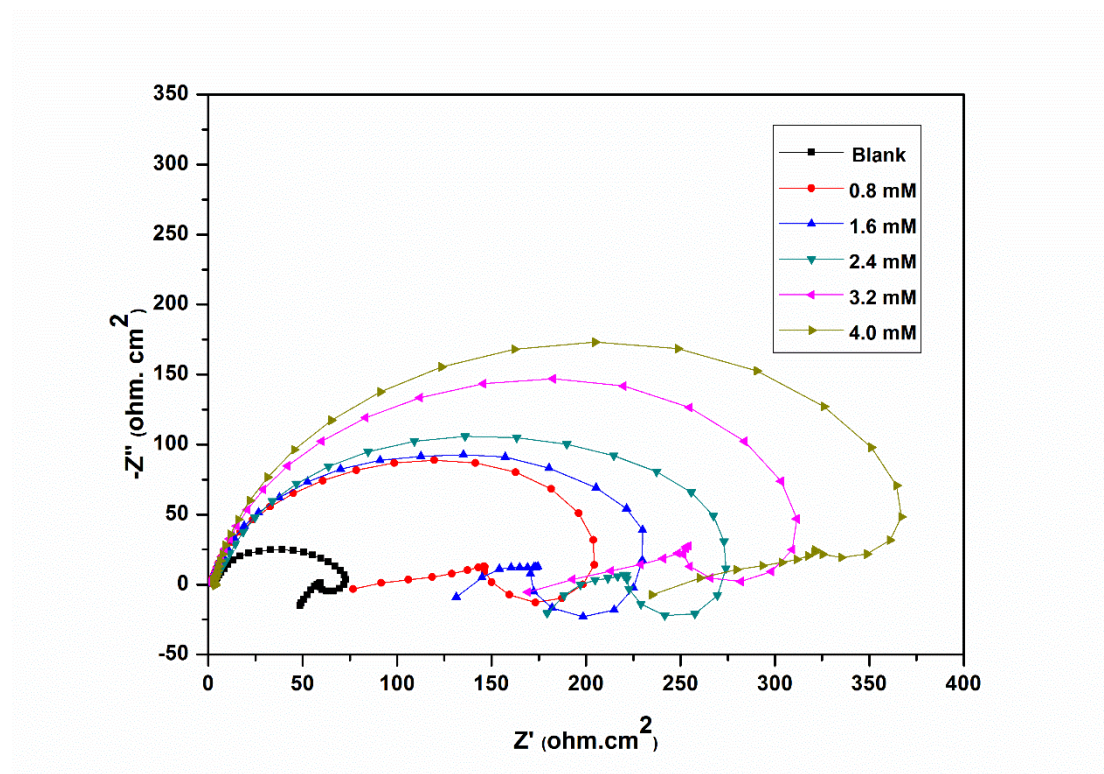
Fig. 3.64: Nyquist plots for the corrosion of GA9 magnesium alloy specimen in 1.0 M NaCl solution containing different concentrations of SDMBS at 40 ℃.

The Nyquist plots are characterized by a capacitive loop, extended from high frequency (HF) to low frequency (LF) range, an inductive loop in the low frequency

region (LF) range and a tail at the medium frequency (MF) range. With the gradual increase of the SDMBS concentration, there is a successive increase in capacitive loops resulted, without a significant change in shape, implying that the added SDMBS reduces corrosion rate without interfering with the mechanism or the corrosion reactions. The equivalent circuit given in Fig. 3.3 is used to fit the experimental data for the corrosion of GA9 magnesium alloy in sodium chloride solution in the presence of SDMBS. As can be seen from the Tables, $R_{ct,}$ value increases and C_{dl} value decreases with the increase in the concentration of SDMBS which suggests the decrease in corrosion rate.

The Bode plots of phase angle and amplitude for the corrosion of the GA9 magnesium alloy immersed in 1.0 M NaCl solution at 40 °C in the presence of varying amounts of SDMBS, are shown in Fig. 3.65 (a) and Fig. 3.65 (b), respectively. As seen from the Bode plots, both the impedance modulus (Z_{mod}) at low frequency and the phase maximum (θ_{max}) at intermediate frequency increase with the increase in SDMBS concentration, which indicates the presence of highly protective surface film, imparting corrosion protection.
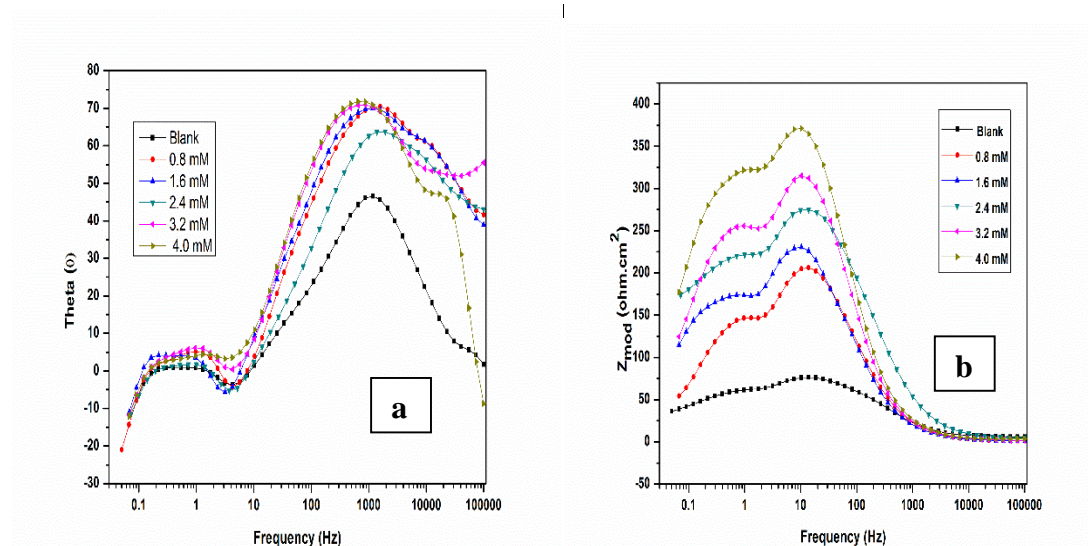
Fig. 3.65: Bode (a) phase angle plots and (b) amplitude plots for the corrosion of GA9 magnesium alloy in 1.0 M NaCl solution containing different concentrations of SDMBS at 40 °C.

3.9.3 Effect of temperature

The potentiodynamic polarization and EIS results pertaining to different temperatures in different concentrations of sodium chloride in the presence of SDMBS have been listed in Tables 3.63 to 3.72. The effect of temperature on corrosion inhibition behaviour of SDMBS is similar to that of SDBS on GA9 magnesium alloy as discussed in the section 3.5.3. The decrease in the inhibition efficiency of SDMBS with the increase in temperature on GA9magnesium alloy surface may be attributed to the physisorption of SDMBS. The Arrhenius plots for the corrosion of GA9 magnesium alloy in 1.0 M sodium chloride solution in the presence of different concentrations of SDMBS are shown in Fig. 3.66. The plots of ln(υ_{corr}/T) versus (1/T) are shown in Fig. 3.67. The calculated values of activation parameters are given in Table 3.73. The observations are similar to the ones obtained in the presence of SDBS and SOBS.
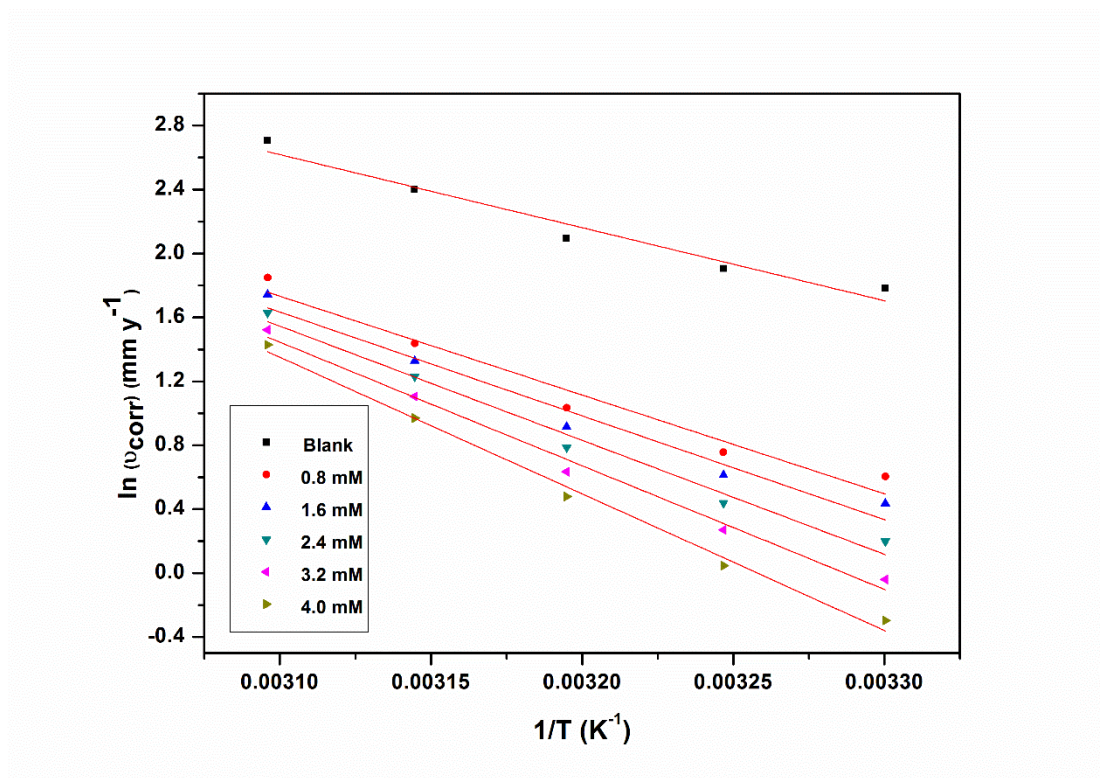
3.66: Arrhenius plots for the corrosion of GA9 magnesium alloy in 1.0 M NaCl solution containing different concentrations of SDMBS.
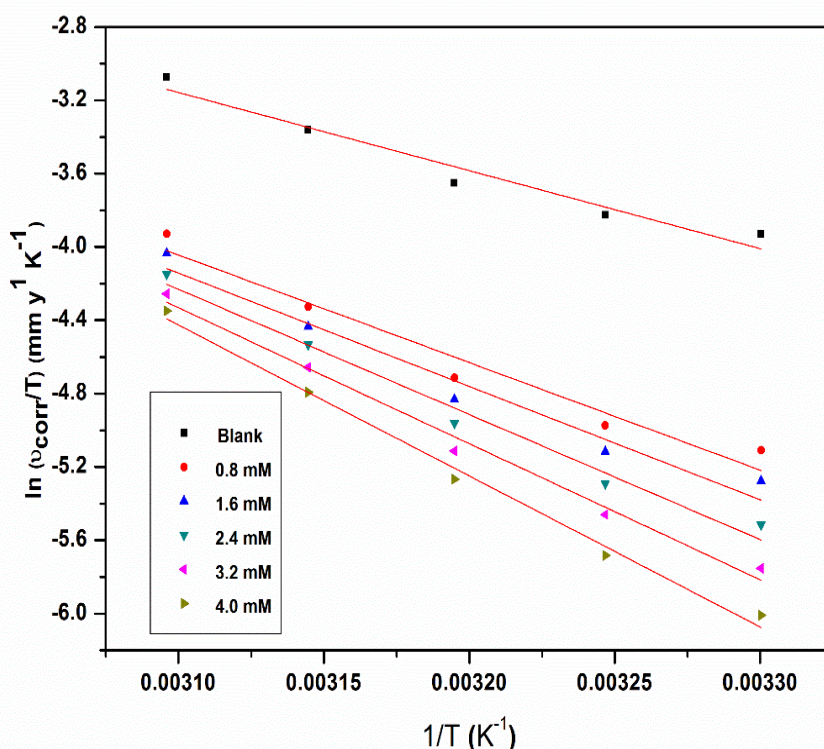
Fig. 3.67: Plots of ln(υ_{corr}/T) versus 1/T for the corrosion of GA9 magnesium alloy in 1.0 M NaCl solution containing different concentrations of SDMBS.

The increase in E_a values with the increase in SDMBS concentration indicates the increase in the energy barrier for the corrosion reaction as discussed in previous sections. The entropy of activation in the absence and presence of SDMBS is large and negative for the corrosion of the alloy. This implies that the activated complex in the rate determining step represents a step of association rather than dissociation, indicating that a decrease in disordering takes place on going from reactants to activated complex. The entropies of activation are higher for the corrosion of GA9 magnesium alloy in inhibited solutions than that in the uninhibited solutions.

3.9.4 Effect of sodium chloride concentration

Table 3.74 summarises the maximum inhibition efficiencies exhibited by SDMBS in sodium chloride solutions of different concentrations. It is evident from both polarization and EIS experimental results that, for a particular concentration of inhibitor, the inhibition efficiency decreases with the increase in sodium chloride

concentration. The highest inhibition efficiency is observed in sodium chloride of 0.1 M concentration.

3.9.5 Adsorption isotherm

The system with SDMBS as the inhibitor showed best agreement with Langmuir adsorption isotherm. The Langmuir adsorption isotherms are shown in Fig. 3.68. The plot of ΔG°_{ads} Vs T is shown in Fig. 3.69. The values of ΔG°_{ads} and ΔH°_{ads} indicate both physisorption and chemisorption of SDMBS on GA9 magnesium alloy with predominant physisorption. The ΔS^{0}_{ads} values indicate the increase in randomness on going from the reactants to the metal adsorbed species.
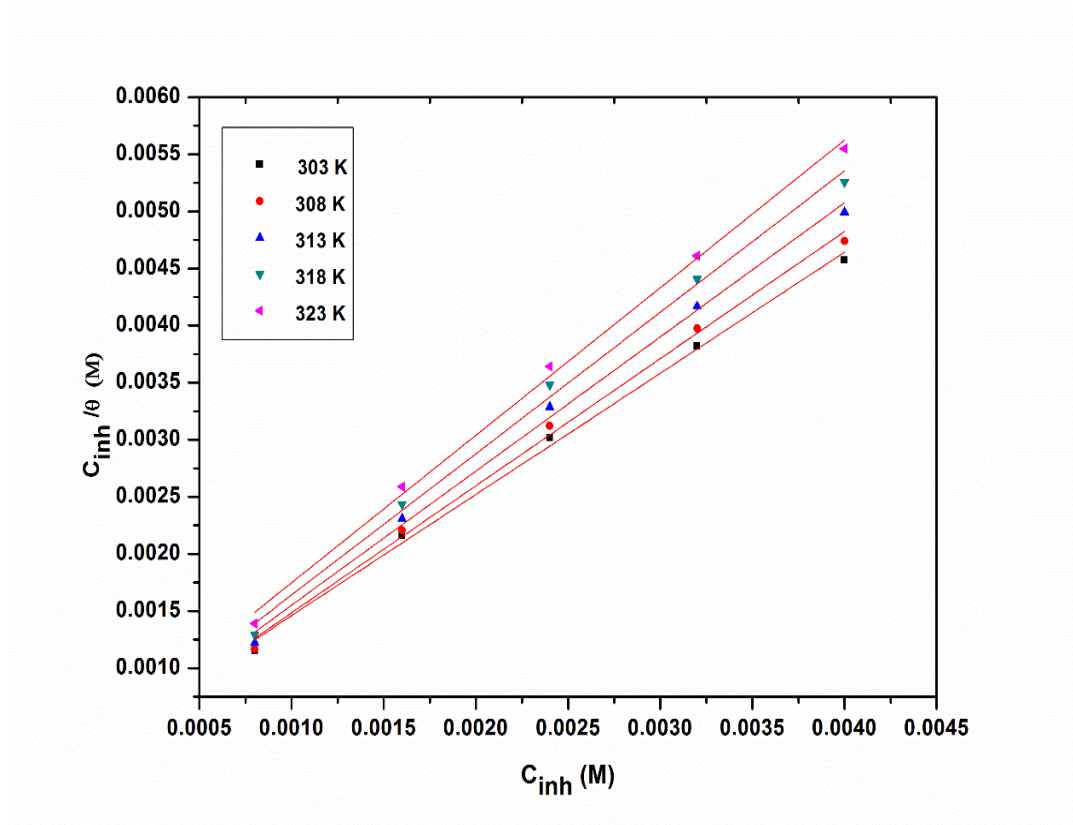
Fig. 3.68: Langmuir adsorption isotherms for the adsorption of SDMBS on GA9 magnesium alloy in 1.0 M NaCl solution at different temperatures.
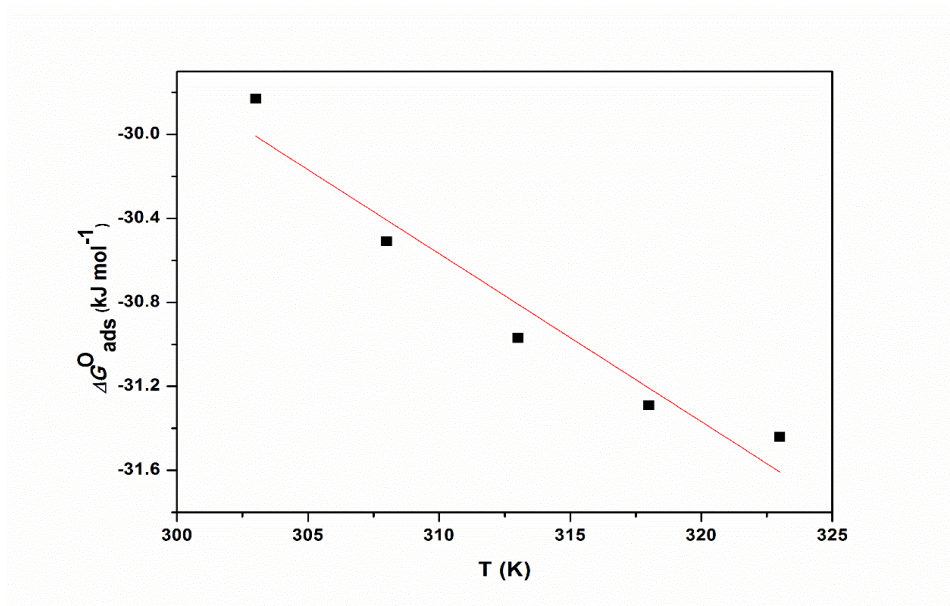
Fig. 3.69: The plot of ΔG°ads vs T for the adsorption of SDMBS on GA9 magnesium alloy in 1.0 M NaCl solution.

3.9.6 Mechanism of corrosion inhibition

The mechanism of corrosion inhibition of GA9 magnesium alloy in the presence of SDMBS is similar to that in the presence of SDBS as discussed under section 3.5.6. The molecules of SDMBS get adsorbed on the alloy surface predominantly by physisorption and to a small extent by chemisorption.

3.9.7 SEM/EDX studies

Fig. 3.70 represents the SEM image of GA9 magnesium alloy after the corrosion tests in a medium of 2.0 M sodium chloride containing 4.0 mM of SDMBS. The image clearly shows a relatively an uncorroded surface due to the presence of adsorbed inhibitor layer on the surface of the alloy.
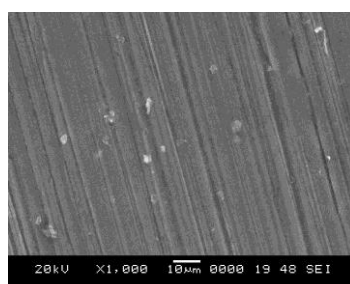
Fig. 3.70: SEM image of the GA9 magnesium alloy after immersion in 2.0 M NaCl solution in the presence of SDMBS.

The EDX spectra for the selected areas on the SEM image of 3.70 in the absence and the presence of inhibitor are shown in Fig. 3.71 (a) and Fig. 3.71 (b). The weight percentage of the elements found in the EDX spectra for corroded metal surface were 86.89% Mg, 8.16% Al, 0.44% Mn, 0.51% Zn and 4.00 % O. The weight percentage of the elements found in the EDX spectra for SDMBS adsorbed metal surface were 77.21% Mg, 9.09% Al, 9.05% O, 0.54% S and 4.10% C and suggested that formation of anticorrosion protective film of SDMBS on the alloy surface.
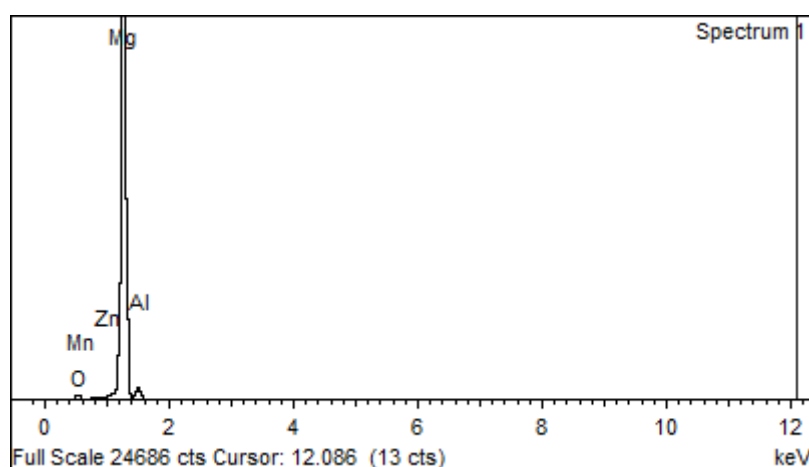
Fig. 3.71 (a): EDX spectra of GA9 magnesium alloy after immersion in 2.0 M NaCl solution in the absence of SDMBS.
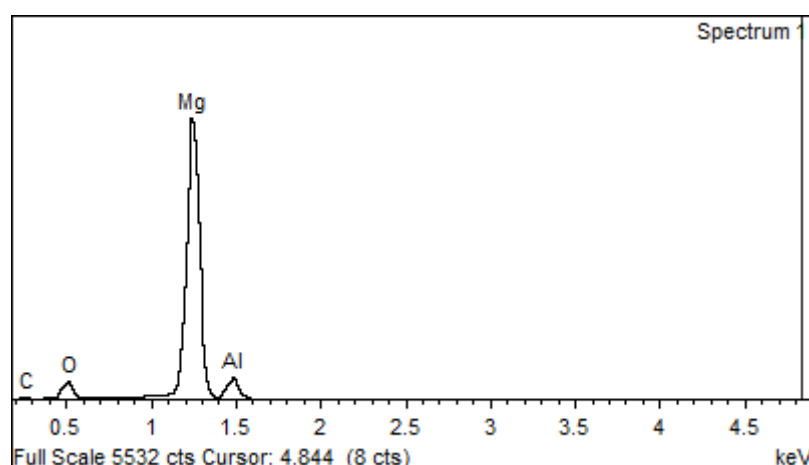
Fig. 3.71 (b): EDX spectra of GA9 magnesium alloy after immersion in 2.0 M NaCl solution in the presence of SDMBS.

Table 3.63: Results of potentiodynamic polarization studies for the corrosion of GA9 magnesium alloy in 0.1 M sodium chloride solution containing different concentrations of SDMBS.

Temperature (℃)	Conc. of inhibitor (mM)	$-E_{corr}$ (mV /SCE)	$-b_c$ (mV dec^{-1})	i_{corr} (μA cm^{-2})	υ_{corr} (mm y^{-1})	η (%)
30	Blank	1449	149	75.1	1.687	
	0.8	1449	123	19.2	0.431	74.5
	1.6	1442	120	15.9	0.357	78.8
	2.4	1445	117	12.7	0.285	83.1
	3.2	1435	115	9.8	0.220	86.9
	4.0	1443	113	7.4	0.166	90.1
35	Blank	1445	157	86.9	1.952	
	0.8	1444	138	22.9	0.515	73.6
	1.6	1448	135	19.2	0.431	77.9
	2.4	1442	131	15.6	0.351	82.0
	3.2	1434	128	12.3	0.276	85.8
	4.0	1436	125	9.6	0.216	89.0
40	Blank	1450	164	108.4	2.435	
	0.8	1449	146	30.4	0.683	72.0
	1.6	1451	143	26.2	0.589	75.8
	2.4	1445	140	21.6	0.485	80.1
	3.2	1442	137	17.5	0.393	83.9
	4.0	1435	133	13.9	0.312	87.2
45	Blank	1465	169	139.1	3.126	
	0.8	1461	153	43.4	0.975	68.8
	1.6	1455	150	39.1	0.879	71.9
	2.4	1458	148	34.1	0.766	75.5
	3.2	1450	145	28.7	0.645	79.4
	4.0	1448	143	23.2	0.521	83.3
50	Blank	1472	173	189.3	4.254	
	0.8	1465	157	70.6	1.586	62.7
	1.6	1463	155	62.7	1.409	66.9
	2.4	1457	152	57.4	1.290	69.7
	3.2	1460	149	52.1	1.171	72.5
	4.0	1452	146	46.9	1.054	75.2

Table 3.64: Results of potentiodynamic polarization studies for the corrosion of GA9 magnesium alloy in 0.5 M sodium chloride solution containing different concentrations of SDMBS.

| Temperature (℃)	Conc. of inhibitor (mM)	$-E_{corr}$ (mV /SCE)	$-b_c$ (mV dec^{-1})	i_{corr} (μA cm^{-2})	υ_{corr} (mm y^{-1})	η (%)
30	Blank	1451	152	160.0	3.595	
	0.8	1443	134	45.1	1.013	71.8
	1.6	1441	131	38.9	0.874	75.7
	2.4	1438	127	31.7	0.712	80.2
	3.2	1436	123	24.5	0.550	84.7
	4.0	1442	118	17.6	0.395	89.0
35	Blank	1473	158	179.3	4.029	
	0.8	1458	142	53.1	1.193	70.4
	1.6	1455	140	44.6	1.002	75.1
	2.4	1465	137	36.6	0.822	79.6
	3.2	1449	135	29.8	0.670	83.4
	4.0	1444	131	23.7	0.533	86.8
40	Blank	1466	167	206.6	4.641	
	0.8	1460	152	65.1	1.463	68.5
	1.6	1463	149	55.2	1.240	73.3
	2.4	1455	145	47.9	1.076	76.8
	3.2	1463	143	40.5	0.910	80.4
	4.0	1448	139	33.3	0.748	83.9
45	Blank	1490	171	285.1	6.405	
	0.8	1485	158	96.9	2.177	66.0
	1.6	1482	155	86.7	1.948	69.6
	2.4	1480	151	76.7	1.723	73.1
	3.2	1475	149	67.0	1.505	76.5
	4.0	1483	144	59.3	1.332	79.2
50	Blank	1497	175	377.1	8.473	
	0.8	1494	163	149.0	3.348	60.5
	1.6	1490	160	134.2	3.015	64.4
	2.4	1495	158	120.3	2.703	68.1
	3.2	1481	155	108.2	2.431	71.3
	4.0	1484	152	98.0	2.202	74.0

Table 3.65: Results of potentiodynamic polarization studies for the corrosion of GA9 magnesium alloy in 1.0 M sodium chloride solution containing different concentrations of SDMBS.

Temperature (℃)	Conc. of inhibitor (mM)	$-E_{corr}$ (mV /SCE)	$-b_c$ (mV dec^{-1})	i_{corr} (µA cm^{-2})	υ_{corr} (mm y^{-1})	η (%)
30	Blank	1474	156	264.5	5.942	
	0.8	1472	144	81.5	1.831	69.2
	1.6	1469	141	68.8	1.546	74.0
	2.4	1465	139	54.2	1.218	79.5
	3.2	1468	135	42.8	0.962	83.8
	4.0	1461	132	33.1	0.744	87.5
35	Blank	1495	162	298.9	6.716	
	0.8	1480	149	94.8	2.130	68.3
	1.6	1468	147	82.2	1.847	72.5
	2.4	1476	143	69.0	1.550	76.9
	3.2	1479	141	58.3	1.310	80.5
	4.0	1469	139	46.6	1.047	84.4
40	Blank	1496	169	361.5	8.122	
	0.8	1482	158	125.1	2.811	65.4
	1.6	1485	155	111.0	2.494	69.3
	2.4	1480	153	97.6	2.193	73.0
	3.2	1477	150	83.9	1.885	76.8
	4.0	1479	148	71.9	1.615	80.1
45	Blank	1496	177	491.0	11.031	
	0.8	1492	166	187.1	4.204	61.9
	1.6	1489	163	167.9	3.772	65.8
	2.4	1494	160	152.2	3.420	69.0
	3.2	1479	157	134.5	3.022	72.6
	4.0	1485	154	117.3	2.636	76.1
50	Blank	1501	179	665.6	14.955	
	0.8	1495	169	282.9	6.356	57.5
	1.6	1490	167	254.3	5.714	61.8
	2.4	1492	164	227.0	5.100	65.9
	3.2	1488	161	203.7	4.577	69.4
	4.0	1477	159	185.7	4.172	72.1

Table 3.66: Results of potentiodynamic polarization studies for the corrosion of GA9 magnesium alloy in 1.5 M sodium chloride solution containing different concentrations of SDMBS.

Temperature (℃)	Conc. of inhibitor (mM)	$-E_{corr}$ (mV /SCE)	$-b_c$ (mV dec^{-1})	i_{corr} (μA cm^{-2})	υ_{corr} (mm y^{-1})	η (%)
	Blank	1497	169	376.5	8.458	
	0.8	1493	157	120.1	2.698	68.1
30	1.6	1490	155	101.7	2.285	73.0
	2.4	1495	151	82.1	1.845	78.2
	3.2	1481	147	65.5	1.472	82.6
	4.0	1487	142	52.3	1.175	86.1
	Blank	1499	173	436.5	9.802	
	0.8	1485	160	141.9	3.188	67.5
	1.6	1493	157	123.5	2.775	71.7
35	2.4	1487	155	104.8	2.355	76.0
	3.2	1494	153	88.6	1.991	79.7
	4.0	1478	149	73.3	1.647	83.2
	Blank	1519	181	552.6	12.416	
	0.8	1511	168	198.9	4.469	64.0
	1.6	1517	165	177.9	3.997	67.8
40	2.4	1503	163	158.0	3.550	71.4
	3.2	1505	161	137.6	3.092	75.1
	4.0	1496	159	117.7	2.645	78.7
	Blank	1520	195	738.2	16.585	
	0.8	1513	184	293.8	6.601	60.2
	1.6	1510	181	266.5	5.988	63.9
45	2.4	1515	179	242.1	5.440	67.2
	3.2	1495	175	214.1	4.811	71.0
	4.0	1502	172	183.1	4.114	75.2
	Blank	1529	210	999.6	22.458	
	0.8	1513	201	435.8	9.792	56.4
	1.6	1519	198	396.8	8.915	60.3
50	2.4	1511	195	357.9	8.041	64.2
	3.2	1499	193	320.9	7.210	67.9
	4.0	1501	190	292.9	6.581	70.7

Table 3.67: Results of potentiodynamic polarization studies for the corrosion of GA9 magnesium alloy in 2.0 M sodium chloride solution containing different concentrations of SDMBS.

Temperature (℃)	Conc. of inhibitor (mM)	$-E_{corr}$ (mV /SCE)	$-b_c$ (mV dec^{-1})	i_{corr} (μA cm^{-2})	υ_{corr} (mm y^{-1})	η (%)
30	Blank	1524	192	447.5	10.055	
	0.8	1515	181	155.7	3.498	65.2
	1.6	1518	179	138.3	3.107	69.1
	2.4	1504	175	119.9	2.694	73.2
	3.2	1496	173	103.8	2.332	76.8
	4.0	1499	170	89.1	2.002	80.1
35	Blank	1525	195	546.9	12.286	
	0.8	1514	185	200.2	4.498	63.4
	1.6	1515	183	180.5	4.056	67.0
	2.4	1519	180	161.9	3.638	70.4
	3.2	1502	177	139.5	3.134	74.5
	4.0	1497	174	122.5	2.752	77.6
40	Blank	1529	206	726.0	16.310	
	0.8	1512	197	286.0	6.426	60.6
	1.6	1518	195	254.1	5.709	65.0
	2.4	1510	192	226.5	5.089	68.8
	3.2	1514	187	199.7	4.487	72.5
	4.0	1498	182	175.0	3.932	75.9
45	Blank	1530	213	986.2	22.157	
	0.8	1514	205	412.2	9.262	58.2
	1.6	1520	203	373.8	8.399	62.1
	2.4	1504	197	338.3	7.601	65.7
	3.2	1508	193	303.7	6.824	69.2
	4.0	1501	188	282.1	6.338	71.4
50	Blank	1535	222	1249.8	28.078	
	0.8	1527	210	578.7	13.003	53.7
	1.6	1513	208	536.2	12.048	57.1
	2.4	1517	204	492.4	11.063	60.6
	3.2	1509	201	453.7	10.194	63.7
	4.0	1507	198	411.2	9.239	67.1

Table 3.68: EIS data for the corrosion of GA9 magnesium alloy in 0.1 M sodium chloride solution containing different concentrations of SDMBS.

Temperature (℃)	Conc. of inhibitor (mM)	R_{ct} (ohm. cm^2)	C_{dl} (μF cm^{-2})	η (%)
	Blank	361.5	11.29	
	0.8	1401.0	8.69	74.2
30	1.6	1681.0	8.57	78.5
	2.4	2102.0	8.31	82.8
	3.2	2698.0	7.95	86.6
	4.0	3615.0	7.52	90.0
	Blank	302.5	11.41	
	0.8	1142.0	9.14	73.5
35	1.6	1388.0	8.79	78.2
	2.4	1709.0	8.58	82.3
	3.2	2176.0	8.25	86.1
	4.0	2854.0	8.07	89.4
	Blank	245.4	15.20	
	0.8	885.9	10.54	72.3
40	1.6	1010.0	10.19	75.7
	2.4	1239.0	9.99	80.2
	3.2	1524.0	9.72	83.9
	4.0	1902.0	9.26	87.1
	Blank	184.5	23.51	
	0.8	595.2	13.87	69.0
45	1.6	661.3	13.41	72.1
	2.4	759.3	12.98	75.7
	3.2	913.4	12.63	79.8
	4.0	1132.0	12.35	83.7
	Blank	132.8	28.95	
	0.8	358.9	17.45	63.0
50	1.6	400.1	17.25	66.8
	2.4	435.4	17.02	69.5
	3.2	481.2	16.64	72.4
	4.0	531.2	16.40	75.0

Table 3.69: EIS data for the corrosion of GA9 magnesium alloy in 0.5 M sodium chloride solution containing different concentrations of SDMBS.

Temperature (℃)	Conc. of inhibitor (mM)	R_{ct} (ohm. cm^2)	C_{dl} (µF cm^{-2})	η (%)
30	Blank	162.9	26.17	
	0.8	581.8	11.22	72.0
	1.6	673.1	11.05	75.8
	2.4	835.4	10.84	80.5
	3.2	1051.0	10.53	84.5
	4.0	1454.0	10.19	88.8
35	Blank	147.0	27.21	
	0.8	498.3	11.50	70.5
	1.6	595.1	11.39	75.3
	2.4	717.1	11.08	79.5
	3.2	869.8	10.71	83.1
	4.0	1081.0	10.27	86.4
40	Blank	127.3	28.63	
	0.8	402.8	12.11	68.4
	1.6	478.6	11.95	73.4
	2.4	553.5	11.75	77.0
	3.2	652.8	11.51	80.5
	4.0	785.8	11.13	83.8
45	Blank	91.0	35.08	
	0.8	269.2	15.57	66.2
	1.6	302.3	15.21	69.9
	2.4	339.6	14.88	73.2
	3.2	388.9	14.40	76.6
	4.0	431.3	13.97	78.9
50	Blank	70.8	40.33	
	0.8	180.2	18.81	60.7
	1.6	199.4	18.45	64.5
	2.4	221.3	18.01	68.0
	3.2	248.4	17.44	71.5
	4.0	274.4	16.80	74.2

Table 3.70: EIS data for the corrosion of GA9 magnesium alloy in 1.0 M sodium chloride solution containing different concentrations of SDMBS.

Temperature (℃)	Conc. of inhibitor (mM)	R_{ct} (ohm. cm²)	C_{dl} (μF cm⁻²)	η (%)
	Blank	99.7	33.50	
	0.8	326.9	11.62	69.5
30	1.6	386.4	11.43	74.2
	2.4	479.3	11.09	79.2
	3.2	604.2	10.65	83.5
	4.0	791.3	10.40	87.4
	Blank	87.4	34.93	
	0.8	277.5	17.07	68.5
35	1.6	314.4	16.70	72.2
	2.4	364.2	16.21	76.0
	3.2	439.2	15.67	80.1
	4.0	549.7	14.89	84.1
	Blank	72.8	39.91	
	0.8	208.6	19.85	65.1
40	1.6	234.8	19.42	69.0
	2.4	268.6	18.87	72.9
	3.2	315.2	18.30	76.9
	4.0	367.7	17.64	80.2
	Blank	52.7	66.70	
	0.8	138.7	30.52	62.0
45	1.6	152.8	30.01	65.5
	2.4	168.4	29.23	68.7
	3.2	191.6	27.59	72.5
	4.0	219.6	26.02	76.0
	Blank	39.0	77.59	
	0.8	92.4	40.50	57.8
50	1.6	103.4	39.26	62.3
	2.4	116.1	38.03	66.4
	3.2	128.7	36.62	69.7
	4.0	141.8	34.33	72.5

Table 3.71: EIS data for the corrosion of GA9 magnesium alloy in 1.5 M sodium chloride solution containing different concentrations of SDMBS.

Temperature (°C)	Conc. of inhibitor (mM)	R_{ct} (ohm. cm^2)	C_{dl} (μF cm^{-2})	η (%)
	Blank	67.9	41.61	
	0.8	210.9	25.32	67.8
30	1.6	252.4	24.95	73.1
	2.4	314.4	23.95	78.4
	3.2	385.8	22.85	82.4
	4.0	474.8	21.79	85.7
	Blank	60.2	61.15	
	0.8	187.5	37.05	67.9
35	1.6	213.5	36.18	71.8
	2.4	248.8	35.14	75.8
	3.2	302.5	33.90	80.1
	4.0	364.8	31.81	83.5
	Blank	47.5	69.71	
	0.8	132.7	41.41	64.2
40	1.6	148.0	40.30	67.9
	2.4	166.7	38.89	71.5
	3.2	192.3	37.94	75.3
	4.0	226.2	35.09	79.0
	Blank	35.5	89.49	
	0.8	89.4	48.41	60.3
45	1.6	97.3	46.63	63.5
	2.4	107.6	44.98	67.0
	3.2	122.0	42.15	70.9
	4.0	140.9	38.82	74.8
	Blank	26.3	107.44	
	0.8	60.3	52.50	56.4
50	1.6	65.9	50.87	60.1
	2.4	73.7	48.10	64.3
	3.2	81.4	45.42	67.7
	4.0	89.5	43.37	70.6

Table 3.72: EIS data for the corrosion of GA9 magnesium alloy in 2.0 M sodium chloride solution containing different concentrations of SDMBS.

Temperature (°C)	Conc. of inhibitor (mM)	R_{ct} (ohm. cm^2)	C_{dl} (µF cm^{-2})	η (%)
	Blank	58.5	58.01	
	0.8	168.6	36.42	65.3
30	1.6	188.7	35.88	69.0
	2.4	219.9	34.80	73.4
	3.2	248.9	33.74	76.5
	4.0	295.5	32.65	80.2
	Blank	48.2	65.11	
	0.8	132.1	39.09	63.5
35	1.6	146.5	38.02	67.1
	2.4	163.4	36.69	70.5
	3.2	188.3	35.21	74.4
	4.0	214.2	33.60	77.5
	Blank	36.2	83.99	
	0.8	91.4	45.02	60.4
40	1.6	102.5	43.55	64.7
	2.4	114.9	41.92	68.5
	3.2	129.7	39.84	72.1
	4.0	147.8	38.01	75.5
	Blank	26.4	109.41	
	0.8	63.0	60.42	58.1
45	1.6	69.8	58.10	62.2
	2.4	77.4	55.75	65.9
	3.2	86.0	52.99	69.3
	4.0	93.3	50.38	71.7
	Blank	21.1	123.26	
	0.8	45.8	64.17	53.9
50	1.6	49.3	62.01	57.2
	2.4	53.7	59.76	60.7
	3.2	58.3	57.32	63.8
	4.0	64.3	54.61	67.2

Table 3.73: Activation parameters for the corrosion of GA9 magnesium alloy in NaCl solutions containing different concentrations of inhibitor SDMBS.

Concentration of NaCl	Conc. of inhibitor (mM)	E_a (kJ mol^{-1})	$\Delta H^{\#}$ (kJ mol^{-1})	$\Delta S^{\#}$ (J mol^{-1} K^{-1})
	Blank	37.67	35.07	-125.49
	0.8	52.60	50.00	-87.93
0.1	1.6	56.10	53.49	-77.97
	2.4	61.63	59.03	-61.69
	3.2	67.99	65.39	-43.01
	4.0	74.21	71.61	-24.93
	Blank	35.31	32.71	-127.16
	0.8	48.50	45.89	-94.38
0.5	1.6	50.89	48.29	-87.90
	2.4	55.24	52.64	-75.29
	3.2	61.33	58.73	-57.28
	4.0	70.06	67.46	-30.94
	Blank	37.98	35.38	-114.14
	0.8	51.39	48.79	-79.94
1.0	1.6	54.00	51.40	-72.67
	2.4	59.37	56.77	-56.77
	3.2	64.27	61.67	-42.40
	4.0	71.05	68.45	-22.18
	Blank	40.24	37.64	-103.66
	0.8	53.66	51.06	-69.15
1.5	1.6	56.70	54.09	-60.44
	2.4	61.44	58.84	-46.42
	3.2	66.00	63.40	-33.12
	4.0	70.90	68.30	-18.83
	Blank	42.98	40.39	-92.91
	0.8	54.43	51.83	-64.03
2.0	1.6	55.88	53.28	-60.24
	2.4	57.90	55.30	-54.71
	3.2	60.59	57.99	-47.13
	4.0	63.27	60.67	-39.52

Table 3.74: Maximum inhibition efficiencies attained in different concentrations of sodium chloride solutions at different temperatures for SDMBS.

Temperature (°C)	Sodium chloride concentration (M)	Concentration of SDMBS (mM)	GA9 magnesium alloy η (%)	
			Potentiodynamic polarization method	EIS method
30	0.1		90.1	90.0
	0.5		89.0	88.8
	1.0	4.0	87.5	87.4
	1.5		86.1	85.7
	2.0		80.1	80.2
35	0.1		89.0	89.4
	0.5		86.8	86.4
	1.0	4.0	84.4	84.1
	1.5		83.2	83.5
	2.0		77.6	77.5
40	0.1		87.2	87.1
	0.5		83.9	83.8
	1.0	4.0	80.1	80.2
	1.5		78.7	79.0
	2.0		75.9	75.5
45	0.1		83.3	83.7
	0.5		79.2	78.9
	1.0	4.0	76.1	76.0
	1.5		75.2	74.8
	2.0		71.4	71.7
50	0.1		75.2	75.0
	0.5		74.0	74.2
	1.0	4.0	72.1	72.5
	1.5		70.7	70.6
	2.0		67.1	67.2

Table 3.75: Thermodynamic parameters for the adsorption of SDMBS on GA9 magnesium alloy surface in sodium chloride solutions at different temperatures.

Molarity of NaCl (M)	Temperature (° C)	$-\Delta G^o_{ads}$ (kJ mol^{-1})	ΔH^o_{ads} (kJ mol^{-1})	ΔS^o_{ads} (J mol^{-1} K^{-1})	R^2	Slope
0.1	30	30.49			0.997	1.05
	35	30.96			0.997	1.06
	40	31.33	-5.04	84.11	0.997	1.08
	45	31.62			0.995	1.14
	50	32.26			0.998	1.26
0.5	30	30.02			0.994	1.05
	35	30.66			0.997	1.08
	40	31.19	-1.42	94.85	0.997	1.12
	45	31.76			0.997	1.20
	50	31.84			0.997	1.27
1.0	30	29.83			0.996	1.06
	35	30.51			0.996	1.11
	40	30.97	-5.77	80.02	0.996	1.17
	45	31.29			0.995	1.24
	50	31.44			0.997	1.29
1.5	30	29.80			0.996	1.08
	35	30.51			0.996	1.13
	40	30.86	-8.41	71.23	0.995	1.20
	45	30.99			0.993	1.25
	50	31.34			0.996	1.32
2.0	30	29.95			0.996	1.17
	35	30.36			0.995	1.21
	40	30.59	-8.21	71.84	0.996	1.23
	45	31.21			0.997	1.31
	50	31.32			0.995	1.40

3.10 SODIUM 2,4-DIMETHYLBENZENESULFONATE (SDMBS) AS CORROSION INHIBITOR ON GA9 MAGNESIUM ALLOY IN SODIUM SULPHATE MEDIUM

3.10.1 Potentiodynamic polarization measurements

The potentiodynamic polarization curves for the corrosion of GA9 magnesium alloy in 1.0 M Na_2SO_4 solution in the presence of different concentrations of SDMBS, at 40 °C are shown in Fig. 3.72. Similar plots were obtained at other temperatures and also in the other concentrations of Na_2SO_4 at the different temperatures studied. The potentiodynamic polarization parameters, calculated from Tafel plots in the presence of different concentrations of SDMBS at different temperatures are summarized in Tables 3.76 to 3.80.
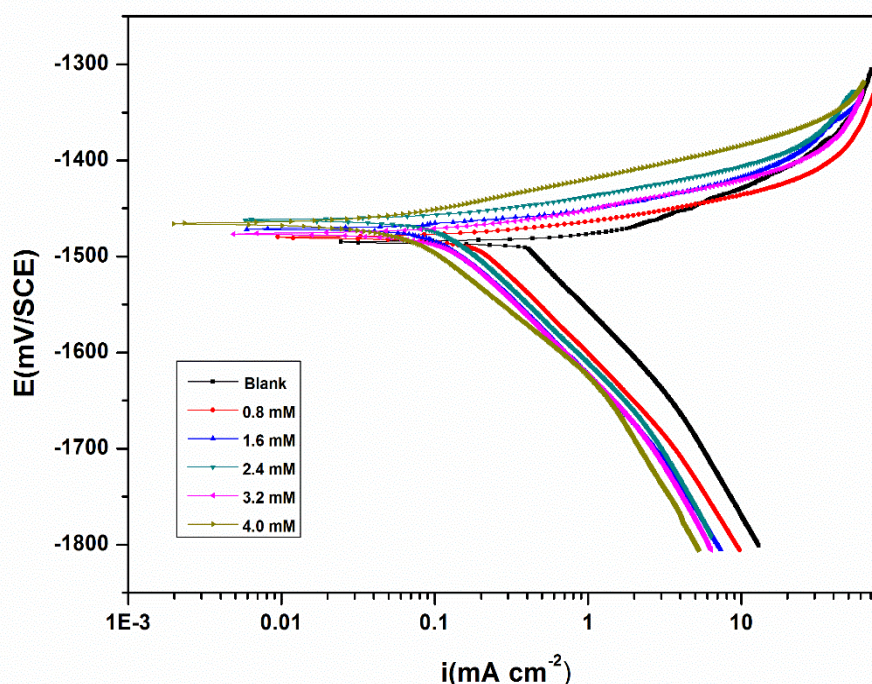
Fig. 3.72: Potentiodynamic polarization curves for the corrosion of GA9 magnesium alloy in 1.0 M Na₂SO₄ solution containing different concentrations of SDMBS at 40 ℃.

The presence of inhibitor brings down the corrosion rate considerably. Polarization curves are shifted to a lower current density region indicating a decrease in corrosion rate (Li et al. 2008). Inhibition efficiency increases with the increase in SDMBS concentration. The presence of inhibitor does not cause any significant shift or a trend for the shift in the E_{corr} value, which implies that the inhibitor, SDMBS, acts as a mixed type inhibitor with a predominant anodic effect. The data in Tables 3.75 to 3.80 show that there is no significant change in the values of cathodic Tafel slope b_c with the increase in the concentration of the inhibitor, indicating the surface-blocking effect of the inhibitor (Ehteshamzadeh et al. 2009 and Ateya et al. 1976).

3.10.2 Electrochemical impedance spectroscopy (EIS) studies

Nyquist plots for the corrosion of GA9 magnesium alloy in 1.0 M sodium sulphate solution in the presence of different concentrations of SDMBS are shown in Fig. 3.73. Similar plots were obtained in other concentrations of sodium sulphate and also at other temperatures. The experimental results of EIS measurements obtained for the corrosion of GA9 magnesium alloy in sodium sulphate solution are summarized in Tables 3.81 to 3.85.

The Nyquist plots are characterized by a capacitive loop, extended from high frequency (HF) to low frequency (LF) range, an inductive loop in the low frequency region (LF) range and a tail at the medium frequency (MF) range in the presence as well as in the absence of inhibitor.

As seen from Fig. 3.73, the capacitive loops of the Nyquist plots are enlarged with increasing SDMBS concentration, while the nature remains the same, suggesting an inhibition achieved without participation in the electrode reactions. The charge transfer resistance (R_{ct}) increases and double layer capacitance decreases with the increase in the concentration of SDMBS, indicating an increase in the inhibition efficiency. SDMBS inhibits corrosion mainly by adsorption and the subsequent formation of a barrier film on the surface of the metal (El Hosary et al. 1972, Sanaa T. 2008). This is consistent with the observations of potentiodynamic polarization measurements.

The equivalent circuit models shown in Fig. 3.3 is used for the interpretation of the Nyquist plots in the presence and absence of SDMBS.
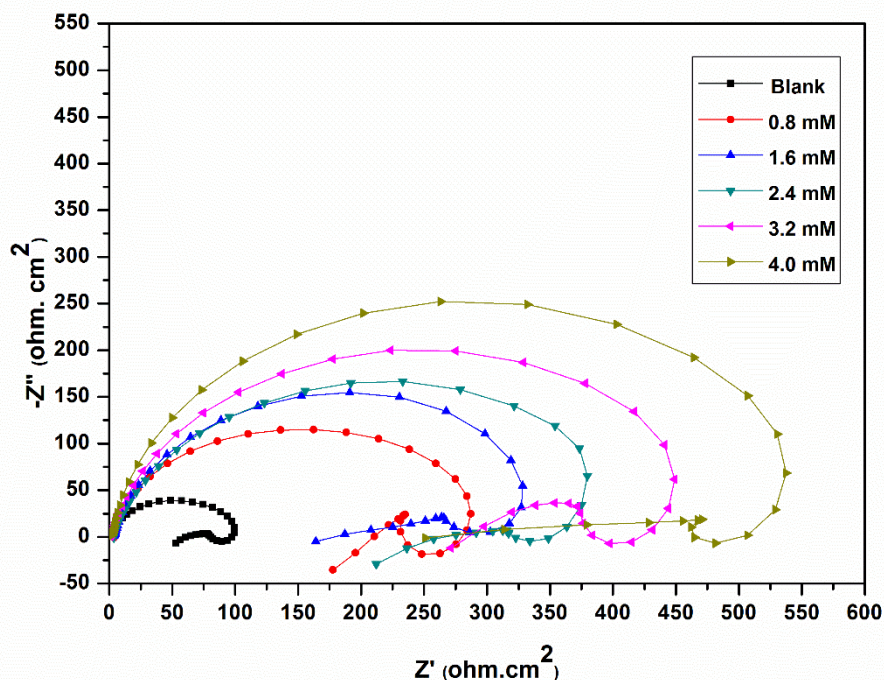
Fig. 3.73: Nyquist plots for the corrosion of GA9 magnesium alloy in 1.0 M Na₂SO₄ solution containing different concentrations of SDMBS at 40 ℃.
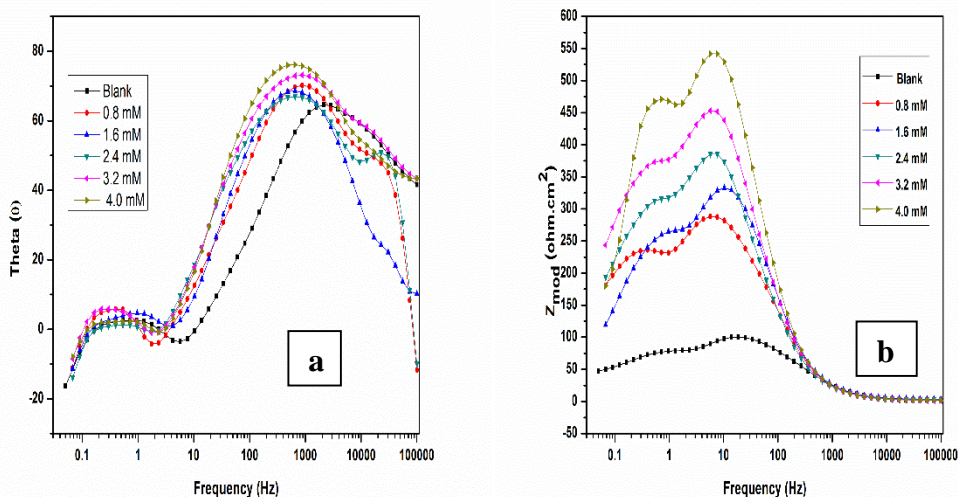
Fig. 3.74: Bode (a) phase angle plots and (b) amplitude plots for the corrosion of GA9 magnesium alloy in 1.0 M Na₂SO₄ solution containing different concentrations of SDMBS at 40 °C.

The Bode plots of phase angle and amplitude for the corrosion of the GA9 magnesium alloy immersed in 1.0 M Na_2SO_4 solution at 40 °C in the presence of varying amounts of SDMBS, are shown in Fig. 3.74 (a) and Fig. 3.74 (b), respectively. As seen from the Bode plots, both the impedance modulus (Z_{mod}) at low frequency and the phase maximum (θ_{max}) at intermediate frequency increase with the increase in SDMBS concentration, which collectively indicates that the presence of highly protective surface film protects the alloy surface.

3.10.3 Effect of temperature

The potentiodynamic polarization and EIS results corresponding to different temperatures in different concentrations of sodium sulphate in the presence of SDMBS, have been listed in the Tables 3.76 to 3.85. The decrease in the efficiency of inhibition with the increase in temperature indicates desorption of the inhibitor molecules from the metal surface when the temperature increases (Poornima et al. 2011). This fact also suggests the physisorption of the inhibitor molecules on the surface of the metal. The Arrhenius plots for the corrosion of GA9 magnesium alloy in the presence of different concentrations of SDMBS in 1.0 M Na_2SO_4 solution are shown in Fig. 3.75. The plots of $\ln(\upsilon_{corr}/T)$ versus $1/T$ in 1.0 M Na_2SO_4 in the presence of different concentrations of SDMBS are shown in Fig. 3.76.
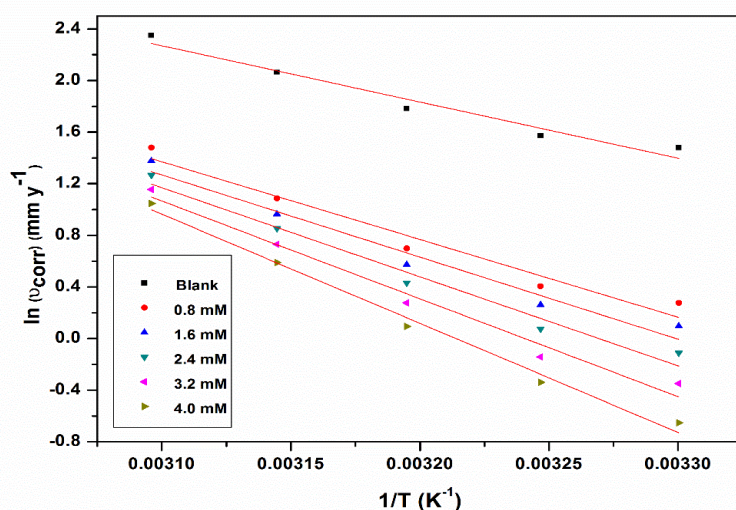
Fig. 3.75: Arrhenius plots for the corrosion of GA9 magnesium alloy in 1.0 M Na_2SO_4 solution containing different concentrations of SDMBS.
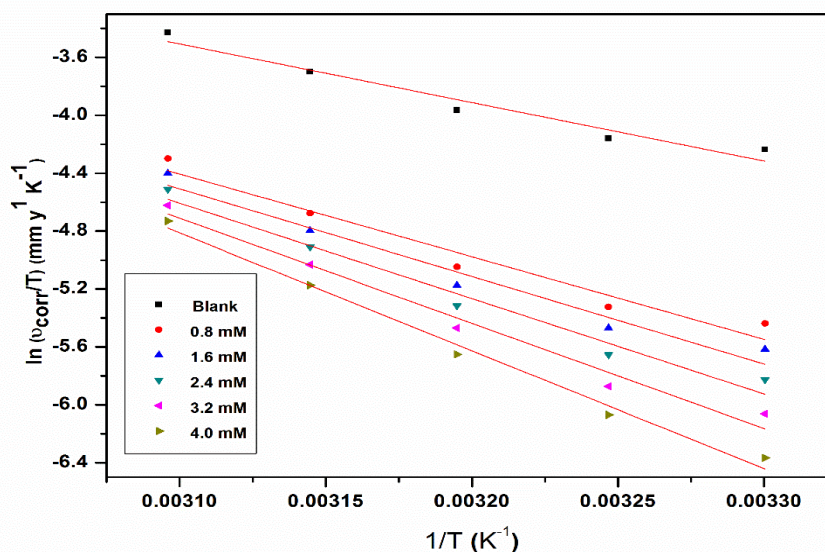
Fig. 3.76: Plots of ln(υ_{corr}/T) versus 1/T for the corrosion of GA9 magnesium alloy in 1.0 M Na₂SO₄ solution containing different concentrations of SDMBS.

The calculated values of E_a, $\Delta H^{\#}$ and $\Delta S^{\#}$ are given in Table 3.86. The increase of the activation energy on the addition of SDMBS can be attributed to the adsorption of SDMBS, providing a barrier on the surface of the alloy (Avci et al. 2008). The values of entropy of activation indicates that the activated complex in the rate determining step represents an association rather than dissociation, resulting in a decrease in randomness on going from the reactants to the activated complex.

3.10.4 Effect of sodium sulphate concentration

Table 3.87 summarizes the maximum inhibition efficiencies exhibited by SDMBS in the Na₂SO₄ solution of different concentrations. It is evident, both from the polarization and from the experimental results of EIS that, for a particular concentration of inhibitor, the efficiency of inhibition decreases with the increase in the concentration of sodium sulphate on GA9 magnesium alloy. The highest inhibition efficiency is observed in sodium sulphate solution of 0.1 M concentration.

3.10.5 Adsorption isotherm

Among the adsorption isotherms considered, Langmuir isotherm was most appropriate to describe the adsorption mediated inhibition by SDMBS. The Langmuir adsorption isotherms for the adsorption of SDMBS on GA9 magnesium alloy surface

at different temperatures in 1.0 M Na_2SO_4 are shown in Fig. 3.77. The plot of ΔG°_{ads} Vs T is shown in Fig. 3.78.
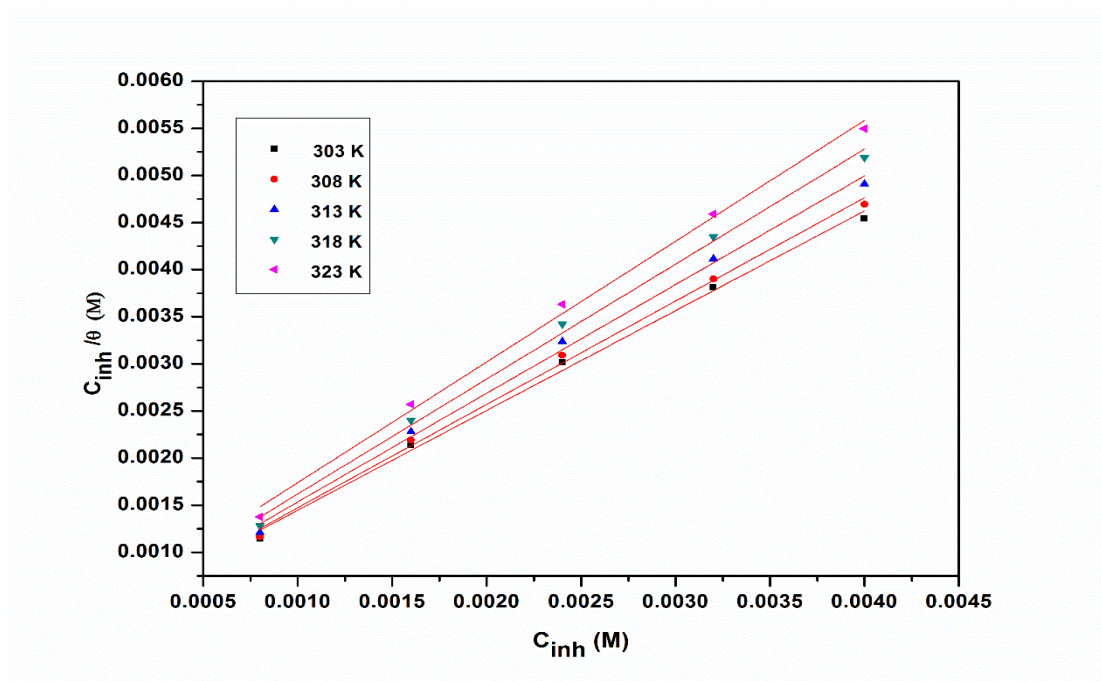
Fig. 3.77: Langmuir adsorption isotherms for the adsorption of SDMBS on GA9 magnesium alloy in 1.0 M Na_2SO_4 solution at different temperatures.

Fig. 3.78: The plot of ΔG°_{ads} Vs T for the adsorption of SDMBS on GA9 magnesium alloy in 1.0 M Na_2SO_4 solution.

212
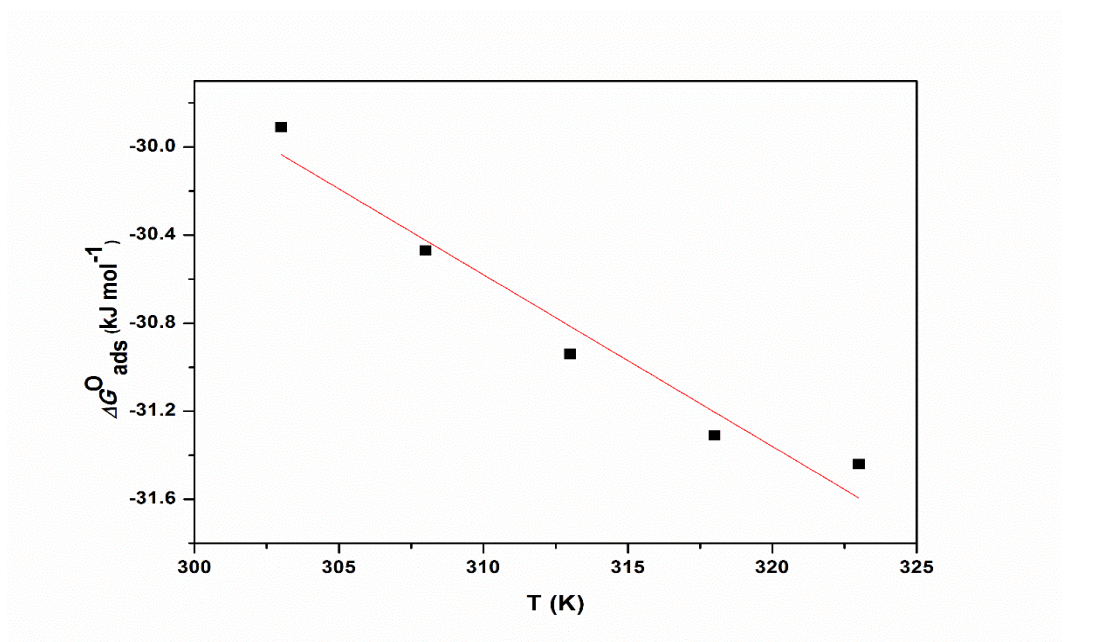
The thermodynamic data obtained for the adsorption of SDMBS on GA9 magnesium alloy are tabulated in Table 3.88. The exothermic $\Delta H°_{ads}$ values of less negative than -41.86 kJ mol^{-1} predict the physisorption of SDMBS on the alloy surfaces (Ashish Kumar et al. 2010). The $\Delta G°_{ads}$ values predict both physisorption and chemisorption of SDMBS. Therefore it can be concluded that the adsorption of SDMBS on GA9 magnesium alloy is predominantly through physisorption. These facts are also supported by the variation of inhibition efficiencies with temperature on the alloy surface.

3.10.6 Mechanism of corrosion inhibition

The corrosion inhibition mechanism of SDMBS in sodium sulphate solution can be explained in the same lines as that of SDMBS in the section 3.9.6. The inhibitor SDMBS protects the alloy surface through predominant physisorption mode in which the SDMBS gets adsorbed on the alloy surface through electrostatic attraction.

3.10.7 SEM/EDX studies

Fig. 3.79 represents the SEM image of GA9 magnesium alloy after the corrosion tests in a medium of 2.0 M sodium sulphate containing 4.0 mM of SDMBS. The image clearly shows a smooth surface due to the adsorbed layer of inhibitor molecules on the alloy surface, thus protecting the metal from corrosion.
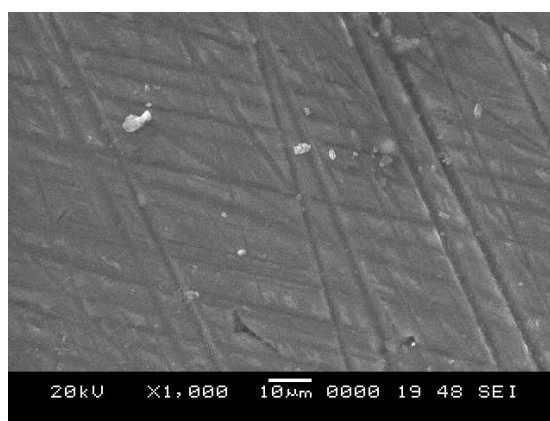
Fig. 3.79: SEM image of GA9 magnesium alloy after immersion in 1.0 M Na$_2$SO$_4$ solution in the presence of SDMBS.

The EDX spectra for the selected areas on the SEM image of 3.61 in the absence and the presence of inhibitor are shown in Fig. 3.80 (a) and Fig. 3.80 (b). The weight

percentage of the elements found in the EDX spectra for corroded metal surface were 86.51% Mg, 9.58% Al, 0.20% Mn, 0.38% Zn and 3.33 % O. The weight percentage of the elements found in the EDX spectra for SDMBS adsorbed metal surface were 82.11% Mg, 9.16% Al, 5.31% O, 0.11% S and 3.33% C and suggested that formation of anticorrosion protective film of SDMBS on the alloy surface.
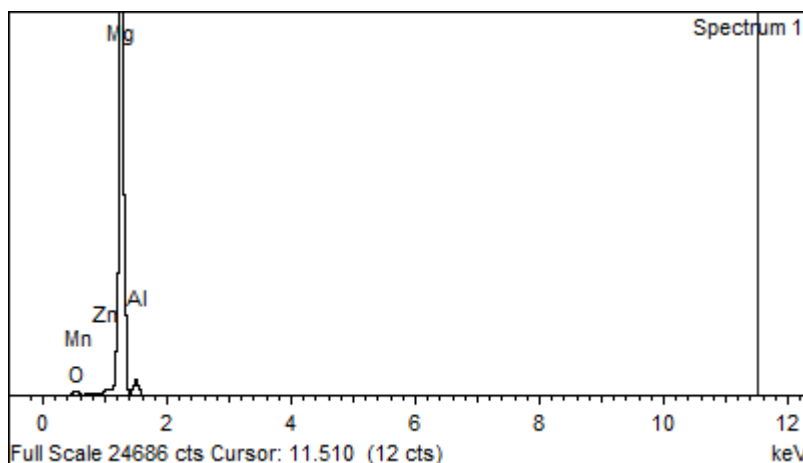
Fig. 3.80 (a): EDX spectra of GA9 magnesium alloy after immersion in 2.0 M Na₂SO₄ solution in the absence of SDMBS.
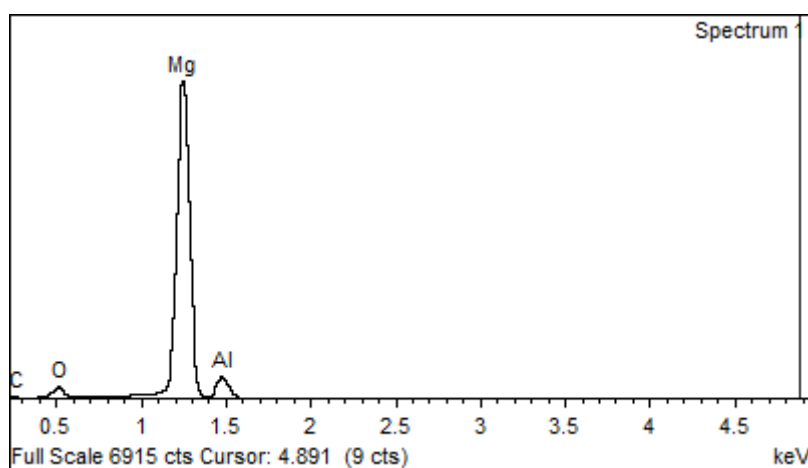
Fig. 3.80 (b): EDX spectra of GA9 magnesium alloy after immersion in 2.0 M Na₂SO₄ solution in the presence of SDMBS.

Table 3.76: Results of potentiodynamic polarization studies for the corrosion of GA9 magnesium alloy in 0.1 M sodium sulphate solution containing different concentrations of SDMBS.

| Temperature (℃)	Conc. of inhibitor (mM)	$-E_{corr}$ (mV /SCE)	$-b_c$ (mV dec^{-1})	i_{corr} (µA cm^{-2})	υ_{corr} (mm y^{-1})	η (%)
30	Blank	1456	139	42.1	0.946	
	0.8	1445	117	10.6	0.238	74.8
	1.6	1449	115	8.6	0.193	79.5
	2.4	1445	113	6.9	0.155	83.7
	3.2	1442	111	5.3	0.119	87.4
	4.0	1444	109	4.0	0.090	90.5
35	Blank	1461	144	47.7	1.071	
	0.8	1454	123	12.4	0.279	73.9
	1.6	1458	121	10.4	0.234	78.3
	2.4	1448	117	8.3	0.186	82.5
	3.2	1449	113	6.6	0.148	86.2
	4.0	1442	111	5.0	0.112	89.6
40	Blank	1463	151	58.4	1.311	
	0.8	1458	131	15.9	0.357	72.7
	1.6	1451	128	13.8	0.310	76.3
	2.4	1455	125	11.2	0.252	80.8
	3.2	1448	123	9.2	0.207	84.3
	4.0	1444	120	7.4	0.166	87.4
45	Blank	1468	159	74.4	1.671	
	0.8	1455	138	22.5	0.506	69.7
	1.6	1459	135	19.9	0.477	73.3
	2.4	1452	133	17.3	0.389	76.7
	3.2	1457	131	14.8	0.333	80.1
	4.0	1449	129	11.9	0.267	84.0
50	Blank	1469	167	97.8	2.197	
	0.8	1461	148	34.0	0.764	65.2
	1.6	1465	146	30.4	0.683	68.9
	2.4	1457	142	26.9	0.604	72.5
	3.2	1451	139	23.8	0.535	75.7
	4.0	1455	135	21.0	0.472	78.5

Table 3.77: Results of potentiodynamic polarization studies for the corrosion of GA9 magnesium alloy in 0.5 M sodium sulphate solution containing different concentrations of SDMBS.

Temperature (°C)	Conc. of inhibitor (mM)	$-E_{corr}$ (mV /SCE)	$-b_c$ (mV dec^{-1})	i_{corr} (µA cm^{-2})	υ_{corr} (mm y^{-1})	η (%)
30	Blank	1461	144	112.4	2.526	
	0.8	1453	123	30.7	0.690	72.7
	1.6	1455	122	26.4	0.593	76.5
	2.4	1449	120	21.7	0.488	80.7
	3.2	1442	118	16.5	0.371	85.3
	4.0	1447	116	11.7	0.263	89.6
35	Blank	1462	149	125.5	2.819	
	0.8	1451	130	36.3	0.816	71.1
	1.6	1455	128	29.9	0.672	76.2
	2.4	1452	125	25.1	0.564	80.0
	3.2	1458	123	20.2	0.454	83.9
	4.0	1444	119	15.7	0.353	87.5
40	Blank	1459	156	161.1	3.619	
	0.8	1460	139	49.6	1.114	69.2
	1.6	1453	136	39.5	0.888	74.4
	2.4	1457	133	36.2	0.813	77.5
	3.2	1445	131	30.8	0.692	80.9
	4.0	1449	128	24.5	0.550	84.8
45	Blank	1475	164	203.3	4.568	
	0.8	1466	147	67.3	1.512	66.9
	1.6	1469	144	60.0	1.348	70.5
	2.4	1461	140	52.9	1.189	74.0
	3.2	1451	138	46.6	1.047	77.1
	4.0	1457	136	40.3	0.905	80.2
50	Blank	1487	173	264.3	5.939	
	0.8	1481	158	98.3	2.209	61.3
	1.6	1484	155	89.9	2.020	65.1
	2.4	1471	153	78.8	1.771	68.8
	3.2	1479	151	70.3	1.580	72.0
	4.0	1465	148	62.4	1.402	75.1

Table 3.78: Results of potentiodynamic polarization studies for the corrosion of GA9 magnesium alloy in 1.0 M sodium sulphate solution containing different concentrations of SDMBS.

Temperature (℃)	Conc. of inhibitor (mM)	$-E_{corr}$ (mV /SCE)	$-b_c$ (mV dec^{-1})	i_{corr} (μA cm^{-2})	υ_{corr} (mm y^{-1})	η (%)
30	Blank	1472	151	195.2	4.386	
	0.8	1465	137	58.6	1.317	70.0
	1.6	1464	135	49.0	1.101	74.9
	2.4	1466	132	39.8	0.894	79.6
	3.2	1457	128	31.4	0.706	83.9
	4.0	1459	125	23.2	0.521	88.1
35	Blank	1477	156	214.2	4.813	
	0.8	1465	144	66.8	1.501	68.8
	1.6	1469	141	57.8	1.299	73.0
	2.4	1472	138	48.0	1.078	77.6
	3.2	1461	134	38.6	0.867	82.0
	4.0	1457	130	31.7	0.712	85.2
40	Blank	1486	160	264.3	5.938	
	0.8	1481	148	89.6	2.013	66.1
	1.6	1472	146	78.8	1.771	70.2
	2.4	1463	143	68.5	1.539	74.1
	3.2	1477	141	56.7	1.319	77.8
	4.0	1466	138	48.9	1.099	81.5
45	Blank	1487	171	350.4	7.872	
	0.8	1474	157	131.8	2.961	62.4
	1.6	1479	154	116.7	2.622	66.7
	2.4	1475	151	104.4	2.346	70.2
	3.2	1480	149	92.5	2.078	73.6
	4.0	1466	145	80.2	1.802	77.1
50	Blank	1490	181	466.3	10.477	
	0.8	1487	168	195.4	4.390	58.1
	1.6	1484	166	176.3	3.961	62.2
	2.4	1488	163	158.1	3.552	66.1
	3.2	1473	161	141.3	3.175	69.7
	4.0	1479	159	126.8	2.849	72.8

Table 3.79: Results of potentiodynamic polarization studies for the corrosion of GA9 magnesium alloy in 1.5 M sodium sulphate solution containing different concentrations of SDMBS.

Temperature (℃)	Conc. of inhibitor (mM)	$-E_{corr}$ (mV /SCE)	$-b_c$ (mV dec^{-1})	i_{corr} (μA cm^{-2})	υ_{corr} (mm y^{-1})	η (%)
30	Blank	1477	158	281.7	6.328	
	0.8	1459	144	88.2	1.982	68.7
	1.6	1466	141	73.5	1.651	73.9
	2.4	1462	139	61.7	1.386	78.1
	3.2	1469	135	49.3	1.108	82.5
	4.0	1455	131	38.9	0.874	86.2
35	Blank	1483	165	339.2	7.621	
	0.8	1473	148	110.6	2.485	67.4
	1.6	1481	146	96.7	2.173	71.5
	2.4	1467	145	82.1	1.845	75.8
	3.2	1472	143	68.9	1.548	79.7
	4.0	1459	141	56.6	1.272	83.3
40	Blank	1482	173	426.8	9.589	
	0.8	1476	159	149.0	3.348	65.1
	1.6	1474	157	132.7	2.982	68.9
	2.4	1480	155	118.2	2.656	72.3
	3.2	1465	153	100.7	2.263	76.4
	4.0	1472	148	89.2	2.004	79.1
45	Blank	1486	182	527.1	11.843	
	0.8	1469	170	202.9	4.559	61.5
	1.6	1475	168	186.6	4.193	64.6
	2.4	1473	166	166.6	3.743	68.4
	3.2	1478	163	148.6	3.339	71.8
	4.0	1465	160	130.2	2.925	75.3
50	Blank	1492	194	707.4	15.894	
	0.8	1485	185	304.2	6.835	57.0
	1.6	1471	182	277.3	6.231	60.8
	2.4	1477	179	249.7	5.610	64.7
	3.2	1483	175	225.0	5.055	68.2
	4.0	1468	172	201.6	4.530	71.5

Table 3.80: Results of potentiodynamic polarization studies for the corrosion of GA9 magnesium alloy in 2.0 M sodium sulphate solution containing different concentrations of SDMBS.

Temperature (℃)	Conc. of inhibitor (mM)	$-E_{corr}$ (mV /SCE)	$-b_c$ (mV dec^{-1})	i_{corr} (μA cm^{-2})	υ_{corr} (mm y^{-1})	η (%)
30	Blank	1488	169	374.6	8.417	
	0.8	1473	160	129.2	2.903	65.5
	1.6	1461	158	115.0	2.584	69.3
	2.4	1467	156	98.9	2.222	73.6
	3.2	1474	153	85.8	1.928	77.1
	4.0	1459	149	71.5	1.606	80.9
35	Blank	1483	176	455.4	10.232	
	0.8	1476	165	165.3	3.714	63.7
	1.6	1473	163	148.5	3.337	67.4
	2.4	1479	160	132.5	2.977	70.9
	3.2	1455	158	112.9	2.537	75.2
	4.0	1460	155	99.7	2.240	78.1
40	Blank	1481	185	597.1	13.415	
	0.8	1479	175	231.7	5.206	61.2
	1.6	1465	173	207.2	4.655	65.3
	2.4	1473	171	185.1	4.159	69.0
	3.2	1478	167	161.8	3.635	72.9
	4.0	1464	163	140.9	3.166	76.4
45	Blank	1489	197	755.8	16.981	
	0.8	1482	187	313.7	7.048	58.5
	1.6	1479	185	284.9	6.401	62.3
	2.4	1484	181	257.7	5.790	65.9
	3.2	1471	176	230.5	5.179	69.5
	4.0	1467	171	209.4	4.705	72.3
50	Blank	1499	209	927.7	20.842	
	0.8	1487	198	424.9	9.547	54.2
	1.6	1474	194	389.6	8.754	58.0
	2.4	1481	190	355.3	7.983	61.7
	3.2	1485	187	321.9	7.233	65.3
	4.0	1471	184	291.3	6.545	68.6

Table 3.81: EIS data for the corrosion of GA9 magnesium alloy in 0.1 M sodium sulphate solution containing different concentrations of SDMBS.

Temperature (℃)	Conc. of inhibitor (mM)	R_{ct} (ohm. cm^2)	C_{dl} (µF cm^{-2})	η (%)
	Blank	604.7	10.53	
	0.8	2419.0	7.19	75.0
30	1.6	2921.0	6.93	79.3
	2.4	3578.0	6.73	83.1
	3.2	4761.0	6.58	87.3
	4.0	6433.0	6.37	90.6
	Blank	545.5	10.98	
	0.8	2106.0	8.11	74.1
35	1.6	2537.0	7.77	78.5
	2.4	3013.0	7.65	81.9
	3.2	3896.0	7.49	86.0
	4.0	5146.0	7.24	89.4
	Blank	447.8	11.35	
	0.8	1665.0	8.57	73.1
40	1.6	1947.0	8.35	77.0
	2.4	2421.0	8.17	81.5
	3.2	3005.0	8.09	85.1
	4.0	3641.0	7.79	87.7
	Blank	356.5	16.50	
	0.8	1181.0	10.30	69.8
45	1.6	1330.0	10.04	73.2
	2.4	1511.0	9.83	76.4
	3.2	1801.0	9.61	80.2
	4.0	2242.0	9.44	84.1
	Blank	273.0	25.71	
	0.8	786.7	15.72	65.3
50	1.6	886.4	15.07	69.2
	2.4	1004.0	14.81	72.8
	3.2	1152.0	14.48	76.3
	4.0	1300.0	14.19	79.0

Table 3.82: EIS data for the corrosion of GA9 magnesium alloy in 0.5 M sodium sulphate solution containing different concentrations of SDMBS.

Temperature (℃)	Conc. of inhibitor (mM)	R_{ct} (ohm. cm^2)	C_{dl} (μF cm^{-2})	η (%)
30	Blank	219.1	18.29	
	0.8	796.7	9.37	72.5
	1.6	928.4	9.18	76.4
	2.4	1124.0	8.91	80.5
	3.2	1501.0	8.70	85.4
	4.0	2148.0	8.57	89.8
35	Blank	200.4	22.81	
	0.8	698.3	10.79	71.3
	1.6	852.8	10.47	76.5
	2.4	1022.0	10.09	80.4
	3.2	1260.0	9.70	84.1
	4.0	1616.0	9.35	87.6
40	Blank	165.0	26.11	
	0.8	541.0	13.03	69.5
	1.6	642.0	12.77	74.3
	2.4	750.0	12.49	78.0
	3.2	877.7	12.10	81.2
	4.0	1107.0	11.61	85.1
45	Blank	128.8	30.77	
	0.8	390.3	14.72	67.0
	1.6	439.6	14.21	70.7
	2.4	501.2	13.95	74.3
	3.2	572.4	13.34	77.5
	4.0	657.1	12.77	80.4
50	Blank	97.8	34.19	
	0.8	254.0	17.82	61.5
	1.6	282.7	17.10	65.4
	2.4	311.5	16.58	68.6
	3.2	350.5	16.35	72.1
	4.0	394.4	16.04	75.2

Table 3.83: EIS data for the corrosion of GA9 magnesium alloy in 1.0 M sodium sulphate solution containing different concentrations of SDMBS.

Temperature (℃)	Conc. of inhibitor (mM)	R_{ct} (ohm. cm^2)	C_{dl} (µF cm^{-2})	η (%)
	Blank	139.0	30.91	
	0.8	469.6	10.92	70.4
30	1.6	560.5	10.55	75.2
	2.4	688.1	10.11	79.8
	3.2	874.2	9.80	84.1
	4.0	1149.0	9.46	87.9
	Blank	122.6	32.17	
	0.8	395.5	12.51	69.0
35	1.6	457.5	12.08	73.2
	2.4	552.3	11.79	77.8
	3.2	692.7	11.27	82.3
	4.0	834.0	10.90	85.3
	Blank	97.4	40.62	
	0.8	289.0	19.41	66.3
40	1.6	329.1	19.02	70.4
	2.4	380.5	18.43	74.4
	3.2	444.7	17.69	78.1
	4.0	538.1	16.43	81.9
	Blank	72.1	45.05	
	0.8	193.3	22.91	62.7
45	1.6	217.8	22.45	66.9
	2.4	243.6	21.60	70.4
	3.2	276.2	20.49	73.9
	4.0	320.4	19.61	77.5
	Blank	55.5	56.30	
	0.8	134.4	26.33	58.7
50	1.6	148.4	25.40	62.6
	2.4	165.2	24.70	66.4
	3.2	185.6	23.41	70.1
	4.0	207.1	22.35	73.2

Table 3.84: EIS data for the corrosion of GA9 magnesium alloy in 1.5 M sodium sulphate solution containing different concentrations of SDMBS.

Temperature (℃)	Conc. of inhibitor (mM)	R_{ct} (ohm. cm^2)	C_{dl} (μF cm^{-2})	η (%)
	Blank	91.6	34.56	
	0.8	290.8	12.75	68.5
30	1.6	348.3	12.39	73.7
	2.4	416.4	12.04	78.0
	3.2	520.5	11.74	82.4
	4.0	659.0	11.33	86.1
	Blank	77.7	40.12	
	0.8	240.6	18.71	67.7
35	1.6	274.6	18.30	71.7
	2.4	322.4	17.92	75.9
	3.2	379.0	17.18	79.5
	4.0	462.5	16.39	83.2
	Blank	62.4	54.17	
	0.8	179.3	28.65	65.2
40	1.6	201.9	27.70	69.1
	2.4	226.9	26.87	72.5
	3.2	267.8	25.45	76.7
	4.0	302.9	24.02	79.4
	Blank	48.7	71.38	
	0.8	126.8	34.59	61.6
45	1.6	138.4	33.29	64.8
	2.4	166.2	32.31	70.7
	3.2	171.5	31.05	71.6
	4.0	198.8	29.74	75.5
	Blank	37.5	88.74	
	0.8	91.2	41.28	58.9
50	1.6	100.1	40.50	62.5
	2.4	107.8	38.99	65.2
	3.2	119.8	36.92	68.7
	4.0	133.9	34.51	72.0

Table 3.85: EIS data for the corrosion of GA9 magnesium alloy in 2.0 M sodium sulphate solution containing different concentrations of SDMBS.

Temperature (°C)	Conc. of inhibitor (mM)	R_{ct} (ohm. cm^2)	C_{dl} (µF cm^{-2})	η (%)
	Blank	67.5	42.55	
	0.8	197.4	19.03	65.8
30	1.6	220.6	18.62	69.4
	2.4	251.9	18.18	73.2
	3.2	293.5	17.29	77.0
	4.0	349.7	16.03	80.7
	Blank	57.4	50.87	
	0.8	157.7	24.88	63.6
35	1.6	176.6	23.71	67.5
	2.4	196.6	22.25	70.8
	3.2	228.7	21.09	74.9
	4.0	257.4	20.01	77.7
	Blank	43.2	69.58	
	0.8	110.8	33.01	61.0
40	1.6	125.2	31.29	65.5
	2.4	140.3	29.04	69.2
	3.2	161.8	27.12	73.3
	4.0	183.8	24.93	76.5
	Blank	34.0	85.41	
	0.8	81.7	43.44	58.4
45	1.6	90.2	40.51	62.3
	2.4	100.3	38.79	66.1
	3.2	112.2	36.21	69.7
	4.0	122.3	33.70	72.2
	Blank	27.8	102.33	
	0.8	60.6	50.02	54.1
50	1.6	66.0	47.53	57.9
	2.4	72.8	45.19	61.8
	3.2	80.6	42.30	65.5
	4.0	89.4	39.44	68.9

Table 3.86: Activation parameters for the corrosion of GA9 magnesium alloy in sodium sulphate solutions containing different concentrations of SDMBS.

Concentration of Na$_2$SO$_4$	Conc. of inhibitor (mM)	E_a (kJ mol^{-1})	$\Delta H^{\#}$ (kJ mol^{-1})	$\Delta S^{\#}$ (J mol^{-1} K^{-1})
	Blank	34.57	31.97	-140.53
	0.8	47.48	44.88	-109.69
0.1	1.6	52.59	49.99	-94.53
	2.4	56.10	53.50	-84.94
	3.2	61.94	59.34	-67.88
	4.0	67.86	65.26	-50.53
	Blank	35.60	32.99	-128.98
	0.8	47.79	45.19	-99.66
0.5	1.6	51.03	48.43	-90.61
	2.4	53.94	51.34	-82.48
	3.2	60.64	58.04	-62.56
	4.0	69.69	67.08	-35.46
	Blank	36.22	33.62	-122.51
	0.8	50.07	47.47	-87.05
1.0	1.6	52.94	50.34	-79.00
	2.4	57.41	54.81	-65.97
	3.2	63.02	60.42	-49.43
	4.0	70.30	67.70	-27.71
	Blank	37.09	34.49	-116.19
	0.8	50.06	47.46	-83.20
1.5	1.6	53.84	51.24	-72.18
	2.4	56.97	54.37	-63.31
	3.2	61.85	59.25	-48.99
	4.0	67.08	64.46	-33.61
	Blank	37.75	35.15	-111.50
	0.8	49.14	46.54	-82.88
2.0	1.6	50.28	47.68	-80.11
	2.4	52.43	49.83	-74.19
	3.2	54.61	52.01	-68.30
	4.0	57.78	55.18	-59.22

Table 3.87: Maximum inhibition efficiencies attained in different concentrations of sodium sulphate solutions at different temperatures for SDMBS.

Temperature (ºC)	GA9 magnesium alloy			
	Sodium sulphate concentration (M)	Concentration of SDMBS (mM)	η (%)	
			Potentiodynamic polarization method	EIS method
30	0.1	4.0	90.5	90.6
	0.5		89.6	89.8
	1.0		88.1	87.9
	1.5		86.2	86.1
	2.0		80.9	80.7
35	0.1	4.0	89.6	89.4
	0.5		87.5	87.6
	1.0		85.2	85.3
	1.5		83.3	83.2
	2.0		78.1	77.7
40	0.1	4.0	87.4	87.7
	0.5		84.8	85.1
	1.0		81.5	81.9
	1.5		79.1	79.4
	2.0		76.4	76.5
45	0.1	4.0	84.0	84.1
	0.5		80.2	80.4
	1.0		77.1	77.5
	1.5		75.3	75.5
	2.0		72.3	72.2
50	0.1	4.0	78.5	79.0
	0.5		75.1	75.2
	1.0		72.8	73.2
	1.5		71.5	72.0
	2.0		68.6	68.9

Table 3.88: Thermodynamic parameters for the adsorption of SDMBS on GA9 magnesium alloy surface in sodium sulphate solutions at different temperatures.

Molarity of Na$_2$SO$_4$ (M)	Temperature (° C)	$-\Delta G^o_{ads}$ (kJ mol^{-1})	ΔH^o_{ads} (kJ mol^{-1})	ΔS^o_{ads} (J mol^{-1} K^{-1})	R^2	Slope
	30	30.54			0.997	1.04
	35	30.95			0.997	1.05
0.1	40	31.45	-5.28	83.41	0.997	1.08
	45	31.80			0.996	1.13
	50	32.20			0.997	1.21
	30	30.09			0.994	1.05
	35	30.74			0.996	1.08
0.5	40	31.26	-2.66	91.07	0.996	1.12
	45	31.81			0.996	1.18
	50	31.83			0.996	1.25
	30	29.91			0.995	1.06
	35	30.47			0.996	1.10
1.0	40	30.94	-6.40	78.01	0.996	1.15
	45	31.31			0.996	1.22
	50	31.44			0.996	1.28
	30	29.93			0.996	1.08
	35	30.46			0.995	1.13
1.5	40	31.04	-8.27	72.08	0.996	1.19
	45	31.24			0.995	1.25
	50	31.34			0.995	1.31
	30	29.89			0.995	1.16
	35	30.36			0.996	1.20
2.0	40	30.60	-10.77	63.41	0.995	1.22
	45	31.09			0.996	1.30
	50	31.11			0.994	1.36

3.11 SODIUM BENZENESULFONATE (SBS) AS CORROSION INHIBITOR ON GA9 MAGNESIUM ALLOY IN SODIUM CHLORIDE MEDIUM

3.11.1 Potentiodynamic polarization measurements

Potentiodynamic polarization curves for the corrosion of GA9 magnesium alloy in 1.0 M NaCl solution in the presence of different concentrations of SBS, at 40 °C are shown in Fig. 3.81. Similar plots were obtained at other temperatures and also in the other concentrations of NaCl at the different temperatures studied. The potentiodynamic polarization parameters are summarized in Tables 3.89 to 3.93. The polarization curves in Fig. 3.81, appear to have shifted to the lower current density region and the shape of the plots is not altered by adding SBS to the blank solution.
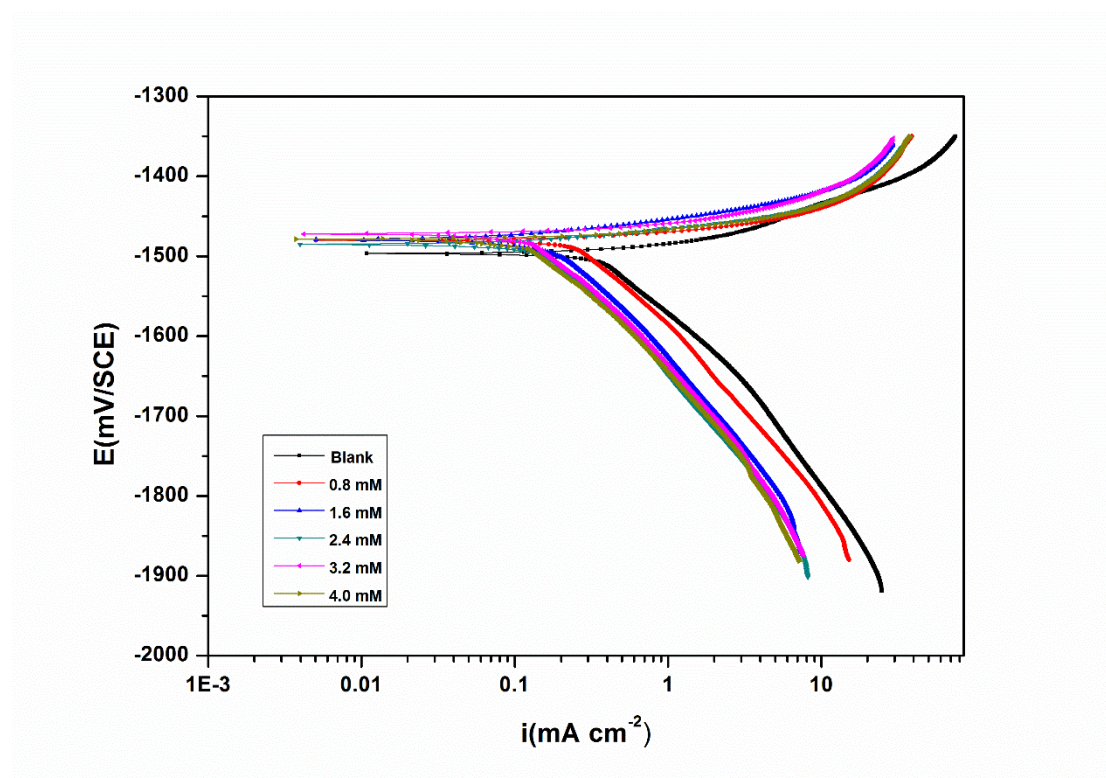
Fig. 3.81: Potentiodynamic polarization curves for the corrosion of GA9 magnesium alloy in 1.0 M NaCl solution containing different concentrations of SBS at 40 ℃.

3.11.2 Electrochemical impedance spectroscopy (EIS) studies

Fig. 3.82 represents the Nyquist plots for the corrosion of GA9 magnesium alloy in 1.0 M NaCl solution in the presence of different concentrations of SBS. Similar plots

were obtained in other concentrations of the sodium chloride and also at other temperatures. The impedance parameters are presented in Tables 3.94 to 3.98.
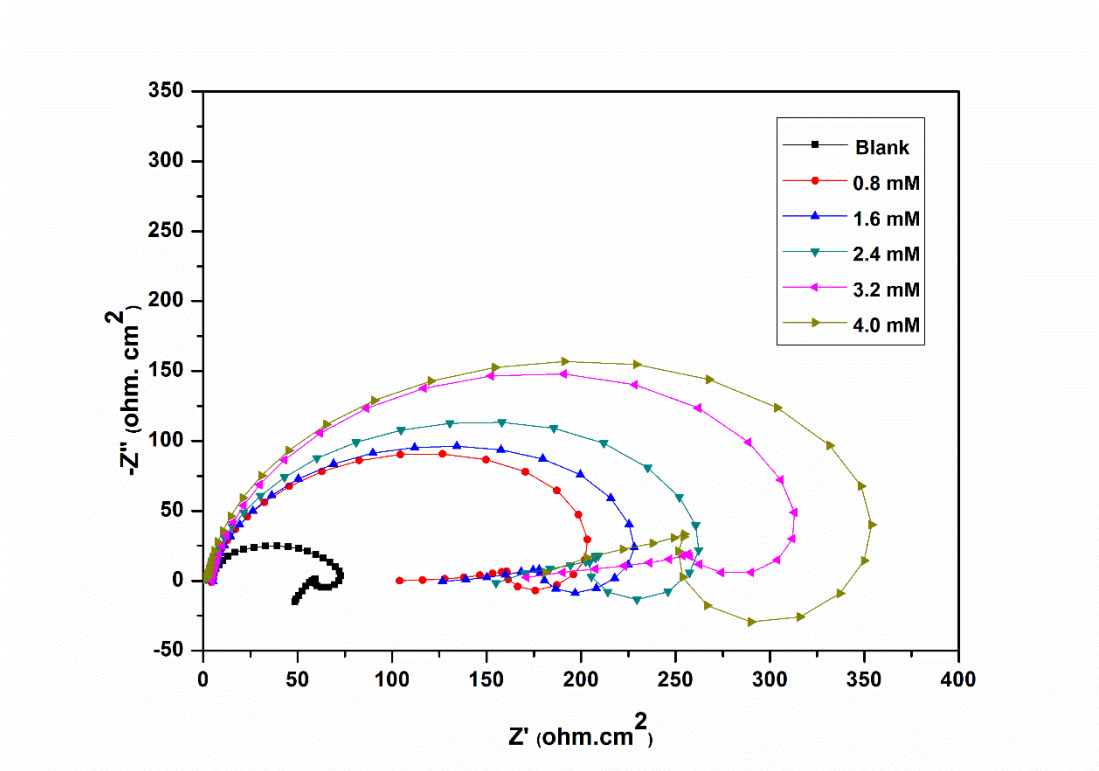
Fig. 3.82: Nyquist plots for the corrosion of GA9 magnesium alloy specimen in 1.0 M NaCl solution containing different concentrations of SBS at 40 ℃.

The Nyquist plots are characterized by a capacitive loop, extended from high frequency (HF) to low frequency (LF) range, an inductive loop in the low frequency region (LF) range and a tail at the medium frequency (MF) range. The addition of SBS in increased concentrations boosts up the resistance towards corrosion as reflected by the enlargement of the capacitive loop. As can be seen from the Tables, R_{ct} value increases and C_{dl} value decreases with the increase in the concentration of SBS which suggest the decrease in the corrosion rate. The equivalent circuit given in Fig. 3.3 is used to fit the experimental data for the corrosion of GA9 magnesium alloy in sodium chloride in the presence of SBS. The values of inhibition efficiency and the pattern of their variation with SBS and medium concentrations are in good agreement with that obtained from the results of polarization studies.

The Bode plots of phase angle and amplitude for the corrosion of the GA9 magnesium alloy immersed in 1.0 M NaCl at 40 °C in the presence of varying amounts

of SBS, are shown in Fig. 3.83 (a) and Fig. 3.83 (b), respectively. As seen from the Bode plots, both the impedance modulus (Z_{mod}) at low frequency and the phase maximum (θ_{max}) at intermediate frequency increase with the increase in SDMBS concentration, which implies the presence of highly protective surface film, able enough to oppose corrosive penetration.
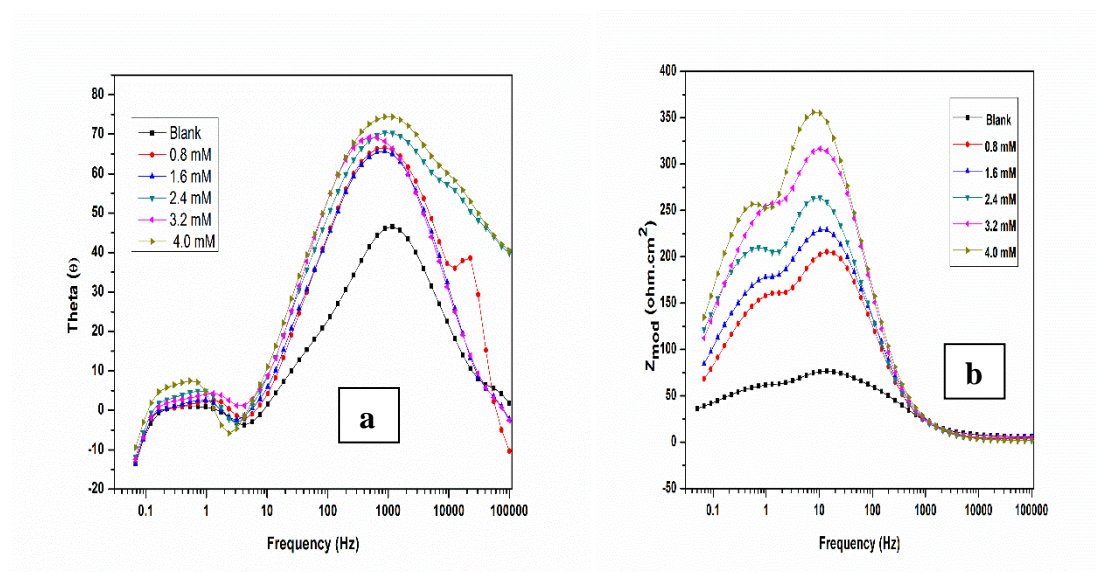
Fig. 3.83: Bode (a) phase angle plots and (b) amplitude plots for the corrosion of GA9 magnesium alloy in 1.0 M NaCl solution containing different concentrations of SBS at 40 ℃.

3.11.3 Effect of temperature

The results of electrochemical studies shown in Tables 3.89 to 3.98 indicate the adversity of higher temperature in the efficiency of SBS inhibition, since in the medium at higher temperatures a lower efficiency is observed together with a higher double layer capacitance and lower charge transfer resistance values, which means the existence of a thin film that offers inferior protection to the underlying alloy. The decrease in the inhibition efficiency of SBS with the increase in temperature on GA9 magnesium alloy may be attributed to the physisorption of SBS. The Arrhenius plots for the corrosion of GA9 magnesium alloy in 1.0 M sodium chloride solution in the presence of different concentrations of SBS are shown in Fig. 3.84. The plots of $\ln(\upsilon_{corr}/T)$ versus $(1/T)$ are shown in Fig. 3.85. The calculated values of activation parameters are given in Table 3.99.
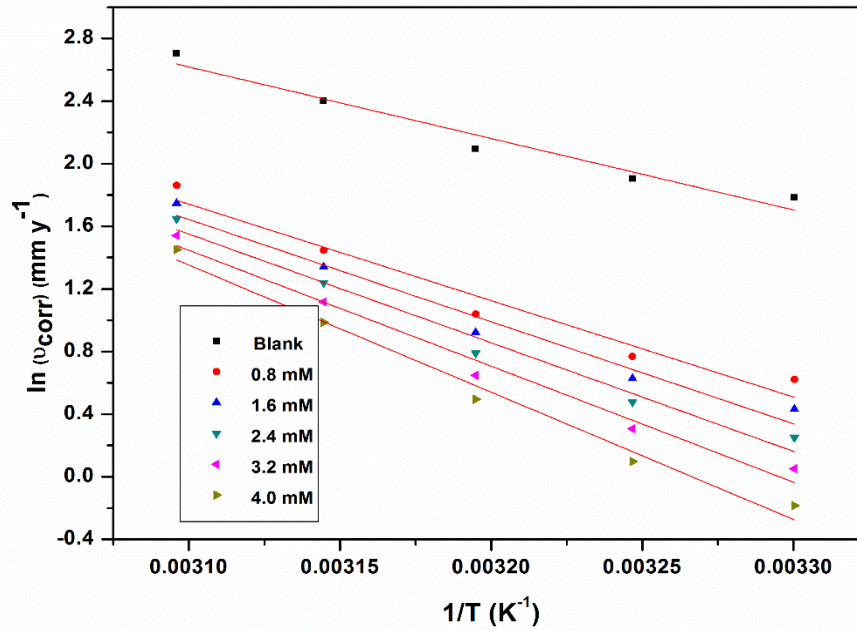
3.84: Arrhenius plots for the corrosion of GA9 magnesium alloy in 1.0 M NaCl solution containing different concentrations of SBS.
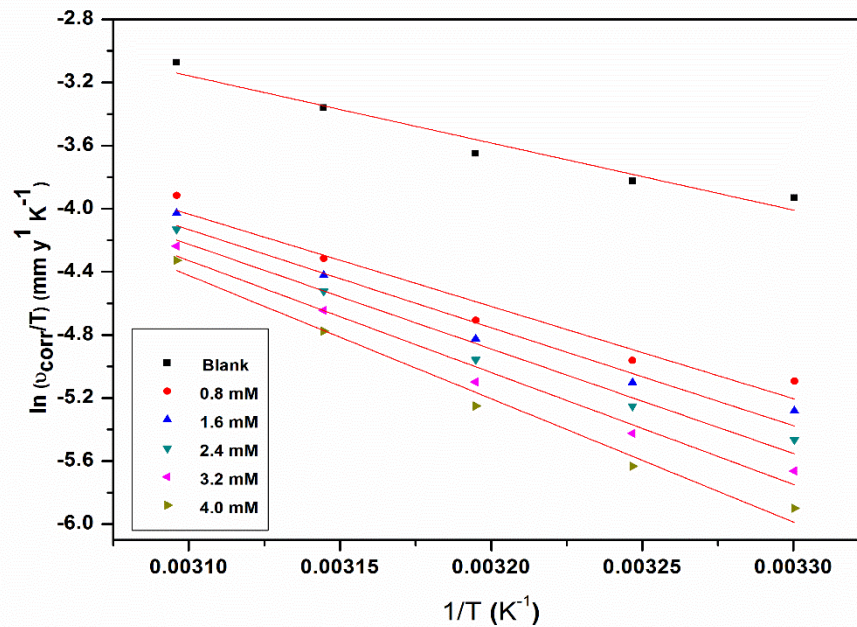
Fig. 3.85: Plots of ln(υ_{corr}/T) versus 1/T for the corrosion of GA9 magnesium alloy in 1.0 M NaCl solution containing different concentrations of SBS.

The increase in E_a values with the increase in SBS concentration indicates the corrosion of GA9 magnesium alloy less favoured. The $\Delta H^{\#}$ values vary in away similar to that of E_a. The entropy of activation in the absence and presence of SBS is large and negative for the corrosion of the alloy. This implies that the activated complex in the rate determining step represents a step of association rather than dissociation, indicating that a decrease in disordering takes place on going from reactants to activated complex. The entropies of activation are higher for the corrosion of GA9 magnesium alloy in inhibited solutions than that in the uninhibited solutions.

3.11.4 Effect of sodium chloride concentration

Table 3.100 summarises the maximum inhibition efficiencies exhibited by SBS in sodium chloride solutions of different concentrations. It is evident from both polarization and EIS experimental results that, for a particular concentration of inhibitor, the inhibition efficiency decreases with the increase in sodium chloride concentration. The highest inhibition efficiency is observed in sodium chloride of 0.1 M concentration.

3.11.5 Adsorption isotherm

The adsorption of SBS on the surfaces of GA9 magnesium alloy was found to obey Langmuir adsorption isotherm. The Langmuir adsorption isotherms for the adsorption of SBS on GA9 magnesium alloy in 1.0 M sodium chloride are shown in Fig. 3.86. The plots of ΔG°_{ads} Vs T are shown in Fig. 3.87.

The thermodynamic parameters for the adsorption of SBS on GA9 magnesium alloy are tabulated in Table 3.101. As seen from Table 3.101, the extent of agreement with the ideal Langmuir isotherm is imprecise, that is, the average regression coefficient equal to 0.99 indicates a substantial agreement, at the same time that the marginal deviation is obvious from the slope values. The suitability of the Langmuir isotherm is accepted by attributing the deviation to the intermolecular interactions of the SBS molecules after adsorption. The values of ΔG°_{ads} and ΔH°_{ads} indicate a spontaneous adsorption which predominantly physisorption. The ΔS°_{ads} value values indicate increase in randomness on going from the reactants to the metal adsorbed species.
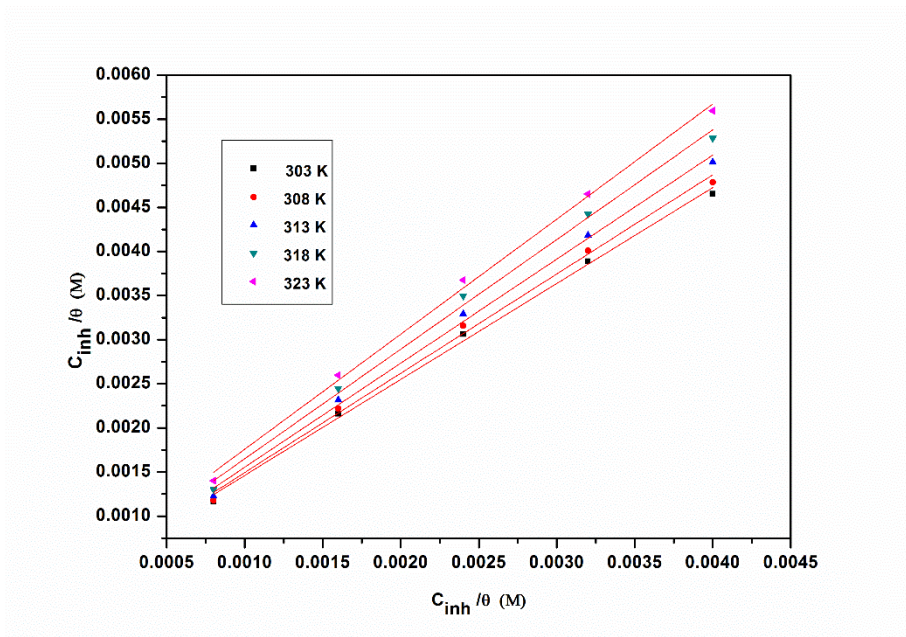
Fig. 3.86: Langmuir adsorption isotherms for the adsorption of SBS on GA9 magnesium alloy in 1.0 M NaCl solution at different temperatures.
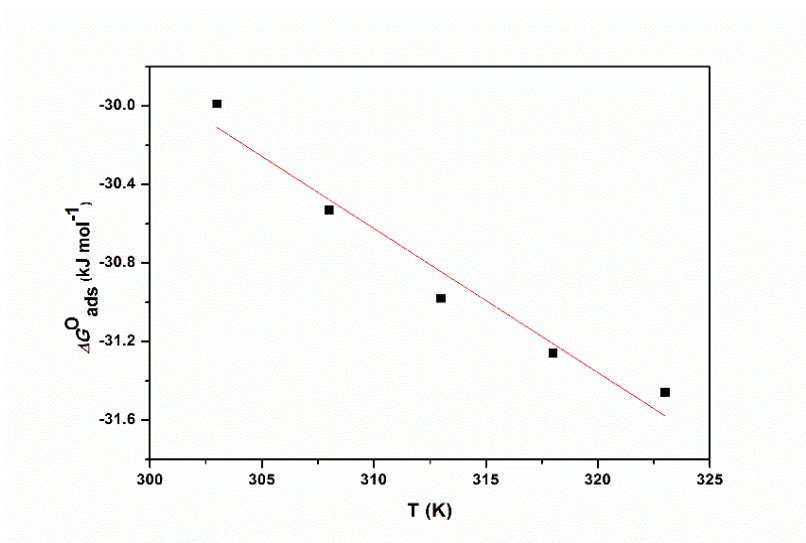
Fig. 3.87: The plot of ΔG°_{ads} vs T for the adsorption of SBS on GA9 magnesium alloy in 1.0 M NaCl solution.

3.11.6 Mechanism of corrosion inhibition

The mechanism of corrosion inhibition of GA9 magnesium alloy in the presence of SDMBS is similar to that in the presence of SDBS as discussed under section 3.5.6. The molecules of SBS get adsorbed on the alloy surface predominantly by physisorption and to a small extent by chemisorption.

3.11.7 SEM/EDX studies

Fig. 3.88 represents SEM image of GA9 magnesium alloy after the corrosion tests in a medium of 2.0 M sodium chloride containing 4.0 mM of SBS. The image clearly shows a relatively smooth surface due to the presence of adsorbed inhibitor layer on the surface of the alloy.
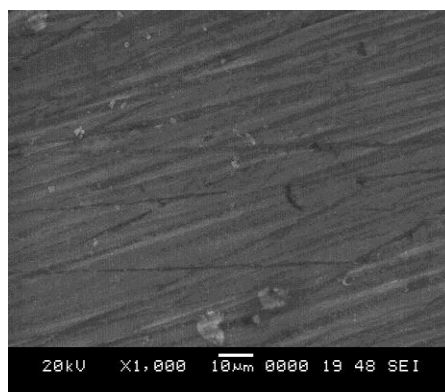
Fig. 3.88: SEM image of the GA9 magnesium alloy after immersion in 2.0 M NaCl solution in the presence of SBS.

The EDX spectra for the selected areas on the SEM image of 3.88 is shown in Fig. 3.89. The weight percentage of the elements found in the EDX spectra for SOBS adsorbed metal surface were 76.22% Mg, 8.66% Al, 11.00% O, 0.48% S and 3.64% C and suggested that formation of anticorrosion protective film of SBS on the alloy surface.
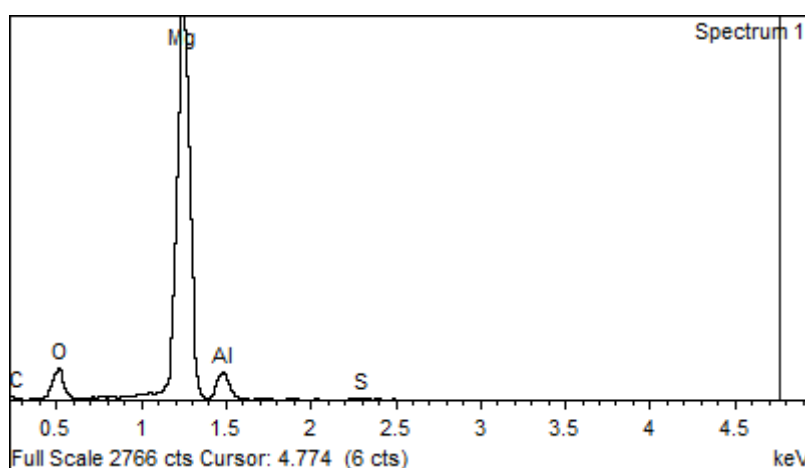
Fig. 3.89: EDX spectra of GA9 magnesium alloy after immersion in 2.0 M NaCl solution in the presence of SBS.

Table 3.89: Results of potentiodynamic polarization studies for the corrosion of GA9 magnesium alloy in 0.1 M sodium chloride solution containing different concentrations of SBS.

| Temperature (℃)	Conc. of inhibitor (mM)	$-E_{corr}$ (mV /SCE)	$-b_c$ (mV dec^{-1})	i_{corr} (μA cm^{-2})	υ_{corr} (mm y^{-1})	η (%)
30	Blank	1449	149	75.1	1.687	
	0.8	1447	124	19.6	0.440	73.9
	1.6	1444	121	16.4	0.368	78.1
	2.4	1436	119	13.5	0.303	82.0
	3.2	1441	117	10.7	0.240	85.7
	4.0	1437	115	7.9	0.178	89.5
35	Blank	1445	157	86.9	1.952	
	0.8	1442	140	23.6	0.530	72.8
	1.6	1435	137	20.2	0.454	76.7
	2.4	1443	134	16.3	0.366	81.2
	3.2	1438	129	13.1	0.294	84.9
	4.0	1432	127	10.2	0.229	88.3
40	Blank	1450	164	108.4	2.435	
	0.8	1445	148	31.3	0.703	71.1
	1.6	1447	145	26.3	0.591	75.7
	2.4	1434	143	22.5	0.506	79.2
	3.2	1439	139	18.6	0.418	82.8
	4.0	1437	135	15.2	0.342	86.0
45	Blank	1465	169	139.1	3.126	
	0.8	1455	155	44.9	1.009	67.7
	1.6	1459	151	40.6	0.912	70.8
	2.4	1454	149	35.5	0.798	74.5
	3.2	1462	147	30.2	0.679	78.3
	4.0	1447	145	25.3	0.568	81.8
50	Blank	1472	173	189.3	4.254	
	0.8	1460	158	71.7	1.611	62.1
	1.6	1464	155	63.2	1.420	66.6
	2.4	1452	153	57.7	1.296	69.5
	3.2	1455	149	52.8	1.186	72.1
	4.0	1449	147	47.9	1.076	74.7

Table 3.90: Results of potentiodynamic polarization studies for the corrosion of GA9 magnesium alloy in 0.5 M sodium chloride solution containing different concentrations of SBS.

Temperature (°C)	Conc. of inhibitor (mM)	$-E_{corr}$ (mV /SCE)	$-b_c$ (mV dec^{-1})	i_{corr} (µA cm^{-2})	υ_{corr} (mm y^{-1})	η (%)
	Blank	1451	152	160.0	3.595	
	0.8	1440	136	46.2	1.038	71.1
	1.6	1442	133	39.4	0.885	75.4
30	2.4	1437	129	32.8	0.737	79.5
	3.2	1441	125	26.9	0.604	83.2
	4.0	1434	121	19.0	0.427	88.1
	Blank	1473	158	179.3	4.029	
	0.8	1454	144	53.3	1.198	70.3
	1.6	1459	142	45.4	1.020	74.7
35	2.4	1449	139	37.8	0.849	78.9
	3.2	1455	136	30.8	0.692	82.8
	4.0	1441	132	25.1	0.564	86.0
	Blank	1466	167	206.6	4.641	
	0.8	1455	154	65.9	1.481	68.1
	1.6	1462	151	56.0	1.258	72.9
40	2.4	1454	148	50.2	1.128	75.7
	3.2	1447	145	42.2	0.948	79.5
	4.0	1451	141	34.7	0.780	83.2
	Blank	1490	171	285.1	6.405	
	0.8	1479	159	98.4	2.211	65.5
	1.6	1483	157	88.1	1.979	69.1
45	2.4	1467	153	77.3	1.737	72.9
	3.2	1471	149	67.6	1.519	76.3
	4.0	1469	145	60.2	1.353	78.9
	Blank	1497	175	377.1	8.473	
	0.8	1492	165	149.3	3.355	60.4
	1.6	1481	162	134.6	3.024	64.3
50	2.4	1486	159	121.4	2.728	67.8
	3.2	1470	156	109.4	2.458	71.0
	4.0	1475	152	99.2	2.229	73.7

Table 3.91: Results of potentiodynamic polarization studies for the corrosion of GA9 magnesium alloy in 1.0 M sodium chloride solution containing different concentrations of SBS.

Temperature (℃)	Conc. of inhibitor (mM)	$-E_{corr}$ (mV /SCE)	$-b_c$ (mV dec^{-1})	i_{corr} (μA cm^{-2})	υ_{corr} (mm y^{-1})	η (%)
30	Blank	1474	156	264.5	5.942	
	0.8	1469	145	82.8	1.860	68.7
	1.6	1461	142	68.5	1.539	74.1
	2.4	1470	139	57.1	1.283	78.4
	3.2	1458	137	46.8	1.052	82.3
	4.0	1463	133	37.0	0.831	86.0
35	Blank	1495	162	298.9	6.716	
	0.8	1481	150	95.9	2.155	67.9
	1.6	1485	148	83.4	1.874	72.1
	2.4	1474	144	71.7	1.611	76.0
	3.2	1469	142	60.4	1.357	79.8
	4.0	1477	139	49.0	1.101	83.6
40	Blank	1496	169	361.5	8.122	
	0.8	1481	160	129.4	2.907	64.2
	1.6	1478	157	114.6	2.575	68.3
	2.4	1485	154	99.4	2.233	72.5
	3.2	1472	152	85.0	1.910	76.5
	4.0	1477	149	74.1	1.665	79.5
45	Blank	1496	177	491.0	11.031	
	0.8	1482	168	189.0	4.247	61.5
	1.6	1488	165	169.9	3.817	65.4
	2.4	1481	162	153.7	3.453	68.7
	3.2	1475	158	136.0	3.056	72.3
	4.0	1479	155	119.3	2.680	75.7
50	Blank	1501	179	665.6	14.955	
	0.8	1485	169	286.2	6.430	57.0
	1.6	1488	167	255.6	5.743	61.6
	2.4	1491	165	231.0	5.190	65.3
	3.2	1479	162	207.7	4.667	68.8
	4.0	1474	159	189.7	4.262	71.5

Table 3.92: Results of potentiodynamic polarization studies for the corrosion of GA9 magnesium alloy in 1.5 M sodium chloride solution containing different concentrations of SBS.

Temperature (°C)	Conc. of inhibitor (mM)	$-E_{corr}$ (mV /SCE)	$-b_c$ (mV dec^{-1})	i_{corr} (μA cm^{-2})	υ_{corr} (mm y^{-1})	η (%)
30	Blank	1497	169	376.5	8.458	
	0.8	1489	159	124.6	2.800	66.9
	1.6	1491	157	106.5	2.393	71.7
	2.4	1482	153	89.6	2.013	76.2
	3.2	1485	149	74.2	1.667	80.3
	4.0	1474	145	59.9	1.346	84.1
35	Blank	1499	173	436.5	9.802	
	0.8	1485	162	151.5	3.404	65.3
	1.6	1481	159	132.3	2.973	69.7
	2.4	1487	157	112.6	2.530	74.2
	3.2	1473	155	96.0	2.157	78.0
	4.0	1477	152	79.4	1.784	81.8
40	Blank	1519	181	552.6	12.416	
	0.8	1507	169	204.5	4.595	63.0
	1.6	1511	167	184.0	4.134	66.7
	2.4	1503	164	163.0	3.662	70.5
	3.2	1506	162	142.0	3.191	74.3
	4.0	1498	160	123.8	2.782	77.6
45	Blank	1520	195	738.2	16.585	
	0.8	1505	186	301.2	6.768	59.2
	1.6	1502	183	275.3	6.186	62.7
	2.4	1510	180	243.6	5.473	67.0
	3.2	1499	177	219.2	4.925	70.3
	4.0	1494	173	196.4	4.413	73.4
50	Blank	1529	210	999.6	22.458	
	0.8	1515	202	447.8	10.061	55.2
	1.6	1501	200	409.8	9.208	59.0
	2.4	1507	197	373.9	8.401	62.6
	3.2	1502	194	338.9	7.615	66.1
	4.0	1495	192	304.9	6.851	69.5

Table 3.93: Results of potentiodynamic polarization studies for the corrosion of GA9 magnesium alloy in 2.0 M sodium chloride solution containing different concentrations of SBS.

Temperature (℃)	Conc. of inhibitor (mM)	$-E_{corr}$ (mV /SCE)	$-b_c$ (mV dec^{-1})	i_{corr} (µA cm^{-2})	υ_{corr} (mm y^{-1})	η (%)
30	Blank	1524	192	447.5	10.055	
	0.8	1513	184	158.9	3.570	64.5
	1.6	1502	181	142.3	3.197	68.2
	2.4	1507	177	126.6	2.845	71.7
	3.2	1493	174	109.6	2.463	75.5
	4.0	1495	172	94.4	2.121	78.9
35	Blank	1525	195	546.9	12.286	
	0.8	1509	187	207.3	4.658	62.1
	1.6	1511	185	187.0	4.202	65.8
	2.4	1505	181	167.4	3.761	69.4
	3.2	1499	179	146.0	3.280	73.3
	4.0	1495	175	130.2	2.925	76.2
40	Blank	1529	206	726.0	16.310	
	0.8	1519	198	296.9	6.671	59.1
	1.6	1503	196	268.6	6.035	63.0
	2.4	1509	194	241.8	5.433	66.7
	3.2	1499	189	216.3	4.860	70.2
	4.0	1501	185	193.1	4.339	73.4
45	Blank	1530	213	986.2	22.157	
	0.8	1509	206	431.0	9.684	56.3
	1.6	1513	202	393.5	8.841	60.1
	2.4	1517	198	358.0	8.044	63.7
	3.2	1502	195	324.5	7.291	67.1
	4.0	1499	191	293.9	6.603	70.2
50	Blank	1535	222	1249.8	28.078	
	0.8	1523	212	594.9	13.366	52.4
	1.6	1509	209	549.9	12.355	56.0
	2.4	1515	206	503.7	11.317	59.7
	3.2	1508	202	464.9	10.446	62.8
	4.0	1501	201	431.2	9.688	65.5

Table 3.94: EIS data for the corrosion of GA9 magnesium alloy in 0.1 M sodium chloride solution containing different concentrations of SBS.

Temperature (℃)	Conc. of inhibitor (mM)	R_{ct} (ohm. cm²)	C_{dl} (µF cm⁻²)	η (%)
	Blank	361.5	11.29	
	0.8	1364.0	8.82	73.5
30	1.6	1621.0	8.64	77.7
	2.4	1986.0	8.37	81.8
	3.2	2493.0	8.05	85.5
	4.0	3379.0	7.61	89.3
	Blank	302.5	11.41	
	0.8	1108.0	9.27	72.7
35	1.6	1304.0	9.01	76.8
	2.4	1671.0	8.74	81.9
	3.2	2044.0	8.40	85.2
	4.0	2677.0	8.13	88.7
	Blank	245.4	15.20	
	0.8	861.1	10.70	71.5
40	1.6	1023.0	10.32	76.0
	2.4	1191.0	10.11	79.4
	3.2	1444.0	9.79	83.0
	4.0	1766.0	9.50	86.1
	Blank	184.5	23.51	
	0.8	576.6	14.02	68.0
45	1.6	640.6	13.62	71.2
	2.4	735.1	13.14	74.9
	3.2	866.2	12.79	78.7
	4.0	1031.0	12.48	82.1
	Blank	132.8	28.95	
	0.8	354.1	17.92	62.5
50	1.6	402.4	17.23	67.0
	2.4	445.6	16.95	70.2
	3.2	495.5	16.52	73.2
	4.0	542.0	16.33	75.5

Table 3.95: EIS data for the corrosion of GA9 magnesium alloy in 0.5 M sodium chloride solution containing different concentrations of SBS.

Temperature (℃)	Conc. of inhibitor (mM)	R_{ct} (ohm. cm^2)	C_{dl} (μF cm^{-2})	η (%)
	Blank	162.9	26.17	
	0.8	567.6	11.50	71.3
30	1.6	675.9	11.21	75.9
	2.4	787.0	10.99	79.3
	3.2	987.3	10.74	83.5
	4.0	1417.0	10.31	88.5
	Blank	147.0	27.21	
	0.8	498.3	11.62	70.5
35	1.6	590.4	11.41	75.1
	2.4	710.1	11.05	79.3
	3.2	875.0	10.60	83.2
	4.0	1081.0	10.22	86.4
	Blank	127.3	28.63	
	0.8	396.6	12.44	67.9
40	1.6	466.3	12.07	72.7
	2.4	515.4	11.83	75.3
	3.2	615.0	11.67	79.3
	4.0	753.3	11.25	83.1
	Blank	91.0	35.08	
	0.8	264.5	15.70	65.6
45	1.6	294.5	15.30	69.1
	2.4	337.0	14.96	73.0
	3.2	385.6	14.51	76.4
	4.0	433.3	14.01	79.0
	Blank	70.8	40.33	
	0.8	179.7	19.02	60.6
50	1.6	199.4	18.57	64.5
	2.4	221.9	18.31	68.1
	3.2	246.7	17.52	71.3
	4.0	272.3	16.93	74.0

Table 3.96: EIS data for the corrosion of GA9 magnesium alloy in 1.0 M sodium chloride solution containing different concentrations of SBS.

Temperature (℃)	Conc. of inhibitor (mM)	R_{ct} (ohm. cm^2)	C_{dl} (μF cm^{-2})	η (%)
30	Blank	99.7	33.50	
	0.8	321.6	11.80	69.0
	1.6	389.5	11.55	74.4
	2.4	468.1	11.19	78.7
	3.2	569.7	10.81	82.5
	4.0	727.7	10.58	86.3
35	Blank	87.4	34.93	
	0.8	270.6	17.38	67.7
	1.6	312.1	17.01	72.0
	2.4	361.2	16.45	75.8
	3.2	430.5	15.80	79.7
	4.0	529.7	15.03	83.5
40	Blank	72.8	39.91	
	0.8	204.5	20.22	64.4
	1.6	231.1	19.71	68.5
	2.4	263.8	19.00	72.4
	3.2	309.8	18.49	76.5
	4.0	353.4	17.80	79.4
45	Blank	52.7	66.70	
	0.8	136.9	30.87	61.5
	1.6	152.8	30.21	65.5
	2.4	168.9	29.51	68.8
	3.2	191.6	27.70	72.5
	4.0	219.6	26.23	76.0
50	Blank	39.0	77.59	
	0.8	91.3	41.03	57.3
	1.6	102.4	39.87	61.9
	2.4	113.0	38.30	65.5
	3.2	126.2	36.85	69.1
	4.0	137.3	34.57	71.6

Table 3.97: EIS data for the corrosion of GA9 magnesium alloy in 1.5 M sodium chloride solution containing different concentrations of SBS.

Temperature (℃)	Conc. of inhibitor (mM)	R_{ct} (ohm. cm^2)	C_{dl} (μF cm^{-2})	η (%)
30	Blank	67.9	41.61	
	0.8	205.8	26.01	67.0
	1.6	241.6	25.13	71.9
	2.4	286.5	24.10	76.3
	3.2	341.2	23.26	80.1
	4.0	424.4	22.02	84.0
35	Blank	60.2	61.15	
	0.8	174.0	38.45	65.4
	1.6	200.1	37.47	69.9
	2.4	231.5	36.31	74.0
	3.2	271.2	34.52	77.8
	4.0	325.4	32.29	81.5
40	Blank	47.5	69.71	
	0.8	129.1	12.10	63.2
	1.6	143.5	40.99	66.9
	2.4	162.1	39.23	70.7
	3.2	186.3	38.32	74.5
	4.0	214.9	35.92	77.9
45	Blank	35.5	89.49	
	0.8	87.7	49.05	59.5
	1.6	95.7	47.03	62.9
	2.4	108.2	45.48	67.2
	3.2	119.9	42.74	70.4
	4.0	134.0	39.20	73.5
50	Blank	26.3	107.44	
	0.8	59.9	52.91	56.1
	1.6	65.3	51.05	59.7
	2.4	71.1	48.55	63.0
	3.2	79.5	45.87	66.9
	4.0	88.0	43.49	70.1

Table 3.98: EIS data for the corrosion of GA9 magnesium alloy in 2.0 M sodium chloride solution containing different concentrations of SBS.

Temperature (℃)	Conc. of inhibitor (mM)	R_{ct} (ohm. cm^2)	C_{dl} (μF cm^{-2})	η (%)
	Blank	58.5	58.01	
	0.8	163.9	37.52	64.3
30	1.6	183.4	36.95	68.1
	2.4	205.3	35.71	71.5
	3.2	237.8	34.50	75.4
	4.0	274.6	33.32	78.7
	Blank	48.2	65.11	
	0.8	126.8	40.10	62.0
35	1.6	141.3	39.01	65.9
	2.4	157.0	37.51	69.3
	3.2	183.3	36.10	73.7
	4.0	204.2	34.15	76.4
	Blank	36.2	83.99	
	0.8	89.4	46.55	59.5
40	1.6	98.6	45.01	63.3
	2.4	109.7	43.37	67.0
	3.2	122.3	41.05	70.4
	4.0	136.6	39.23	73.5
	Blank	26.4	109.41	
	0.8	60.7	62.31	56.5
45	1.6	66.3	60.04	60.2
	2.4	73.1	57.90	63.9
	3.2	80.5	54.53	67.2
	4.0	89.2	52.00	70.4
	Blank	21.1	123.26	
	0.8	44.6	66.24	52.7
50	1.6	48.1	64.09	56.1
	2.4	52.6	61.55	59.9
	3.2	57.3	58.89	63.2
	4.0	61.9	56.11	65.9

Table 3.99: Activation parameters for the corrosion of GA9 magnesium alloy in NaCl solutions containing different concentrations of inhibitor SBS.

Concentration of NaCl	Conc. of inhibitor (mM)	E_a (kJ mol^{-1})	$\Delta H^{\#}$ (kJ mol^{-1})	$\Delta S^{\#}$ (J mol^{-1} K^{-1})
	Blank	37.67	35.07	-125.49
	0.8	52.54	49.94	-82.91
0.1	1.6	55.12	52.52	-80.87
	2.4	59.79	57.18	-67.29
	3.2	65.39	62.79	-50.86
	4.0	73.09	70.49	-27.92
	Blank	35.31	32.71	-127.16
	0.8	47.95	45.35	-96.02
0.5	1.6	50.56	47.96	-88.86
	2.4	54.03	51.43	-78.93
	3.2	58.24	55.64	-66.83
	4.0	67.84	65.24	-37.76
	Blank	37.98	35.38	-114.14
	0.8	51.27	48.63	-80.38
1.0	1.6	54.28	51.68	-71.72
	2.4	57.75	55.15	-61.74
	3.2	61.57	58.97	-50.77
	4.0	67.55	64.95	-32.99
	Blank	40.24	37.64	-103.66
	0.8	52.68	50.07	-71.98
1.5	1.6	55.66	53.06	-63.40
	2.4	58.93	56.33	-54.05
	3.2	62.76	60.16	-42.96
	4.0	67.60	65.00	-28.75
	Blank	42.98	40.39	-92.91
	0.8	54.83	52.23	-62.47
2.0	1.6	56.08	53.48	-59.22
	2.4	57.26	54.66	-56.39
	3.2	59.97	57.37	-48.65
	4.0	62.64	60.04	-41.05

Table 3.100: Maximum inhibition efficiencies attained in different concentrations of sodium chloride solutions at different temperatures for SBS.

Temperature (ºC)	GA9 magnesium alloy			
	Sodium chloride concentration (M)	Concentration of SBS (mM)	η (%)	
			Potentiodynamic polarization method	EIS method
30	0.1	4.0	89.5	89.3
	0.5		88.1	88.5
	1.0		86.0	86.3
	1.5		84.1	84.0
	2.0		78.9	78.7
35	0.1	4.0	88.3	88.7
	0.5		86.0	86.4
	1.0		83.6	83.5
	1.5		81.8	81.5
	2.0		76.2	76.4
40	0.1	4.0	86.0	86.1
	0.5		83.2	83.1
	1.0		79.5	79.4
	1.5		77.6	77.9
	2.0		73.4	73.5
45	0.1	4.0	81.8	82.1
	0.5		78.9	79.0
	1.0		75.7	76.0
	1.5		73.4	73.5
	2.0		70.2	70.4
50	0.1	4.0	74.7	75.5
	0.5		73.7	74.0
	1.0		71.5	71.6
	1.5		69.5	70.1
	2.0		65.5	65.9

Table 3.101: Thermodynamic parameters for the adsorption of SBS on GA9 magnesium alloy surface in sodium chloride solutions at different temperatures.

Molarity of NaCl (M)	Temperature (° C)	$-\Delta G^o_{ads}$ (kJ mol^{-1})	ΔH^o_{ads} (kJ mol^{-1})	ΔS^o_{ads} (J mol^{-1} K^{-1})	R^2	Slope
	30	30.43			0.996	1.06
	35	30.86			0.997	1.07
0.1	40	31.43	-3.65	88.42	0.997	1.10
	45	31.62			0.995	1.16
	50	32.26			0.998	1.27
	30	30.06			0.994	1.07
	35	30.72			0.997	1.09
0.5	40	31.19	-2.49	91.43	0.996	1.14
	45	31.69			0.997	1.20
	50	31.86			0.997	1.28
	30	29.99			0.996	1.09
	35	30.53			0.996	1.13
1.0	40	30.98	-7.87	73.41	0.996	1.18
	45	31.26			0.995	1.24
	50	31.46			0.997	1.30
	30	29.82			0.995	1.11
	35	30.27			0.995	1.14
1.5	40	30.79	-8.16	71.85	0.995	1.21
	45	31.06			0.996	1.27
	50	31.22			0.995	1.34
	30	29.94			0.995	1.19
	35	30.31			0.996	1.23
2.0	40	30.58	-11.24	61.80	0.996	1.28
	45	30.90			0.996	1.33
	50	31.19			0.996	1.42

3.12 SODIUM BENZENESULFONATE (SBS) AS CORROSION INHIBITOR ON GA9 MAGNESIUM ALLOY IN SODIUM SULPHATE MEDIUM

3.12.1 Potentiodynamic polarization measurements

Potentiodynamic polarization curves for the corrosion of GA9 magnesium alloy in 1.0 M Na_2SO_4 solution in the presence of different concentrations of SBS, at 40 °C are shown in Fig. 3.90. Similar plots were obtained at other temperatures and also in the other concentrations of sodium sulphate at the different temperatures studied. The potentiodynamic polarization parameters were calculated from Tafel plots in the presence of different concentrations of SBS at different temperatures and are summarized in Tables 3.102 to 3.106.
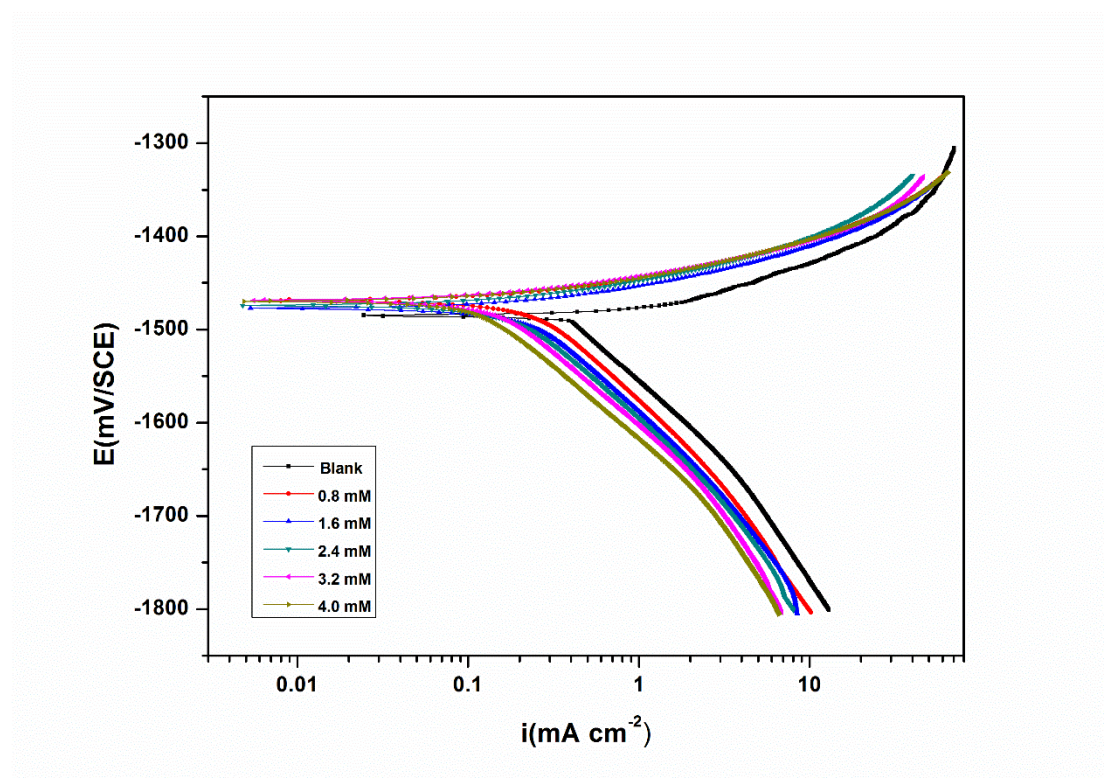
Fig. 3.90: Potentiodynamic polarization curves for the corrosion of GA9 magnesium alloy in 1.0 M Na_2SO_4 solution containing different concentrations of SBS at 40 ℃.

The presence of inhibitor brings down the corrosion rate considerably. Polarization curves are shifted to a lower current density region indicating a decrease in corrosion rate (Li et al. 2008). Inhibition efficiency increases with the increase in SBS concentration. The insignificant shift in the E_{corr} value, in the presence of the

inhibitor implies that the inhibitor SBS, acts as a mixed type inhibitor with a predominant anodic effect.

3.12.2 Electrochemical impedance spectroscopy (EIS) studies

Nyquist plots for the corrosion of GA9 magnesium alloy in 1.0 M sodium sulphate solution in the presence of different concentrations of SBS, at 40 °C are shown in Fig. 3.91. Similar plots were obtained in other concentrations of sodium sulphate and also at other temperatures. The experimental results of EIS measurements obtained for the corrosion of GA9 magnesium alloy in sodium sulphate solution of different concentrations at different temperatures are summarized in Tables 3.106 to 3.111.
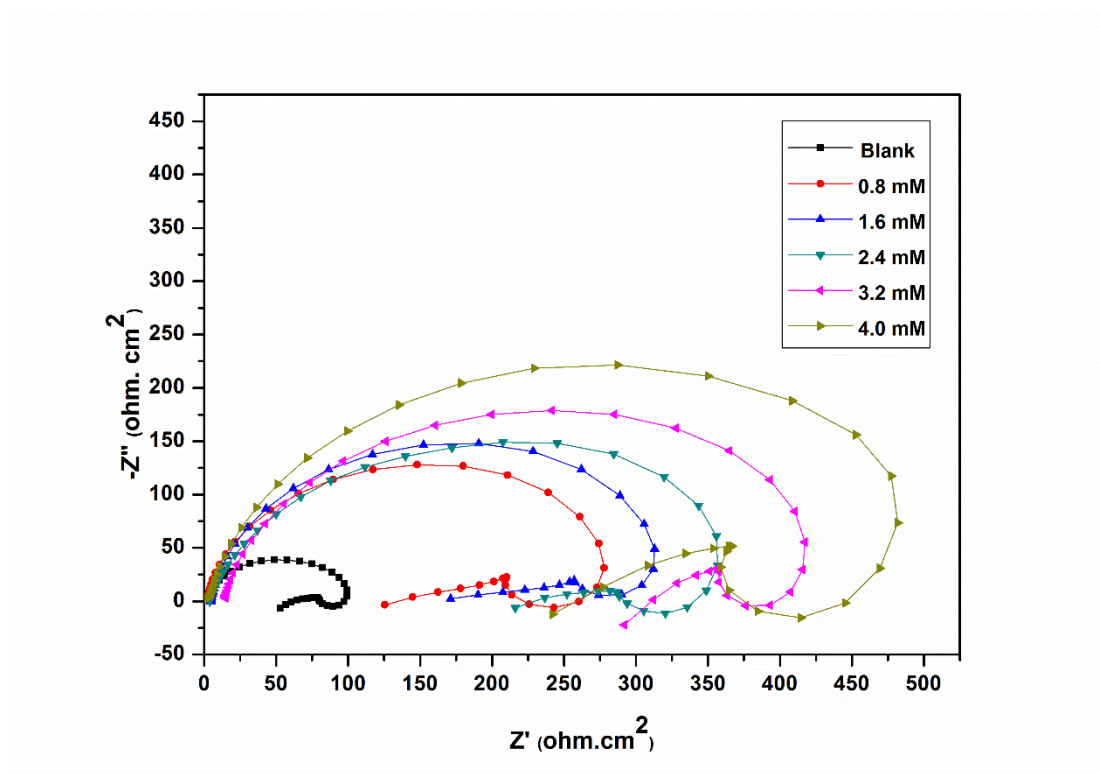
Fig. 3.91: Nyquist plots for the corrosion of GA9 magnesium alloy in 1.0 M Na₂SO₄ solution containing different concentrations of SBS at 40 ℃.

As seen from Fig. 3.91, the capacitive loops of the Nyquist plots are enlarged sequentially with increasing SBS concentration, while the nature remains the same, suggesting an inhibition achieved without the participation of the inhibitor in the electrode reactions. This indicates that the corrosion of GA9 magnesium alloy is controlled by a charge transfer process and the addition of SBS does not alter the

reaction mechanism of the corrosion of sample in Na_2SO_4 solution (Amin et al. 2007). The charge transfer resistance (R_{ct}) increases and double layer capacitance decreases with the increase in the concentration of SBS, indicating an increase in the inhibition efficiency.

The Bode plots of phase angle and amplitude for the corrosion of the GA9 magnesium alloy immersed in 1.0 M Na_2SO_4 at 40 °C in the presence of varying amounts of SBS, are shown in Fig. 3.92 (a) and Fig. 3.92 (b), respectively. As seen from the Bode plots, both the impedance modulus (Z_{mod}) at low frequency and the phase maximum (θ_{max}) at intermediate frequency increase with the increase in SBS concentration, which suggests the presence of highly protective surface film, protects the alloy surface.
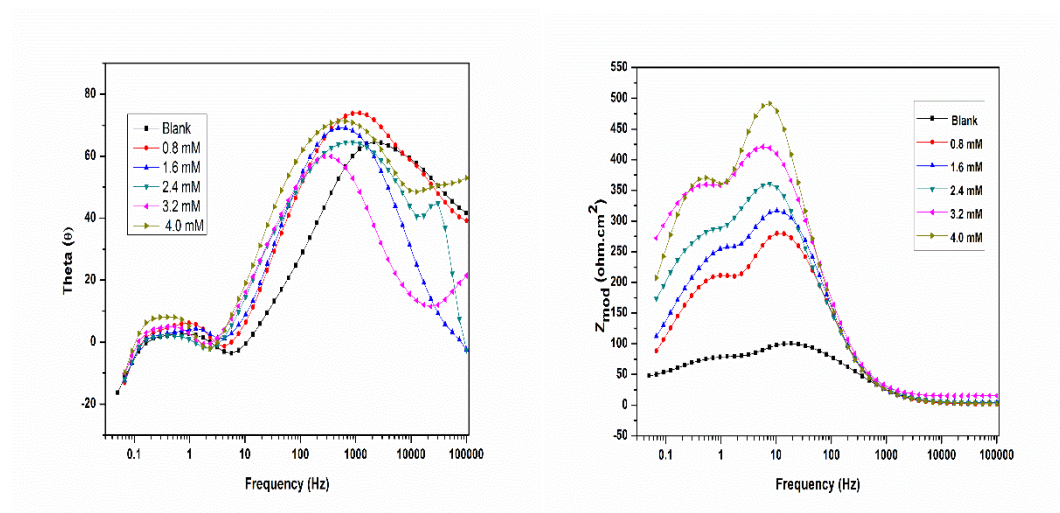
Fig. 3.92: Bode (a) phase angle plots and (b) amplitude plots for the corrosion of GA9 magnesium alloy in 1.0 M Na_2SO_4 solution containing different concentrations of SBS at 40 ℃.

3.12.3 Effect of temperature

The potentiodynamic polarization and EIS results corresponding to different temperatures in different concentrations of sodium sulphate in the presence of SBS, have been listed in the Tables 3.101 to 3.111. The decrease in the efficiency of inhibition with the increase in temperature indicates desorption of the inhibitor molecules from the metal surface when the temperature increases (Poornima et al. 2011). This fact also suggests the physisorption of the inhibitor molecules on the surface of the metal. The Arrhenius plots for the corrosion of GA9 magnesium alloy in

the presence of different concentrations of SBS in 1.0 M Na$_2$SO$_4$ are shown in Fig. 3.93. The plots of ln(υ_{corr}/T) versus 1/T in 1.0 M Na$_2$SO$_4$ in the presence of different concentrations of SBS are shown in Fig. 3.94.
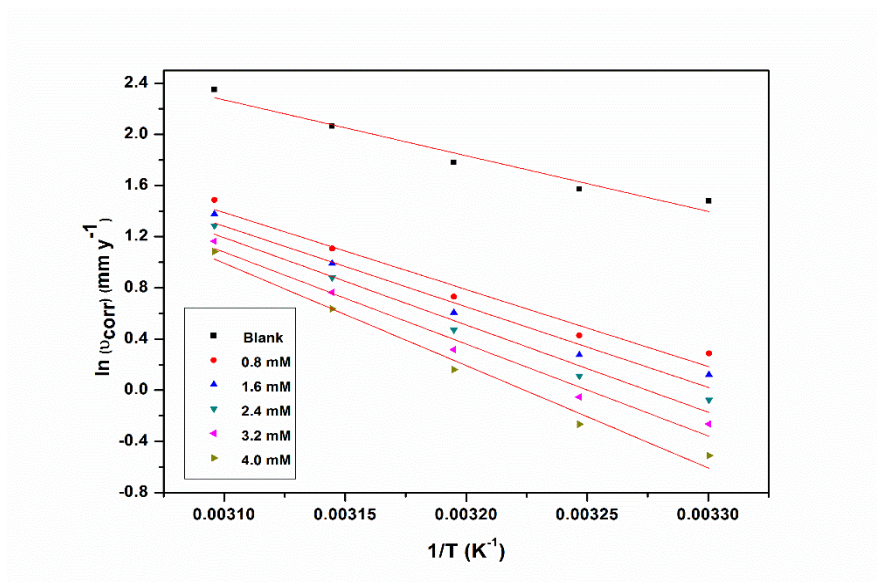
Fig. 3.93: Arrhenius plots for the corrosion of GA9 magnesium alloy in 1.0 M Na$_2$SO$_4$ solution containing different concentrations of SBS.
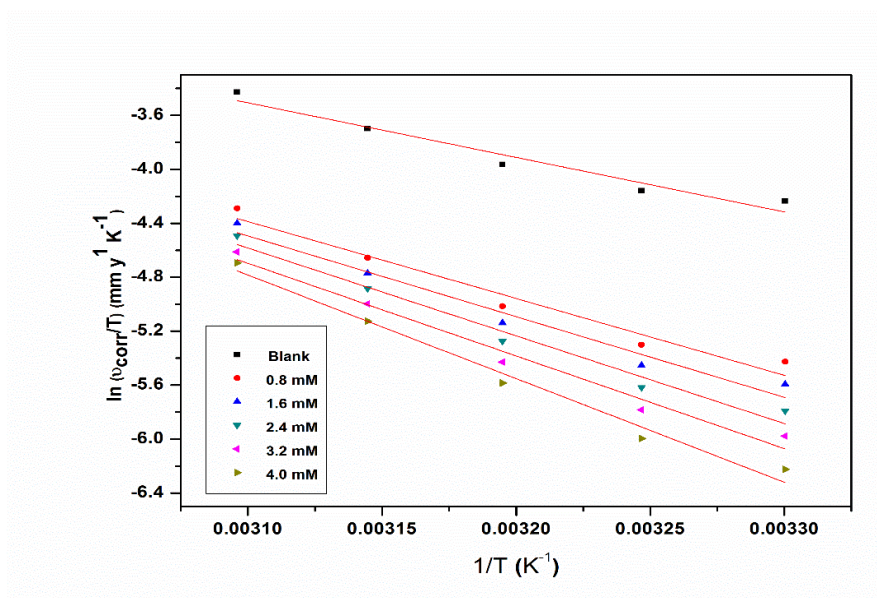
Fig. 3.94: Plots of ln(υ_{corr}/T) versus 1/T for the corrosion of GA9 magnesium alloy in 1.0 M Na$_2$SO$_4$ solution containing different concentrations of SBS.

The calculated values of E$_a$, ΔH$^{\#}$ and ΔS$^{\#}$ are given in Table 3.112. The increase of the activation energy on the addition of SBS can be attributed to the adsorption of

251

SBS, providing a barrier on the surface of the alloy (Avci et al. 2008). The values of entropy of activation indicates that the activated complex in the rate determining step represents an association rather than dissociation, resulting in a decrease in randomness on going from the reactants to the activated complex.

3.12.4 Effect of sodium sulphate concentration

Table 3.113 summarizes the maximum inhibition efficiencies exhibited by SBS in the Na_2SO_4 solution of different concentrations. It is evident, both from the experimental results of polarisation and EIS, that, for a particular concentration of inhibitor, the efficiency of inhibition decreases with the increase in the concentration of sodium sulphate on GA9 magnesium alloy. The highest inhibition efficiency is observed in sodium sulphate of 0.1 M concentration.

3.12.5 Adsorption isotherm

Among the adsorption isotherms considered, Langmuir isotherm was most appropriate to describe the adsorption mediated inhibition by SBS. The Langmuir adsorption isotherms for the adsorption of SBS on GA9 magnesium alloy surface at different temperatures in 1.0 M Na_2SO_4 solution are shown in Fig. 3.95. The plot of ΔG°_{ads} Vs T is shown in Fig. 3.96.
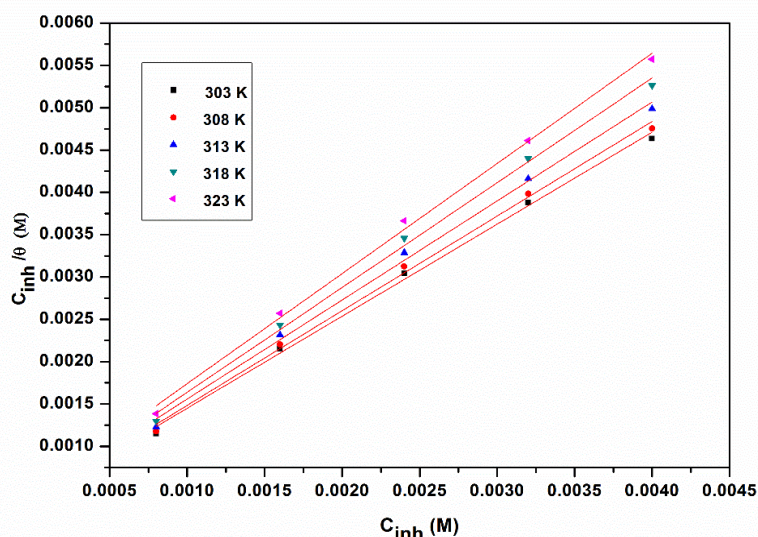
Fig. 3.95: Langmuir adsorption isotherms for the adsorption of SBS on GA9 magnesium alloy in 1.0 M Na_2SO_4 solution at different temperatures.

The calculated thermodynamic parameters like ΔG°_{ads}, ΔH°_{ads} and ΔS°_{ads} along with slope and linear regression coefficient (R^2) for the adsorption of SBS at different temperatures in sodium sulphate are listed in Table 3.114. The small deviation from ideal Langmuir behaviour as evident from the slope values is the consequence of interactions among the adsorbed SBS molecules. The thermodynamic parameters collectively suggest a spontaneous adsorption of SBS, which is predominantly physisorption and accompanied by increase in entropy of the system.
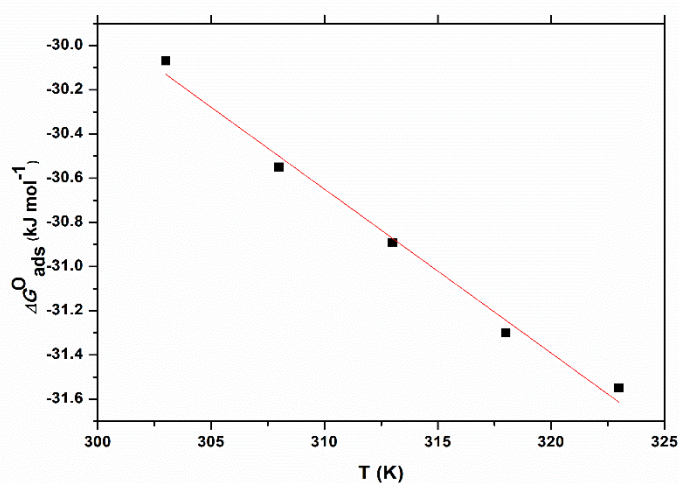
Fig. 3.96: The plot of ΔG°_{ads} Vs T for the adsorption of SBS on GA9 magnesium alloy in 1.0 M Na₂SO₄ solution.

3.12.6 Mechanism of corrosion inhibition

The corrosion inhibition mechanism of SBS in sodium sulphate solution can be explained in the same lines as that of SBS in the section 3.11.6. The inhibitor SBS protects the alloy surface through predominant physisorption mode in which the SBS gets adsorbed on the alloy surface through electrostatic attraction.

3.12.7 SEM/EDX studies

Fig. 3.97 represents the SEM image of GA9 magnesium alloy after the corrosion tests in a medium of 2.0 M sodium sulphate containing 4.0 mM of SBS. The image clearly shows a smooth surface due to the adsorbed layer of inhibitor molecules on the alloy surface, thus protecting the metal from corrosion.
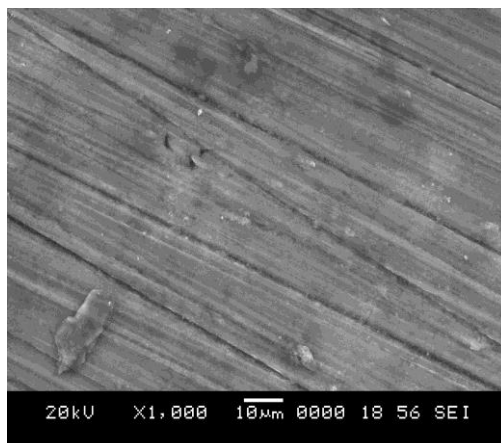
Fig. 3.97: SEM image of GA9 magnesium alloy after immersion in 2.0 M Na$_2$SO$_4$ solution in the presence of SBS.

The EDX spectra for the selected areas on the SEM image of 3.97 is shown in Fig. 3.98. The weight percentage of the elements found in the EDX spectra for SBS adsorbed metal surface were 81.79% Mg, 9.62% Al, 5.35 % O, 0.08% S and 3.16% C and suggested that formation of anticorrosion protective film of SBS on the alloy surface.
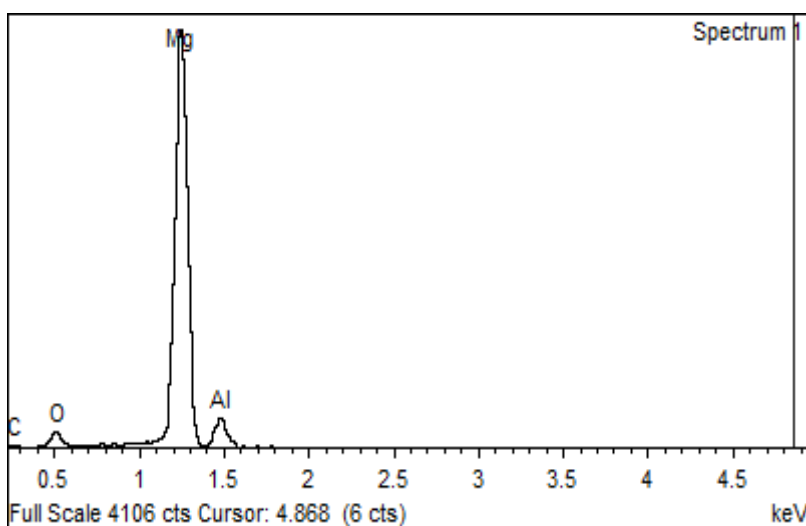
Fig. 3.98: EDX spectra of GA9 magnesium alloy after immersion in 2.0 M Na$_2$SO$_4$ solution in the presence of SBS.

254

3.12.8 Effect of structure on inhibition efficiency

The inhibition efficiencies of the four inhibitors vary in the following order in both the media is SDBS > SOBS > SDMBS > SBS. Inhibition efficiency act synonymously with the concentration of the inhibitor and anonymously with the temperature and concentration of the media. The higher inhibition have been observed in SDBS could be explained with the help of skeletal structure. SDBS could accumulate on greater surface area of the alloy due to the presence of larger alkyl chain attached to the benzene ring of the sulfonate, which hinders the corrosion attack of the media. In comparison with SDBS, SOBS possesses a smaller alkyl chain attached to the benzene ring, hence inhibition efficiency of SOBS is less than that of SDBS and inhibition efficiency of SDMBS. The inhibition efficiency of SBS is still less than that of SOBS as it does not possess alkyl chain.

Table 3.102: Results of potentiodynamic polarization studies for the corrosion of GA9 magnesium alloy in 0.1 M sodium sulphate solution containing different concentrations of SBS.

Temperature (℃)	Conc. of inhibitor (mM)	$-E_{corr}$ (mV /SCE)	$-b_c$ (mV dec^{-1})	i_{corr} (μA cm^{-2})	υ_{corr} (mm y^{-1})	η (%)
30	Blank	1456	139	42.1	0.946	
	0.8	1448	119	10.7	0.240	74.5
	1.6	1441	117	9.3	0.209	78.7
	2.4	1445	114	7.3	0.164	82.6
	3.2	1439	112	5.8	0.130	86.2
	4.0	1440	110	4.3	0.097	89.9
35	Blank	1461	144	47.7	1.071	
	0.8	1452	125	12.7	0.285	73.4
	1.6	1455	122	10.9	0.245	77.2
	2.4	1448	118	8.7	0.195	81.7
	3.2	1445	115	7.0	0.157	85.3
	4.0	1441	113	5.3	0.119	88.8
40	Blank	1463	151	58.4	1.311	
	0.8	1455	133	16.4	0.368	72.0
	1.6	1457	130	13.7	0.308	76.5
	2.4	1451	127	11.2	0.252	80.9
	3.2	1448	125	9.3	0.209	84.0
	4.0	1443	122	7.5	0.169	87.2
45	Blank	1468	159	74.4	1.671	
	0.8	1453	139	23.0	0.517	69.1
	1.6	1449	137	19.9	0.447	73.2
	2.4	1452	134	17.9	0.402	75.9
	3.2	1444	132	15.3	0.344	79.4
	4.0	1441	130	12.4	0.279	83.3
50	Blank	1469	167	97.8	2.197	
	0.8	1459	151	35.0	0.786	64.2
	1.6	1462	148	31.6	0.710	67.7
	2.4	1457	145	28.5	0.640	70.9
	3.2	1448	141	25.7	0.577	73.7
	4.0	1451	138	23.4	0.526	76.1

Table 3.103: Results of potentiodynamic polarization studies for the corrosion of GA9 magnesium alloy in 0.5 M sodium sulphate solution containing different concentrations of SBS.

Temperature (℃)	Conc. of inhibitor (mM)	$-E_{corr}$ (mV /SCE)	$-b_c$ (mV dec^{-1})	i_{corr} (μA cm^{-2})	υ_{corr} (mm y^{-1})	η (%)
30	Blank	1461	144	112.4	2.526	
	0.8	1449	124	31.5	0.708	72.0
	1.6	1454	123	26.8	0.602	76.2
	2.4	1452	121	22.5	0.506	80.0
	3.2	1447	119	18.1	0.407	83.9
	4.0	1441	117	13.2	0.297	88.3
35	Blank	1462	149	125.5	2.819	
	0.8	1455	131	36.8	0.827	70.7
	1.6	1451	129	31.0	0.697	75.3
	2.4	1445	126	25.7	0.577	79.5
	3.2	1448	124	21.1	0.474	83.2
	4.0	1442	121	16.7	0.375	86.7
40	Blank	1459	156	161.1	3.619	
	0.8	1455	141	50.6	1.137	68.6
	1.6	1451	138	43.0	0.966	73.3
	2.4	1448	135	37.1	0.834	77.0
	3.2	1441	133	31.3	0.703	80.6
	4.0	1445	130	25.8	0.580	84.0
45	Blank	1475	164	203.3	4.568	
	0.8	1463	148	69.1	1.553	66.0
	1.6	1455	146	61.4	1.380	69.8
	2.4	1459	142	54.5	1.225	73.2
	3.2	1461	139	47.4	1.065	76.7
	4.0	1451	138	41.9	0.941	79.4
50	Blank	1487	173	264.3	5.939	
	0.8	1475	160	99.6	2.238	62.3
	1.6	1480	158	90.4	2.031	65.8
	2.4	1471	155	81.9	1.840	69.0
	3.2	1465	153	73.7	1.656	72.1
	4.0	1467	149	66.6	1.496	74.8

Table 3.104: Results of potentiodynamic polarization studies for the corrosion of GA9 magnesium alloy in 1.0 M sodium sulphate solution containing different concentrations of SBS.

Temperature (°C)	Conc. of inhibitor (mM)	$-E_{corr}$ (mV /SCE)	$-b_c$ (mV dec^{-1})	i_{corr} (μA cm^{-2})	v_{corr} (mm y^{-1})	η (%)
30	Blank	1472	151	195.2	4.386	
	0.8	1463	139	59.3	1.332	69.6
	1.6	1465	138	50.2	1.128	74.3
	2.4	1459	134	41.2	0.926	78.9
	3.2	1461	130	34.2	0.768	82.5
	4.0	1455	128	26.7	0.600	86.3
35	Blank	1477	156	214.2	4.813	
	0.8	1464	145	68.3	1.535	68.1
	1.6	1474	142	58.7	1.319	72.6
	2.4	1470	139	49.7	1.117	76.8
	3.2	1459	136	42.2	0.948	80.3
	4.0	1463	132	34.1	0.766	84.1
40	Blank	1486	160	264.3	5.938	
	0.8	1471	151	92.5	2.078	65.0
	1.6	1479	148	81.7	1.836	69.1
	2.4	1474	145	71.4	1.604	73.0
	3.2	1467	143	61.1	1.373	76.9
	4.0	1470	140	52.3	1.175	80.2
45	Blank	1487	171	350.4	7.872	
	0.8	1471	159	134.6	3.024	61.6
	1.6	1475	157	119.8	2.692	65.8
	2.4	1466	153	107.2	2.409	69.4
	3.2	1469	151	95.7	2.150	72.7
	4.0	1470	147	84.1	1.890	76.0
50	Blank	1490	181	466.3	10.477	
	0.8	1479	169	197.2	4.431	57.7
	1.6	1482	167	176.3	3.961	62.2
	2.4	1475	165	160.9	3.615	65.5
	3.2	1472	162	142.7	3.206	69.4
	4.0	1477	161	131.5	2.955	71.8

Table 3.105: Results of potentiodynamic polarization studies for the corrosion of GA9 magnesium alloy in 1.5 M sodium sulphate solution containing different concentrations of SBS.

Temperature (℃)	Conc. of inhibitor (mM)	$-E_{corr}$ (mV /SCE)	$-b_c$ (mV dec^{-1})	i_{corr} (µA cm^{-2})	υ_{corr} (mm y^{-1})	η (%)
30	Blank	1477	158	281.7	6.328	
	0.8	1455	147	93.0	2.090	67.0
	1.6	1457	144	79.2	1.780	71.9
	2.4	1462	142	66.5	1.494	76.4
	3.2	1457	138	54.9	1.234	80.5
	4.0	1453	134	44.2	0.993	84.3
35	Blank	1483	165	339.2	7.621	
	0.8	1467	151	117.7	2.645	65.3
	1.6	1461	148	103.8	2.332	69.4
	2.4	1465	145	88.9	1.997	73.8
	3.2	1458	143	76.3	1.714	77.5
	4.0	1460	140	63.4	1.425	81.3
40	Blank	1482	173	426.8	9.589	
	0.8	1471	162	157.1	3.530	63.2
	1.6	1475	160	140.8	3.164	67.0
	2.4	1466	158	125.5	2.820	70.6
	3.2	1463	155	110.1	2.474	74.2
	4.0	1468	151	95.2	2.139	77.7
45	Blank	1486	182	527.1	11.843	
	0.8	1471	172	210.3	4.725	60.1
	1.6	1475	170	192.4	4.323	63.5
	2.4	1468	168	172.4	3.874	67.3
	3.2	1459	165	155.5	3.494	70.5
	4.0	1465	162	138.6	3.114	73.7
50	Blank	1492	194	707.4	15.894	
	0.8	1484	186	311.3	6.994	56.0
	1.6	1471	183	285.1	6.406	59.7
	2.4	1475	179	261.0	5.864	63.1
	3.2	1466	176	237.0	5.325	66.5
	4.0	1469	175	216.5	4.864	69.4

Table 3.106: Results of potentiodynamic polarization studies for the corrosion of GA9 magnesium alloy in 2.0 M sodium sulphate solution containing different concentrations of SBS.

Temperature (°C)	Conc. of inhibitor (mM)	$-E_{corr}$ (mV /SCE)	$-b_c$ (mV dec^{-1})	i_{corr} (µA cm^{-2})	υ_{corr} (mm y^{-1})	η (%)
30	Blank	1488	169	374.6	8.417	
	0.8	1477	162	133.7	3.004	64.3
	1.6	1469	160	120.2	2.701	67.9
	2.4	1473	157	107.5	2.415	71.3
	3.2	1458	154	93.7	2.105	75.0
	4.0	1463	152	80.5	1.809	78.5
35	Blank	1483	176	455.4	10.232	
	0.8	1475	167	171.7	3.858	62.3
	1.6	1467	165	154.8	3.478	66.0
	2.4	1470	162	138.0	3.101	69.7
	3.2	1466	160	120.7	2.712	73.5
	4.0	1458	158	107.5	2.415	76.4
40	Blank	1481	185	597.1	13.415	
	0.8	1469	177	242.4	5.446	59.4
	1.6	1464	175	219.1	4.923	63.3
	2.4	1458	174	197.0	4.426	67.0
	3.2	1471	169	176.1	3.957	70.5
	4.0	1472	165	157.0	3.528	73.7
45	Blank	1489	197	755.8	16.981	
	0.8	1481	189	332.6	7.473	56.0
	1.6	1482	187	303.8	6.826	59.8
	2.4	1471	183	276.6	6.215	63.4
	3.2	1474	179	251.7	5.655	66.7
	4.0	1467	175	226.7	5.094	70.0
50	Blank	1499	209	927.7	20.842	
	0.8	1486	201	446.2	10.025	51.9
	1.6	1481	198	410.0	9.212	55.8
	2.4	1469	194	375.7	8.441	59.5
	3.2	1475	190	348.8	7.837	62.4
	4.0	1472	188	323.8	7.275	65.1

Table 3.107: EIS data for the corrosion of GA9 magnesium alloy in 0.1 M sodium sulphate solution containing different concentrations of SBS.

Temperature (℃)	Conc. of inhibitor (mM)	R_{ct} (ohm. cm^2)	C_{dl} (µF cm^{-2})	η (%)
30	Blank	604.7	10.53	
	0.8	2326.0	7.25	74.0
	1.6	2774.0	7.01	78.2
	2.4	3436.0	6.79	82.4
	3.2	4319.0	6.64	86.0
	4.0	5651.0	6.43	89.3
35	Blank	545.5	10.98	
	0.8	2043.0	8.22	73.3
	1.6	2372.0	7.89	77.0
	2.4	2997.0	7.70	81.8
	3.2	3762.0	7.56	85.5
	4.0	4744.0	7.33	88.5
40	Blank	447.8	11.35	
	0.8	1617.0	8.71	72.3
	1.6	1922.0	8.48	76.7
	2.4	2369.0	8.37	81.1
	3.2	2834.0	8.23	84.2
	4.0	3526.0	7.95	87.3
45	Blank	356.5	16.50	
	0.8	1165.0	10.51	69.4
	1.6	1335.0	10.22	73.3
	2.4	1492.0	9.96	76.1
	3.2	1774.0	9.75	79.9
	4.0	2161.0	9.53	83.5
50	Blank	273.0	25.71	
	0.8	777.8	15.79	64.9
	1.6	840.0	15.42	67.5
	2.4	928.6	14.97	70.6
	3.2	1034.0	14.61	73.6
	4.0	1138.0	14.30	76.0

Table 3.108: EIS data for the corrosion of GA9 magnesium alloy in 0.5 M sodium sulphate solution containing different concentrations of SBS.

Temperature (℃)	Conc. of inhibitor (mM)	R_{ct} (ohm. cm^2)	C_{dl} (µF cm^{-2})	η (%)
	Blank	219.1	18.29	
	0.8	785.3	9.51	72.1
30	1.6	932.3	9.25	76.5
	2.4	1153.0	8.98	81.0
	3.2	1387.0	8.81	84.2
	4.0	1939.0	8.64	88.7
	Blank	200.4	22.81	
	0.8	679.3	11.02	70.5
35	1.6	804.8	10.72	75.1
	2.4	987.2	10.27	79.7
	3.2	1179.0	9.84	83.0
	4.0	1553.0	9.43	87.1
	Blank	165.0	26.11	
	0.8	532.3	13.39	69.0
40	1.6	627.4	13.01	73.7
	2.4	723.7	12.60	77.2
	3.2	863.9	12.32	80.9
	4.0	1044.0	11.94	84.2
	Blank	128.8	30.77	
	0.8	382.2	14.95	66.3
45	1.6	430.8	14.49	70.1
	2.4	489.7	14.11	73.7
	3.2	562.4	13.50	77.1
	4.0	637.6	12.92	79.8
	Blank	97.8	34.19	
	0.8	263.6	18.05	62.9
50	1.6	291.1	17.42	66.4
	2.4	318.6	16.82	69.3
	3.2	355.6	16.45	72.5
	4.0	391.2	16.10	75.0

Table 3.109: EIS data for the corrosion of GA9 magnesium alloy in 1.0 M sodium sulphate solution containing different concentrations of SBS.

Temperature (℃)	Conc. of inhibitor (mM)	R_{ct} (ohm. cm^2)	C_{dl} (μF cm^{-2})	η (%)
30	Blank	139.0	30.91	
	0.8	455.7	11.20	69.5
	1.6	543.0	10.74	74.4
	2.4	643.5	10.33	78.4
	3.2	785.3	10.02	82.3
	4.0	985.8	9.59	85.9
35	Blank	122.6	32.17	
	0.8	378.4	12.74	67.6
	1.6	441.0	12.31	72.2
	2.4	519.5	11.96	76.4
	3.2	613.0	11.40	80.0
	4.0	752.1	11.04	83.7
40	Blank	97.4	40.62	
	0.8	275.1	20.10	64.6
	1.6	312.2	19.37	68.8
	2.4	358.1	18.80	72.8
	3.2	418.0	18.03	76.7
	4.0	489.4	16.85	80.1
45	Blank	72.1	45.05	
	0.8	189.2	23.21	61.9
	1.6	200.3	22.59	64.0
	2.4	236.4	21.77	69.5
	3.2	265.1	20.63	72.8
	4.0	301.7	19.90	76.1
50	Blank	55.5	56.30	
	0.8	132.1	26.60	58.0
	1.6	148.0	25.51	62.5
	2.4	162.8	24.83	65.9
	3.2	183.2	23.55	69.7
	4.0	198.9	22.48	72.1

Table 3.110: EIS data for the corrosion of GA9 magnesium alloy in 1.5 M sodium sulphate solution containing different concentrations of SBS.

Temperature (℃)	Conc. of inhibitor (mM)	R_{ct} (ohm. cm^2)	C_{dl} (μF cm^{-2})	η (%)
	Blank	91.6	34.56	
	0.8	273.4	12.90	66.5
30	1.6	321.4	12.47	71.5
	2.4	381.7	12.17	76.0
	3.2	465.0	11.83	80.3
	4.0	579.7	11.42	84.2
	Blank	77.7	40.12	
	0.8	222.6	19.03	65.1
35	1.6	256.4	18.50	69.7
	2.4	293.2	18.11	73.5
	3.2	342.3	17.32	77.3
	4.0	413.3	16.55	81.2
	Blank	62.4	54.17	
	0.8	171.0	29.23	63.5
40	1.6	190.2	28.10	67.2
	2.4	210.1	27.35	70.3
	3.2	241.9	25.78	74.2
	4.0	283.6	24.31	78.0
	Blank	48.7	71.38	
	0.8	122.4	35.10	60.2
45	1.6	134.9	33.69	63.9
	2.4	152.2	32.74	68.0
	3.2	168.5	31.41	71.1
	4.0	188.8	30.01	74.2
	Blank	37.5	88.74	
	0.8	85.6	42.59	56.2
50	1.6	94.0	41.70	60.1
	2.4	102.7	40.14	63.5
	3.2	112.3	38.02	66.6
	4.0	123.0	35.47	69.5

Table 3.111: EIS data for the corrosion of GA9 magnesium alloy in 2.0 M sodium sulphate solution containing different concentrations of SBS.

Temperature (℃)	Conc. of inhibitor (mM)	R_{ct} (ohm. cm^2)	C_{dl} (µF cm^{-2})	η (%)
	Blank	67.5	42.55	
	0.8	188.0	20.10	64.1
30	1.6	211.6	19.47	68.1
	2.4	232.8	18.98	71.0
	3.2	265.7	18.01	74.6
	4.0	311.1	16.85	78.3
	Blank	57.4	50.87	
	0.8	153.1	25.74	62.5
35	1.6	170.8	24.52	66.4
	2.4	191.3	23.08	70.0
	3.2	217.4	21.90	73.6
	4.0	246.4	20.71	76.7
	Blank	43.2	69.58	
	0.8	105.6	34.12	59.1
40	1.6	116.4	32.40	62.9
	2.4	129.0	30.19	66.5
	3.2	145.5	28.05	70.3
	4.0	163.0	25.59	73.5
	Blank	34.0	85.41	
	0.8	76.7	45.16	55.7
45	1.6	84.0	43.09	59.5
	2.4	92.4	40.77	63.2
	3.2	101.5	38.13	66.5
	4.0	112.6	35.31	69.8
	Blank	27.8	102.33	
	0.8	57.7	52.54	51.8
50	1.6	63.2	50.01	56.0
	2.4	68.3	47.39	59.3
	3.2	73.2	45.00	62.0
	4.0	79.2	42.19	64.9

Table 3.112: Activation parameters for the corrosion of GA9 magnesium alloy in sodium sulphate solution containing different concentrations of SBS.

Concentration of Na_2SO_4	Conc. of inhibitor (mM)	E_a (kJ mol^{-1})	$\Delta H^{\#}$ (kJ mol^{-1})	$\Delta S^{\#}$ (J mol^{-1} K^{-1})
	Blank	34.57	31.97	-140.53
	0.8	48.14	45.54	-107.39
0.1	1.6	49.38	46.78	-104.61
	2.4	55.87	53.27	-85.34
	3.2	61.03	58.43	-70.33
	4.0	68.61	65.85	-47.89
	Blank	35.60	32.99	-128.98
	0.8	47.60	44.99	-100.12
0.5	1.6	50.55	47.95	-91.86
	2.4	54.11	51.51	-81.69
	3.2	58.68	56.08	-68.46
	4.0	67.48	64.85	-42.05
	Blank	36.22	33.62	-122.51
	0.8	49.99	47.40	-87.11
1.0	1.6	52.35	49.75	-80.73
	2.4	56.70	54.09	-67.98
	3.2	59.70	57.10	-59.60
	4.0	66.46	63.86	-39.39
	Blank	37.09	34.49	-116.19
	0.8	48.66	46.06	-87.35
1.5	1.6	51.65	49.05	-78.76
	2.4	55.22	52.62	-68.41
	3.2	59.12	56.52	-57.05
	4.0	64.39	61.79	-41.48
	Blank	37.75	35.15	-111.50
	0.8	49.96	47.36	-79.90
2.0	1.6	50.87	48.27	-77.77
	2.4	52.01	49.41	-75.01
	3.2	54.70	52.09	-67.32
	4.0	57.40	54.79	-59.63

Table 3.113: Maximum inhibition efficiencies attained in different concentrations of sodium sulphate solution at different temperatures for SBS.

Temperature (ºC)	Sodium sulphate concentration (M)	Concentration of SBS (mM)	GA9 magnesium alloy η (%)	
			Potentiodynamic polarization method	EIS method
30	0.1		89.9	89.3
	0.5		88.3	88.7
	1.0	4.0	86.3	85.9
	1.5		84.3	84.2
	2.0		78.5	78.3
35	0.1		88.8	88.5
	0.5		86.7	87.1
	1.0	4.0	84.1	83.7
	1.5		81.3	81.2
	2.0		76.4	76.7
40	0.1		87.2	87.3
	0.5		84.0	84.2
	1.0	4.0	80.2	80.1
	1.5		77.7	78.0
	2.0		73.7	73.5
45	0.1		83.3	83.5
	0.5		79.4	79.8
	1.0	4.0	76.0	76.1
	1.5		73.7	74.2
	2.0		70.0	69.8
50	0.1		76.1	76.0
	0.5		74.8	75.0
	1.0	4.0	71.8	72.9
	1.5		69.4	69.5
	2.0		65.1	64.9

Table 3.114: Thermodynamic parameters for the adsorption of SBS on GA9 magnesium alloy surface in sodium sulphate solution at different temperatures.

Molarity of Na_2SO_4 (M)	Temperature ($^\circ$C)	$-\Delta G^o_{ads}$ (kJ mol^{-1})	ΔH^o_{ads} (kJ mol^{-1})	ΔS^o_{ads} (J mol^{-1} K^{-1})	R^2	Slope
	30	30.50			0.996	1.05
	35	30.90			0.997	1.06
0.1	40	31.46	-1.69	95.09	0.997	1.08
	45	31.83			0.996	1.14
	50	32.41			0.998	1.25
	30	30.20			0.995	1.07
	35	30.73			0.997	1.09
0.5	40	31.19	-0.96	96.61	0.997	1.12
	45	31.74			0.997	1.19
	50	32.11			0.997	1.27
	30	30.07			0.996	1.09
	35	30.55			0.996	1.12
1.0	40	30.89	-7.65	74.25	0.996	1.17
	45	31.30			0.996	1.24
	50	31.55			0.997	1.30
	30	29.94			0.996	1.06
	35	30.31			0.995	1.15
1.5	40	30.84	-6.27	78.23	0.995	1.21
	45	31.22			0.996	1.28
	50	31.44			0.996	1.35
	30	29.94			0.995	1.20
	35	30.33			0.996	1.23
2.0	40	30.61	-11.68	60.04	0.996	1.27
	45	30.87			0.995	1.34
	50	31.18			0.996	1.43

CHAPTER 4

SUMMARY AND CONCLUSION

4.1 SUMMARY

The corrosion behaviour of GA9 magnesium alloy in sodium chloride and sodium sulphate media was established. The in-depth investigation was an electrochemical approach that essentially used potentiodynamic polarization and electrochemical impedance techniques to understand the overall phenomenon. The environmental factors such as concentration of the medium, solution temperature and pH were varied to understand the influence of each of these factors on anodic dissolution of GA9. In addition, the study of the corrosion of GA9 at various temperatures was fundamental for the evaluation of the activation parameters. The results of the electrochemical and surface analyses studies have confirmed the existence of a protective surface film having a remarkable impact on the corrosion behaviour of the GA9 alloy.

Four alkylsulfonates: SDBS, SOBS, SDMBS and SBS were examined for their effectiveness in mitigating the corrosion of GA9 magnesium alloy in solution containing sodium chloride and sodium sulphate. The inhibition test was performed at different medium concentration and temperatures to determine the effect of ionic concentration of the medium and the temperature on the sulfonates inhibition efficiency. At each concentration and medium temperature, the study was extended by varying the concentration of sulfonate. The activation parameters for the corrosion of the alloy in the absence and presence of the inhibitors were calculated and analysed. The thermodynamic parameters like free energy of adsorption (ΔG°_{ads}), enthalpy of adsorption (ΔH°_{ads}) and entropy of adsorption (ΔS°_{ads}) have been calculated and analysed to determine the type and adsorption of inhibitor molecules on the alloy surface.

The electrochemical results together with SEM and EDX analyses were considered to propose a plausible mechanism for the inhibition of the corrosion of GA9 by sulfonates. A slight deviation from the ideal behaviour of Langmuir was observed and was attributed to intermolecular forces such as, van der Waals interactions existing between the alkylsulfonates of the adsorbed molecules. It was believed that such mutual interactions contributed more to the densification of the film.

4.2 CONCLUSIONS

From the above results and discussion, the main conclusions can be summarized in the following points:

1. The corrosion rates of the GA9 magnesium alloy in sodium chloride medium and sodium sulphate medium are substantial.

2. The corrosion rate of the alloy increases with the increase in solution temperature and concentration of chloride ions and sulphate ions.

3. The corrosion kinetics follows Arrhenius law in both the media.

4. The corrosion behaviour of GA9 magnesium alloy in sodium chloride and sodium sulphate solutions are strongly influenced by the medium pH. The corrosion rate decreases with the increase in medium pH. The relatively high corrosion resistance in basic solutions is attributed to the formation of the stable $Mg(OH)_2$ barrier film on the alloy surface.

5. The inhibitors, SDBS, SOBS, SDMBS and SBS act as mixed type inhibitors. SDMBS and SBS are predominantly affect anodic reaction of metal dissolution.

6. The inhibition efficiencies of all the four inhibitors decrease with the increase in temperature and concentrations of the chloride and sulphate ions.

7. The adsorption of all the four inhibitors on the surface of GA9 magnesium alloy obey Langmuir adsorption isotherm with a little interaction between the adsorbed molecules in both the media.

8. The adsorption of all the four inhibitors is through both physisorption and chemisorption, with predominant physical adsorption on GA9 magnesium alloy in both the media.

9. The inhibition efficiencies of the four inhibitors vary in the following order in both the media is SDBS > SOBS > SDMBS > SBS.

4.3 SCOPE FOR FUTURE WORK

The following extensions are recommended to the work presented in this thesis

1. Above study can be extended to other structurally related inhibitors to understand the effect of structure of inhibitor on corrosion inhibition.

2. The electrochemical studies can be performed by varying the immersion time to understand the effectiveness of the surface film during long exposure periods of exposure.

3. Study of corrosion behaviour and inhibition of GA9 magnesium alloy in presence of carboxylates as inhibitors.

References

Abd EI Rehim, S.S., Hassan, H.H. and Amin, M.A. (2003). ''The corrosion inhibition study of sodium dodecyl benzene sulphonate to aluminium and its alloys in 1.0 M HCl solution.'' *Mater. Chem. Phys.,* 78, 337–348.

Abd Ei-Rehim, S.S., Ibrahim, M.A.M. and Khaled, K.F. (1999). "4-Aminoantipyrine as an inhibitor of mild steel corrosion in HCl solution." *J. Appl. Electrochem.,* 29, 593-599.

Altum, H. and Sen, S. (2004). "Studies on the influence of chloride ion concentration and pH on the corrosion and electrochemical behavior of AZ63 magnesium alloy."*Mater. Des.,* 25, 637-643.

Ambat, R., Aung, N. N. and Zhou, W. (2000). "Studies on the influence of chloride ion and pH on the corrosion and electrochemical behaviour of AZ91D magnesium alloy." *J. Appl. Electrochem., 30, 865-874.*

Amin, M.A., Abd El-Rehim, S.S., El-Sherbini, E.E.F. and Bayyomi, R.S. (2007). "The inhibition of low carbon steel corrosion in hydrochloric acid solutions by succinic acid: Part I. Weight Loss, Polarization, EIS, PZC, EDX and SEM Studies." *Electrochim. Acta,* 52, 3588 -3600.

Amy Forsgren (2006). "*Corrosion control through organic coatings."* CRC Press LLC, Taylor & Francis.

Arrabal, R., Pardo, A., Merino, M. C., Mohedano, M., Casajus, P., Paucar, K. and Garces, G. (2012). "Effect of Nd on the corrosion behaviour of AM50 and AZ91D magnesium alloys in 3.5 wt.% NaCl solution." *Corros, Sci.,* 55, 301-312.

Ashish Kumar, S. and Quraishi, M.A. (2010) "Effect of cefazolin on the corrosion of mild steel in HCl solution." *Corros. Sci.,* 52, 152–160.

Ateya, B.G., El-Khair, M.B.A. and Abdel-Hamed, I.A. (1976). "Thiosemicarbazide as an Inhibitor for the Acid Corrosion of Iron." *Corros. Sci.,* 16, 163–169.

Atta, N.F., Fekry, A.M. and Hassaneen, H.M. (2011*). "Corrosion inhibition, hydrogen evolution and antibacterial properties of newly synthesized organic inhibitors on 316L stainless steel alloy in acid medium." *Int. J. Hydrogen Energy.,* 36, 6462-6471.

Avci, G. (2008). "Corrosion inhibition of indole-3-acetic acid on mild steel in 0.5 M HCl." *Colloids Surf.,* 317, 730 -736.

Badaway, W., Hilal N., El-Rabiee M., Nady H. (2010). "Electrochemical behavior of Mg and some Mg alloys in aqueous solutions of different pH." *Electrochim. Acta.,* 55, 1880-1887.

Banerjee, S.N. (1985). *An introduction to science of corrosion and its inhibition*, Oxonian press, New Delhi.

Baghni, M., Wu, Y., Li, J., Zhang, W. (2004). "Corrosion behaviour of magnesium alloys." *Trans. Nonferrous. Met. Soc. China.,* 14, 1-10.

Balwert, C., Hort, N. and Kainer, K.U. (2004). "Automotive applications of magnesium and its alloys." *Trans. Indian Inst. Met.*, 57, 397-408.

Baril, G. and Pebere, N. (2001). "The corrosion of pure magnesium in aerated and deaerated sodium sulphate solutions." *Corros. Sci.,* 43, 471-484.

Barouni, K., Bazzi,L., Salghi, R., Mihit, M., Hammouti, B., Albourine, A. and El Issami, S. (2008). "Some amino acids as corrosion inhibitors for copper in nitric acid solution." *Mater. Lett*., 62, 3325-3327.

Bentiss, F., Lebrini, M. and Lagrenee, M. (2005). "Thermodynamic characterization of metal dissolution and inhibitor process in mild steel/2,5–bis(n-Thienyl)-1,3,4-thiadiazoles/Hydrochloric Acid System." *Corros. Sci.,* 47, 2915-2931.

Bouklah, M., Hammouti, B., Aounti, A. and Benhadda, T. (2004). "Thiophene derivatives as effective inhibitors for the corrosion of steel in 0.5 M H_2SO_4." *Prog Org Coat*., 49, 227 -235.

Bouklah, M., Hammouti, B., Benkaddour, M. and Benhadda, T. (2005). "Thiophene derivatives as effective inhibitors for the corrosion of steel in 0.5 M H_2SO_4." *J. Appl. Electrochem.*, 35, 1095-1101.

Cao, F.H., Len, V.H., Zhang, Z. and Zhang, J.Q. (2007). "Corrosion behavior of magnesium and its alloy in NaCl solution." *Russ. J. Electrochem.*, 43, 837-843.

Cao, H., Li, Q., Chen, F.N., Dai, Y., Luo, F. and li, L. (2011). "Study of the corrosion inhibition effect of sodium silicate on AZ91D magnesium alloy." *Corros. Sci.*, 53, 1401-1407.

Carlson, B.E. and Jones, J.W. (1993). *"The metallurgical aspects of the corrosion behaviour of cast Mg-Al alloys, In: Light metals processing and applications."* METSOC conference, Quebec.

Chao, C., Zhao, Z., Zhong-ling, W., Jain-feng, Y. and Jin-feng, L. (2012). "Electrochemical and corrosion of pure Mg in neutral 1.0% NaCl solution." *Trans. Nonferrous Met. Soc. China*, 22, 970-976.

Chen, J., Wang, J., Han, E., Dong, J. and Ke, W. (2007). "AC impedance spectroscopy study of the corrosion behavior of an AZ91 magnesium alloy in 0.1 M sodium sulfate solution." *Electrochim. Acta.*, 52, 3299-3309.

Correa, P.S., Malfatti, C.F. and Azambuja, D.S. (2011). "Corrosion behavior study of AZ91 magnesium alloy coated with methyltriethoxysilane doped with cerium ions." *Prog. Org. Coat.*, 72, 739-747.

Daloz, D., Rapin, C., Steinmetz, P. and Michot, G. (1998). "Corrosion inhibition of rapidly solidified Mg-3%Zn-15%Al magnesium alloy with sodium carboxylates." *Corrosion*, 54, 444-450.

Davis, J.R. and Davis Associates (2000). *"Corrosion Understanding the basics"* ASM international, Ohio.

Dinodi, N. and Shetty, A. N. (2014). "Investigation of influence of medium pH and sulfate ion concentrations on corrosion behavior of magnesium alloy ZE41." *Surf. Eng. Appl. Electrochem.,* 50, 149-156.

Dinodi, N. and Shetty, A. N. (2014). "Alkyl carboxylates as efficient and green inhibitors of magnesium alloy ZE41corrosion in aqueous salt solution." *Corros. Sci.,* 85, 411-427.

Ehteshamzadeh, M., Jafari, A.H., Naderi, E. and Hosseini, M.G. (2009*).* "Effect of carbon steel microstructure and molecular structure of two new schiff base compounds on inhibition performance in 1 N HCl solution by EIS." *Mater. Chem. Phys.,* 113, 986–993.

Einar Bardal (2003). *"Corrosion and Protection''* Springer-Verlag London Limited, United States of America.

El Hosary, A. A., Saleh, R. M. and Shams El Din, A.M. (1972). "Corrosion inhibition by naturally occurring substances -I. The effect of hibiscus subdariffa (karkade) extract on the dissolution of Al and Zn." *Corros. Sci*., 12, 897-904.

El-Sayed, A. (1997). "Phenothiazine as inhibitor of the corrosion of cadmium in acidic solutions." *J. Appl. Electrochem.,* 27, 89-94.

El-Sayed, M.S. (2011). "Effects of 5-(3-Aminophenyl)-tetrazole as a corrosion inhibitor on the corrosion of Mg/Mn alloy in Arabian Gulf water." *Int. J. Electrochem. Sci.,* 6, 5372-5387.

Fabiola, B., Snihirova, D.V., Xue, H., Montemor, M.F., Lamaka, S.V. and Ferreira, M.G.S. (2012). "Hybrid epoxy-silane coatings for improved corrosion protection of Mg alloy." *Corros. Sci.,* 23, 673-679.

Fekry, A.M. and Ameer, M.A. (2010). "Corrosion inhibition of mild steel in acidic media using newly synthesized heterocyclic organic molecules." *Int. J. Hydrogen Energy.,* 35, 7641 - 7651.

Fontana, M.G., (1986). *"Corrosion Engineering"* 3rd ed., McGraw-Hill, New York, Inc.282.

Froes, F.H., Ellezer, D., Aghion, E., (1998). *"The Science, Technolgy and Applications of Magnesium"* JOM. 50, 30-34.

Frignai, A., Grassi, V., Zanotto, F. and Zucchi, F. (2012). "Inhibition of AZ31 Mg alloy corrosion by anionic surfactants." *Corros. Sci.,* 63, 29-39.

Gadag, R.V. and Shetty, A. N. (2010). "Corrosion and its control." *Engineering chemistry,* second edition, IK International, New Delhi, 54-77.

Gao, H., Li, Q., Dai, Y., Luo, F. and Zhang, H.X. (2010). "High efficiency corrosion inhibitor 8-hydroxyquinoline and its synergistic effect with sodium dodecylbenzenesulphonate on AZ91D magnesium alloy." *Corros. Sci.,* 52, 1603-1609.

Gao, H., Li, Q., Chen, F.N., Dai, Y., Luo, F. and Li, L. Q. (2011). "Study of the corrosion inhibition effect of sodium silicate on AZ91D magnesium alloy." *Corros. Sci.,* 53, 1401-1407.

Geetha, M. P., Nayak, J. and Shetty, A. N. (2011). "Corrosion inhibition of 6061Al-15 vol.pct.SiC(p) composite and its base alloy in a mixture of sulphuric acid and hydrochloric acid by 4-(N,N-dimethylamino) benzaldehyde thiosemicarbazone." *Mater. Chem. Phys.*, 125, 628-640.

Guo, K.W. (2010). "A review of magnesium/magnesium alloy corrosion and its protection." *Recent Patents on Corros. Sci.,* 2, 13-21.

Guohua, W., Yu, F., Hongtao, G., Chunquan, Z. and Ping Z.Y. (2005). "The effect of Ca and rare earth elements on the microstructure, mechanical properties and corrosion behaviour of AZ91D." *Mater. Sci. Eng. A.,* 408, 255-263.

Gupta, M. and Sharon, N.M.L. (2011). "Introduction to magnesium." *Magnesium, and magnesium alloys and msgnesium composites,* John Wiley & Sons, New Jersey, 1-11.

Heakal, F.E., Shehata, O.S. and Tantawy, N.S. (2012). "Enhanced corrosion resistance of magnesium alloy AM60 by cerium(III) in chloride solution." *Corros. Sci.,* 56, 86-95.

Helal, N.H. (2010). "Corrosion inhibition and behavior of methionine on Mg-Al-Zn alloy." *Chem. Eng. Mater. Sci.,* 2, 28-38.

Helal, N.H. and Badaway, W.A. (2011*). "Environmentally safe corrosion inhibition of Mg-Al-Zn alloy in chloride free neutral solutions by amino acids." Electrochim. Acta*., 56, 6581-6587.

Hosseini, M., Mertens S.F.L. and Arshadi M.R. (2003). "Synergism and antagonism in mild steel corrosion inhibition by sodium dodecyl benzenesulphonate and hexamethylenetetramine." *Corros. Sci*., 45, 1473-1482.

Hu, J., Huang, d., Zhang, G., Song, G.L. and Guo, X. (2011). "The synergistic inhibition effect of organic silicate and inorganic Zn salt on corrosion of Mg-10Gd-3Y magnesium alloy." *Corros. Sci.,* 53, 4093-4101.

Hu, J., Huang, d., Zhang, G., Song, G.L. and Guo, X. (2012). "Research on the inhibition mechanism of tetraphenylporphyrin on AZ91D magnesium alloy." *Corros. Sci.,* 63, 367-378.

Hu, J., Zeng. D., Zhing. Z., Shi. T., Song. G.L. and Guo. X. (2013). "2-hydroxy-4-methoxy-acetophenone as an environment-friendly corrosion inhibitor for AZ91D magnesium alloy." *Corros. Sci.,* 49, 1657-1665.

Huang, D., Hu, J., Song, G.-L. and Guo, X. (2011). "Inhibition effect of inorganic and organic inhibitors on the corrosion of Mg-10Gd-3Y-0.5Zr alloy in an ethylene glycol solution at ambient and elevated temperatures." *Electrochim. Acta*, 56, 10166-10178.

Karavai, o.V., Bastos, A.C., Zheludkevich, M. L., Taryaba, M.G., lamaka, S.V. and Ferreira, M.G.S. (2010). "Localized electrochemical study of corrosion inhibition in microdefects on coated AZ31 magnesium alloy." *Electrochim. Acta,* 49, 456-462.

Lasia, A. (1999). "Electrochemical impedance spectroscopy and its applications." *Modern aspects of electrochemistry,* B.E. Conway., J. Bockris and R.E. White, eds., Kluwer Academic/ Plenum Publishers, New York, 143-248.

Lei, J., Li. L., Pan. F. (2012). "Corrosion inhibition of sodium benzoate on AZ31 alloy." *Chem. Eng. Mater. Sci*, 3, 58-68.

Li, W.H., He, Q., Pei, C.L., Hou and B.R., H. (2008). "Some new triazole derivatives as inhibitors for mild steel corrosion in acidic medium." *J Appl Electrochem.,* 38, 289–295.

Li, L.-J., Yao, Z.-M., Lei, J.-L., Xu, H., Zhang, S.-T. Pang, F.-S. (2009). "Adsorption and corrosion behaviour of sodium dodecylbenzenesulfonate on AZ31 magnesium alloy." *Acta Phys-Chim. Sin.,* 25, 1332-1336.

Liu, W., Cao, F., chang, L., Zhang, Z. and Zhang, J. (2009). "Effect of rare earth element Ce and La on corrosion behavior of AM60 magnesium alloy." *Corros. Sci.,* 51, 1334-1343.

Logan, S.D. (2007). "Lightweight automobile body concept featuring ultra-large, thin wall structural magnesium castings." *Magnesium technology*, R.S. Beals, A.A. Luo, N.R. Neelameggham and M.O. Pekuleryuz, eds., TMS, Warrendale, Pennsylvania, 41.

Luo, A.A. (2002). "Magnesium; current and potential automotive applications." JOM, 54, 42-48.

Malik, M.A., Hashim, M.A., Nabi, F., Al-Thabaiti., S.A. and Khan, Z. (2011). "Anti-corrosion ability of surfactants: A review." *Int. J. Electrochem. Sci.,* 6, 1927-1948.

Mansfeld, F. Tsai, C.H. and Shih, H. (1992). "Software for simulation and analysis of electrochemical impedance spectroscopy (EIS) data." *Computer modeling in corrosion*, R.S. Munn, eds., ASTM, Philadelphia, 186-196.

Martinez, S., Stern, I. (2002). "Thermodynamic characterization of metal dissolution and inhibitor adsorption processes in the low carbon steel/mimosa tannin/H_2SO_4 system." *Appl. Surf. Sci.,* 199, 83-99.

Mathaudhu, S. and Nyberg, E. A. (2010). "Magnesium technology: Magnesium alloys in U.S. military applications: past, current and future solutions." *Magnesium technology 2010,* S.R. Agnew, eds., TMS, Warrendale, Pa., 27-33.

McCafferty, E. (2010). *Introduction to corrosion science*, Springer, New York.

Mesbah, A., juers, C., lacouture, F., Mathieu, S., Rocca, E., Francois, M. and Steinmetz, J. (2007). "Inhibitors for magnesium corrosion: Metal-organic frameworks." *Solid state Sci.,* 9, 322-328.

Migahed, M.A. and Al-Sabagh, A.M. (2009). "Beneficial role of surfactants as corrosion inhibitors in petroleum chemistry: a review article." *Chem. Eng. Commun.,* 196, 1054-1075.

Montemor, M. and ferrerira, M.G.S. (2008). "Analytical characterization and corrosion behaviour of bis-aminosilane coatings modified with carbon nanotubes activated with rare-earth salts applied on AZ31 magnesium alloy." *Surf. Coat. Technol.,* 202, 4766-4774.

Morad, M.S. and Kamal El-Dean, A.M. (2006). "2, 2'-Dithiobis (3-cyano-4,6-dimethylpyridine): A New Class of Acid Corrosion Inhibitors for Mild Steel." *Corros. Sci.*, 48, 3398–3412.

Nestor Perez (2004). *"Electrochemistry and Corrosion science."* Kluwer Academic Publishers, Boston.

Oguzie, E. E., Njoku, V.O., Enenebeak, C.K., Akalezi, C.O. and Obi, C. (2008). "Effect of hexamethylpararosaniline chloride (crystal violet) on mild steel corrosion in acidic media." *Corros Sci.*, 50, 3480-3486.

Papavinasam, S. (2011). "Evaluation and selection of corrosion inhibitors." *Uhlig's corrosion handbook,* R. W. Revie, eds., John Wiley & Sons, New Jersey, 1169-1178.

Philip Schweitzer, A. (2007). *"Corrosion Engineering Handbook."* 2nd edition, Taylors and Francis Group, CRC Press, United States of America.

Pierre Roberge, R. (2008). *"Corrosion Engineering Principles and Practice"* McGrawHill, New Delhi.

Polmer, I.J. (1992). *"Physical Metallurgy of Magnesium alloys, DGM Informationsgesellschaft"* Oberursel, Germany. p. 201.

Poornima, T. Nayak, J. and Shetty, A.N. (2010). "Studies on corrosion of annealed and aged 18 ni 250 grade maraging steel in sulphuric acid medium." *Port. Electrochim. Acta,* 28 (3), 173-188.

Poornima, T. Nayak, J. and Shetty. A.N. (2011). "Effect of 4-(N, N-diethylamino) benzaldehyde thiosemicarbazone on the corrosion of aged 18 Ni 250 grade maraging steel in phosphoric acid solution." *Corros. Sci.,* 53, 3688 – 3696.

Poornima, T., Nayak, J. and Shetty, A. N. (2010). "Corrosion of aged and annealed 18 Ni 250 grade maraging steel in phosphoric acid medium." *Int. J. Electrochem. Sci.*, 5, 56 – 71.

Poornima, T., Nayak, J. and Shetty, A. N. (2011). "3, 4-Dimethoxy benzaldehyde thiosemicarbazone as corrosion inhibitor for aged 18Ni 250 grade maraging steel in 0.5 M sulfuric acid." *J. Appl. Electrochem.*, 41, 223-233.

Pourbaix, M. (1974). *"Atlas of Electrochemical Equlibria Aqueous Solutions."* Houston: NACE. p. 139.

Prabhu, R. A., Shanbhag, A. V. and Venkatesha, T. V. (2007). "Influence of tramadol [2-[(dimethylamino) methyl]-1-(3- methoxyphenyl) cyclohexanol hydrate] on corrosion inhibition of mild steel in acidic media." *J. Appl. Electrochem.*, 37, 491- 497.

Prabhu, R.A., Venkatesha, T.V., Shanbhag, A.V., Kulkarni, G.M. and Kalkhambkar, R, G. (2008). "Inhibition effects of some Schiff's bases on the corrosion of mild steel in hydrochloric acid solution." *Corros. Sci.*, 50, 3356–3362.

Quraishi, M.A. and Jamal, D. (2002). "Inhibition of Mild Steel Corrosion in the Presence of Fatty Acid Triazoles." *J. Appl. Electrochem..* 32, 425-430.

Rosen, G.I., Segal, G. And Lumbinsky, A. (2005). "Large profile magnesium alloy extrusions for automotive applications." *Magnesium technology* 2005, N.R. neelameggham, H.I. Kalpan and B.R. Powell, eds., TMS, California, 61.

Sahin, M. Bilgic, S. and Yilmaz, H. (2002). "The inhibition effects of some cyclic nitrogen compounds on the corrosion of the steel in NaCl mediums." *Appl. Surf. Sci.,* 195, 1-7.

Salman, S. A., Ichino, R. and Okido, M. A. (2010). "A comparative electrochemical study of AZ31 and AZ91 magnesium alloy."*Int. J. Corros.,* 1.

Sanaa, T. A. (2008). "Inhibition Action of Thiosemicabazone and some of it is r-substituted compounds on the corrosion of iron-base metallic glass alloy in 0.5 M H2SO4 at 30 °C." *Mater. Res. Bull*., 43, 510–521.

Sastri, V.S., Edward Ghali and Mimoun Elboujdaini (2007). "*Corrosion Prevention and Protection Practical Solutions*." John Wiley & Sons Ltd, England.

Satpati, A.K. and Ravindran, P.V. (2008). ''Electrochemical study of the inhibition of corrosion of stainless steel by 1,2,3-benzotriazole in acidic media.'' *Mater. Chem. Phys.,* 109, 352-359.

Schweitzer, P. A. (2010). *Fundamentals of corrosion: Mechanisms, causes and preventive methods*, CRC Press, Yew York.

Seifzadeh, D., Bezaatpour, A. and joghani, R.A. (2014). "Corrosion inhibition effect of N,N'-bis(2-pyridylmethylidene)-1,2-diaminoethane on AZ91D magnesium alloy in acidic media." *T.. Nonferr. Met. Soc., China,* 24, 3441-3451.

Sheng, N. and Ohtsuka, T. (2012). "Preparation of conducting poly-pyrole layer on zinc coated Mg alloy of AZ91D for corrosion protection." *Prog. Org. Coat.,* 6, 57-65.

Sherif, E.M. and Almajid, A.A. (2011). "Corrosion of magnesium/magnesium alloy in chloride solutions and its inhibition by 5-(3-aminophenyl)-tetrazole." *Int. J. electrochem. Sci.,* 6, 2131-2148.

Shi, H., Liu, F. and Han, E. (2009). "Corrosion protection of AZ91D magnesium alloy with sol-gel coating containing 2-methyl piperidine." *Prog. Org. Coat.,* 66, 183-191.

Song, G. L. and Atrens, A. (1999). "Corrosion mechanisms of magnesium alloys." *Adv. Eng. Mater.,* 1, 11-13.

Song, G. and Atrens, A. (2003). *Understanding magnesium corrosion-a framework for improved alloy performance, Adv. Eng. Mater.,* 1, 11-13.

Song G., Atrens. A. and Dargusch, m. (1999). "Influence of microstructure on the corrosion of diecast AZ91D." *Corros, Sci.,* 41, 249-273.

Song, G. and Atrens, A. (2007). *Recent insights into the mechanism of magnesium corrosion and research suggestions, Adv. Eng. Mater.,* 9, 177-183.

Song, G., Atrens, A., John, D. S., Wu, X. and Nairn, J. (1997). "The anodic dissolution of magnesium in chloride and sulphate solutions." *Corros, Sci.,* 39, 1981-2004.

Song, G., Atrens, A., Wu, X. and Zhang, B. (1998). "Corrosion behavior of AZ21, AZ501and AZ91 in sodium chloride." *Corros. Sci.*, *40,* 1769-1791.

Song, D., Ma, A., Jiang, J., Lin, P., Yang, D. and Fan, J. (2010). "Corrosion behavior of equal-channel-angular-pressed pure magnesium in NaCl aqueous solution." *Corros. Sci.,* 52, 481-490.

Song, G. and St. John, D. (2004). "Corrosion behavior of magnesium in ethylene glycol." *Corros. Sci.,* 46, 1381-1399.

Stansbury, E.E. and Buchanan, R.A. (2000). *"Fundamentals of Electrochemical Corrosion."* ASM International, Materials Park, Ohio.

Taner A., Fatma K., Eno, E. E., Ian, L. and Hailemichael, A. (2009). "Quantum chemical studies on the corrosion inhibition of some sulphonamideson mild steel in acidic medium." *Corros. Sci.*, 51, 35 – 47.

Tao, Z. Zhang, S. Li, W. and Hou, B. (2010) "Adsorption and corrosion inhibition behavior of mild steel by one derivative of benzoic-triazole in acidic solution." *Ind. Eng. Chem. Res.,* 49, 2593-2599.

Thomson, N.G., and payer, G.H. (1998). "DC electrochemical test methods." *Corrosion testing made easy*, national Association of Corrosion Engineers, Houston.

Udhayan, R. and Bhat D.P. (1986). "On the corrosion behavior of magnesium and its alloys using electrochemical techniques." *J. Power Sources,* 63, 103-107.

Wang, L., Zang, B., Shinohara, T. (2010). "Corrosion behavior of GA9 magnesium alloy in dilute NaCl solutions." *Mater. Des.,* 31, 857-863.

Williams, G., McMurray, H.N. and Grace, R. (2010). "Inhibition of magnesium localized corrosion in chloride containing electrolyte." *Electrochim. Acta,* 55, 7824-7833.

Winston Revie, R. (2000). *"Uhling's corrosion handbook"* John Wiley & Sons Inc., Canada.

Yang, X., Pan, F.-S. and zhang, D.F. (2009). "A study on corrosion inhibitor for magnesium alloy." *Mater. Sci. Forum,* 610, 920-926.

Yang L., Wei Y., Hou L. and Zhang D. (2010). "Corrosion behavior of die-cast AZ91D magnesium alloy in aqueous sulphate solutions." *Corros. Sci*., 52, 345-351.

Yang, L., Li, Y., Qian, B. and Hou, B. (2015). "Polyaspartic acid as a corrosion inhibitor for WE43 magnesium alloy." *J. Mag. and alloys.,* 3, 47-51.

Yu, F., Guohua, W., Hongtao, G., Guanqun, L. and Chunquan, Z. (2006). "Influence of lanthanum on the microstructure, mechanical property and corrosion resistance of magnesium alloy." *Mater. Sci. Eng. A* 433, 208-215.

Zhang, L., Mohammed, E.A.A. and Adriaens, A. (2016). "Synthesis and electrochemical behavior of a magnesium fluoride-polydopamine-stearic acid composite coating on AZ31 magnesium alloy." *Surf. Coat. Technolo.,* 307, 56-64.

Zhao, M.C., Liu, M., Song, G. and Atrens, A. (2008). "Influence of the β-phase morphology on the corrosion of the Mg alloy AZ91." *Corros. Sci*., 50, 1939-1953.

Zhao, M.C., Liu, M., Song, G. and Atrens, A. (2008). "Influence of pH and chloride ion concentration on the corrosion of Mg alloy ZE41." *Corros. Sci*., 50, 3168-3178.

Zucchi, F., Frignani, A., Grassi, V., Balbo, A. and Trabanell, G. (2008). "Organo-silane coatings for AZ31 magnesium alloy corrosion protection." *Mater. Chem. Phy.,* 263-268.

LIST OF PUBLICATION

a) **In Journals**

1. Sudarshana Shetty, Jagannath Nayak and A. Nityananda Shetty. (2014). "Electrochemical investigation on corrosion behaviour of Mg-Al-Mn-Zn (GA9) alloy in sodium chloride medium." *J. Electrochem. Plat. Tech*. DOI: 10.12850/ISSN2196-0267.JEPT3343.

2. Sudarshana Shetty, Jagannath Nayak and A. Nityananda Shetty. (2015). "Influence of sulfate ion and pH on the corrosion of Mg-Al-Mn-Zn (GA9) magnesium alloy." *J. Mag. Alloys,* 3 (2015) 258-270.

b) **Papers presented in conferences**

1. Sudarshana Shetty, Jagannath Nayak and A. Nityananda Shetty. (2013). "Electrochemical investigation on corrosion behaviour of magnesium GA9 alloy in sodium chloride medium." *ICRAMST- 13*, January 17-19, NITK Surathkal.

2. Sudarshana Shetty, Jagannath Nayak and A. Nityananda Shetty. (2015). "Corrosion Inhibition of Mg-Al-Mn-Zn (GA9) alloy Sodium Dodecylbenzenesulfonate as Eco-Friendly Material." *Chemistry and Life*, August 7-8, Poornaprajna College, Udupi.

3. Sudarshana Shetty, Jagannath Nayak and A. Nityananda Shetty. (2016). "Sodium xylenesulfonate as agreen corrosion inhibitor of Mg-Al-Zn-Mn (GA9) alloy in chloride medium." *NCRTCS-2016*, January 11-12, MIT Manipal.

4. Sudarshana Shetty, Jagannatha Nayak and A. Nityananda Shetty. (2017). "Corrosion inhibition of sodium 4-n-octylbenzenesulfonate on Mg-Al-Zn-Mn (GA9) alloy." *NCCSF-2017*, January 27-28, Sri Dharmasthala Manjunatheshwara College, Ujire.

5. Sudarshana Shetty, Jagannath Nayak and A. Nityananda Shetty. (2017). "The corrosion inhibition of sodium dodecylbenzenesulfonate on Mg-Al-Zn-Mn (GA9) alloy in 1.0M sodiumsulphate solution." *GCNOC-2017*, Febrauary 27-28, St. Aloysius College, Mangalore.

BIODATA

Mr. SUDARSHANA SHETTY

S/o: RATHNAKARA SHETTY

"SIRI" Cholebettu,

Kukkehalli Post

Udupi-576124.

State: Karnataka

Phone: +91- 9611562468 (M)

E-mail: sudashetty25@gmail.com

Date of Birth: 01/06/1986

Academic Details

Course	Institution	Year	Class
Master of Science- Organic Chemistry	Karnatak University Dharwad.	2009	I
Bachelor of Science- Physics, Chemistry, Mathematics	Milagres College, Kallianpur.	2007	I
Pre-University Course	Milagres P.U. College, Kallianpur	2004	I
S.S.L.C	Sri Vishwakarma High School, Bellampalli.	2002	I

Professional Experience

		Position	Year
Pre-University	Oxford P.U. Science College, Nagarbetta, Vijapura	Lecturer	July 2009 - April 2011
Under Gratuate	Pooraprajna College, Udupi	Lecturer and HOD	June 2011 - Till date